

STRUCTURAL MATERIALS: MANUFACTURE, PROPERTIES, CONDITIONS OF USE

Collective monograph

UDC 669.01

S89

Published in 2023
by TECHNOLOGY CENTER PC
Shatylova dacha str., 4, Kharkiv, Ukraine, 61165

S89

Authors:

Orest Ostash, Svitlana Polyvoda, Andrii Titov, Kostyantyn Balushok, Roman Chepil, Natalia Zlochevska, Anatoliy Nariivskiy, Oleg Shinsky, Inna Shalevska, Yuliia Kvasnitska, Pavlo Kaliuzhnyi, Maksym Kovzel, Valentyna Kutzova

Structural materials: manufacture, properties, conditions of use: collective monograph. – Kharkiv: TECHNOLOGY CENTER PC, 2023. – 176 p.

Collective monograph highlights the results of systematic scientific research devoted to the problems of forming alloys with specified properties. The considered alloys of the Al-Mg and Al-Mg-Sc systems, alloyed and reinforced aluminum, iron-carbon and heat-resistant alloys of cast and composite structural materials, in particular for the blades of gas turbine engines (GTE), deformable aluminum alloys and heat-resistant chromium-nickel alloys "Nikorin". Technological solutions for the production of such alloys are proposed and their characteristics are given.

The monograph is intended for theoreticians and practitioners involved in the development and implementation of alloys, as well as their manufacturing technologies for various operational applications, which can provide an opportunity to increase the competitiveness of enterprise products.

Figures 94, Tables 40, References 164 items.

All rights reserved. No part of this book may be reprinted or reproduced or utilised in any form or by any electronic, mechanical, or other means, now known or hereafter invented, including photocopying and recording, or in any information storage or retrieval system, without permission in writing from the authors. This book contains information obtained from authentic and highly regarded sources. Reasonable efforts have been made to publish reliable data and information, but the author and publisher cannot assume responsibility for the validity of all materials or the consequences of their use. The authors and publishers have attempted to trace the copyright holders of all material reproduced in this publication and apologize to copyright holders if permission to publish in this form has not been obtained. If any copyright material has not been acknowledged please write and let us know so we may rectify in any future reprint.

The publisher, the authors and the editors are safe to assume that the advice and information in this book are believed to be true and accurate at the date of publication. Neither the publisher nor the authors or the editors give a warranty, express or implied, with respect to the material contained herein or for any errors or omissions that may have been made.

Trademark Notice: product or corporate names may be trademarks or registered trademarks, and are used only for identification and explanation without intent to infringe.

DOI: 10.15587/978-617-7319-97-8

ISBN 978-617-7319-97-8 (on-line)

Cite as: *Structural materials: manufacture, properties, conditions of use (2023)*. Kharkiv: TECHNOLOGY CENTER PC, 176. doi: <https://doi.org/10.15587/978-617-7319-97-8>



9 786177 319978

Copyright © 2023 Authors
This is an open access paper under the Creative Commons CC BY license

AUTHORS

CHAPTER 1

OREST OSTASH

Professor, Head of Laboratory
Laboratory of Microstructural Fracture Mechanics
Karpenko Physico-Mechanical Institute of National Academy
of Sciences of Ukraine

 ORCID ID: <https://orcid.org/0000-0001-6441-3830>

SVITLANA POLYVODA

Researcher
Department of Alloy Smelting and Refining Processes
Physico-Technological Institute of Metals and Alloys of
National Academy of Sciences of Ukraine

 ORCID ID: <http://orcid.org/0009-0002-8906-0693>

ANDRII TITOV

PhD, Associate Professor
Department of Applied Hydroaeromechanics and
Mechatronics
National Technical University of Ukraine "Igor Sikorsky Kyiv
Polytechnic Institute"

 ORCID ID: <https://orcid.org/0000-0002-2245-5650>

KOSTYANTYN BALUSHOK

PhD, Chief Engineer
Motor Sich JSC

 ORCID ID: <https://orcid.org/0000-0002-8212-9275>

ROMAN CHEPIL

PhD, Senior Researcher
Laboratory of Microstructural Fracture Mechanics
Karpenko Physico-Mechanical Institute of National Academy
of Sciences of Ukraine

 ORCID ID: <https://orcid.org/0000-0002-9861-4291>

NATALIA ZLOCHEVSKA

PhD, Associate Professor
Department of Aircraft Production Technologies
National Technical University of Ukraine "Igor Sikorsky Kyiv
Polytechnic Institute"

 ORCID ID: <https://orcid.org/0000-0002-7252-9566>

CHAPTER 2

ANATOLIY NARIVSKIY

Doctor of Technical Sciences, Professor, Corresponding
Member National Academy of Sciences of Ukraine,
Director of Institute
Physico-Technological Institute of Metals and Alloys of
National Academy of Sciences of Ukraine

 ORCID ID: <http://orcid.org/0000-0002-1596-6401>

OLEG SHINSKY

Doctor of Technical Sciences, Professor, Head of
Department
Department of Physics and Chemistry of Foundry Processes
Physico-Technological Institute of Metals and Alloys of
National Academy of Sciences of Ukraine

 ORCID ID: <http://orcid.org/0000-0001-6200-0709>

INNA SHALEVSKA

Doctor of Technical Sciences, Associate Professor,
Leading Researcher
Department of Physics and Chemistry of Foundry Processes
Physico-Technological Institute of Metals and Alloys of
National Academy of Sciences of Ukraine

 ORCID ID: <http://orcid.org/0000-0002-8410-7045>

YULIYA KVASNITSKA

Doctor of Technical Sciences, Senior Researcher, Leading
Researcher
Department of Physics and Chemistry of Foundry Processes
Physico-Technological Institute of Metals and Alloys of
National Academy of Sciences of Ukraine

 ORCID ID: <http://orcid.org/0000-0003-3790-2035>

PAVLO KALIUZHNYI

PhD, Senior Researcher
Department of Physics and Chemistry of Foundry Processes
Physico-Technological Institute of Metals and Alloys of
National Academy of Sciences of Ukraine

 ORCID ID: <http://orcid.org/0000-0002-1111-4826>

SVITLANA POLYVODA

Researcher
Department of Alloy Smelting and Refining Processes
Physico-Technological Institute of Metals and Alloys of
National Academy of Sciences of Ukraine

 ORCID ID: <http://orcid.org/0009-0002-8906-0693>

CHAPTER 3

MAKSYM KOVZEL

Senior Researcher
Department of Problems Strain-Heat Treatment of
Structural Steels
Iron and Steel Institute of Z. I. Nekrasov of National
Academy of Sciences of Ukraine
 ORCID ID: <https://orcid.org/0000-0001-5720-1186>

VALENTYNA KUTZOVA

Doctor of Technical Sciences, Professor, Head of
Department
Department of Material Science and Heat Treatment of
Metals
Institute of Industrial and Business Technologies Ukrainian
State University of Science and Technologies
 ORCID ID: <https://orcid.org/0000-0003-2413-679X>

CHAPTER 4

ANATOLIY NARIVSKIY

Doctor of Technical Sciences, Professor, Corresponding
Member National Academy of Sciences of Ukraine,
Director of Institute
Physico-Technological Institute of Metals and Alloys of
National Academy of Sciences of Ukraine
 ORCID ID: <http://orcid.org/0000-0002-1596-6401>

OLEG SHINSKY

Doctor of Technical Sciences, Professor, Head of
Department
Department of Physics and Chemistry of Foundry Processes
Physico-Technological Institute of Metals and Alloys of
National Academy of Sciences of Ukraine
 ORCID ID: <http://orcid.org/0000-0001-6200-0709>

INNA SHALEVSKA

Doctor of Technical Sciences, Associate Professor,
Leading Researcher
Department of Physics and Chemistry of Foundry Processes
Physico-Technological Institute of Metals and Alloys of
National Academy of Sciences of Ukraine
 ORCID ID: <http://orcid.org/0000-0002-8410-7045>

YULIYA KVASNITSKA

Doctor of Technical Sciences, Senior Researcher, Leading
Researcher
Department of Physics and Chemistry of Foundry Processes
Physico-Technological Institute of Metals and Alloys of
National Academy of Sciences of Ukraine
 ORCID ID: <http://orcid.org/0000-0003-3790-2035>

PAVLO KALIUZHNYI

PhD, Senior Researcher
Department of Physics and Chemistry of Foundry Processes
Physico-Technological Institute of Metals and Alloys of
National Academy of Sciences of Ukraine
 ORCID ID: <http://orcid.org/0000-0002-1111-4826>

SVITLANA POLYVODA

Researcher
Department of Alloy Smelting and Refining Processes
Physico-Technological Institute of Metals and Alloys of
National Academy of Sciences of Ukraine
 ORCID ID: <http://orcid.org/0009-0002-8906-0693>

ABSTRACT

Collective monograph highlights the results of systematic scientific research devoted to the problems of forming alloys with specified properties for various operating conditions of parts made from them. It also considers the characteristics of alloys of several systems, mechanisms of structure formation, properties and technological features of obtaining such alloys.

Chapter 1 presents the results of studies of the effect of reducing the magnesium content and alloying with scandium, zirconium, manganese, chromium, and SRM on the structure, phase composition, strength, plasticity, and crack resistance, as well as the corrosion potential and current of alloys of the Al-Mg and Al-Mg-Sc systems, obtained using a magnetohydrodynamic foundry. A positive effect of reducing the magnesium content, as well as the replacement of manganese with chromium and doping with lanthanum in alloys of the Al-Mg-Sc system in the cast state and after extrusion, pressing and rolling has been established. It is shown that due to dispersion strengthening by secondary intermetallics of chromium and lanthanum, this alloy in the cast state after homogenization is superior in strength to the well-known alloys of grades 1570 and 1545. After hot and cold rolling, it is not inferior to these alloys in terms of strength and plasticity, but has higher corrosion resistance characteristics. In terms of structural strength, which is comprehensively determined by the characteristics of strength and cyclic crack resistance, such alloys are superior to the well-known Al-Mg-Sc, Al-Mg and Al-Cu-Mg systems.

Chapter 2 presents the results of the development of new highly efficient foundry technologies for the production of cast and composite structural materials and products with high operational characteristics from alloyed and reinforced aluminum, iron-carbon and heat-resistant alloys. In particular, the results of obtaining blades of gas turbine engines (GTE) with a regular directional casting structure using the method of jet gas cooling of molds in a vacuum are presented. Promising technologies for obtaining cast iron and steel reinforced structures based on gasification patterns by liquid-phase combination of system components have been developed.

Chapter 3 is devoted to determining the patterns of structure formation, phase composition, and tribological properties of heat-resistant chrome-nickel alloys "Nikorin". New solutions to the scientific and practical problem, which consists in increasing the complex of tribological properties and heat resistance of chromium-nickel alloys for modern engineering, are presented. The composition of heat-resistant chrome-nickel alloys, the distribution of alloying elements between phases and structural components have been studied, and the dependence of changes in mechanical properties on the parameters of the structure and phase composition has been established. The results of determining the structure, phase composition, and microhardness of the structural components of the heat-resistant chrome-nickel alloy "Nikorin" after quenching at different temperatures, as well as the tribological properties of chrome-nickel alloys in the cast state, are given.

Chapter 4 presents the results of determining the influence of electromagnetic mixing and alloying on the properties of deformable aluminum alloys, on the phase state and structural stability of heat-resistant corrosion-resistant alloys used for the manufacture of turbine blades of gas turbine engines (GTE). The results of studies on the effect of alloying a heat-resistant nickel-based alloy with tantalum and rhenium on its operational characteristics are presented. It has been proven that under the controlled influence of technological factors and excess pressure (2...6 MPa) on liquid metal and during its crystallization, it is possible to increase the mechanical strength and reduce the porosity of cast iron and steel castings by 15...30 %, compared to gravity casting according to models, which are gasified.

KEYWORDS

Aluminum alloys, Al-Mg-Sc system, alloying, modification, deformation treatment, structural strength, corrosion resistance, vacuum magnetohydrodynamic mixer, heat-resistant corrosion-resistant nickel alloys, blades of gas turbine engines, directional crystallization, iron-carbon alloys, lost foam casting, chrome-nickel alloys, wear rate, wear resistance index.

CIRCLE OF READERS AND SCOPE OF APPLICATION

The monograph is intended for researchers dealing with issues of synthesis of alloys and the development of technologies for their production based on modern phenomena about the mechanisms of formation of structure and properties for various operational applications.

The monograph is also useful for practitioners – designers, metallurgists, technologists who implement modern solutions in the field of materials science of metals and alloys in the practical conditions of their enterprises and are interested in increasing the competitiveness of their products.

CONTENTS

List of Tables	xi
List of Figures	xiii
Introduction	1
1 Cast and deformation strengthened alloys of the Al-Mg-Sc system	2
1.1 Structure and mechanical and corrosion properties of cast alloys of the Al-Mg-Sc system	3
1.2 Strength and cyclic crack resistance of heat-deformed alloys of the Al-Mg-Sc system	8
1.3 The influence of rare-earth metals on the structure and properties of cast and deformed alloys of the Al-Mg-Cr-Sc-Zr system	14
1.4 Pressing of semi-finished products from alloys of the Al-Mg-Sc system in isothermal conditions	23
References	28
2 Modern technological processes of obtaining cast products and structures of responsible purpose from aluminum, ferrous carbon and heatresistant alloys	32
2.1 Modern processes of obtaining cast structural materials from aluminum alloys of responsible purpose	34
2.2 Effective processes for obtaining cast turbine blades for marine and power gas turbine engines	43
2.2.1 Modern technologies for obtaining working blades of gas turbine engines	43
2.2.2 Experimental studies using the GCC technological process	47
2.3 Promising technologies for obtaining cast iron and steel reinforced structures by lost foam casting	51
2.3.1 Methods of obtaining products with high special properties	51
2.3.2 Production technologies of cast reinforced structures, which are obtained by liquid-phase combination of system components	52
2.3.3 Research of heat and mass exchange processes in reinforced castings from iron-carbon alloys	57
2.3.4 Selection of functional schemes for obtaining cast reinforced structures and optimization of their technological parameters	59
Conclusions	62
References	63

3 Regularities of the formation of structure, phase composition and tribological properties of heat-resistant chromium-nickel alloys "Nikorin"	68
3.1 A contemporary view about the patterns of structure formation, phase composition, mechanical and tribological properties of high-chromium and chromium-nickel alloys	69
3.1.1 Patterns of structure formation in heat-resistant high-chromium and chromium-nickel alloys	69
3.1.1.1 Features of structure formation in high-chromium alloys	69
3.1.1.2 Formation of the structure of chromium-nickel alloys	71
3.1.2 Structural transformations in chromium-nickel alloys	73
3.1.2.1 Formation of γ' -phase	73
3.1.2.2 Ordering by Ni_2Cr type	74
3.1.2.3 Formation of α -phase	74
3.1.2.4 Carbide forming	75
3.1.3 Carbides in heat-resistant chromium-nickel alloys	76
3.1.4 Influence of alloying elements on the structure and properties of high-chromium nickel alloys	78
3.1.5 Heat resistance of chromium-nickel alloys	82
3.1.6 Modern trends in the development and use of high-temperature nickel-chromium alloys "Nikorin" for the manufacture of mandrels for tube rolling mills	84
3.1.7 Statement of the research problem	88
3.2 Material and methodology of research	88
3.3 Investigation of the regularities of the structure formation, phase composition, properties and distribution of alloying elements between the phases and structural components of nickel-chromium alloys "Nikorin" in the as-cast state	92
3.4 Calorimetric analysis of research chromium-nickel alloys	101
3.5 Structure, phase composition, microhardness of phases and structural components of prototypes of nickel-chromium alloy "Nikorin" after quenching from different temperatures	103
3.6 Influence of the structural-phase state on the mechanical and tribological properties of chromium-nickel alloys in the cast state	110
Conclusions	115
References	116
4 The influence of external actions and methods of alloying alloys on the operational characteristics of cast products	121
4.1 Modern processes of production of cast structural materials from aluminum alloys for products of responsible purpose	122

4.1.1	The influence of external actions and melt alloying methods on the structures and properties of products made of deformable aluminum alloys	122
4.2	Influence of alloying elements on special properties of heat-resistant alloys.....	131
4.3	The influence of excess pressure on the properties and quality of castings from iron-carbon alloys when lost foam casting	136
4.3.1	Features of thermal destruction of polystyrene under the action of excess pressure	136
4.3.2	The influence of technological parameters of lost foam casting under regulated pressure on the physical and mechanical characteristics of cast structures made of iron-carbon alloys	143
4.3.3	Technological scheme of obtaining reinforced castings by lost foam casting under regulated pressure	151
	Conclusions	153
	References.....	154

LIST OF TABLES

1.1	Chemical composition (wt. %) of the investigated alloys	3
1.2	Mechanical characteristics of alloys	4
1.3	Local content (wt. %) of chemical elements in the investigated alloys	6
1.4	Chemical composition (wt. %) of alloys	9
1.5	Mechanical characteristics of the studied alloys in the cast and thermo-deformed states and their comparison with those known in the literature	10
1.6	Mechanical characteristics and parameter of structural strength of aluminum alloys	14
1.7	Chemical composition (wt. %) of the investigated alloys	15
1.8	Mechanical characteristics of the studied alloys in the cast state	16
1.9	Influence of the cooling rate and homogenization of castings on the mechanical characteristics of alloy No. 5	16
1.10	Local content of alloying elements in castings of alloy No. 5 (mold at 300 °C, homogenization at 360 °C, cooled in air)	18
1.11	Local content (wt. %)* of the main alloying elements in deformed alloy No. 5	19
1.12	Mechanical characteristics of deformed alloy No. 5 and their comparison with those known in the literature	20
1.13	Mechanical characteristics and parameter of structural strength of aluminum alloys	22
1.14	Average chemical composition of alloys	23
1.15	Temperature change in yield strength (MPa) of alloys during compression tests	23
2.1	Chemical composition of heat-resistant alloy based on nickel	49
3.1	The chemical composition of the prototypes of the nickel-chromium alloy "Nikorin"	89
3.2	Quantitative data of X-ray structural analysis of prototypes of the nickel-chromium alloy "Nikorin"	96
3.3	The value of the microhardness of the matrix and eutectic carbide in research chromium-nickel alloys	96
3.4	Distribution of alloying elements between phases and structural components in the chrome-nickel alloy "Nikorin" (alloy No. 1)	100
3.5	Distribution of alloying elements between phases and structural components in the chrome-nickel alloy "Nikorin" (alloy No. 2)	100
3.6	Distribution of alloying elements between phases and structural components in the chrome-nickel alloy "Nikorin" (alloy No. 3)	100
3.7	Temperatures of the onset of crystallization/melting of samples of chromium-nickel alloy "Nikorin" during heating/cooling	103
3.8	Microhardness of the matrix and carbides in the samples of the nickel-chromium alloy "Nikorin" after quenching from various temperatures	109

3.9	Measurement data of the high-temperature hardness of the nickel-chromium alloy "Nikorin"	110
3.10	Results of studies on the wear resistance of the nickel-chromium alloy "Nikorin" under friction conditions at various loads	111
3.11	The results of studies on the wear resistance of the nickel-chromium alloy "Nikorin" under friction conditions at elevated temperatures and a load of 500 N	111
3.12	Quantitative data of X-ray structural analysis of the research chromium-nickel alloy "Nikorin" before and after friction wear at room temperature	114
3.13	Microhardness of matrix, eutectic carbide and hardness of samples of chromium-nickel alloy "Nikorin" before and after friction wear	115
4.1	Technological parameters of the preparation of secondary alloy AD31 and continuous casting of ingots from it	124
4.2	Conditions for experimental melting of alloy 1545 and results of mechanical tests of samples in the cast state	126
4.3	Mechanical properties of hot-pressed billets from the B96C1 alloy	129
4.4	Mechanical properties of products from experimental alloys	131
4.5	Chemical composition of modern global heat-resistant alloys for high-pressure turbine blades of gas turbines	132
4.6	Results of calculations of the composition of the experimental alloy with the addition of rhenium and tantalum using linear regression analysis	134
4.7	Characteristics of experimental alloys	134
4.8	Mechanical properties of samples of experimental alloys	136
4.9	Corrosion indicators of experimental alloys	136
4.10	Number of gaseous, vapor-liquid and solid phases during thermal destruction of a polystyrene foam sample weighing 2.4 g	140
4.11	Experiment planning matrix	144

LIST OF FIGURES

1.1	Microstructure of alloys: <i>a, b</i> – No. 1; <i>c, d</i> – 2; <i>e, f</i> – 3; <i>g, h</i> – 8	5
1.2	Polarization curves and electrochemical characteristics of alloys according to their number in the Table 1.1	7
1.3	Corroded surface of alloy samples No. 1 (<i>a</i>); No. 2 (<i>b</i>); No. 3 (<i>c</i>) and No. 8 (<i>d</i>). Alloy number according to the Table 1.1	8
1.4	Temperature dependence of yield strength under compression for alloys No. 1 (●) and No. 2 (▲)	9
1.5	Microstructure (<i>a, b</i>) and local chemical composition of intermetallic compounds (<i>c, d</i>) and matrix (<i>e, f</i>) of alloys No. 1 (<i>a, c, e</i>) and No. 2 (<i>b, d, f</i>) after rolling	11
1.6	Diagrams of fatigue macrocrack growth rates: <i>a</i> – for rolled alloys No. 1 (●, △) and No. 2 (■) under tensile (●) and bending (△, ■) loads; <i>b</i> – comparison with literature data for heat-deformed alloys of type 1570: 1 – alloy No. 1, $D_g=50\dots150\ \mu\text{m}$; 2 – $6\dots10\ \mu\text{m}$ [12]; 3 – $70\dots170\ \mu\text{m}$ [9]; 4 – $\sim 1\ \mu\text{m}$ [9]; 5 – [3]; 6 – [2]	12
1.7	Microfractograms of samples from alloys No. 1 (<i>a, c</i>) and No. 2 (<i>b, d</i>) at $\Delta K=15$ (<i>a, b</i>) and $25\ \text{MPa}\cdot\sqrt{\text{m}}$ (<i>c, d</i>)	13
1.8	Microstructure of alloy No. 5 depending on the cooling rate during crystallization (<i>a, b</i>) and after homogenization (<i>c, d</i>) casting: <i>a, b</i> – mold at 300 °C and 20 °C; <i>c, d</i> – cooling in water and air	17
1.9	Microstructure of alloy No. 5 after hot (<i>a</i>) and cold rolling of samples with a thickness of 4 mm (<i>b, d</i>) and 2 mm (<i>c</i>); <i>d</i> – electron microscopy	19
1.10	The corroded surface of samples of hot-rolled alloys 1570 (<i>a</i>), 1545 (<i>b</i>) and No. 5 (<i>c</i>) and their electrochemical characteristics	20
1.11	Diagrams of fatigue macrocrack growth rates (<i>a</i>) in alloy No. 5: 1 – HR(6), $D_g=10\dots30\ \mu\text{m}$; 2 – HRV(6)+A ₁ ; 3 – CR(4), $D_g=10\dots15\ \mu\text{m}$; 4 – CR(4)+A ₂ ; 5 – CR(2), $D_g=5\dots10\ \mu\text{m}$; 6 – CR(2)+A ₂ (designation see Table 1.12) and their comparison with literature results for deformed alloys of type 1570: 7 – $D_g\approx 6\ \mu\text{m}$ [12]; 8 – $D_g\approx 1\ \mu\text{m}$ [3], as well as microfractograms of samples of alloy No. 5 after CR (<i>b</i>) and CR (<i>c</i>) at $da/dN\approx 1.10^6\ \text{m/cycle}$	21
1.12	Calculation scheme (<i>a</i>) and general view of the hot pressing installation (<i>b</i>): I, II, III – deformation zones. The arrows point to the movement speed vectors (the length of the arrow is proportional to the movement speed)	24
1.13	Distribution of the intensity of deformation rates ϵ_t at the moment of establishment of a stable pressing mode: <i>a</i> – in the ZY plane; <i>b</i> – in the XZ plane	25

1.14	Shear deformations ε_{yz} (<i>a</i>) and the distribution of their intensity according to Mises at the time of establishment of a constant deformation force (<i>b</i>), in particular, in sections <i>ZY</i> along the <i>Y</i> axis (<i>c</i>) and <i>ZY</i> along the <i>Z</i> axis (<i>d</i>)	26
1.15	Change in the microstructure of alloy 1570 along the strip thickness: <i>a</i> – near-surface zone; <i>b</i> – the middle	26
1.16	Comparison of the dependences of the pressing force <i>P</i> on the displacement <i>a</i> of the punch, determined experimentally for blanks made of alloys 1545 (curve 1) and 1570 (curve 2), and calculated: 3 – $\mu=0.5$; 4 – 0.3; 5 – 0.1	27
1.17	Distribution of damage ω in a strip with a thickness of 12 mm	28
2.1	Vacuum MHD equipment for the preparation of aluminum alloys and continuous casting of ingots from them	35
2.2	Flow diagram of the melt in the heat nozzle	36
2.3	Device for feeding the ligature rod into the melt	36
2.4	Scheme of a crystallizer for creating a protective atmosphere around the solid-liquid phase of the ingot	37
2.5	Diagram of a centrifugal casting machine	38
2.6	Schematic of MHD equipment for obtaining rapidly crystallized aluminum fibers and powder	39
2.7	Scheme of the MHD unit for processing aluminum alloys with fine crystalline particles	40
2.8	Diagram: <i>a</i> – of the equipment for obtaining aluminum powder; <i>b</i> – the movement of the melt in the crucible of the resistance furnace during electromagnetic stirring	40
2.9	Scheme of melt processing with a vacuum-plasma unit	41
2.10	Scheme of a high-gradient installation for obtaining castings with directional crystallization	45
2.11	Comparative parameters of DC methods	47
2.12	Scheme of a foundry installation with an additional cooling unit	48
2.13	Thermo-kinetic curves of five experimental melting thermocouples with DC	50
2.14	Macrostructure of the sample in the cast state: <i>a</i> – appearance of the sample; <i>b</i> – macrostructure of the middle part of the sample; <i>c</i> – section from the seed (near the cone)	51
2.15	Microstructure of test samples in the cast state at different magnifications	51
2.16	Microstructure of a two-layer casting made of cast iron with a diaphragm made of a steel plate St3 with a thickness of 0.7 mm	54
2.17	Physical model of production of cast reinforced structures	56
2.18	Kinetics of solidification and cooling of a casting (F 50×200 mm) made of 45L steel in a hollow form	57
2.19	Kinetics of solidification and cooling of a casting (F 50×200 mm) made of 45L steel in a mold with MRP (0.5 D_{cast})	58
2.20	Kinetics of MRP heating and cooling (0.5 D_{cast})	59

2.21	Selection and optimization of materials and basic technological parameters for obtaining reinforced cast structures and castings with differential properties using macroreinforcing phase (MRP)	61
3.1	Diagram of the state of the Ni-Cr system: <i>a</i> – according to the data [13]; <i>b</i> – according to the data [14]	72
3.2	The effect of chromium on the hardness of binary alloys Ni-Cr after 1 g tempering at 600–900 °C. Quenching from 1100 °C in water (figures in Cr % curves)	75
3.3	Mandrel drawings	86
3.4	Scheme of shell rolling	87
3.5	Scheme of rolling the shell in a continuous state	87
3.6	Scheme of rolling the shell on the machine-state	87
3.7	Scheme of rolling the shell on the machine-state (in details)	88
3.8	General view of the installation for hardening-microstructural analysis	90
3.9	Diagram of the working space of the furnace for hardening-microstructural analysis	90
3.10	Appearance of tribological contact at a load of 1000 N and a sliding speed of 2 m/s	91
3.11	Microstructure of heat-resistant chromium-nickel alloy "Nikorin" (alloy No. 1): <i>a</i> – casting surface $\times 150$; <i>b</i> – surface of casting $\times 600$; <i>c</i> – central part of casting $\times 600$	92
3.12	Microstructure of heat-resistant chromium-nickel alloy "Nikorin" (alloy No. 2): <i>a</i> – longitudinal section of Cr_7C_3 carbides; <i>b</i> – cross section of Cr_7C_3 ; <i>c</i> – coarsely differentiated austenite-carbide eutectic based on Cr_7C_3 chromium carbide	93
3.13	Microstructure of nickel-chromium alloy "Nikorin" (alloy No. 3): <i>a</i> – cross-section of Cr_7C_3 ; <i>b</i> – longitudinal section of Cr_7C_3 carbides; <i>c</i> – carbide <i>t</i> and, which grows together with chromium carbide Cr_7C_3	93
3.14	Scheme of the diffractogram of the prototype (alloy No. 1) of the nickel-chromium alloy "Nikorin"	94
3.15	Scheme of the diffractogram of the prototype (alloy No. 2) of the nickel-chromium alloy "Nikorin"	94
3.16	Scheme of the diffraction pattern of the prototype (alloy No. 3) of the nickel-chromium alloy "Nikorin"	95
3.17	Scheme of the diffraction pattern of the carbide analysis of the prototype (alloy No. 2) of the nickel-chromium alloy "Nikorin"	95
3.18	Scheme of the diffractogram of the carbide analysis of the prototype (alloy No. 3) of the nickel-chromium alloy "Nikorin"	96
3.19	Distribution of alloying elements between phases and structural components in the nickel-chromium alloy "Nikorin" (alloy No. 1)	97
3.20	Distribution of alloying elements between phases and structural components in the nickel-chromium alloy "Nikorin" (alloy No. 2)	98

3.21	Distribution of alloying elements between phases and structural components in the nickel-chromium alloy "Nikorin" (alloy No. 3)	99
3.22	Thermogram of the nickel-chromium alloy "Nikorin": <i>a</i> – heating; <i>b</i> – cooling	102
3.23	Microstructure of samples of chromium-nickel alloy "Nikorin" after quenching from different temperatures ($\times 1000$): <i>a</i> – hardening temperature 1390 °C; <i>b</i> – hardening temperature 1373 °C; <i>c</i> – hardening temperature 1280 °C; <i>d</i> – hardening temperature 1170 °C; <i>e</i> – hardening temperature 1150 °C; <i>f</i> – hardening temperature 1100 °C; <i>g</i> – hardening temperature 1100 °C ($\times 500$)	104
3.24	Microstructure of a sample quenched from a temperature of 1280 °C: <i>a</i> – $\times 500$; <i>b</i> , <i>c</i> – $\times 1000$	105
3.25	Microstructure of samples, chromium-nickel alloy "Nikorin" after quenching at different temperatures: <i>a</i> – hardening temperature 1085 °C; <i>b</i> – hardening temperature 526 °C	106
3.26	Schemes of diffraction patterns of the nickel-chromium alloy "Nikorin" after quenching at different temperatures: <i>a</i> – hardening temperature 1390 °C; <i>b</i> – hardening temperature 1373 °C; <i>c</i> – hardening temperature 1286 °C	106
3.27	Schemes of diffraction patterns of the nickel-chromium alloy "Nikorin" after quenching from different temperatures: <i>a</i> – hardening temperature 1280 °C; <i>b</i> – hardening temperature 1190 °C; <i>c</i> – hardening temperature 1170 °C	107
3.28	Schemes of the diffraction patterns of the nickel-chromium alloy "Nikorin" after quenching at different temperatures: <i>a</i> – hardening temperature 1150 °C; <i>b</i> – hardening temperature 1110 °C; <i>c</i> – hardening temperature 1085 °C; <i>d</i> – hardening temperature 526 °C	108
3.29	Schematic of the diffraction pattern of a sample of nickel-chromium alloy "Nikorin" quenched from a temperature of 1150 °C	109
3.30	Schematic diffraction pattern of a sample of nickel-chromium alloy "Nikorin" quenched from a temperature of 1100 °C	109
3.31	Temperature dependence of the hot hardness of the prototypes of the nickel-chromium alloy "Nikorin"	111
3.32	Graph of the dependence of the wear rate on the specific load of the nickel-chromium alloy "Nikorin"	112
3.33	Graph of the dependence of the wear resistance index of the nickel-chromium alloy "Nikorin" on the specific load	113
3.34	Microstructure of the nickel-chromium alloy "Nikorin" in the cast state after testing at a temperature of 20 °C and a specific load of 0.04 kg/mm ² : <i>a</i> – $\times 200$; <i>b</i> – $\times 500$; <i>c</i> – $\times 1000$	113
3.35	Section of the diffraction pattern of the research chromium-nickel alloy "Nikorin" in the cast state after tests at a temperature of 20 °C and a specific load of 0.04 kg/mm ²	114

LIST OF FIGURES

4.1	Vacuum MHD complex for the preparation of aluminum alloys and continuous casting of ingots from them	124
4.2	Macrostructure of experimental ingots from secondary alloy AD31: <i>a</i> – melt No. 1; <i>b</i> – melt No. 2; <i>c</i> – melt No. 3	125
4.3	Scheme of liquid metal movement during electromagnetic stirring in the crystallizer	127
4.4	Macrostructure of the longitudinal section of a continuously cast ingot Ø90 mm from the B96Ts alloy: the upper part – without electromagnetic stirring; the lower one – with electromagnetic stirring of the alloy in the ingot	128
4.5	Microstructure of continuously cast ingots with a diameter of 150 mm from the B96Ts1 alloy: <i>a</i> – produced according to traditional technology; <i>b</i> – modified with a ligature bar Al–2.5 % by wt. Zr	129
4.6	Vacuum MHD mixer with plasmatron	130
4.7	Microstructure of continuously cast ingots with a diameter of 250 mm from experimental alloys: <i>a</i> – B93pch; <i>b</i> – B93pch+Ti+PN	131
4.8	Microstructure of samples of heat-resistant alloys in the cast state: <i>a</i> – CM88Y; <i>b</i> – experimental alloy	135
4.9	Scheme of the unit (<i>a</i>) and sleeve (<i>b</i>) for studying thermal destruction of polystyrene when high pressure is applied to the metal	137
4.10	Kinetics of gasification of a polystyrene model when pressure ($P=0.5$ MPa) is applied to the crystallizing liquid metal	139
4.11	The influence of the metal rising speed in a mold with a gasifying model on the degree of gasification (<i>n</i>) and the accumulation of the liquid phase (ε) during the casting of iron-carbon alloys under high pressure ($P>0.5$ MPa)	140
4.12	Scheme of the equipment for researching the influence of the main technological factors on the gas-hydrodynamic features, technical and technological properties of metal castings when lost foam casting, under excess adjustable pressure	143
4.13	Influence of pressure P_1 and the degree of metal overheating on the strength σ_B in: <i>a</i> – carbon steel; <i>b</i> – alloy steel	146
4.14	Influence of pressure P_1 and the degree of metal overheating θ_1 on the strength σ_B of: <i>a</i> – high-strength cast iron; <i>b</i> – gray cast iron	146
4.15	Influence of pressure P_1 and the degree of metal overheating on porosity P in castings made of: <i>a</i> – stainless (X18H10) steel; <i>b</i> – carbon steel	147
4.16	Influence of pressure P_1 and the degree of metal overheating θ_1 on the porosity of: <i>a</i> – high-strength cast iron; <i>b</i> – gray cast iron	147
4.17	Influence of pressure P_1 and the degree of metal overheating θ_1 on the linear shrinkage of: <i>a</i> – carbon (Steel 45L) steel; <i>b</i> – alloy (X18H10) steel	148
4.18	Influence of pressure P_1 and the degree of metal overheating θ_1 on the linear shrinkage of: <i>a</i> – gray cast iron; <i>b</i> – high-strength cast iron	149

4.19	Carbon steel cooling curves depending on the amount of added pressure ($R_1 = 15$ mm)	150
4.20	Solidification kinetics of a cast iron casting ($R_1 = 15$ mm) during gravity casting and lost foam casting	150
4.21	Technological scheme of obtaining LAM castings using external pressure: <i>a</i> – mold installation on the movable traverse; <i>b</i> – heating of the mold; <i>c</i> – pouring of the matrix alloy (MCA into the receiving bowl); <i>d</i> – transfer of the bowl from the MA to the pouring position; <i>e</i> – setting of the mold to the pouring position; <i>f</i> – filling of the form and LAM solidification under pressure; <i>g</i> – cooling the mold and removing the bowl	152

INTRODUCTION

The competitiveness of machine-building enterprises largely depends on the quality and operational reliability of machines manufactured at these enterprises. Such indicators are largely formed by the materials of parts and assemblies of mechanisms and machines, the vast majority of which are alloys of various systems. The synthesis of such alloys and technological solutions for their production is based on knowledge of the mechanisms of structure formation and properties during the production process.

Given the increased requirements for the operational properties of parts, researchers are faced with the need to complicate alloy systems while simultaneously determining the most effective technological processes for manufacturing alloys. Therefore, scientific applied research in this direction is relevant.

The presented collective monograph contains original solutions obtained by systematic studies of alloys of various systems for some applied applications. Among such systems, the alloys of the Al-Mg and Al-Mg-Sc systems obtained using a magnetohydrodynamic casting plant are considered, which after hot and cold rolling are not inferior to alternative alloys in terms of strength and plasticity, but have higher corrosion resistance characteristics. In terms of structural strength, the proposed alloys are superior to the known Al-Mg-Sc, Al-Mg and Al-Cu-Mg systems.

The presented results of the development of new highly efficient casting technologies for the production of cast and composite structural materials from alloyed and reinforced aluminum, iron-carbon and heat-resistant alloys can be used in the manufacture of blades of gas turbine engines (GTE) with a regular directional casting structure.

The determined regularities of the formation of the structure, phase composition and tribological properties of heat-resistant chrome-nickel alloys "Nikorin" can be used to develop such technological solutions that will ensure an increase in the complex of tribological properties and heat resistance of chrome-nickel alloys for modern engineering.

The studied effect of alloying a heat-resistant nickel-based alloy with tantalum and rhenium can be used for the development of technological measures that will improve the operational characteristics of parts. In particular, among such measures, the influence of technological factors and excess pressure on liquid metal can be controlled, which allows, during its crystallization, to increase the mechanical strength and reduce the porosity of cast iron and steel castings by 15–30 %, compared to gravity casting according to gasification patterns.

All these issues are given in the presented monograph, and the developments proposed in it have both theoretical and practical value.

CHAPTER 1

CHAPTER 1

CAST AND DEFORMATION STRENGTHENED ALLOYS
OF THE Al-Mg-Sc SYSTEMABSTRACT

The effect of reducing the magnesium content and doping with scandium, zirconium, manganese, chromium, and rare-earth metals on the structure, phase composition, strength, plasticity, and crack resistance, as well as the potential and corrosion current of alloys of the Al-Mg and Al-Mg-Sc systems obtained using magnetohydrodynamic foundry was investigated. Installation a positive effect of reducing the magnesium content, replacing manganese with chromium, and alloying with lanthanum in alloys of the Al-Mg-Sc system in the cast state and after deformation processing (extrusion, pressing, and rolling) was established. It is shown that due to dispersion strengthening by secondary intermetallics of chromium and lanthanum, this alloy in the cast state after homogenization is superior in strength to the well-known alloys of grades 1570 and 1545. After hot and cold rolling, it is not inferior to these alloys in terms of strength and plasticity, but has higher corrosion resistance characteristics. It was found that in terms of structural strength, which is comprehensively determined by the characteristics of strength and cyclic crack resistance, such alloys are superior to the well-known Al-Mg-Sc, Al-Mg and Al-Cu-Mg systems. The results of modeling the stress-strain state and damage of strips of different thicknesses during hot isothermal pressing are presented. The temperature-force parameters of the process and the geometry of the pressed strip are set to obtain its minimal damage.

KEYWORDS

Aluminum alloys, Al-Mg-Sc system, alloying, chrome, REM, deformation treatment, structure, structural strength, corrosion resistance, damage.

The high characteristics of plasticity, corrosion resistance and weldability, as well as the absence of the need to perform strengthening heat treatment, determine the wide use of alloys of the Al-Mg system (AMg type) in mechanical engineering, in particular in aerospace engineering. But their disadvantage is low strength [1], which is increased by structural (shredding structural

elements) and solid-solution or intermetallic strengthening, in particular, alloying with transition metals, among which scandium is one of the most effective [2, 3]. Doping with scandium ensures the formation of a dendritic structure of castings with small crystals of solid aluminum solution in the form of cells and dispersed intermetallic inclusions. At the same time, in order to increase the corrosion resistance and weldability and manufacturability in a high-strength state, it is considered appropriate to reduce the magnesium content from 6.0...6.5 to 4.0...4.5 by wt. % [3, 4].

1.1 STRUCTURE AND MECHANICAL AND CORROSION PROPERTIES OF CAST ALLOYS OF THE Al-Mg-Sc SYSTEM

The properties of cast alloys depend significantly on the casting technology: homogenization of the melt, speed of crystallization, etc. Today, one of the progressive technologies is the technology based on the use of magnetohydrodynamic (MHD) foundry installations. Here, the simultaneously controlled thermal and force effects on the liquid metal contribute to the rapid and complete assimilation of alloying and modifying elements, the uniformity of the chemical composition and the grinding of the structure, as well as the intensification of vacuum refining [5, 6].

The structure and properties of alloys of the Al-Mg and Al-Mg-Sc systems [7] were studied, in particular the well-known AMg₆ (option No. 1) and 1570 and 1545 with different Mg contents (options No. 2, 3), as well as experimental alloys with different contents Zr, Mn and Cr (options No. 4–8 in **Table 1.1**). Samples were cut from castings obtained by MHD mixing of the melt at 700 ± 10 °C. To homogenize the structure of the casting during the decomposition of the solid solution, the alloys were crystallized in a steel mold heated to 300 °C.

◆ **Table 1.1** Chemical composition (wt. %) of the investigated alloys

Alloy No.	Mg	Mn	Sc	Zr	Cr	Fe	Si
1	6.28	0.39	–	–	–	0.12	0.18
2	5.96	0.40	0.24	0.09	–	0.28	0.16
3	4.61	0.43	0.28	0.12	–	0.31	0.17
4	4.50	–	–	0.49	–	0.23	0.17
5	4.47	–	–	0.75	–	0.14	0.16
6	4.53	0.42	–	0.25	–	0.21	0.18
7	4.70	–	–	0.30	0.43	0.10	0.09
8	4.60	–	0.26	0.13	0.47	0.14	0.10

Note: the averaged chemical composition is given; all alloys also contain ~0.03 wt. % Ti and ~0.003 wt. % Be, Al – the rest

AMg₆ alloy (option No. 1) has low strength and plasticity (**Table 1.2**), which is characteristic of this type of cast alloys, when a non-dendritic cellular matrix structure with a large grain

size (up to 100...200 μm) and a network of large (micro-sized) discharges is formed secondary phase up to 20...40 μm in size (**Fig. 1.1, a, b**). Based on the results of local chemical analysis (**Table 1.3**), it can be stated that the matrix is a solid solution of Mg, Mn, and Ti in aluminum, and the secondary phase is intermetallics such as Al_3Mg_2 , Al_6Mg_5 , $\text{Al}_6(\text{Fe, Mn})$, Mg_2Si [8].

● **Table 1.2** Mechanical characteristics of alloys

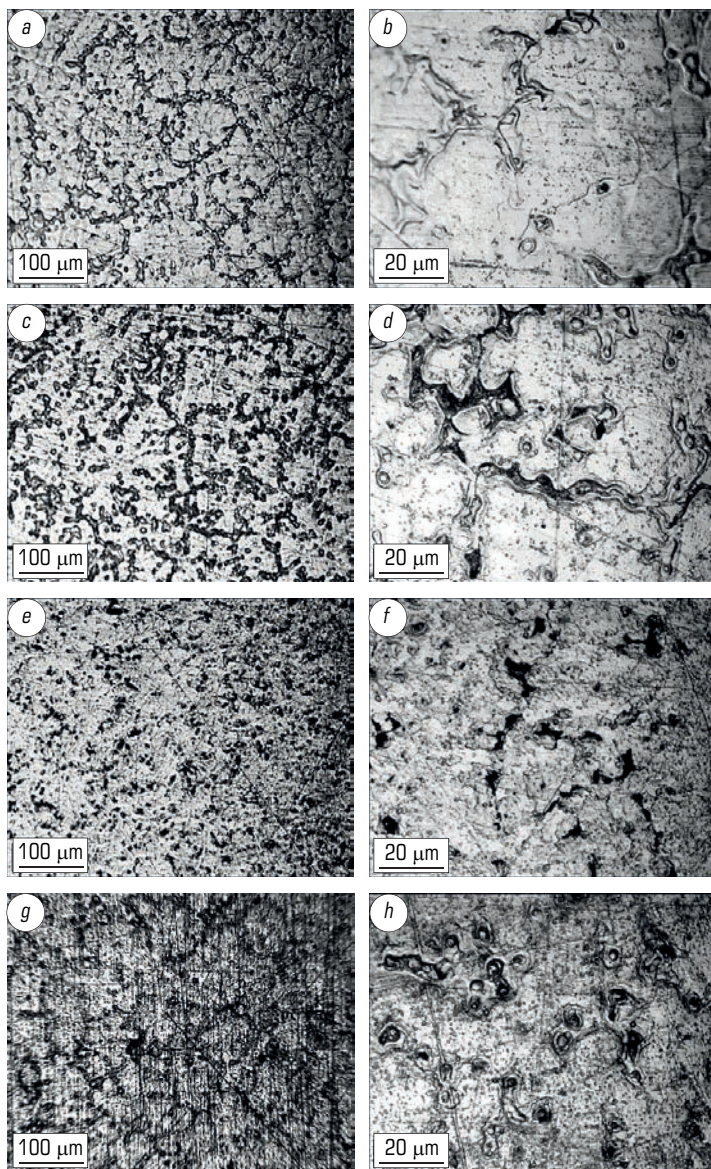
Characteristics	Alloy No.							
	1	2	3	4	5	6	7	8
$\sigma_{0.2}$, MPa	137	152	178	90	91	93	109	175
σ_B , MPa	213	234	284	214	204	205	244	280
Δ_5 , %	8	11	14	16	11	15	18	15

Note: alloy number according to **Table 1.1**; averaged test data of 3–5 samples are presented

Scandium and zirconium in alloy type 1570 (option No. 2) increase its mechanical characteristics compared to option No. 1 (**Table 1.2**) primarily due to grinding of the matrix grain (**Fig. 1.1, c** vs. **Fig. 1.1, a**). The morphology of large intermetallics did not change significantly (**Fig. 1.1, d** vs. **Fig. 1.1, b**). At the same time, as evidenced by the data in the **Table 1.3**, a dispersed (nano-sized) Al_3Sc strengthening phase is formed in the matrix [2, 3], but zirconium (together with scandium) is contained only in large intermetallics. A high iron content was recorded here (**Table 1.3**). Obviously, in addition to $\text{Al}_6(\text{Fe, Mn})$ -type precipitates, Al_3Fe -type intermetallics are formed [8]. Iron-based intermetallics negatively affect the properties of Al-Mg-Sc alloys [8, 9], so it is suggested to limit the content of iron and silicon in them: $[\text{Fe} + \text{Si}] \leq 0.12$ wt. %.

An unexpected result was obtained by studying an alloy of type 1545 with a reduced magnesium content (option No. 3 in **Table 1.1**). It is known that the strength of alloys of the Al-Mg system increases with increasing magnesium content. Option No. 3 shows the opposite trend (**Table 1.2**), when with a decrease in magnesium content from 5.96 to 4.61 wt. %, but with a slightly higher content of scandium and zirconium (**Table 1.1**), the strength and plasticity of the alloy increased significantly. There was a transformation of the morphology of the structure of large discharges of the secondary phase (**Fig. 1.1, e, f** vs. **Fig. 1.1, c, d**), in particular, their size decreased and their distribution became more uniform. However, the nature of the matrix changed the most (**Table 1.3**): zirconium appeared here, which indicates the formation of a dispersed $\text{Al}_3(\text{Sc}_{1-x}\text{Zr}_x)$ phase at an optimal ratio of $\text{Sc}/\text{Zr} \approx 2/1$. This phase determines the grinding of the grain, provides a more homogeneous non-dendritic structure and strengthening of the alloy, which, in our opinion, is also facilitated by the used MHD technology.

Increasing the amount of zirconium (0.25...0.75 wt. %) in alloys with a reduced magnesium content without and with manganese (options No. 4–6 in **Table 1.1**) did not have a positive effect on improving their mechanical characteristics compared to option No. 1 (**Table 1.2**).



○ Fig. 1.1 Microstructure of alloys: *a, b* – No. 1; *c, d* – 2; *e, f* – 3; *g, h* – 8

● **Table 1.3** Local content (wt. %) of chemical elements in the investigated alloys

Structural component	Chemical element	Alloy No.				
		1	2	3	8	
Matrix	Al	94.34	95.31	96.26	96.20	
	Mg	5.23	4.25	3.02	2.76	
	Mn	0.36	0.22	0.28	–	
	Sc	–	0.22	0.24	0.22	
	Zr	–	–	0.11	0.12	
	Cr	–	–	–	0.64	
	Ti	0.04	0.05	0.05	0.04	
	Fe	–	–	–	–	
	Si	–	–	–	–	
Micro-sized intermetallics	Zone A	Al	83.17	86.02	88.06	88.02
		Mg	15.85	13.12	10.22	10.60
		Mn	0.48	0.10	0.48	–
		Sc	–	0.13	0.32	0.38
		Zr	–	0.16	0.05	0.07
		Cr	–	–	–	0.16
		Ti	–	–	–	–
		Fe	0.32	0.45	0.63	0.36
		Si	0.16	–	0.22	0.40
	Zone B	Al	76.18	67.09	68.69	73.50
		Mg	23.44	8.60	10.12	11.40
		Mn	0.12	1.40	2.87	–
		Sc	–	0.39	0.47	0.60
		Zr	–	0.21	0.28	0.35
		Cr	–	–	–	13.72
		Ti	0.05	–	–	–
		Fe	–	22.06	17.27	0.41
		Si	0.18	0.23	0.26	–

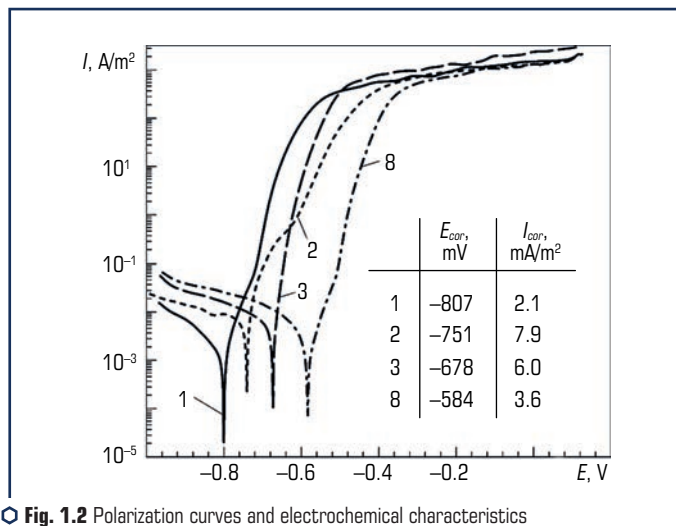
Note: alloy number according to table 1; averaged data of 3–5 measurements are provided; zone A is dark, and zone B is the light part of intermetallics (Fig. 1, b, d, f, h)

In alloys of the Al-Mg-Sc-Zr system, manganese content is 0.2...0.6 wt. % increases their strength and corrosion resistance [2, 4]. There are also known attempts to alloy such alloys with manganese (~0.5 wt. %) and chromium (~0.5 wt. %) in order to additionally form a strengthening phase of the Al₇Cr type [10]. The influence of chromium on the properties of alloys of the Al-Mg and Al-Mg-Sc system has been little studied. Although, to improve the properties of the weld metal

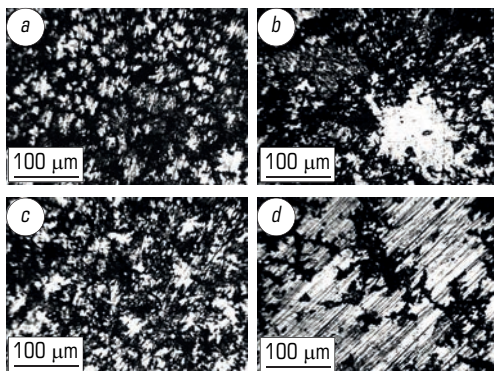
of welded joints of these alloys, welding wires with the addition of chromium were used [2]. However, the properties of such alloys after replacing manganese with chromium were not investigated.

In alloys of the Al-Mg-Zr system, such a replacement (options No. 6, 7 in **Table 1.1**) led to a noticeable increase in the strength and plasticity of alloy No. 7 compared to option No. 6 (**Table 1.2**). Therefore, they studied alloy type 1545 (option No. 3), which contained 0.47 wt. % Cr instead of 0.43 wt. % Mn (option No. 8). For this alloy, a matrix structure with a grain size of 50...100 μm was recorded (**Fig. 1.1, g**) with a uniform distribution of globular particles of the intermetallic phase with an average size of $\sim 10 \mu\text{m}$ (**Fig. 1.1, h**). Scandium, zirconium and chromium were found in the matrix (**Table 1.3**), which may indicate the formation of dispersed strengthening phases of the type $\text{Al}_3(\text{Sc}_{1-x}\text{Zr}_x)$ and Al_7Cr . These elements in large quantities (especially chromium) are present in large intermetallics, where the iron content is quite low compared to option No. 3. As a result, alloying with chromium instead of manganese ensured the strength and plasticity of alloy No. 8 at the level of alloy No. 3 (**Table 1.2**), but had a significant positive effect on its corrosion resistance.

Electrochemical studies revealed (**Fig. 1.2**) that with an increased magnesium content (6.0...6.3 wt. %) the alloy type 1570 (option No. 2) compared to the alloy type AMg₆ (option No. 1) has a slightly better corrosion potential E_{cor} , but the corrosion current I_{cor} is almost 4 times higher (**Fig. 1.2**), which causes a greater intensity of corrosion of the surface of the samples in a 3 % NaCl solution (**Fig. 1.3, b** vs. **Fig. 1.3, a**). Such an increase in I_{cor} values can be associated with an increase in the heterogeneity of the structure of alloy No. 2, in particular, with the formation of large intermetallics with a high iron content (**Table 1.3**).



○ **Fig. 1.2** Polarization curves and electrochemical characteristics of alloys according to their number in the **Table 1.1**



○ **Fig. 1.3** Corroded surface of alloy samples No. 1 (a); No. 2 (b); No. 3 (c) and No. 8 (d). Alloy number according to the **Table 1.1**

With a decrease in the magnesium content, which is among the first (standard electrode potential $z^{\circ} = -2.363$ V) in the range of activity of metals [11], the polarization curve of alloy No. 3 shifts to the right and down, i.e., the values of E_{cor} and I_{cor} improve (**Fig. 1.2**), which is manifested in a decrease in the intensity of corrosion of the sample surface (**Fig. 1.3, c** vs. **Fig. 1.3, b**). However, the optimal situation was observed for alloy No. 8: here the best combination of E_{cor} and I_{cor} characteristics was recorded (**Fig. 1.2**), and the traces of corrosion on the surface of the sample are the smallest (**Fig. 1.3, d**), which is a consequence of the positive effect of chromium, for which $z^{\circ} = -0.744 \dots 0.913$ V versus -1.180 V for manganese [11].

Thus, in contrast to the known literature data, an increase in the strength limit was recorded due to a decrease in the magnesium content in alloys of the Al-Mg-Sc system, obtained using the technology of magnetohydrodynamic mixing of the melt at 700 °C and its crystallization in a steel mold heated to 300 °C. It was established that chromium effectively replaces manganese in these alloys, ensuring their strengthening and a significant increase in corrosion resistance in a 3 % NaCl solution.

1.2 STRENGTH AND CYCLIC CRACK RESISTANCE OF HEAT-DEFORMED ALLOYS OF THE Al-Mg-Sc SYSTEM

Optimum characteristics of strength and plasticity are achieved after thermo-deformation processing of cast blanks: extrusion, pressing, rolling, etc. The chemical composition and structural phase state can have different effects on the strength and crack resistance of deformed alloys of the Al-Mg-Sc system under cyclic loading, in particular on the fatigue threshold [12]. Therefore, the structural strength of materials, especially for aerospace purposes, when the principle

of safe damage is applied during their operation, depends on the optimal combination of strength and crack resistance characteristics. It can be effectively estimated [13] by the complex parameter $P = [\sigma_B \cdot \Delta K_{th} \cdot \Delta K_{fc}]$, where σ_B – the limit of strength; ΔK_{th} – the fatigue threshold and ΔK_{fc} – the cyclic fracture toughness, which are characteristics of the cyclic crack resistance (CCR) of the material [14].

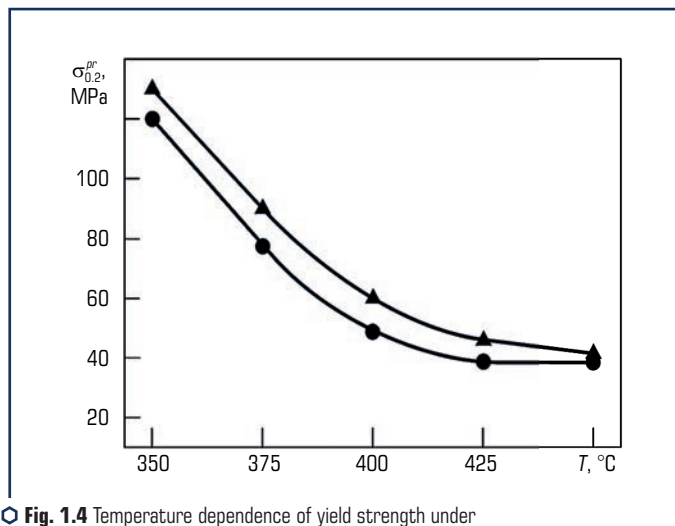
Alloys 1570 and 1545 with different magnesium content were studied (Table 1.4). Castings were obtained by MHD mixing of the melt at 700 ± 10 °C and crystallization in a steel mold heated to 300 °C to homogenize the structure of the casting.

The resistance to plastic deformation of the metal was evaluated based on the temperature dependence of the yield strength under compression (Fig. 1.4), determined on standard samples cut from castings. On this basis, thermal deformation treatment was carried out in different ways: by extrusion of castings $\varnothing 30$ mm to $\varnothing 20$ mm at 390 ± 10 °C (alloy No. 1) and 420 ± 10 °C (alloy No. 2); pressing castings $\varnothing 30$ mm into a strip 6 mm thick at 420 ± 10 °C; by rolling pressed blanks 20 mm thick onto a plate 4.5 mm thick at 420 ± 10 °C (alloy No. 1) and 460 ± 10 °C (alloy No. 2) [15].

● Table 1.4 Chemical composition (wt. %) of alloys

Alloy No.	Mg	Mn	Sc	Zr	Ti	Be	Fe	Si	Al
1	6.12	0.37	0.26	0.09	<0.03	<0.003	0.09	0.05	Rest
2	4.85	0.32	0.24	0.12	<0.03	<0.003	0.08	0.04	

Note: the averaged chemical composition is given



○ Fig. 1.4 Temperature dependence of yield strength under compression for alloys No. 1 (●) and No. 2 (▲)

As during the test at room temperature [7], at ≤ 400 °C, a slightly higher resistance to plastic deformation of alloy No. 2 was recorded compared to alloy No. 1, and in the range of 400...450 °C for both alloys it changed slightly (**Fig. 1.4**). Some shift of this dependence for cast alloy No. 2 towards higher temperatures compared to alloy No. 1 can be attributed to the difference in the secondary phase that strengthens the matrix: in alloy No. 2 it is an intermetallic $Al_3(Sc_{1-x}Zr_x)$, and in alloy No. 1 is Al_3Sc [7]. According to literature data, alloys of the Al-Mg-Sc system are processed by thermal deformation in the range of 300...480 °C, although it is recommended to process them at ≤ 420 °C. Therefore, in order to obtain a wider database, alloys No. 1, 2 were studied after extrusion, pressing and rolling in the range of 390...460 °C (**Table 1.5**).

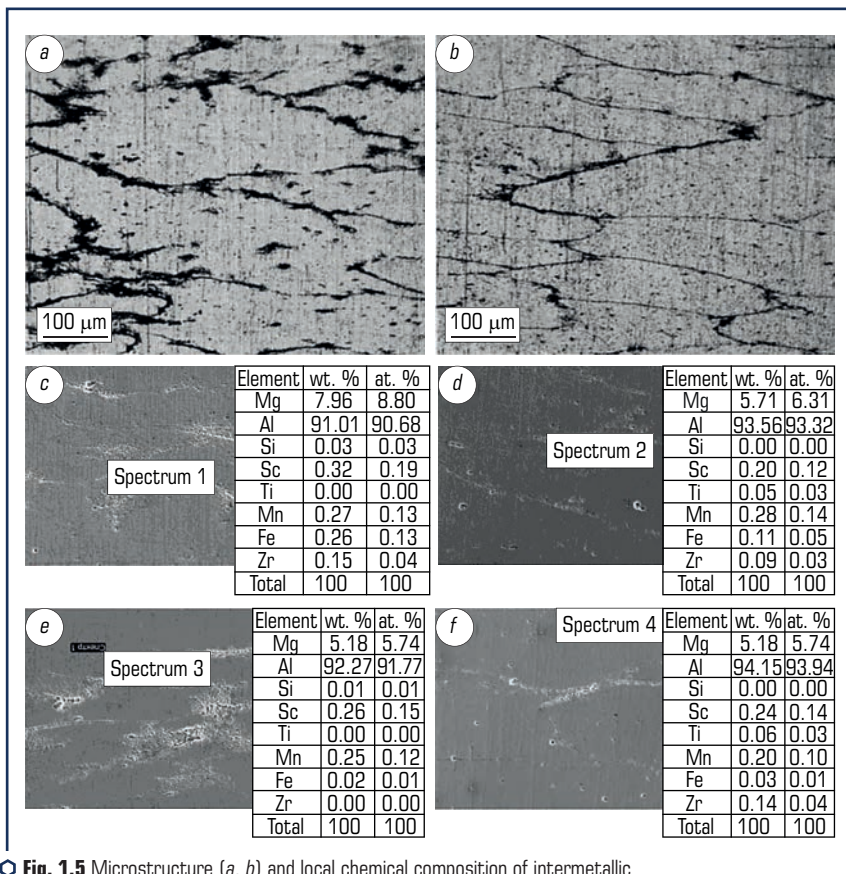
In the cast state, alloy No. 2 is superior to alloy No. 1 in terms of mechanical characteristics (**Table 1.5**), which significantly increase after deformation treatment: $\sigma_{0.2}$ – from 153...162 to 305...374 MPa; σ_B – from 236...270 to 396...452 MPa; Δ_5 – from 11...15 to 12...17 % depending on its method. The highest strength of alloy No. 1 was obtained after multiple (8 passes) rolling, and for alloy No. 2 – after extrusion. The lower value of σ_B for this alloy after rolling (**Table 1.5**) is probably caused by too high a processing temperature, i.e. the recommendation of an optimal temperature of ≤ 420 °C for alloys of the Al-Mg-Sc system is confirmed. The obtained results agree with the literature results for similar alloys (**Table 1.5**). It should be noted here that heat-deformed alloys No. 1, 2 show, as a rule, higher values of the yield strength $\sigma_{0.2}$ compared to those known in the literature (**Table 1.5**), which may be a consequence of the use of MHD technology.

◆ **Table 1.5** Mechanical characteristics of the studied alloys in the cast and thermo-deformed states and their comparison with those known in the literature

Alloy	Processing	$\sigma_{0.2}$, MPa	σ_B , MPa	Δ_5 , %
No. 1	Casting	153	236	11
	Extrusion (390 °C)	310	397	12
	Pressing (420 °C)	326	413	13
	Rolling (420 °C)	374	450	12
No. 2	Casting	162	270	15
	Extrusion (420 °C)	350	452	16
	Pressing (420 °C)	309	405	16
	Rolling (460 °C)	305	396	17
01570 [2] (5.8 % Mg)	Extrusion	305...345	430...445	15...18
	Hot rolling	270...300	390...420	15...20
1570 C [2] (5.0...5.6 % Mg)	Pressing and hot rolling	245...300	375...400	15...20
1575 C [16] (6 % Mg)	Rolling (300 °C, $\epsilon=70$ %)	295	450	20
1545 [16] (4.57 % Mg)	Rolling (360 °C, $\epsilon=70$ %)	280	385	20
1545 [17] (4.57 % Mg)	Rolling (320...360 °C)	260	395	17
	Cold rolling ($\epsilon=20...70$ %)	375...450	440...490	8...10

Note: averaged test results of at least three samples are provided for alloys No. 1, 2

The microstructure of alloys after rolling is noticeably different. The grain size transverse to the direction of rolling in alloy No. 1 is 50...150 μm (**Fig. 1.5, a**), and in alloy No. 2 it is 50...100 μm (**Fig. 1.5, b**). In alloy No. 1, significant separation of intermetallics along the grain boundaries was recorded, while in alloy No. 2 with a reduced magnesium content, they are much less. Local chemical analysis revealed (**Fig. 1.5, c, d**) that in both alloys, these are primary allocations of intermetallics: aluminum and magnesium; aluminum, manganese and iron; aluminum, scandium and zirconium (such as Al_3Mg_2 , $\text{Al}_6(\text{Fe, Mn})$, $\text{Al}_3(\text{Sc, Zr})$) [8].



○ **Fig. 1.5** Microstructure (*a, b*) and local chemical composition of intermetallic compounds (*c, d*) and matrix (*e, f*) of alloys No. 1 (*a, c, e*) and No. 2 (*b, d, f*) after rolling

The difference was found by analyzing their matrix: zirconium is absent in alloy No. 1 (**Fig. 1.5, e**), while it is present in alloy No. 2 (**Fig. 1.5, f**). This shows that in the first case, the Al_3Sc secondary

phase is released in the matrix, and in the second case, $Al_3(Sc_{1-x}Zr_x)$, which is more dispersed, therefore strengthens the alloy more effectively. A similar result was previously obtained for an alloy with a reduced magnesium content in the cast state [7], as well as other researchers for a heat-deformed alloy [16].

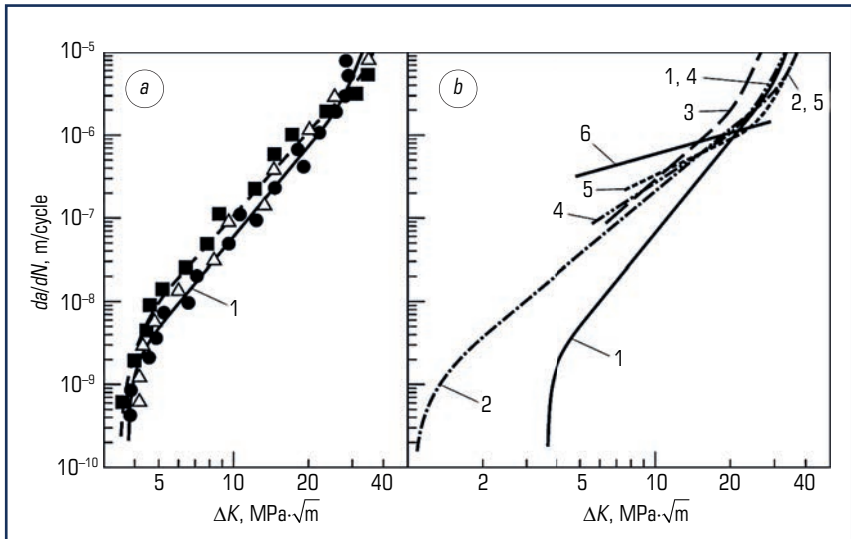
Increased strength of alloys of the Al-Mg-Sc system is achieved, first of all, by alloying with scandium, which structurally strengthens the alloy by grinding the grain, which predicts the Hall-Petch equation. However, it is known that the size of the grain affects the characteristics of strength and CCR ambiguously. In particular, for steels, this dependence for strength and fatigue threshold ΔK_{th} is opposite [18]:

$$\sigma_{0.2} = \sigma_i + k_y D_g^{-0.5}, \quad (1.1)$$

$$\Delta K_{th} = A + B D_g^{0.5}, \quad (1.2)$$

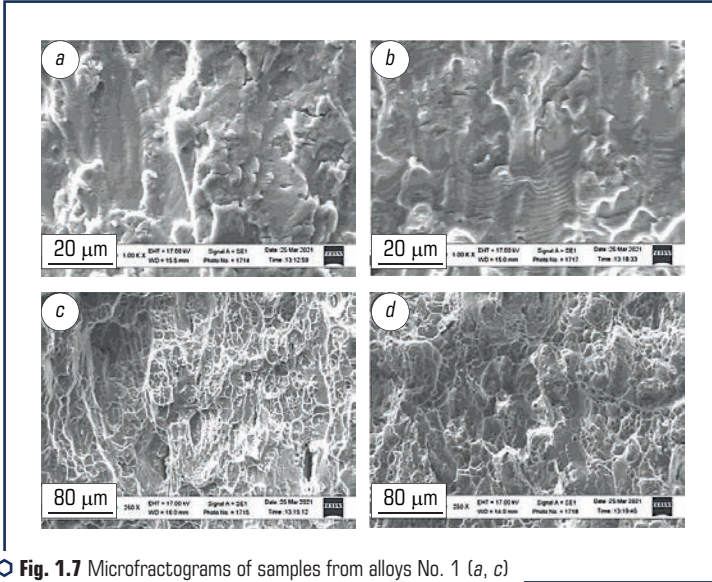
where D_g – the grain size; σ_i , k_y , A , B – material constants. The ΔK_{th} characteristic is important for assessing the durability of structural elements, as it is directly correlated with the resistance to fatigue macrocrack initiation and the fatigue limit of materials [14].

Diagrams of fatigue macrocrack growth rates show (Fig. 1.6, a) that alloy No. 1 after rolling has a somewhat larger CCR in the medium-amplitude part of the diagram and a lower one in the high-amplitude part of the diagram compared to alloy No. 2.



○ Fig. 1.6 Diagrams of fatigue macrocrack growth rates: a – for rolled alloys No. 1 (●, △) and No. 2 (■) under tensile (●, △) and bending (△, ■) loads; b – comparison with literature data for heat-deformed alloys of type 1570: 1 – alloy No. 1, $D_g=50\text{...}150 \mu\text{m}$; 2 – $60\text{...}100 \mu\text{m}$ [12]; 3 – $70\text{...}170 \mu\text{m}$ [9]; 4 – $\sim 1 \mu\text{m}$ [9]; 5 – [3]; 6 – [2]

Note that the diagram for alloy No. 1 (similar to the known results [19]) is invariant with respect to the geometry and method of sample loading, that is, it is a characteristic of the material. Both alloys have a high resistance to fatigue macrocrack growth, which is caused by high-energy micro-mechanisms of destruction: at $\Delta K \approx 15 \text{ MPa} \cdot \sqrt{\text{m}}$, this is a fatigue groove (**Fig. 1.7, a, b**); at $\Delta K \approx 25 \text{ MPa} \cdot \sqrt{\text{m}}$ – it is mainly pitted (**Fig. 1.7, c, d**).



○ **Fig. 1.7** Microfractograms of samples from alloys No. 1 (*a, c*) and No. 2 (*b, d*) at $\Delta K = 15$ (*a, b*) and $25 \text{ MPa} \cdot \sqrt{\text{m}}$ (*c, d*)

Both alloys with a relatively large grain size ($D_g = 50 \dots 150 \mu\text{m}$) show a relatively high fatigue threshold $\Delta K_{th} = 3.3 \dots 3.8 \text{ MPa} \cdot \sqrt{\text{m}}$, which distinguishes them from the known ones (**Fig. 1.6, b**, line 1 vs. 2): for alloy 1570 with a small grain size ($D_g = 6 \dots 10 \mu\text{m}$) $\Delta K_{th} = 1.1 \text{ MPa} \cdot \sqrt{\text{m}}$ [12], which confirms the above considerations. In the high-amplitude region ($\Delta K = 15 \dots 30 \text{ MPa} \cdot \sqrt{\text{m}}$), these diagrams agree well with the results of other authors (**Fig. 1.6, b**). They also show (lines 4 and 6) that alloys with fine grain ($D_g \sim 1 \mu\text{m}$) show low CCR in the low-amplitude region of the diagram ($\Delta K < 5 \text{ MPa} \cdot \sqrt{\text{m}}$). Therefore, taking into account the ambiguous influence of the structure on the strength and CCR of alloys of the Al-Mg-Sc system, their mechanical behavior under operating conditions should be evaluated according to the above structural strength parameter P (**Table 1.6**).

Among the aluminum alloys of different alloying systems, alloy No. 1 has the highest value of the P parameter, and alloy No. 2 has the lowest value, although it is practically equal to the high-strength D16T alloy, but it is higher compared to the medium-strength AMg5M alloy,

which is widely used in aerospace engineering. Note that the fine-grained structure of the alloy, causing a very low fatigue threshold ΔK_{th} , determines the lowest value of the P parameter, despite the relatively high strength of this alloy (item 3 in **Table 1.6**).

● **Table 1.6** Mechanical characteristics and parameter of structural strength of aluminum alloys

No.	Alloy (alloying system)	Alloy condition	σ_B , MPa	ΔK_{th} , MPa $\cdot\sqrt{m}$	ΔK_{IC} , MPa $\cdot\sqrt{m}$	P , MPa $^3\cdot m$
1	No. 1 (Al-Mg-Sc)	Hot rolling	450	3.8	33	56430
2	No. 2 (Al-Mg-Sc)	– –	396	3.4	35	47124
3	O1570 [12] (Al-Mg-Sc)	Hot rolling, annealing	410	1.1	35	15785
4	AMg5M [20] (Al-Mg)	– –	315	3.2	33	33264
5	D16M [20] (Al-Cu-Mg)	– –	235	3.5	32	26320
6	D16T [20] (Al-Cu-Mg)	Hot rolling, hardening, natural age hardening	415	3.2	34	45152

Thus, in order to achieve increased structural strength, alloys of the Al-Mg-Sc system should have an average grain size, obviously several tens of micrometers.

1.3 THE INFLUENCE OF RARE-EARTH METALS ON THE STRUCTURE AND PROPERTIES OF CAST AND DEFORMED ALLOYS OF THE Al-Mg-Cr-Sc-Zr SYSTEM

It was revealed that the Al-Mg-Sc system alloy, which has a reduced magnesium content (4.55...4.65 wt. %) and instead of manganese contains 0.4...0.5 wt. % chromium, in terms of corrosion and mechanical characteristics, the well-known alloy 1545 prevails, but it also needs to increase the strength in the cast state.

Considering the high cost of scandium, an effective means of influencing the structure and physical and mechanical properties of alloys of the Al-Mg-Sc system is microalloying with rare-earth metals (REM). Having a specific electronic structure of the d-shell and the size of the atom, they are able to form complex alloyed solid solutions and intermetallics in these alloys, which contributes to grain grinding, increasing the purity of grain boundaries, increasing microhardness, and improving their mechanical and corrosion properties. First of all, this applies to erbium and lanthanum [21–26]. It was established that lanthanum is most similar to scandium in its effect [26], and the effectiveness of erbium is low at reduced scandium content [25]. It is believed that ~0.10 wt. % is the optimal content of erbium or lanthanum in the alloys of this system [21, 26].

The effect of erbium and lanthanum on the structure, phase composition, and mechanical and corrosion properties of an alloy of the Al-Mg-Sc system, in which the magnesium content is reduced and manganese is replaced by chromium, was studied after plastic deformation of castings

obtained by MHD technology [27]. The well-known alloy 1545 with a reduced magnesium content (No. 1 in **Table 1.7**) was chosen as the base. In alloys No. 2, 4–7, manganese is replaced by chromium to increase corrosion resistance [7]. The effect of erbium was studied on alloys No. 3, 4, and lanthanum on alloys No. 5–7.

● **Table 1.7** Chemical composition (wt. %) of the investigated alloys

Alloy No.	Mg	Mn	Cr	Sc	Zr	Er	La	Fe	Si
1	4.64	0.43	–	0.28	0.09	–	–	0.21	0.16
2	4.70	–	0.45	0.26	0.13	–	–	0.14	0.10
3	4.62	0.36	–	0.28	0.12	0.06	–	0.11	0.14
4	4.72	–	0.49	–	0.35	0.15	–	0.22	0.12
5	4.67	–	0.45	0.25	0.12	–	0.08	0.10	0.07
6	4.65	–	0.40	0.15	0.10	–	0.11	0.11	0.09
7	4.63	–	0.42	0.10	0.1	–	0.25	0.10	0.10

Note: the averaged chemical composition is given; all alloys also contain ~0.03 wt. % Ti and ~0.003 wt. % Be, the rest – Al

Castings were obtained by MHD mixing of the melt at 700 ± 10 °C and crystallization in a steel mold at 20 °C and heated to 300 °C for the initial homogenization of the casting structure. Castings were homogenized at 360 °C for 5 hours with cooling in water or in air at 20 °C.

Considering that the temperature of 360 °C is optimal for thermo-deformation processing of alloys of the Al-Mg-Sc system [25, 28, 29], the homogenized castings were pressed at this temperature into strips 12 mm thick and then rolled into plates 6 mm thick. After annealing at 360 °C for 1 hour they were thinned by cold rolling first to a thickness of 4 mm and annealed at 200 °C for 1 hour, and then to a thickness of 2 mm and also annealed at 200 °C for 1 hour.

Cast alloys. An increase in the mechanical characteristics $\sigma_{0.2}$ and σ_B was recorded after replacing manganese with chromium in alloys with a reduced (4.64...4.70 wt. %) magnesium content (No. 1, 2 in **Table 1.8**), which was associated with the intensification of the release of intermetallics $Al_3(Sc_{1-x}Zr_x)$. Doping with erbium (0.06 and 0.15 wt. %) of alloys with manganese or chromium led to a decrease in strength characteristics, which increases with an increase in the content of erbium (up to 0.15 wt. %) and zirconium (up to 0.35 wt. %) in the absence of scandium (No. 3, 4 vs. No. 1, 2). In the paper [25], they also did not find a positive effect of erbium on the mechanical properties of the thermoformed alloy of the Al-Mg-Mn-Sc-Zr system when it was reduced from 0.25 to 0.12 wt. % of scandium content.

Doping with lanthanum (0.08 wt. %), on the contrary, leads to an increase in strength characteristics with a slight decrease in plasticity (No. 5 vs. No. 2). At the same time, as with erbium doping, increasing the lanthanum content (up to 0.11...0.25 wt. %) with a reduced (from 0.25 to 0.10...0.15 wt. %) scandium content does not have a positive effect: strength decreases

significantly with increasing plasticity (No. 6, 7 vs. No. 5). However, it should be noted here that with a 2.5-fold reduction in the content of precious scandium after alloying with lanthanum, a highly plastic and sufficiently strong alloy was obtained in the cast state (No. 7 vs. No. 5).

● **Table 1.8** Mechanical characteristics of the studied alloys in the cast state

Characteristics	Alloy No.						
	1	2	3	4	5	6	7
$\sigma_{0.2}$, MPa	162	175	152	132	204	152	132
σ_B , MPa	270	280	260	248	292	255	250
Δ_5 , %	16	15	17	18	12	21	22

Note: alloy number according to **Table 1.7**; averaged test results of 3–5 samples are given

Next, alloy No. 5 was studied. The structure and properties of the cast metal depend on the cooling rate during crystallization and after homogenization of the casting. It was established (**Table 1.9**) that during its growth during the crystallization of the casting (mold at a temperature of 20 °C versus heated to 300 °C), the microhardness of the grain body and the strength characteristics of alloy No. 5 decrease somewhat. The mechanical properties of the casting obtained in a mold heated to 300 °C improve after homogenization at 360 °C. At the same time, they also depend on the speed of cooling after homogenization: they increase more significantly when it is lower, that is, during cooling in air. As the homogenization temperature increases to 420 °C, the microhardness and strength characteristics decrease (**Table 1.9**).

● **Table 1.9** Influence of the cooling rate and homogenization of castings on the mechanical characteristics of alloy No. 5

Alloy condition	$HV_{0.1}$, GPa	$\sigma_{0.2}$, MPa	σ_B , MPa	Δ_5 , %
Cast (molded at 300 °C)	0.74	204	292	12
Cast (molded at 20 °C)	0.69	200	285	14
Homogenization (360 °C, cooled in water)	1.00	225	310	12
Homogenization (360 °C, cooled in air)	1.05	240	320	13
Homogenization (420 °C, cooled in air)	0.85	209	281	12

Note: averaged values based on the results of 3–5 measurements are given; the microhardness of the grain body was determined

The change in the mechanical characteristics of alloy No. 5 correlates with the features of its microstructure. After crystallization in a heated mold, there is a non-dendritic structure with a grain size of 50...100 μm with the release of intermetallics of the Al_3Mg_2 type [30] along the

grain boundaries (**Fig. 1.8, a**), which worsen the mechanical properties. Therefore, the decrease in the strength of the alloy after crystallization in the mold at 20 °C (**Table 1.9**) is caused by the more intense release of these intermetallics (**Fig. 1.8, b**), even with a certain decrease (to 50...70 μm) in the grain size. The growth of the $HV_{0.1}$, $\sigma_{0.2}$ and σ_B characteristics of the alloy after homogenization during cooling in water (**Table 1.9**) can be associated with the separation of the secondary phase in the body of the grain (**Fig. 1.8, c**). At the same time, as there are more discharges after homogenization with air cooling (**Fig. 1.8, d**), the mechanical characteristics of the alloy increase significantly (**Table 1.9**).

Local chemical analysis shows (**Table 1.10**) that for the highest strength characteristics of alloy No. 5 after crystallization in a mold heated to 300 °C and homogenization with cooling in air (**Table 1.10**) with an almost unchanged content of the main alloying elements (Mg, Cr, Sc, Zr, and Ti) in the matrix and intermetallics, the content of lanthanum changes noticeably: it decreases by three times in the primary intermetallics along the grain boundaries and increases by the same number of times in the matrix and secondary intermetallics in the body of the grain. Thus, microalloying with lanthanum (~0.1 wt. %) can increase the strength of the cast alloy of the Al-Mg-Cr-Sc-Zr system by dispersion strengthening with secondary intermetallics of the types Al_3La [24], $Al_3(Sc_{1-x}P3M_x)$ [31], $(Al, Cr)_3(Zr, REM)$ [32] after homogenization of the casting.

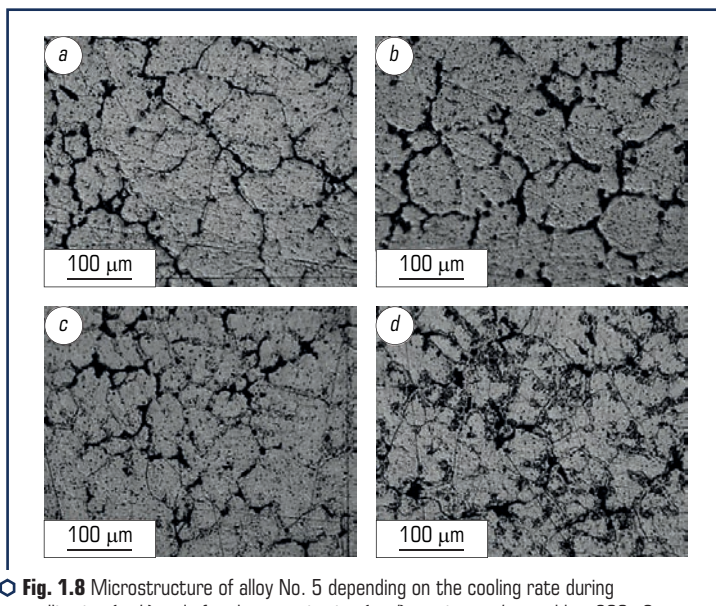


Fig. 1.8 Microstructure of alloy No. 5 depending on the cooling rate during crystallization (*a, b*) and after homogenization (*c, d*) casting: *a, b* – mold at 300 °C and 20 °C; *c, d* – cooling in water and air

● **Table 1.10** Local content of alloying elements in castings of alloy No. 5 (mold at 300 °C, homogenization at 360 °C, cooled in air)

Structural zone	Alloy condition	Elements, wt. %								
		Mg	Cr	Sc	Zr	La	Ti	Fe	Si	Al
Matrix	Cast	3.75	0.55	0.26	0.29	0.03	0.05	–	–	Rest
	After homogenization	3.62	0.54	0.23	0.26	0.11	0.08	0.03	–	– –
Intermetallics	Cast	7.55	0.29	0.31	0.11	0.15	0.02	0.28	0.10	– –
	After homogenization	6.95	0.35	0.36	0.10	0.05	0.02	0.17	0.06	– –

Note: The average content is given based on the results of 3–5 measurements

Deformed alloys. The effect of hot and cold plastic deformation was studied on castings of alloy No. 5 after crystallization in a mold heated to 300 °C and homogenization at 360 °C for 5 hours with air cooling, which demonstrated the highest mechanical properties (**Table 1.10**).

It has an anisotropic microstructure traditional for rolled materials, where the grains are elongated along the direction of rolling (**Fig. 1.9**), and their size depends on the mode of deformation processing of the samples: it is 10...30 μm for hot-rolled ones (**Fig. 1.9, a**) and 10...15 μm (**Fig. 1.9, b**) and 5...10 μm (**Fig. 1.9, c**) – for cold-rolled ones with a thickness of 4 and 2 mm, respectively. Note that after cold rolling, the primary intermetallics are crushed and their shape is mostly globular. The size of intermetallic inclusions is 1...5 μm and they are fairly evenly located in the volume of the material (**Fig. 1.9, d**).

Local chemical analysis shows that, compared to the cast state (**Table 1.10**), in the deformed alloy No. 5 (**Table 1.11**), the qualitative picture of the distribution of the main alloying elements in the matrix and intermetallics is similar. But the content of magnesium, chromium, scandium and zirconium increases in the intermetallics of the deformed alloy. At the same time, the concentration of alloying elements in the matrix, except for zirconium, is practically the same as in castings after homogenization. This also applies to lanthanum, i.e. secondary allocations of Al-Sc-Zr, Al-La or Al-Cr-Zr-La systems are preserved in the matrix of the deformed alloy [32]. In addition, chromium and titanium are found in the solid solution of the matrix. Thus, based on the results of these analyses, it can be stated that deformed alloy No. 5 should have high mechanical characteristics due to structural (grain crushing), solid-solution and dispersion strengthening.

Compared with castings after homogenization (**Table 1.9**), the strength of alloy No. 5 after hot pressing and rolling increases by 20...23 % with the same plasticity (**Table 1.12**). After cold rolling, this tendency increases significantly: compared to the cast state, the yield strength increases by 1.6–1.8 times, depending on the degree of deformation, and the strength limit by 1.3–1.5 times. Annealing after rolling slightly reduces these characteristics due to the increase in plasticity of the alloy, although they remain sufficiently high. The obtained

characteristics of deformed alloy No. 5 are at the level of the best-known results for alloys 1570 and 1545 (Table 1.12).

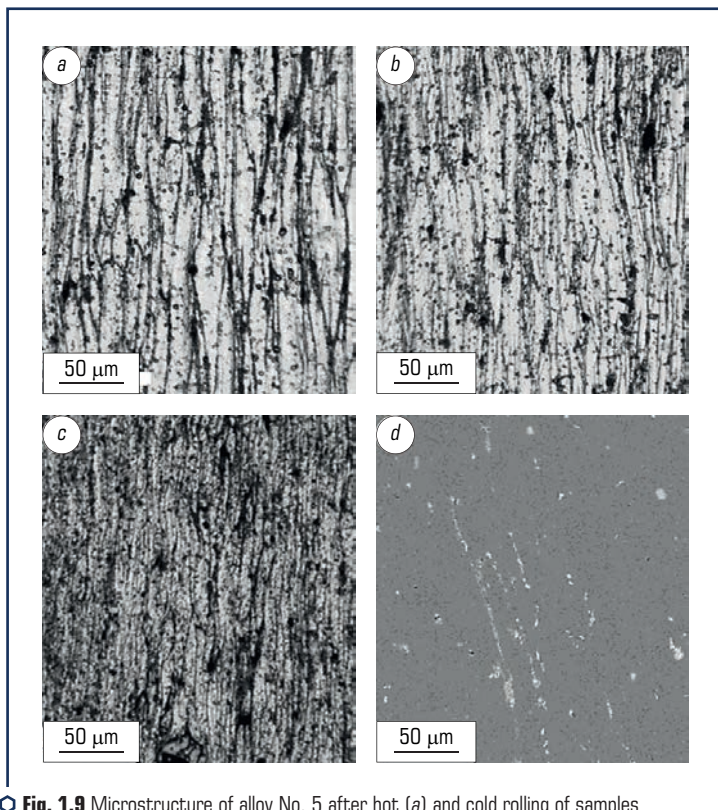


Fig. 1.9 Microstructure of alloy No. 5 after hot (a) and cold rolling of samples with a thickness of 4 mm (b, d) and 2 mm (c); d – electron microscopy

Table 1.11 Local content (wt. %)° of the main alloying elements in deformed alloy No. 5

Processing	Structural zone	Mg	Cr	Sc	Zr	Ti	La
Hot rolling	M	3.57	0.41	0.23	0.11	0.03	0.12
	I	10.14	14.51	0.80	0.46	–	0.05
Cold rolling	M	3.48	0.42	0.24	0.14	0.04	0.11
	I	10.10	14.95	0.51	0.37	0.01	0.03

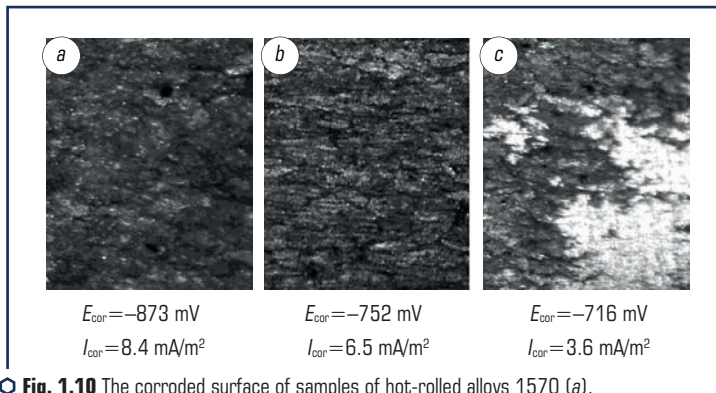
Note: ° averaged data of 3–5 measurements; M – matrix; I – intermetallics

● **Table 1.12** Mechanical characteristics of deformed alloy No. 5 and their comparison with those known in the literature

Alloy	Processing (plate thickness, mm)	$\sigma_{0.2}$, MPa	σ_B , MPa	Δ_s , %
No. 5	HR(12)	280	378	14
	HR(6)	292	395	13
	HR(6)+A ₁	283	380	16
	CR(4)	385	423	8
	CR(4)+A ₂	350	418	13
	CR(2)	430	472	7
	XB(2)+A ₂	361	422	10
01570 [33]	HR [*] (5)	297	376	7
	CR(3)	429	470	5
	CR(3)+A [*]	312	383	14
P-1580 [33]	HR [*] (5)	312	389	12
	CR(3)	409	453	5
	CR(3)+B [*]	277	390	14
1545 [17]	HR (320...360 °C)	260	395	17
	CR ($\epsilon=20...70$ %)	375...450	440...490	8...10

Note: 1 hour; HR^{*} – at 450 °C; A^{*} – at 350 °C, 3 hours; ϵ_i – the deformation value; averaged test data of 3–5 samples are presented

Deformed alloy No. 5, in which the magnesium content is reduced and manganese is replaced by chromium with additional microalloying with lanthanum, similar to the cast state, has higher corrosion resistance compared to deformed alloys 1570 and 1545 (**Fig. 1.10, c** vs. **Fig. 1.10, a, b**).

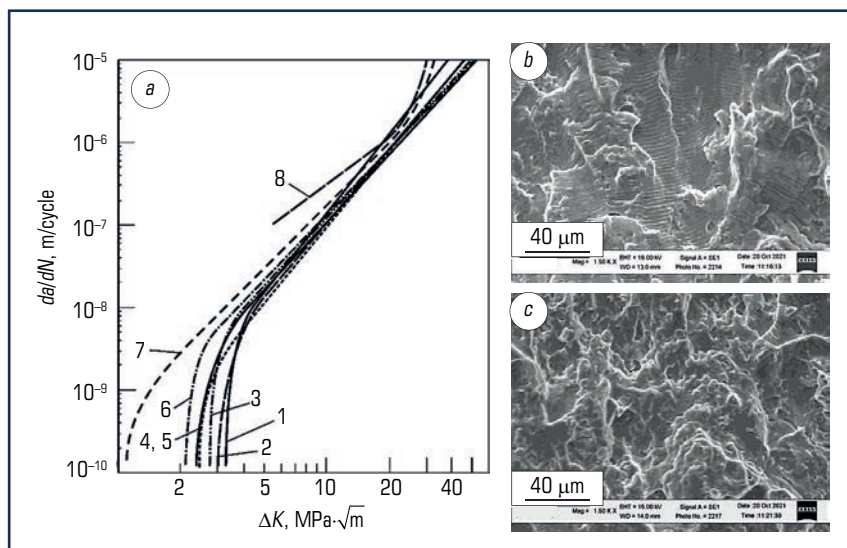


○ **Fig. 1.10** The corroded surface of samples of hot-rolled alloys 1570 (a), 1545 (b) and No. 5 (c) and their electrochemical characteristics

Its electrochemical characteristics are better: the corrosion potential E_{cor} increases, and the corrosion current I_{cor} decreases. This is due to the positive effect of lanthanum [34], in addition to chromium [7], on cleaning the grain boundaries and improving the electrochemical potential.

Structural strength of alloys. The performance of materials, when the principle of safe damage is applied during their operation, depends on the optimal combination of strength characteristics and CCR, so it can be effectively evaluated by the complex parameter of structural strength P . Increasing the strength of alloys of the Al-Mg-Sc system is achieved, first of all, by alloying with scandium, which structurally strengthens them by grinding the grain. However, its size has the opposite effect on the strength and CCR of materials: the strength increases according to the Hall-Petch equation, and the fatigue threshold ΔK_{th} decreases [15, 35].

The obtained diagrams of fatigue macrocrack growth rates show (Fig. 1.11, a) that alloy No. 5 after various treatments has high CCR characteristics, especially in the high-amplitude region, when $\Delta K_{fc} \approx 50 \text{ MPa} \cdot \sqrt{\text{m}}$.



○ **Fig. 1.11** Diagrams of fatigue macrocrack growth rates (a) in alloy No. 5: 1 – HR(6), $D_g = 10 \dots 30 \mu\text{m}$; 2 – HRV(6) + A_1 ; 3 – CR(4), $D_g = 10 \dots 15 \mu\text{m}$; 4 – CR(4) + A_2 ; 5 – CR(2), $D_g = 5 \dots 10 \mu\text{m}$; 6 – CR(2) + A_2 (designation see **Table 1.12**) and their comparison with literature results for deformed alloys of type 1570: 7 – $D_g \approx 6 \mu\text{m}$ [12]; 8 – $D_g \approx 1 \mu\text{m}$ [3], as well as microfractograms of samples of alloy No. 5 after CR (b) and CR (c) at $da/dN \approx 1.10^6 \text{ m/cycle}$

Annealing after hot and cold rolling leads to a slight decrease in the fatigue threshold ΔK_{th} and an increase in the cyclic fracture toughness ΔK_{fc} (curve 2 vs. curves 1, 4 vs. curve 3, and

curve 6 vs. curve 5). The smaller grain size of the material after cold rolling compared to hot rolling (**Fig. 1.9**) leads to a decrease in the fatigue threshold ΔK_{th} (curves 3 and 5 versus 1), i.e., here the trend is opposite to the change in strength characteristics (**Table 1.12**). This regularity is confirmed by the results for other alloys of the Al-Mg-Sc system (**Fig. 11, a**): with a grain size of 1...6 μm , they have a lower CCR, especially in the threshold area (curves 7, 8), compared to alloy No. 5 with grains 5...30 μm after various treatments (curves 1–6).

The high CCR characteristics of alloy No. 5, in particular the cyclic fracture toughness ΔK_{fc} , are due to the implementation of energy-intensive micromechanisms of viscous fracture: classic grooved after hot rolling (**Fig. 1.11, b**) and pitted with the formation of deformation ridges after cold (**Fig. 1.11, c**).

As a result, the structural strength parameter P of various modifications of alloy No. 5 is quite high (**Table 1.13**): after hot rolling and annealing, it is ~4 times greater than for the fine-grained alloy O1570, and compared to the D16T alloy widely used in aerospace engineering, it is ~1.3 times. Alloy No. 5 surpasses this alloy in terms of the P parameter also in the state after cold rolling (**Table 1.13**), when it has the highest (472 MPa) strength.

● **Table 1.13** Mechanical characteristics and parameter of structural strength of aluminum alloys

Alloy	Processing	σ_B , MPa	ΔK_{th} , MPa $\cdot\sqrt{\text{m}}$	ΔK_{fc} , MPa $\cdot\sqrt{\text{m}}$	P , MPa $^3\cdot\text{m}$
No. 5, $D_g=3...30 \mu\text{m}$	HR(6)	395	3.2	38	48030
	HR(6)+A ₁	380	3.0	52	59280
	CR(4)	423	2.7	49	55960
	CR(4)+A ₂	418	2.4	51	51160
	CR(2)	472	2.4	46	52110
	CR(2)+A ₂	422	2.1	50	44310
O1570, $D_g=6...10 \mu\text{m}$ [15]	HR+A	410	1.1	35	15790
D16T [15]	HR+hardening and age hardening	415	3.2	34	45150

Note: designation see **Table 1.12**

Therefore, the alloy of the Al-Mg-Cr-Sc-Zr-La system in the cast state has increased strength characteristics after crystallization in a mold heated to 300 °C and homogenization at 360 °C with cooling in air due to additional dispersion strengthening with lanthanum intermetallics. After hot (at 360 °C) and cold rolling, it is not inferior in terms of strength and plasticity to known alloys of the Al-Mg-Mn-Sc-Zr system (grades 1570 and 1545), but it surpasses them in terms of corrosion resistance, which is due to the positive influence of lanthanum and chromium for cleaning the grain boundaries and refining the electrochemical potential, as well as for the characteristics of cyclic crack resistance.

1.4 PRESSING OF SEMI-FINISHED PRODUCTS FROM ALLOYS OF THE Al-Mg-Sc SYSTEM IN ISOTHERMAL CONDITIONS

Aluminum alloys can be significantly strengthened by deformation processing, in particular, hot pressing, hot and cold rolling, etc. However, with the selection of suboptimal temperature and force parameters of such processing, micro- and macro-damage is formed in semi-finished products from these alloys, especially in the near-surface layers, due to which the physico-mechanical properties of the deformed metal deteriorate. Therefore, let's study how to optimize the temperature-force parameters of hot pressing in isothermal conditions of a cast cylindrical billet from alloys of the Al-Mg-Sc system in order to form strips of different thicknesses with minimal damage [36].

Let's study castings from alloys 1570 and 1545 (**Table 1.14**), which were obtained after crystallization in a steel mold preheated to 300 °C. At the same time, the melt at 700 ± 10 °C was subjected to magnetohydrodynamic stirring. Therefore, the castings were not homogenized.

● **Table 1.14** Average chemical composition of alloys

Alloy	Element content, wt. %						
	Mg	Mn	Sc	Zr	Fe	Si	Al
1570	5.96	0.40	0.24	0.09	0.28	0.16	Rest
1545	4.61	0.43	0.28	0.12	0.31	0.17	— —

The pressing temperature was chosen based on the results of standard compression tests of samples and it was found that the temperature dependences of the yield strength of alloys 1570 and 1545 are qualitatively similar (**Table 1.15**). Let's take into account, on the one hand, the temperature at which a sharp drop in the resistance to plastic deformation of the samples begins, and on the other hand, the need to reduce the processing temperature, therefore, a pressing temperature of 360 ± 5 °C was adopted for both alloys.

● **Table 1.15** Temperature change in yield strength (MPa) of alloys during compression tests

Alloy	Test temperature, °C						
	150	250	350	375	400	425	450
1570	139	130	120	75	50	40	40
1545	149	139	130	90	60	47	40

Note: average test results of 3–5 samples are given

Simulation of pressing was carried out in the DEFORM3D software complex [37] and full-scale pressing of cast blanks. The correctness of the calculations was assessed by comparing them with the experimentally determined force parameters. The cylindrical workpiece 1 (\varnothing 30 mm and

length 50 mm) cut from the casting was pressed through the matrix 2 by the punch 3 with the output of a strip 4 with a width of 30 mm and a given thickness (**Fig. 1.12, a**).

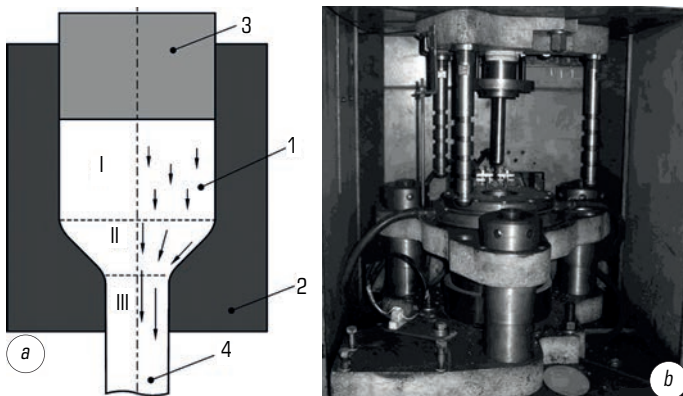


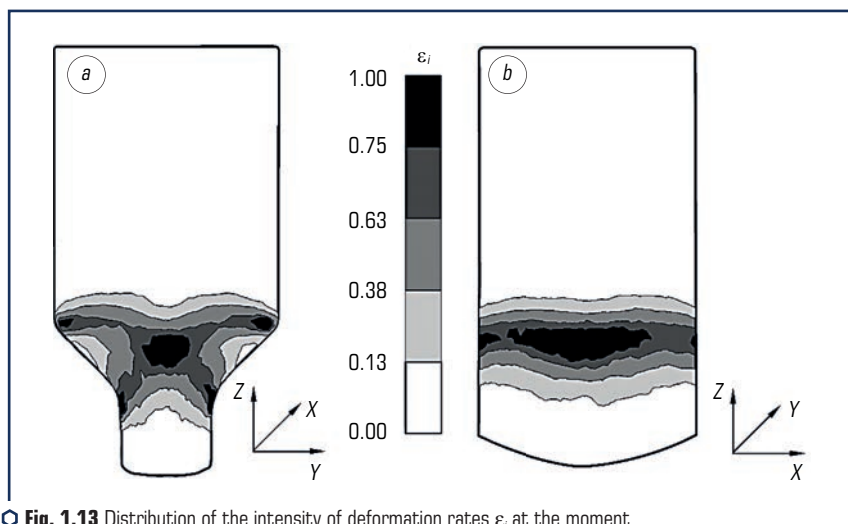
Fig. 1.12 Calculation scheme (a) and general view of the hot pressing installation (b): I, II, III – deformation zones. The arrows point to the movement speed vectors (the length of the arrow is proportional to the movement speed)

It was assumed that the matrix and punch are absolutely rigid and the Siebel law of contact friction is fulfilled, and the following initial data were also accepted: Coulomb friction coefficient $\mu=0.1\dots0.5$; temperature of the workpiece and tools $t=360\text{ }^{\circ}\text{C}$; speed of the deforming tool $V_0=5\text{ mm/s}$; the model material is aluminum alloy 5056 (similar to the investigated alloys in terms of deformation properties).

Natural isothermal hot pressing of the strip was carried out on a PD-476 hydraulic press (**Fig. 1.12, b**), the working unit of which was heated to the selected temperature. Process parameters (force, punch speed and temperature) were monitored by appropriate sensors with computer recording. The workpieces were heated to the specified temperature in an electric furnace SNOL 30/1300 with an error of $\pm 5\text{ }^{\circ}\text{C}$.

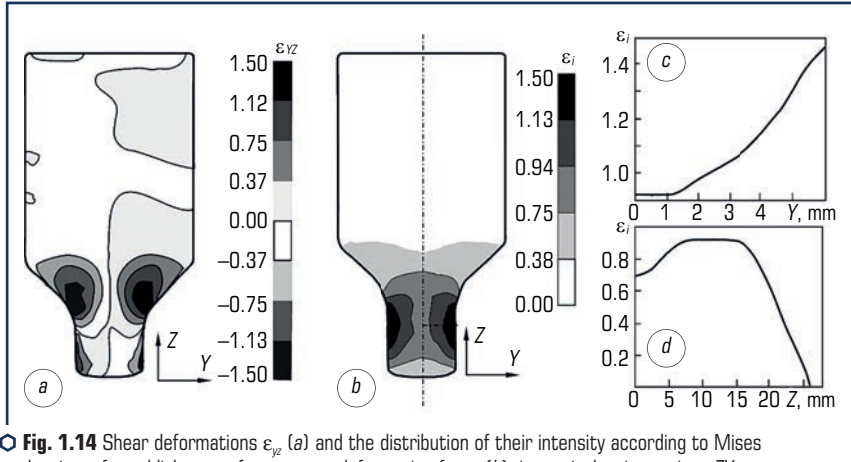
The general field of metal movement velocities at the time of establishment of a stable pressing mode can be conditionally divided into three characteristic zones (**Fig. 1.12, a**): I – here the workpiece retains its cylindricality, the speed along the Z and Y axes is uniform and equal to the punch movement speed; the size of this zone is variable and depends on the distance of the plane of the face of the punch to the point where the narrowing of the matrix channel begins; II – the zone from the beginning of the narrowing of the matrix channel to the calibration hole; here, the largest deformations occur and a structure with the corresponding properties of the strip material is formed, which is calibrated in zone III.

In the II zone, the velocity vectors change the direction of movement of the metal particles depending on the profile of the cone of the matrix. Due to the symmetry of the cross-section of the workpiece, two streams of metal meet here, which increases the speed of movements in this place. Therefore, their distribution along the Y axis is uneven: the maximum speed value is on the axis of symmetry, and the minimum value is on the working contour of the matrix profile. This is confirmed by the results of the calculation of deformation rates, the intensity distribution of which is shown in **Fig. 1.13** for a stable pressing mode. The maximum rate of deformation is characteristic of the center of zone II in sections ZY and XZ. At the same time, it decreases along the X coordinate in the XZ section to the working contour of the matrix. As a result of this distribution of velocities along the strip thickness, a zone of residual deformations with a value of 0.95...1.0 is formed in the middle along the Z axis, which decrease towards the edge of the strip (along the X coordinate) to 0.75...0.8. Along the Z axis, the values and distribution of deformations practically do not change. An exception is the zone of entry of the cylindrical workpiece into the working calibration part of the matrix and the exit of the workpiece. The non-uniformity of the intensity of deformations in the cross-section of the strip reaches 15...17 %.



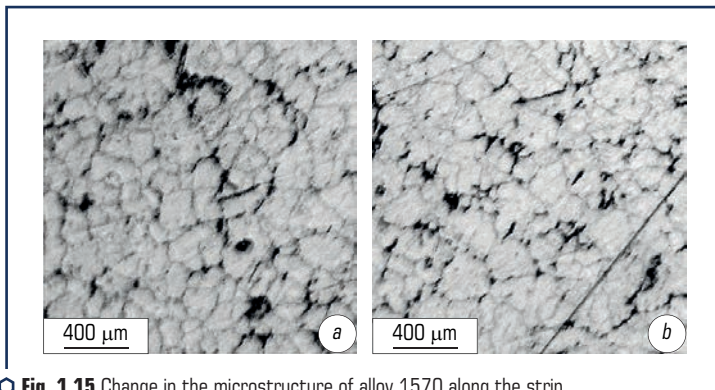
○ **Fig. 1.13** Distribution of the intensity of deformation rates ϵ_i at the moment of establishment of a stable pressing mode: *a* – in the ZY plane; *b* – in the XZ plane

Along the thickness of the band in the cross-section ZY, the distribution of deformations is more complicated due to the occurrence of significant shear deformations in zone II on inclined conical surfaces (**Fig. 1.14, a**). As a result, their intensity sharply increases on the calibration surfaces of the matrix (**Fig. 1.14, b, c**).



○ **Fig. 1.14** Shear deformations ε_{yz} (a) and the distribution of their intensity according to Mises at the time of establishment of a constant deformation force (b), in particular, in sections ZY along the Y axis (c) and ZY along the Z axis (d)

The calculation showed that after pressing, the distribution of the intensity of the residual deformations along the thickness of the strip is uneven, which was confirmed experimentally. The grain size of the material in the cross-section of the strip varies noticeably: in the near-surface zone it is ~ 2 times smaller than in the middle (**Fig. 1.15**), which corresponds to the nature of the influence of the intensity of deformations on the conditions of recrystallization of the deformed grain during hot pressing.



○ **Fig. 1.15** Change in the microstructure of alloy 1570 along the strip thickness: a – near-surface zone; b – the middle

By comparing calculated and experimental values of force during hot pressing of the strip, it was found (**Fig. 1.16**) that with a friction coefficient of $\mu=0.5$, the error of the calculated

compared to the actual value does not exceed 20...22 %. By reducing the friction coefficient to 0.1...0.3, it is possible to significantly weaken the pressing force (curves 4 and 5 in **Fig. 1.16**), which is achieved by using high-temperature lubricant on the surfaces of the workpiece and matrix.

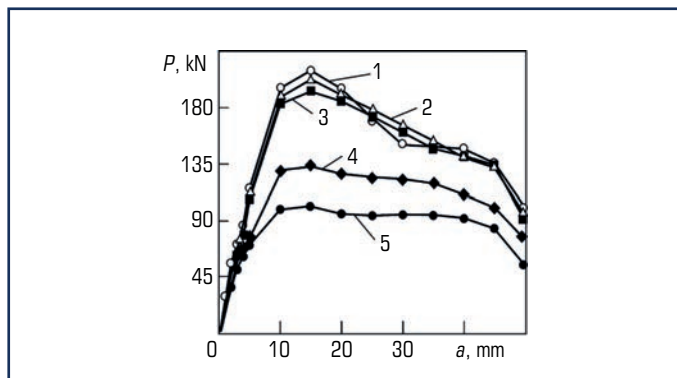


Fig. 1.16 Comparison of the dependences of the pressing force P on the displacement a of the punch, determined experimentally for blanks made of alloys 1545 (curve 1) and 1570 (curve 2), and calculated: 3 – $\mu=0.5$; 4 – 0.3; 5 – 0.1

It was established that the average compressive stress on the surface of the calibration belt reaches 110...120 MPa, which exceeds the yield point of the material at the pressing temperature (**Table 1.15**), i.e., destruction due to deformational damage may occur here. In the phenomenological theory of destruction [38], damageability ω is taken as the calculation parameter. Taking into account that the deformations during pressing are monotonous, a linear model in the form of:

$$\omega = \int_t \frac{\dot{\varepsilon}_i dt}{\Lambda_p(\Pi_\sigma, T)}, \quad (1.3)$$

where ε_i – the intensity of deformation rates; t – deformation time; $\Lambda_p(\Pi_\sigma, T)$ – metal fracture deformation; Π_σ – load stiffness index; T – the temperature of the metal during deformation. Here,

$$\Pi_\sigma = \frac{3\sigma_m}{\sigma_i}, \quad (1.4)$$

where $\sigma_m = 1/3(\sigma_1 + \sigma_2 + \sigma_3)$ – average tension; σ_i – stress intensity. The deformation of metal fracture at a given process temperature was determined on samples under uniaxial tension. This approach gives estimated results, the error of which does not exceed 15–20 %.

It was believed that in the initial state of the metal (before deformation) $\omega=0$; at the time of band destruction $\omega=1$. Intermediate values of ω determine the accumulation of micro- and macro-defects in the metal. Some threshold values of damage were established [39, 40–42]: $0 \leq \omega \leq 0.2$,

when deformation defects disappear after recrystallization annealing; $0.2...0.4 \leq \omega \leq 0.6...0.8$ – microdefects are formed in the metal that are not healed during heat treatment, and the metal loses its bearing capacity (mechanical characteristics decrease); $\omega > 0.6...0.8$ – there is a possibility of metal destruction.

The calculated distribution of damage – $\omega = 0.35...0.45$, and with a decrease in thickness to 6 mm – $\omega = 0.50...0.55$. At the same time, it was experimentally recorded that in the first case the strip is without visible defects, and in the second – with surface macrocracks.



○ Fig. 1.17 Distribution of damage ω in a strip with a thickness of 12 mm

Therefore, for the optimized selection of geometric parameters of the strip and equipment for pressing, it is proposed to determine the calculated damage rate ω at the process design stage. It was found that at $\omega = 0.35...0.45$ there is no visually observable crack formation, and when this parameter increases ($\omega = 0.50...0.55$), macrocracks appear on the strip surface.

CONFLICT OF INTEREST

The authors declare that they have no conflict of interest in relation to this research, whether financial, personal, authorship or otherwise, that could affect the research and its results presented in this paper.

REFERENCES

1. Ostash, O. P., Fedirko, V. M., Uchanin, V. M., Bychkov, S. A., Moliar, O. H., Semenets, O. I. (2007). Mitsnist i dovhovichnist aviatsiinykh materialiv ta elementiv konstruktsii. Lviv: SPOLOMB, 1068.
2. Filatov, Yu. A., Yelagin, V. I., Zakharov, V. V. (2000). New Al-Mg-Sc alloys. Materials Science and Engineering: A, 280 (1), 97–101. doi: [https://doi.org/10.1016/s0921-5093\(99\)00673-5](https://doi.org/10.1016/s0921-5093(99)00673-5)

3. Li, M., Pan, Q., Wang, Y., Shi, Y. (2014). Fatigue crack growth behavior of Al-Mg-Sc alloy. *Materials Science and Engineering: A*, 598, 350–354. doi: <https://doi.org/10.1016/j.msea.2014.01.045>
4. Fernandes, M. T. (2001). Pat. PCT/US00/19559. Aluminium-magnezium-scandium alloys with hafnium. Publ. 22.02.2001.
5. Polyvoda, S. L., Siryi, O. V., Hordynia, O. M., Puzhailo, L. P. (2017). Pat. No. 119406 UA. Plavylno – lyvarnyi kompleks dlia napivbezperernogo lyttia zlyvkiv z aliuminiievykh splaviv. MPK B22D 11/14. No. u201703178; declared: 03.04.2017; published: 25.09.2017, Bul. No. 18. Available at: <https://uapatents.com/5-119406-plavilno-livarnijj-kompleks-dlya-napivbezperernogo-littya-zlyvkiv-z-alyumniehvikh-splaviv.html>
6. Puzhailo, L. P., Siryi, O. V., Polyvoda, S. L. (2015). Pat. No. 108781 UA. Sposib rafinuvannia aliuminiievoho splavu u vakuumi. MPK C22B 21/00, C22B 9/04. No. a201310432. declared: 27.08.2013; published: 10.06.2015, Bul. No. 11. Available at: <https://uapatents.com/4-108781-sposib-rafinuvannya-alyumniehvogo-splavu-u-vakuumi.html>
7. Ostash, O. P., Polyvoda, S. L., Narivskiy, A. V., Chepil, R. V., Podhurska, V. Ya., Kulyk, V. V. (2020). Vplyv khimichnoho skladu na strukturu ta mekhanichni i koroziini vlastyivosti lytykh splaviv systemy Al-Mg-Sc. *Fyzyko-khimichna mekhanika materialiv*, 56 (4), 122–127.
8. Gavras, A. G., Chenelle, B. F., Lados, D. A. (2010). Effects of microstructure on the fatigue crack growth behavior of light metals and design considerations. *Matéria (Rio de Janeiro)*, 15 (2), 319–329. doi: <https://doi.org/10.1590/s1517-70762010000200033>
9. Avtokratova, E., Sitdikov, O., Kaibyshev, R., Watanabe, Y. (2008). Fatigue-Crack-Growth Behavior of Ultrafine-Grained Al-Mg-Sc Alloy Produced by ECAP. *Materials Science Forum*, 584-586, 821–826. doi: <https://doi.org/10.4028/www.scientific.net/msf.584-586.821>
10. Mann, V. Kh., Krokhin, A. Iu., Alabin, A. N., Khromov, A. P. (2019). Pat. No. 2 683 399 C1 RU. Splav na osnove aliuminiia. Opubl. 23.03.2019; Biul. No. 10.
11. Derkach, F. A. (1968). *Khimiiia*, Lviv: Lvivsk. universytet, 311.
12. Ostash, O. P., Kostyk, E. M., Kudriashov, V. G., Andreiko, I. N., Skotnikov, I. A. (1990). Nizkotemperaturnaia tsiklicheskaia treshchinostoikost vysokoprochnykh aliuminievykh splavov na stadiakh zarozhdeniia i rosta treshchiny. *Fiziko-khimicheskaia mekhanika materialov*, 26 (3), 40–49.
13. Ostash, O. P., Labur, T. M., Holovatiuk, Yu. V., Vira, V. V., Koval, V. A., Shynkarenko, V. S., Yavorska, M. R. (2019). Konstruktsiina mitsnist zvarnykh ziednan termozmitsnenoho splavu systemy Al-Cu-Mg. *Fyzyko-khimichna mekhanika materialiv*, 4, 81–87.
14. Ostash, O. P. (2006). Novi pidkhody v mekhanitsi vtomnoho ruinuvannia. *Fyzykokhimichna mekhanika materialiv*, 26 (3), 13–25.
15. Ostash, O. P., Chepil, R. V., Titov, V. A., Polyvoda, S. L., Voron, M. M., Podhurska, V. Ya. (2021). Mitsnist i tsyklichna trishchynostiikist termodeformovanykh splaviv systemy Al-Mg-Sc. *Fyzyko-khimichna mekhanika materialiv*, 57 (3), 118–125.
16. Zhemchuzhnikova, D., Mogucheva, A., Kaibyshev, R.; Weiland, H., Rollett, A., Cassada, W. (Eds.) (2012). *Mechanical properties of Al-Mg-Sc-Zr alloys at cryogenic and ambient*

- temperatures. Proc. 13th Int. Conf. on Aluminium Alloys (ICAA13). The Minerals, Metals and Materials Society, 879–884. doi: <https://doi.org/10.1002/9781118495292.ch131>
17. Mogucheva, A., Babich, E., Kaibyshev, R.; Weiland, H., Rollett, A., Cassada, W. (Eds.) (2012). Microstructure and mechanical properties of an Al-Mg-Sc-Zr alloy subjected to extensive cold rolling. Proc. 13th Int. Conf. on Aluminium Alloys (ICAA13). The Minerals, Metals and Materials Society, 1773–1778. doi: https://doi.org/10.1007/978-3-319-48761-8_265
 18. Ostash, O. P., Kostyk, E. M., Levina, I. N. (1988). Vlianie nizkoi temperatury na zarozhdenie i rost ustalostnykh treshchin v stali O8kp s razlichnym razmerom zerna. Fiziko-khimicheskaia mekhanika materialov, 24 (4), 63–71.
 19. Ivasyshyn, A. D., Vasylyv, B. D. (2001). Vplyv rozmiriv i formy vrazkiv na diahramu shvydkostei rostu vtomnykh trishchyn. Fyzyko-khimichna mekhanika materialiv, 37 (6), 119–120.
 20. Holovatiuk, Yu. V., Pokliatskiy, A. H., Ostash, O. P., Labur, T. M. (2018). Pidvyshchennia konstruktivnoi mitsnosti zvarnykh z'iednan lystiv zi splavu systemy Al-Cu-Mg. Fyzyko-khimichna mekhanika materialiv, 54 (3), 112–119.
 21. Nie, Z. R., Fu, I. B., Zou, I. X., Jin, T. N., Yang, I. I., Xu, G. F., et al.; Nie, I. E., Morton, A. J., Muddle, B. C. (Eds.) (2004). Advanced aluminium alloys containing rare-earth erbium. Proc. 9th Int. Conf. on Aluminium Alloys. Brisbane, 197–201.
 22. He, L. Z., Li, X. H., Liu, X. T., Wang, X. J., Zhang, H. T., Cui, J. Z. (2010). Effects of homogenization on microstructures and properties of a new type Al-Mg-Mn-Zr-Ti-Er alloy. Materials Science and Engineering: A, 527 (29-30), 7510–7518. doi: <https://doi.org/10.1016/j.msea.2010.08.077>
 23. la Torre, E. A.-D., Pérez-Bustamante, R., Camarillo-Cisneros, J., Gómez-Esparza, C. D., Medrano-Prieto, H. M., Martínez-Sánchez, R. (2013). Mechanical properties of the A356 aluminium alloy modified with La/Ce. Journal of Rare Earths, 31 (8), 811–816. doi: [https://doi.org/10.1016/s1002-0721\(12\)60363-9](https://doi.org/10.1016/s1002-0721(12)60363-9)
 24. Zhang, X., Wang, Z. H., Zhou, Z. H., Xu, J. M., Zhong, Z. J., Yuan, H. L., Wang, G. W. (2015). Effects of Rare Earth on Microstructure and Mechanical Properties of Al-3.2Mg Alloy. Materials Science Forum, 817, 192–197. doi: <https://doi.org/10.4028/www.scientific.net/msf.817.192>
 25. Pozdniakov, A. V., Yarasu, V., Barkov, R. Yu., Yakovtseva, O. A., Makhov, S. V., Napalkov, V. I. (2017). Microstructure and mechanical properties of novel Al-Mg-Mn-Zr-Sc-Er alloy. Materials Letters, 202, 116–119. doi: <https://doi.org/10.1016/j.matlet.2017.05.053>
 26. Ibrokhimov, S. Zh. (2018). Struktura i svoistva splava AMg4, legirovannogo redkozemelnymi metallami (Sc, Y, La, Pr, Nd). Dushanbe.
 27. Ostash, O. P., Polivoda, S. L., Chepil, R. V., Titov, V. A., Gogaev, K. O., Kulik, V. V. et al. (2021). Vplyv ridkisnozemelnykh metaliv na strukturu i vlastivosti litikh ta deformovanykh splaviv sistemi Al-Mg-Cr-Sc-Zr. Fiziko-khimichna mekhanika materialiv, 57 (6), 120–127.
 28. Estrin, Y., Vinogradov, A. (2013). Extreme grain refinement by severe plastic deformation: A wealth of challenging science. Acta Materialia, 61 (3), 782–817. doi: <https://doi.org/10.1016/j.actamat.2012.10.038>

29. Zhemchuzhnikova, V. A. (2016). Vlianie deformatsii na strukturu i mekhanicheskie svoistva Al-Mg-Sc-Zr splava. Belgorod.
30. Ren, L., Gu, H., Wang, W., Wang, S., Li, C., Wang, Z., Zhai, Y., Ma, P. (2020). The Microstructure and Properties of an Al-Mg-0.3Sc Alloy Deposited by Wire Arc Additive Manufacturing. *Metals*, 10 (3), 320. doi: <https://doi.org/10.3390/met10030320>
31. Harada, Y., Dunand, D. C. (2009). Microstructure of Al₃Sc with ternary rare-earth additions. *Intermetallics*, 17 (1-2), 17–24. doi: <https://doi.org/10.1016/j.intermet.2008.09.002>
32. Fang, H. C., Shang, P. J., Huang, L. P., Chen, K. H., Liu, G., Xiong, X. (2012). Precipitates and precipitation behavior in Al-Zr-Yb-Cr alloys. *Materials Letters*, 75, 192–195. doi: <https://doi.org/10.1016/j.matlet.2012.02.013>
33. Iakiviuk, O. V. (2018). Razrabotka tekhnologii polucheniiia dlinnomernykh deformirovannykh polufabrikatov iz splavov sistemy Al-Mg, legirovannykh skandiem, i issledovanie ikh svoistv. Krasnoiar'sk.
34. Bethencourt, M., Botana, F. J., Calvino, J. J., Marcos, M., Rodríguez-Chacón, M. A. (1998). Lanthanide compounds as environmentally-friendly corrosion inhibitors of aluminium alloys: a review. *Corrosion Science*, 40 (11), 1803–1819. doi: [https://doi.org/10.1016/s0010-938x\(98\)00077-8](https://doi.org/10.1016/s0010-938x(98)00077-8)
35. Cavaliere, P. (2009). Fatigue properties and crack behavior of ultra-fine and nanocrystalline pure metals. *International Journal of Fatigue*, 31 (10), 1476–1489. doi: <https://doi.org/10.1016/j.ijfatigue.2009.05.004>
36. Titov, A. V., Balushok, K. B., Ostash, O. P., Titov, V. A., Korieva, V. O., Polyvoda, S. L., Chepil, R. V. (2022). Presuvannia napivfabrykativ zi splaviv systemy Al-Mg-Sc v izotermichnykh umovakh. *Fyzyko-khimichna mekhanika materialiv*, 58 (5), 120–127.
37. Design Environment for FORMing. Available at: <https://www.deform.com/products/deform-3d/>
38. Kolmogorov, V. L. (1970). Napriazheniya, deformatsyy, razrushenye. Moscow: Metallurhiya, 229.
39. Bohatov, A. A., Myzhyrytskyi, O. Y., Smyrnov, S. V. (1984). Resurs plastychnosti metallov pry obrabotke davlenyem. Moscow: Metallurhiya, 144.
40. Mykhalevych, V. M., Dobraniuk, Yu. V., Kraievskiy, V. O. (2018). Porivnialne doslidzhennia modelei hranychnykh plastychnykh deformatsii. *Visnyk mashynobuduvannia ta transportu*, 2 (8), 56–64.
41. Shao, Y., Peng, W., Cao, F., Oleksandr, M., Titov, V. (2022). Effect of process parameters on AA6061/Q345 bimetal composite for hot stamping. *Proceedings of the Institution of Mechanical Engineers, Part E: Journal of Process Mechanical Engineering*, 236 (6), 2515–2525. doi: <https://doi.org/10.1177/09544089221096204>
42. Yu, Z., Peng, W., Zhang, X., Oleksandr, M., Titov, V. (2022). Evolution of microstructure of aluminum alloy hollow shaft in cross wedge rolling without mandrel. *Journal of Central South University*, 29 (3), 807–820. doi: <https://doi.org/10.1007/s11771-022-4950-8>

CHAPTER 2

**MODERN TECHNOLOGICAL PROCESSES OF OBTAINING
CAST PRODUCTS AND STRUCTURES OF RESPONSIBLE
PURPOSE FROM ALUMINUM, FERROUS CARBON
AND HEATRESISTANT ALLOYS****ABSTRACT**

The chapter presents the results of scientific research and development of new highly efficient foundry technologies for the production of cast and composite structural materials and products with high operational characteristics from alloyed and reinforced aluminum, iron-carbon and heat-resistant alloys.

The latest technological processes for the production of cast construction materials from aluminum alloys combine the influence of electromagnetic, plasma kinetic, centrifugal actions on metal systems in a vacuum, which makes it possible to obtain large-sized custom products for the space and atomic industries by the casting method.

The results of theoretical and experimental studies using the method of jet gas cooling of molds in a vacuum for obtaining blades of gas turbine engines (GTE) with a regular directional casting structure are given.

Promising technologies for obtaining cast iron and steel reinforced structures based on gasification patterns by liquid-phase combination of system components have been developed. The results of the study of the thermal state of the reinforced casting by the methods of mathematical and computer modeling are presented, the physical model of mass and heat transfer of reinforcing elements and matrix alloy during the formation of the structure and properties of cast reinforced structures is presented.

The works carried out by the authors at the Physical and Technological Institute of Metals and Alloys of the National Academy of Sciences of Ukraine are of high scientific and practical importance for the development of foundry production and will be useful for foundry product manufacturers, scientific and scientific-pedagogical workers in the specialty "Metallurgy" (Foundry production).

KEYWORDS

Aluminum alloys, vacuum magnetohydrodynamic mixer, continuous ingot casting machine, modification, heat-resistant corrosion-resistant nickel alloys, gas turbine engine blades,

directional crystallization, composite castings, cast reinforced structures, iron-carbon alloys, lost foam casting.

The development of mechanical engineering is largely related to the production of cast products from aluminum, iron-carbon and heat-resistant alloys with the required level of physical, mechanical and operational characteristics, the improvement of existing ones and the creation of new materials and technologies based on them with enhanced functionality.

A promising direction is the use in industry of composite materials that have high anti-friction properties, thermal and electrical conductivity in a wide temperature range. Currently, various technologies for obtaining composite products are being created and their nomenclature is expanding. At the same time, the requirements for operational characteristics and special properties of structural materials are constantly growing, and modern processes of their production do not provide the necessary technical and economic indicators.

The high quality of structural materials can be ensured by using the latest methods of preparing alloys, based on the intensification of the processes of interaction of gas, liquid and solid phases with the melt. The use of plasma, centrifugal and electromagnetic actions on metal systems in a vacuum provides wide opportunities for the creation of effective technologies for mass and special purpose metal production, based on the processes of treating alloys with dispersed and active reagents in a highly reactive state.

The creation of such breakthrough technologies for obtaining high-quality structural materials with economical consumption of energy resources and materials is relevant and meets the requirements of science and practice at the current stage.

It is at the basis of the further recovery and development of the domestic foundry industry that the above concept will be used to provide the machine-building complex of Ukraine with mono- and reinforced cast structural materials and products from high-strength aluminum and iron-carbon alloys with a reduced mass by 2...3 times and an increase in resource by 3...5 times, and this will provide the needs of highly competitive products for the Ukrainian and foreign consumers, as well as make it possible to reduce the overall metal content of engineering products, primarily vehicles, by 25...30 %, increase its resource by 1.5...2 times and at the same time reduce material costs and energy costs during its production by 30...50 %.

To achieve the goal, the authors used original methods of strengthening alloys with transition and rare earth metals and particles synthesized in the matrix melt under magnetodynamic, centrifugal, vacuum, and plasmakinetic effects on the processes of mass transfer, physicochemical, and interphase interactions in metal systems; the influence of the reinforcement of alloys in the liquid phase state on structure formation and heat and mass exchange processes during the production of castings by lost foam casting was investigated and determined; the technology of obtaining blades of gas turbine engines (GTE) with a regular directional casting structure was researched and improved.

2.1 MODERN PROCESSES OF OBTAINING CAST STRUCTURAL MATERIALS FROM ALUMINUM ALLOYS OF RESPONSIBLE PURPOSE

The high quality of structural materials made of aluminum alloys is ensured by new technologies for their preparation, which are based on the intensification of the processes of interaction of gas, liquid and solid phases in the melt. The use of electromagnetic, plasma, centrifugal and vacuum effects on metal melts allows for effective processing of alloys with dispersed and active reagents in a highly reactive (liquid, vaporous and gaseous) state. The creation of such technologies for the production of high-quality construction materials with economical consumption of energy resources meets the requirements of science and practice at the current stage.

The Physical and Technological Institute of Metals and Alloys of the National Academy of Sciences of Ukraine (PTIMA of the National Academy of Sciences of Ukraine) has developed and successfully operates electromagnetic melting and pouring equipment for the preparation of aluminum alloys and the production of continuously cast ingots from them [1]. The equipment includes a vacuum magneto-hydrodynamic mixer (MHD-mixer) and a continuous ingot casting machine (CICM) (Fig. 2.1).

The operation of the MHD mixer is based on the process of converting electrical energy into thermal energy, in which the primary winding is an inductor, and the secondary winding is a flow of liquid metal in the channel and mixer crucible. The operation of such equipment is as follows: after filling the U-shaped horizontal channel with liquid metal, voltage is applied to the inductor and electromagnet. As a result, an alternating electric current is induced by the magnetic flux of the inductor in the melt, which fills the horizontal channel. This current heats the alloy at a rate that depends on its magnitude. As a result of the interaction of the current in the melt and the magnetic field of the electromagnet, the alloy circulates in the channel and crucible of the mixer.

When the voltage on the electromagnet of the MHD-mixer increases, the electromagnetic force increases, under the influence of which the melt moves along the metal conduit to the crystallizer. At the same time, the alloy is affected by an electric current, a magnetic field, hydrodynamic and vortex pulsations in the liquid metal. Such actions intensify the processes of assimilation of alloying and modifying elements by the melt and average its chemical composition in the entire volume. At the same time, in the channel of the MHD mixer, in the area of the melt, through which the magnetic flux from the electromagnet passes, an "active zone" is formed, in which the alloying and modifying components introduced into the alloys are maximally influenced by magnetohydrodynamic factors. The presence of such factors makes it possible to intensify the dissolution processes of the introduced components at reduced heating temperatures of aluminum alloys [2]. As a result, the content of gases in the melt and its oxidation, as well as the consumption of electricity for the alloy preparation process, are reduced.

The channel, crucible and electromagnetic system of the MHD mixer are placed in a vacuum chamber, where the liquid metal is refined with its constant stirring. Regardless of the initial content of hydrogen in the melt, vacuum refining in the MHD mixer allows reducing its residual concentration in the alloy to $0.05...0.12 \text{ cm}^3/100 \text{ g}$ of metal, which allows obtaining ingots without

gas porosity. For the vacuum refining of aluminum alloys with a high (more than 4 % by mass) zinc content, a technology has been developed that allows to eliminate the loss of alloying elements by evaporation [3]. For products of responsible purpose, a method of refining alloys using successive vacuum pulses has been created, which ensures the residual content of hydrogen in ingots at the level of 0.01...0.03 cm³/100 g of metal [4]. Methods of operational control of hydrogen content in liquid metal [5] were also developed, which made it possible to automate the processes of preparing alloys with the help of industrial devices.

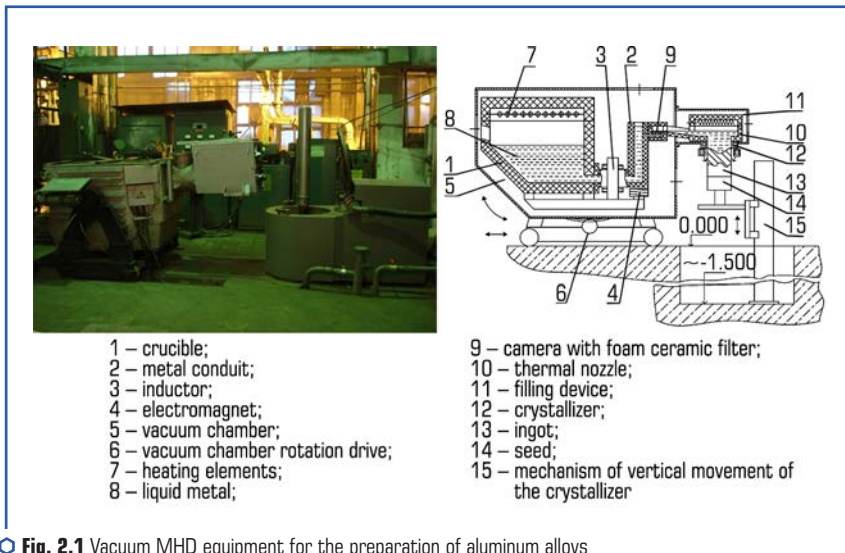


Fig. 2.1 Vacuum MHD equipment for the preparation of aluminum alloys and continuous casting of ingots from them

After vacuuming, the alloy from the MHD mixer is passed through a chamber with a porous ceramic filter under adjustable electromagnetic pressure. As a result of filtration, the alloy is cleaned of oxide inclusions to a residual concentration of ≤ 0.05 vol. %. The purified alloy enters the pouring unit, which is attached to the front wall of the vacuum chamber of the MHD mixer and is also a vacuum chamber in which the thermal nozzle is placed. The melt fills the thermal nozzle with two laminar flows (Fig. 2.2), which contributes to the mixing of the melt, averaging its temperature, and excludes mixing of oxide films into the alloy. The thermal nozzle is equipped with heating elements, which allows to compensate for the heat loss of the melt on the way of its movement from the MHD mixer to the crystallizer, and also reduces the temperature gradient along the height of the overflow part of the ingot, thereby creating favorable conditions for its directional crystallization.

Continuous modification of the alloy during the production of ingots at the CICM can be carried out with a ligature rod, which is fed into the liquid metal during pouring (Fig. 2.3). It is expedient

to insert the rod into the zone of melt vortices formed by its two tangential flows of melt. As a result, intermetallics and modifiers are evenly distributed throughout the volume of the liquid phase of the ingot during crystallization.

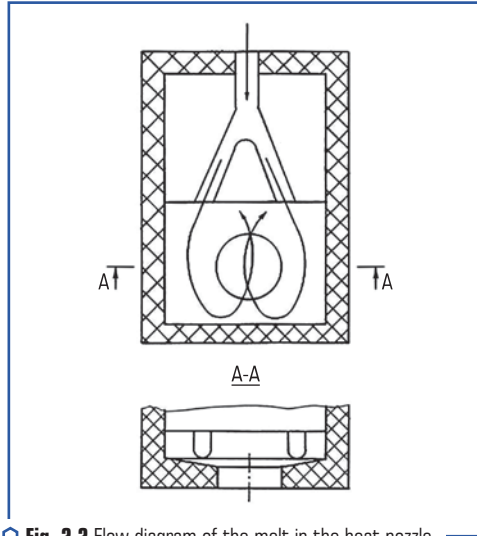


Fig. 2.2 Flow diagram of the melt in the heat nozzle

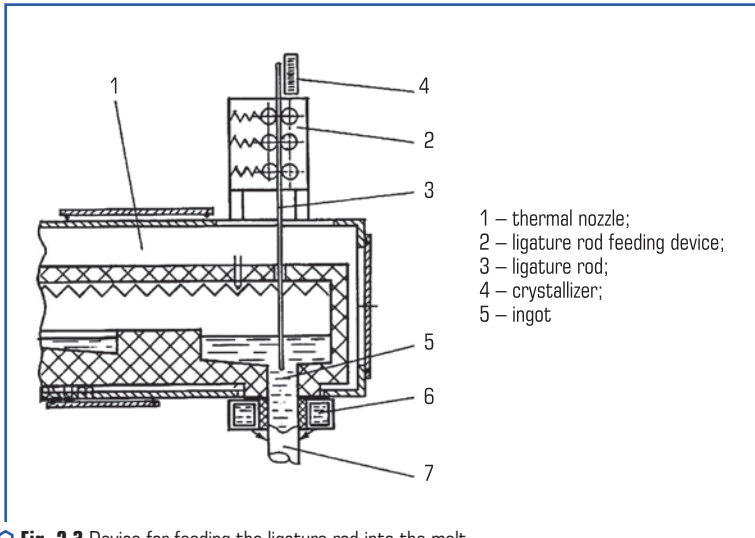
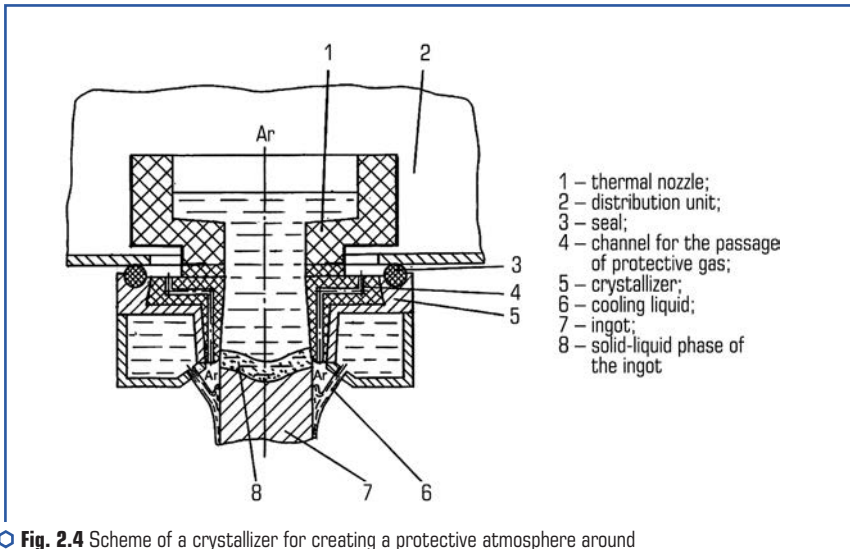


Fig. 2.3 Device for feeding the ligature rod into the melt

The complex of vacuum MHD equipment includes a vertical type CICM with smooth adjustment of the speed of movement of the casting table. The CICM is equipped with a low ($h - 33$ mm) crystallizer, the feature of which is the use of a heat-insulating lining layer with low thermal conductivity [6], which ensures the absence of radial heat dissipation from the liquid metal along the height of the crystallizer and leads to a significant decrease in the depth of the hole and the height of the transition zone of the ingot during crystallization and positively affects its structure. A gas-forming coating is applied to the inner surface of the crystallizer, during sublimation of which a gaseous layer is formed around the perimeter of the ingot, which also reduces heat removal from the ingot through the wall of the crystallizer. Thus, a thin film of crystallized metal is formed in the crystallizer, and the crystallization of the inner layers of the ingot takes place in the water-cooling zone below the level of the crystallizer. The speed of heat removal from the crystallizing ingot is a key parameter for controlling the structure of the ingots, therefore, the CICM is equipped with a system of adjustable coolant supply to the ingot.

When preparing highly oxidizable alloys in the MHD mixer, such as the Al-Mg system, it becomes necessary to protect the melt using an inert gas. For this purpose, it is possible to seal not only the furnace space of the MHD mixer, but also the entire metal tract, including the crystallizer of the machine for continuous casting of ingots [7] (Fig. 2.4).



○ Fig. 2.4 Scheme of a crystallizer for creating a protective atmosphere around the solid-liquid phase of the ingot

Electromagnetic stirring of the liquid phase of the crystallizing ingot affects heat and mass transfer processes, the intensity of convective flows in the melt, and also creates shear stresses

along the crystallization front of the alloy. As a result, the dendritic structure in the alloy is destroyed with transformation into a globular form [8]. An electromagnetic stirrer of the liquid phase of the ingot can be placed on the CICM crystallizer, which increases the efficiency of the processes of dispersing structural components in ingots during continuous casting.

The created MHD equipment makes it possible to obtain high-quality ingots from aluminum deformable alloys with high chemical uniformity, without internal defects, having a homogeneous fine crystal structure and a smooth shiny surface that does not require mechanical processing before pressing. Technical characteristics of the complex of vacuum MHD equipment: the maximum capacity of the crucible is 200 kg, diameters of ingots are from 50 to 250 mm; the length of ingots is up to 1500 mm.

The vacuum MHD mixer can also be used for casting under combined (electromagnetic and pneumatic) pressure, for dosing and controlled programmable electromagnetic pouring of liquid aluminum alloys into casting molds, including in the hopper of centrifugal casting machines for obtaining custom blanks.

The space and atomic industries require large-sized custom products made of aluminum alloys (rings, bushings, bandages, pipes), which are most often obtained by welding rolled sheets or rolling continuously cast ingots after piercing them. These technologies have a low rate of metal use, high labor intensity and cost. It is more expedient to obtain custom-made products by the centrifugal casting method, which allows to intensify the process of crystallization of the alloy and disperse its structure. During crystallization of alloys under the action of centrifugal forces, the density and homogeneity of cast products increase. Crystallization of alloys under high pressure leads to a shift in the boundaries of phase transformations. At the same time, phases absent in the equilibrium diagrams can be obtained. In addition, it is possible to achieve wetting between phases, if it was absent under normal conditions. For the implementation of centrifugal casting technologies, the PTIMA of the National Academy of Sciences of Ukraine produced a machine for the production of custom castings, bushings and pipes up to 800 mm in length and up to 450 mm in diameter at an adjustable casting speed of up to 3000 rpm (**Fig. 2.5**).

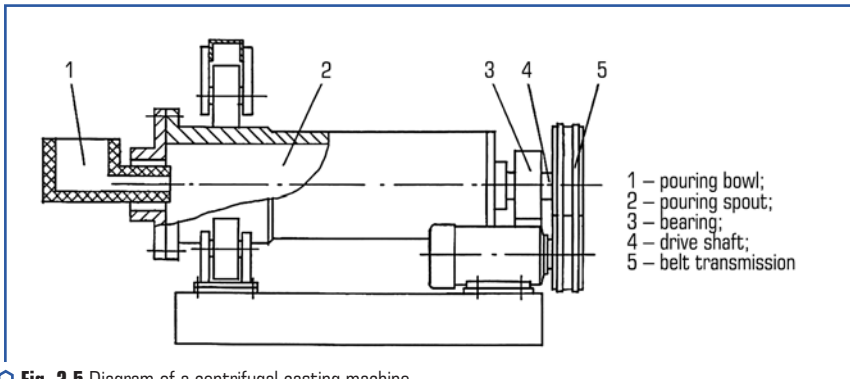
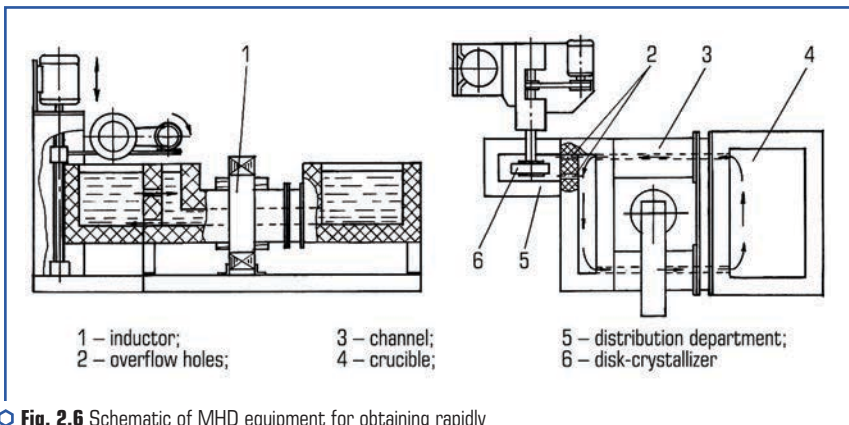


Fig. 2.5 Diagram of a centrifugal casting machine

For the production of cast and composite products from aluminum alloys, dispersed particles, fibers and powders are widely used. In foundry production, it is also advisable to use quickly crystallized ligatures. Such dispersed materials with a homogeneous structure can be produced by the method of extracting the melt in an electromagnetic field [9]. For the implementation of such technologies, electromagnetic equipment [10] has been created at the PTIMA of the National Academy of Sciences of Ukraine, which includes an MHD installation and a water-cooled disk-crystallizer with adjustable rotation speed (**Fig. 2.6**). When the crystallizer disk comes into contact with the surface of the melt, the alloy freezes on its ribbed surface, from which it is thrown into a separate hopper. The shape of the crystallized particles varies depending on the geometry of the disc's ribbed surface and the speed of its rotation.

For the modification (alloying) of aluminum alloys with fine-crystalline particles and fibers, a method was proposed and equipment for melt processing was created [11]. According to this method, the liquid metal modification operation is carried out in a vacuum with dispersed particles, which are extracted from the matrix melt during the preparation of the alloy in the MHD installation (**Fig. 2.7**).

The alloy solidifying on the crystallizer disk is thrown onto the screen by centrifugal forces in the form of particles and fibers. Dispersed particles of the alloy are reflected from the screen and fall into the liquid metal bath. Fine-crystalline fibers and particles that fall into the metal, related to the matrix alloy, are well wetted and assimilated by it. As a result, the processes of nucleation in the alloy during crystallization are intensified, which contributes to the grinding of structural components in the cast metal. The technology of obtaining powder from aluminum melt, which is in an electromagnetic field, has been introduced into industrial production. MHD mixer (**Fig. 2.8, a**) is installed on the melting furnace with a capacity of 1.5 tons, which is made in the form of a U-shaped horizontal channel with an open vertical section for installing a nozzle. The channel is connected to the melting crucible of the furnace and covers the inductor with a W-shaped magnetic conductor, on the central rod of which there are coils.



○ **Fig. 2.6** Schematic of MHD equipment for obtaining rapidly crystallized aluminum fibers and powder

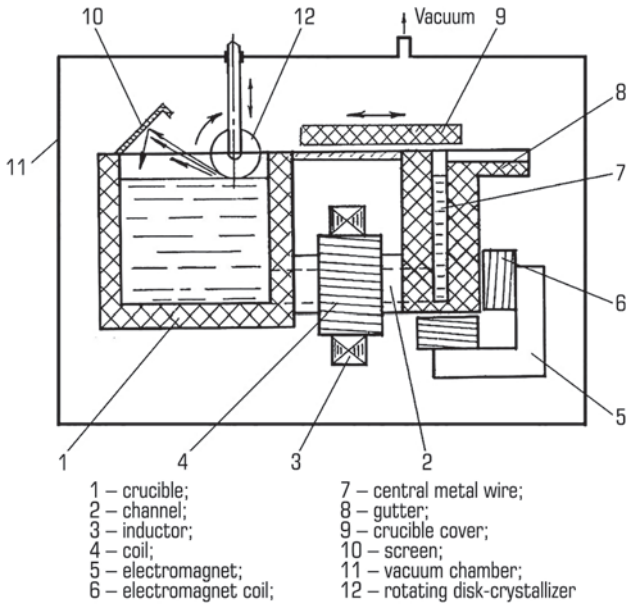


Fig. 2.7 Scheme of the MHD unit for processing aluminum alloys with fine crystalline particles

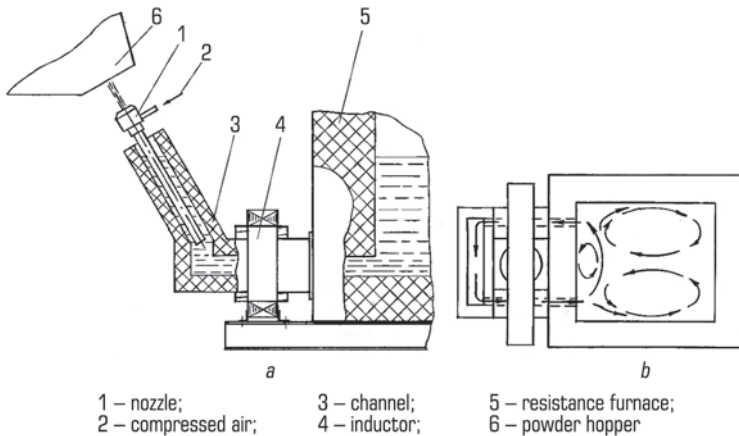
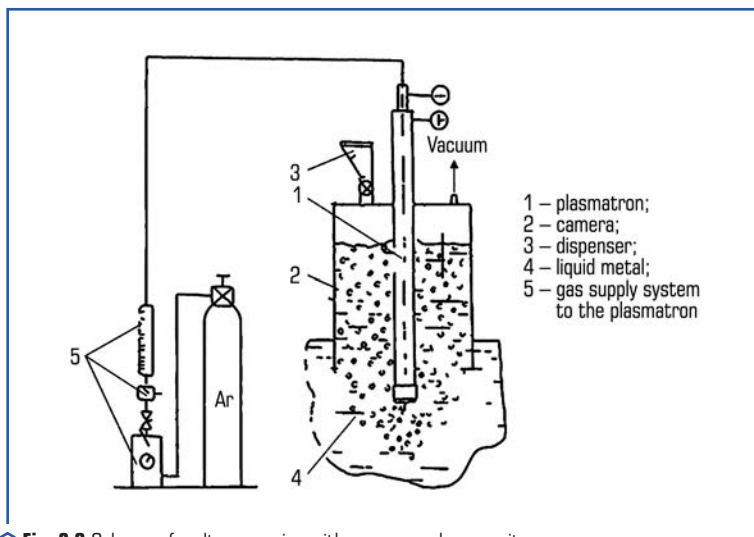


Fig. 2.8 Diagram: *a* – of the equipment for obtaining aluminum powder; *b* – the movement of the melt in the crucible of the resistance furnace during electromagnetic stirring

The use of continuous electromagnetic stirring made it possible to eliminate the formation of stagnant zones in the melt (**Fig. 2.8, b**), reduce overheating and stabilize its temperature at the level of $790 \pm 10 \text{ }^\circ\text{C}$. Lowering the alloy preparation temperature by $50 \dots 60 \text{ }^\circ\text{C}$ made it possible to reduce the oxidation of crystallized particles and improve the quality of the powder. Due to the heating of the melt in the active zone of the annular horizontal channel, the temperature of the metal at the exit from the nozzle is $840 \dots 850 \text{ }^\circ\text{C}$. At such injection temperature regimes, crystallization of the melt near the nozzle of the nozzle is excluded and its service life is increased. At the same time, the productivity of aluminum powder production increases from 300 to 500 kg/h.

The use of plasma technology opens up wide possibilities for the creation of combined processes that will allow treating alloys with a high-temperature gas jet with simultaneous heating, melting or evaporating fluxes and special additives. The plasma thermo-kinetic influence brings the reagents into a highly reactive physico-chemical state, which intensifies the processes of their interphase interaction with the melt.

The Physical and Technological Institute of Metals and Alloys of the National Academy of Sciences of Ukraine has created processes for vacuum-plasma processing of non-ferrous alloys that have no analogues abroad [12–16]. Such technologies make it possible to process alloys with plasma in a vacuum during portioned and continuous pouring of metal with the help of simple equipment (**Fig. 2.9**). The plasmatron together with the camera is immersed in the melt and a vacuum is created. The metal in the chamber rises to a certain height, which depends on the amount of vacuum above the surface of the liquid bath. Vacuum sealing of the chamber during alloy processing provides the melt in which it is immersed.



○ **Fig. 2.9** Scheme of melt processing with a vacuum-plasma unit

The diameter of the chamber and the location of the plasmatron nozzle are chosen so that all gas bubbles enter the chamber during metal blowing. In this case, the surface of the melt outside the chamber is in a calm state, the oxide film or the flux applied to its surface prevent the inflow of hydrogen from the atmosphere into the melt during processing.

The necessary reagents are preloaded into the dispenser, and then fed into the chamber in the process of metal processing. The reagents are mixed in the upper layers of the melt, where the highest intensity of mass transfer is achieved during blowing with a gas jet, and are evenly distributed in the metal.

The industrial development of such technologies has shown that vacuum-plasma processing of aluminum alloys allows: to heat the melt in the process of refining or modification; reduce the amount of non-metallic inclusions in the alloy by 1.5...2 times, the hydrogen content – up to 80 %; reduce by 3–4 times (or eliminate the use of) the consumption of reagents for the processing of alloys. Along with this, after vacuum-plasma treatment in the melt, the average size of microclusters decreases by 2–2.5 times (from 26.8 to 11.2 nm), the tensile strength of the cast metal increases by 14–25 %, the relative elongation by 1.5...1.8 times.

Employees of the PTIMA of the National Academy of Sciences of Ukraine have also developed complex environmentally friendly processes for processing and pouring aluminum melts using the created MHD equipment, in which vacuum-plasma systems are installed [17–21]. Such technologies, due to thermoforce effects on liquid metal, allow:

- intensify structural and phase transformations in alloys;
- disperse intermetallics and microgroups in alloys;
- evenly distribute alloying and strengthening particles in the liquid metal bath;
- control the rate of crystallization of the alloy;
- effectively doping alloys with active metals, in particular, using consumable electrodes in plasmatrons;
- treat alloys with carbon and silicon nanoparticles synthesized by reactions of carbon with silicon-containing media on crystalline metal centers and compounds that are introduced into the melt;
- increase the efficiency of plasma heating of liquid metal to ≥ 90 %;
- change the structure and properties of cast products by effective plasma effects on alloys (dissociation of gases, ionization of atoms, controlled energy and density of charged particles, etc.).

According to the results of research of hydrodynamic, heat-mass transfer and physico-chemical processes in metal melts during their deep processing with plasma reagent media, the following were determined:

1. The temperature of the plasma jet immersed in the liquid metal increases to 5000 °C when approaching the plasmatron nozzle. In the zone of introduction of a deep plasma jet into the melt, the temperature of the alloy is 400–600 °C higher (with cold blowing – ~100 degrees lower) than its average mass temperature. As a result, during plasma treatment, the processes of gas-reactive interaction in alloys, as well as mass transfer of hydrogen in the superheated melt, are intensified.

2. The rate of heating of solid particles with a dispersion of 50...100 μm in the plasma jet is 350...490 degrees/ms. Reagents used for processing aluminum and copper alloys, when introduced through a plasmatron, are heated and enter the melt in a highly reactive (liquid and vapor) state. As a result, the processes of interaction of reagents with the melt intensify and the degree of their assimilation increases.

3. It was established that during the cooling of plasma-heated argon bubbles to the average mass temperature of the aluminum melt (0.1...0.4 ms), their radii decrease by 15...40 %, and the boundary layer renewal time on them decreases by 1.5...2.5 times.

4. When blowing with a plasma jet, the intensity of mass transfer processes in the melt is 25–70 % higher than with cold argon. Treatment of the melt with reagents in the liquid state makes it possible to increase the rate of mass exchange in the bath by 20...30 % compared to the solid one. At the same time, regardless of the depth of outflow of the cold or plasma jet, the maximum mixing and turbulization of the melt occurs in the surface layers of the bath.

5. In the reaction zone of the plasma jet, along with the thermo-time treatment of the alloy, evaporation of its components with rapid cooling ("condensation") of vapors in the melt being processed is possible. Dispersed particles of such "condensate" intensify the process of nucleation of components in alloys and contribute to the emergence of synthesized strengthening phases in the melt. At the same time, intermetallic and oxide inclusions are destroyed under the high-temperature influence ("thermal shock") of the plasma jet.

2.2 EFFECTIVE PROCESSES FOR OBTAINING CAST TURBINE BLADES FOR MARINE AND POWER GAS TURBINE ENGINES

2.2.1 MODERN TECHNOLOGIES FOR OBTAINING WORKING BLADES OF GAS TURBINE ENGINES

Increasing the service life of gas turbine engine (GTE) blades is associated not only with the development of new composite heat-resistant alloys, but also with methods of controlling the process of crystallization of castings from these alloys. In this regard, research is being carried out on such processes that ensure the formation of given structures in the parts, which guarantee the preservation of the necessary characteristics of the part during the given resource of its operation [22–25]. It is known that GTE blades are obtained by two methods, namely, equiaxial casting and casting with directional crystallization (DC).

Nickel alloys have high strength at high temperatures, because the formation of fatigue cracks occurs between grains. Therefore, it is better to have a blade with fewer grains and the ability to control their orientation. These questions are studied in many scientific centers of domestic and foreign scientists. The main reasons for the destruction of turbine blades are the grain boundaries, which are perpendicular to the direction of the external load. In order to improve the long-term strength of nickel heat-resistant alloys, it is necessary to have a directional structure in which the

grain boundaries are parallel to the direction of action of the principal stresses. One of the ways to further develop DC technologies is to obtain blades with a monocrystalline structure. Studies show that the destruction of the blades occurs mainly through the grain boundaries, which are perpendicular to the vector of the external load on the turbine blades.

In order to improve the long-term strength of nickel heat-resistant alloys, it is necessary to provide a directional structure in which the grain boundaries will be parallel to the direction of the main stresses. The use of monocrystalline blades can significantly increase the resource and capacity of gas turbines by 20...30 % and 10...15 %, respectively, which makes them more efficient [26, 27].

Although the casting of blades with a polycrystalline structure is more common than casting with a directional or monocrystalline structure, many researchers are engaged in the development of new methods of manufacturing blades with a more directional structure to increase their strength and durability.

One of the main factors determining the prevalence of casting blades with a polycrystalline structure is the lower complexity of the technological process compared to casting with directional and monocrystalline structures. To achieve better quality when casting GTE blades with a polycrystalline structure, vacuum melting units with heated molds (VMUHM) are used. One of the main parameters that are controlled during such a process is the depth of the vacuum, the temperature of the melt during the melting process, and the temperature of the mold heating furnace.

As a rule, at enterprises, turbine cooling blades are melted to obtain a polycrystalline structure, since it is impossible to obtain such blades by the method of directional crystallization with the required crystallographic orientation. At gas turbine manufacturers, cast turbine blades without internal cooling are produced with a directional structure or a monostructure, depending on the responsibility of the purpose.

Numerous methods of obtaining oriented dendritic and single crystal structures are presented and analyzed in the scientific and patent literature, such as the Bridgman, Shubnikov, Kiropoulos, Stockberger, Chochralsky method [28]. These methods can differ both in the method of heating and maintaining high temperatures in a ceramic mold with a crystallized melt, and in cooling the finished product, that is, in the method of heat removal.

The main methods of heating during the production of parts with a directional structure include, first of all, the following: direct induction heating, use of a resistance heater. The world's leading manufacturers of gas turbine installations use the Bridgman-Stockbarger (High Rate Solidification – HRS) method for manufacturing gas turbine blades [29]. The essence of the method is that in the heating zone, the alloy is poured into a ceramic mold that stands on a copper cooling crystallizer. Then the crystallizer is vertically moved into the cooling zone at a given speed, as a result of which a temperature difference is created at the crystallization front. Intensive heat removal is carried out in the lower part of the mold through a copper crystallizer, the upper part of the mold with melt is cooled by heat radiation from the side surface of the mold to the walls of the chamber. Such heat removal leads to slow cooling rates of castings, as a result of which a directional structure is formed.

The main tasks of thermal calculation in the development of the directional crystallization process are the determination of the following technological parameters: cooling rate of castings; temperature gradient at the crystallization front; crystallization speed of parts; the length of the transitional solid-liquid zone of the alloy and its location relative to the level of the cooler or heater.

A mandatory condition for obtaining a directional structure is the support during melting of the directional solidification of the liquid metal of the flat crystallization front. During the heat flow, the speed of advancement of the crystallization front practically becomes constant, which depends on the method of removal of the heat of crystallization.

In the practice of manufacturing-oriented parts, the so-called high-speed directional crystallization using a liquid metal cooler – the Liquid Metal Cooling (LMC) method [30] has received wide industrial application. This method makes it possible to obtain an oriented structure with crushed dendrites, small inter-dendritic distances and more dispersed and homogeneous secondary phases (carbides, intermetallics) in conditions of high-gradient cooling of the mold, for example, in liquid aluminum or tin, which leads to a significant increase in the mechanical level of alloys, including its long-term strength and plasticity.

Furnaces with liquid metal cooling (**Fig. 2.10**) can be used both for casting blades from eutectic heat-resistant alloys and from nickel-based alloys with intermetallic strengthening. The rate of crystallization in the first case is 0.1...0.2 mm/min, in the second 10...15 mm/min. Accelerated cooling of the alloy leads to the formation of a current dendritic structure, while endurance can be increased by 15–20 % compared to an alloy cast at a lower speed.

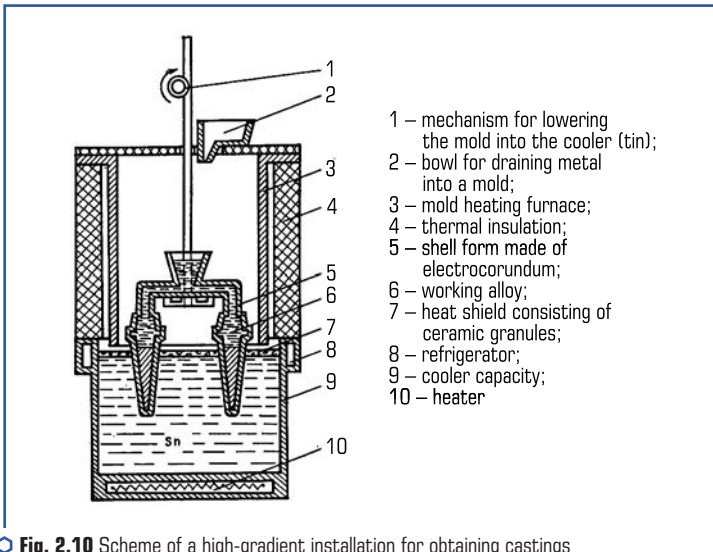


Fig. 2.10 Scheme of a high-gradient installation for obtaining castings with directional crystallization

Domestic gas turbine manufacturers use UVNK-8B industrial units with a tin crystallizer and UVNK-8P with an aluminum crystallizer. The alloys obtained by this technology have a small (8–10 times smaller) microporosity (up to 0.1 %) and a finely dispersed homogeneous structure (inter-dendritic distance 100–150 μm), which provides an increase in strength by 10–15 % and fatigue properties by 20...25 % compared to alloys obtained at normal temperature gradients (20...30 degrees/cm) [31]. The best results are obtained if the melt is preliminarily subjected to high-temperature treatment, and the obtained blanks are subjected to thermovacuum treatment. This ensures minimum values of dispersion of service properties and maximum reliability of blades. The liquid metal used for mold cooling must meet a number of requirements: high thermal conductivity and heat capacity, relatively low melting point, small value of partial pressure at the contact temperature, low adhesion to the surface of the molds, low cost and non-scarcity. In addition, the accidental ingress of liquid metal coolant into the alloy should not lead to deterioration of the latter's properties.

Since the production of GTE blades from heat-resistant alloys is carried out in a vacuum, only metal melts with low vapor elasticity in a vacuum at temperatures of contact with the mold (1100 °C) can be used as liquid cooling media.

When casting large-sized blades, there are difficulties associated with the use of a bulky beam containing a large volume of molten aluminum. During the immersion of the mold in aluminum, there is a significant change in the level of the melt in the bath, which slows down the speed of drawing the mold and, accordingly, reduces the productivity of the casting process to achieve the necessary longitudinal gradient during crystallization. Also, during casting, the installation is contaminated with aluminum (Al) and silicon (Si) oxide sublimates, which creates a risk of foaming of the aluminum melt. In the event of a mold break with heat-resistant alloy melt, it is necessary to replace the bath with aluminum. In addition, in molten aluminum, the solidified areas of the vane are cooled at an excessively high rate, which can lead to warping and cracking of the vanes, especially in the area of oversized banded vanes.

The company Houmet takes the first place in castings of monocrystalline large-sized blades of powerful energy turbines up to 600 mm long. Since 2005, they have been successfully using the GCC (Gas Cooling Casting) method of jet gas cooling of molds in a vacuum [32]. The GCC technological process involves convective jet cooling with argon in a vacuum of ceramic molds during directional crystallization while preserving the effect of cooling the molds by radiation. This process allows for optimal temperature control during casting, ensuring high quality and perfect crystal structure of the blades. From **Fig. 2.11**, it can be seen that the process of jet gas cooling of forms provides an increase in the productivity of single-crystal casting in comparison with liquid metal cooling by 2...3 times and 1.5 times, respectively. The use of such a process does not require special design and manufacture of new equipment. For this purpose, available in the industry installations with liquid metal cooling can be used, with the dismantling of the aluminum bath and the modification of the installation for the supply and distribution of inert gas.

One of the most effective ways to ensure the necessary characteristics of cyclic strength and durability of blades is to choose the optimal crystallographic orientation relative to the geometry of the blade, taking into account the large anisotropy of mechanical properties. The complete

crystallographic orientation of the blade is determined by the axial and azimuthal orientations. Based on the results of numerous studies and practical experience, it has been confirmed that for turbine blades with optimal axial orientation, a set of strength properties is achieved in the [001] direction with an accuracy of $\alpha[001]=10...15^\circ$. Directionally crystallized and single-crystal turbine blades of modern gas turbines are manufactured with this axial orientation [32].

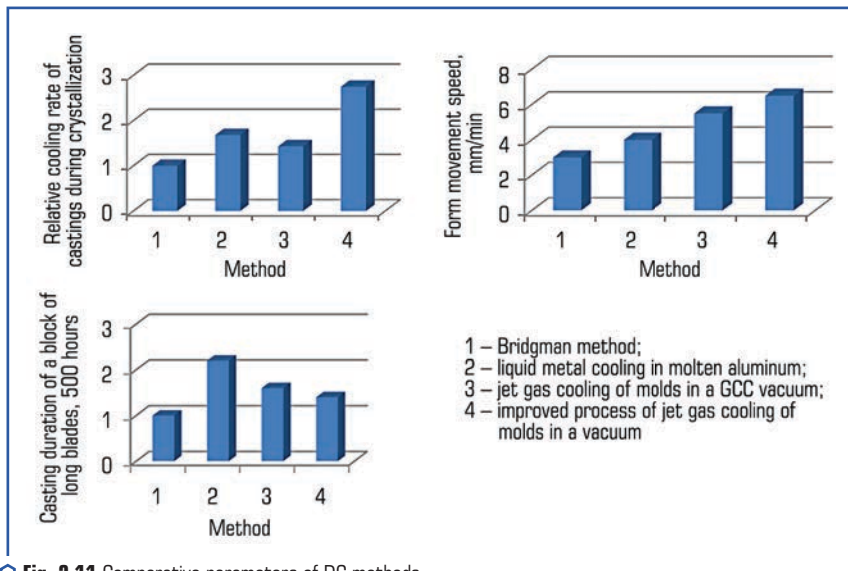


Fig. 2.11 Comparative parameters of DC methods

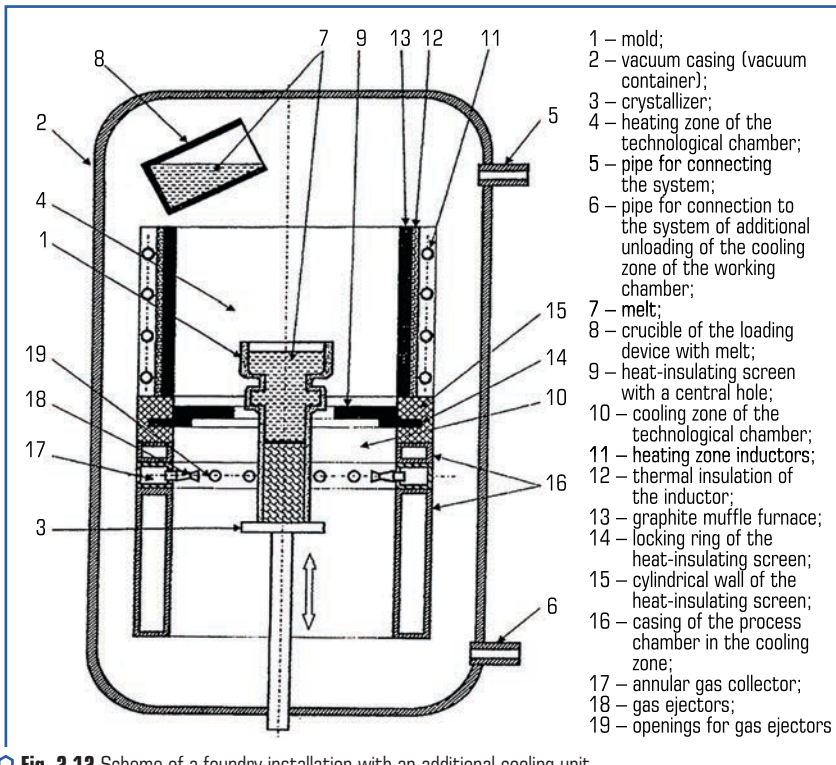
To achieve a given orientation in cast castings, the seeding method is used [32]. When melting gas turbine blades from heat-resistant nickel alloys, Ni-W alloy is used as a primer (Ni is the base, W 32...36 % by weight).

2.2.2 EXPERIMENTAL STUDIES USING THE GCC TECHNOLOGICAL PROCESS

The analysis of the data presented in subsection 2.2.1 indicates the need to develop new technologies for the production of special purpose products. Among the various options, one of the most promising is the method of jet gas cooling of molds in a vacuum. Within the framework of this method, theoretical and experimental studies were conducted to obtain a regular directional structure of the casting with [001] orientation depending on the conditions of product formation.

For research, a modernized foundry plant was used, which is implemented in the VIM-25-175C unit of the vertical type, which can be used, including for obtaining an oriented dendritic structure

in castings. The improvement included the installation of an additional cooling unit using an inert gas, namely argon. In **Fig. 2.12** it is possible to see the installation where the compatible casting crystallization process is implemented. The initial crystallization front is provided using the Bridgman-Stockbarger method (see section 2.2.1), and then, through a special crystallizer and a starting cone, the directed growth of grains in the blades is formed by directed argon blowing through a special system of nozzles. Up to 15 kg of material can be placed in the DC crucible, and the maximum pouring speed is 15 kg/sec per second. The dimensions of the ceramic mold are as follows: diameter – 200 mm, height – 400 mm. To control the temperature of the liquid metal, a thermocouple and an optical two-color pyrometer were used, in particular, a device of the Mikron type, model M-780. The time required to reach a working vacuum of 7×10^{-2} Pa after loading the charge was 2 minutes.



○ **Fig. 2.12** Scheme of a foundry installation with an additional cooling unit

For cooling, the inert gas supply device is implemented in the form of a ring gas collector, which is equipped with gas ejectors. Ejectors are located in a row at a distance of 45...75 mm from the lower surface of the heat-insulating screen. These ejectors allow to change the direction

of the gas flow for cooling. They are also designed in such a way that it is possible to change the direction of the gas flow for cooling and are located in a row at a distance of 45...75 mm from the lower surface of the heat-insulating screen.

In the inner wall of the annular collector, holes for ejectors are provided, which can be closed with plugs, for the possibility of positioning the ejectors in different variants. For this process, the critical diameter of the nozzles is 0.7...0.9 mm, the opening angle of the bell is 10...15°, and the gas pressure in the critical section of the nozzle is $(7...10) \times 10^5$ Pa. The use of this cooling method contributes to the intensification of the melt crystallization process and changes the temperature gradient at the crystallization front in comparison with convective cooling in a vacuum. As a result, the kinetics of structure formation changes significantly (**Fig. 2.12**).

The temperature-speed conditions of the crystallization process, which depend on the speed of movement of the ceramic mold (V_f , mm/min) and the temperature gradient at the crystal growth front (G , K/mm), have a significant effect on the intragranular structure, dispersion, and phase composition of the alloy [33]. Thermal analysis data were used to determine the optimal temperature intervals that affect the structural and phase characteristics of the DC process. With the help of the experiment, the optimal technological parameters for the DC process in the production of working non-cooling blades of the II stage of the power turbine were established. These parameters include the following: top heater temperature is (1560 ± 10) °C, cooler temperature is (1560 ± 10) °C, pouring temperature is (1570 ± 10) °C, crystallization front speed is 10–12 mm/min.

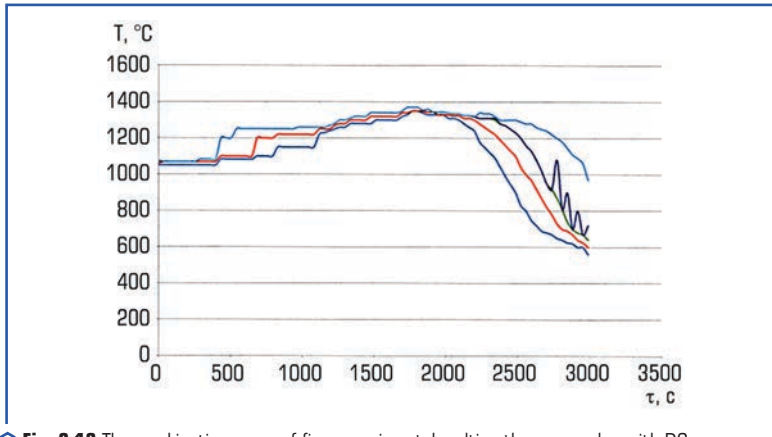
For conducting experimental fusions, a serial heat-resistant corrosion-resistant nickel-based alloy SM88 was used, the chemical composition of which is shown in **Table 2.1** [34]. In order to determine the local values of the parameters of the directional crystallization process during melting, the temperature distribution in the volume of the casting was measured experimentally at five points along the axis of the casting using tungsten-rhenium thermocouples (BP 5/20) with an electrode diameter of 0.30 mm. To obtain turbine blades with a directional structure, a technology was used, in which for each casting, a seed composition of Ni – base, W 32...36 % by weight was added to the bottom of the mold and [001] orientation. By analyzing thermo-kinetic curves built on the basis of the results of experimental measurements (**Fig. 2.13**), it is possible to determine the distribution of temperatures in the metal at any moment in time. The speed of immersion of the mold in the cooling zone directly affects the speed of crystallization of the melt.

● **Table 2.1** Chemical composition of heat-resistant alloy based on nickel

Element content, wt. %													
C	Cr	Co	Mo	Ti	Al	W	Nb	Fe	B	Zr	Si	Hf	Zr
0.09	15.6	10.7	1.9	4.6	3.0	5.3	0.11	0.5	0.05	0.05	0.04	0.5	0.05

Analysis of the microstructure of the alloy samples was carried out using a scanning electron microscope JSM-35CF of the company "JEOL" (Japan). The resolution of the microscope is up

to 1.2 nm, and the accelerating voltage is from 0.5 to 30 kV. Grids for metallographic studies were subjected to chemical etching using the Marble reagent ($\text{CuSO}_4 - 4 \text{ g}$, $\text{HCl} - 20 \text{ ml}$, water - 20 ml). Phase analysis of alloys and parameters of crystal lattices of phases were determined on the "DRON-3M" installation in $\text{CuK}\alpha$ radiation ($\lambda_{\text{CuK}\alpha} = 0.154187 \text{ nm}$).



○ Fig. 2.13 Thermo-kinetic curves of five experimental melting thermocouples with DC

The study of the structure after melting according to the above regimes in the modernized unit showed that the crystallographic orientation (CGO) of the obtained blades, which was determined by the X-ray diffraction method on each block sample, was [001]. The deviation from the orientation does not exceed the permissible angle of deviation from the main axis up to 20 degrees, according to the data presented in [35]. In all cross-sections (Fig. 2.14), the macrostructure shows a regular structure that meets the requirements concerning the structure of the second-degree blade samples, according to the technical standards of the enterprise [35].

The microstructure of the as-cast samples is mainly characterized by dendritic heterogeneity, as shown in Fig. 2.15. The strengthening γ' -phase has a size variation both in the axes of the dendrites and in the intermediate spaces between them. In the latter, the formation of a carbide phase in the rail morphology is observed, which indicates its eutectic nature. Eutectic structures $\gamma-\gamma'$ can also be observed in the intermediate spaces in a limited amount, so the next necessary component of obtaining high-quality products is their heat treatment according to the enterprise standard.

The introduction of additional cooling in the improved design of the casting unit VIM-25-175C led to the improvement of the cooling process of the crystallizer during directional crystallization and ensured obtaining a regular structure of castings.

The analysis of the technical literature, the current state of the issue and experimental studies showed that the works devoted to improving the quality of structure formation of blade castings with directional crystallization are promising and require further improvement.

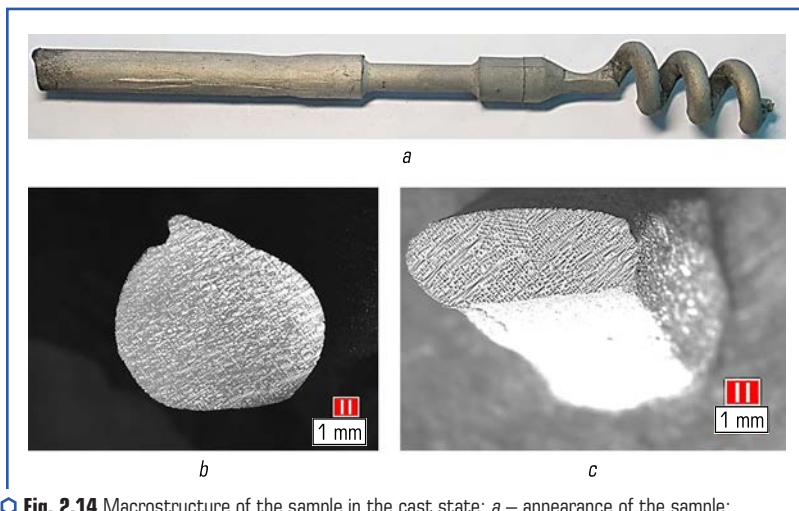


Fig. 2.14 Macrostructure of the sample in the cast state: *a* – appearance of the sample; *b* – macrostructure of the middle part of the sample; *c* – section from the seed (near the cone)

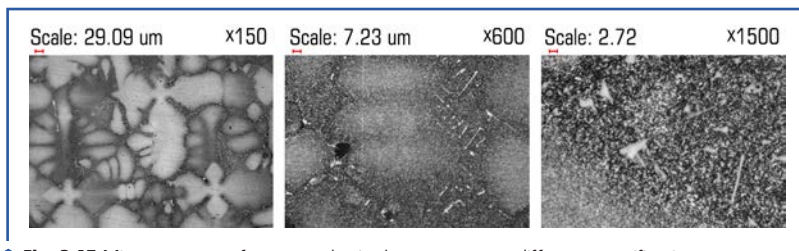


Fig. 2.15 Microstructure of test samples in the cast state at different magnifications

2.3 PROMISING TECHNOLOGIES FOR OBTAINING CAST IRON AND STEEL REINFORCED STRUCTURES BY LOST FOAM CASTING

2.3.1 METHODS OF OBTAINING PRODUCTS WITH HIGH SPECIAL PROPERTIES

Special properties in products are obtained by various methods: mechanical or chemical-thermal treatment of materials, casting, forging, welding, riveting and combined methods, but some methods do not allow to ensure the strength characteristics of the joint zone at the level of the main material, which reduces the duration of product operation [36].

When obtaining products with special properties, the most acceptable methods are types of casting, in which the joining of casting layers occurs due to diffusion penetration or sub-melting,

which makes it possible to use products under dynamic, shock and static loads. Usually, such castings are obtained by centrifugal and continuous casting methods, and sometimes by other methods.

In the manufacture of composite products, Al_2O_3 , SiO_2 , SiC , titanium carbides, vanadium, tungsten and others are used as reinforcing fillers.

One of the necessary conditions for obtaining a high-quality casting with special properties is the presence of a strong connection of its various layers. When used for the separation of two liquid metals, the interphase diffusion processes at the interface between the liquid metal and the partition have a great influence, thanks to which mass transfer, structural and phase transformations occur.

As research has shown, taking into account the fact that the diffusion coefficient in a liquid iron-carbon alloy is 4–6 orders of magnitude higher than in a solid one, the formation of the transition zone occurs mainly during solidification in the liquid phase. The longer the period when the alloy is in a liquid state, the wider the transition zone [37].

To obtain cast composite materials, various methods of liquid-phase connection of a metal matrix with high-strength reinforcing material of the required configuration are used.

The main technological schemes for obtaining composite castings are presented in the chapter [38]. The authors considered the general theoretical provisions of the processes occurring in the mold and which make it possible to obtain composite (reinforced) castings, recommended matrix alloys and grades of reinforcing phase (RP). It should be noted that castings with volumetric reinforcement, for example: metal rods, should be made by lost foam casting, because this method is "flexible" from the point of view of controlling the properties of the casting, and the mold and polystyrene pattern can be used as an active-functional system and tool for introducing reinforcing elements [39].

The liquid-phase method has significant advantages over other methods of obtaining reinforced structures and makes it possible to manufacture high-precision products with minimal force impact on reinforcing elements with the possibility of mechanization, automation and implementation of continuous technological processes. The RP mixing with the matrix melt is carried out under the influence of convection and circulation flows that arise in the liquid metal during the RP filling [38].

2.3.2 PRODUCTION TECHNOLOGIES OF CAST REINFORCED STRUCTURES, WHICH ARE OBTAINED BY LIQUID-PHASE COMBINATION OF SYSTEM COMPONENTS

The most effective method of obtaining materials with special functional properties from iron-carbon alloys is reinforcement during the liquid-phase combination of system components [38].

There are known options for manufacturing composite cast iron, which is locally reinforced with ceramics to increase abrasive wear resistance. At the same time, to ensure a uniform distribution of particles in the casting, it is necessary to fix the ceramic insert in the cavity of the mold, which leads to an increase in labor intensity during the production of castings [40].

The technology of casting according to gasified models is the most suitable for obtaining reinforced castings. There are options for local strengthening of cast materials by introducing

wear-resistant inserts to create locally strengthened areas based on refractory carbides in the polystyrene foam pattern [41].

It is also possible to modify gray cast iron with ferrosilicon FeSi45 using a dispersion-filled polystyrene pattern [42], that is, the polystyrene pattern is used as a tool for introduction into the mold cavity.

In order to obtain cast reinforced structures of guaranteed quality, the structure of the materials must be heterogeneous and consist of solid grains evenly distributed in the elastic-plastic matrix, and the adhesive bond must be maintained between the components. The maximum strength of the matrix alloy can be ensured using the pressure casting method, in which the pressure on the matrix alloy is maintained during the crystallization of the cast reinforced structure (CRS) using the direct impact of a pressing punch [43].

The liquid-phase method of combining the components of the reinforced system is divided into two groups: involuntary (gravitational) and forced impregnation.

When implementing the process of involuntary (gravitational) impregnation, reinforcing frames can be tied, simply placed in a casting mold or pre-aggregated (pre-tied). With this method, it is impossible to obtain reinforced castings of a complex shape, gas-shrinkage defects and the formation of an imperfect structure may occur during the CRS production.

During the process of forced impregnation with the help of additional mechanical influence on the matrix melt, there is an intensification of the flow of the melt on the surface of the reinforcing filler and the achievement of a better connection of the CRS components [44]. In order to obtain optimal reinforced systems and achieve maximum operational characteristics, it is necessary to establish technological parameters that determine the choice of composition and quantity of RP and matrix alloy (MA).

In order to achieve perfect results regarding the combination of the components of reinforced systems, a clear understanding of the technological bases of such combination is necessary, primarily from the point of view of the formation of macro-heterogeneous structures, the emergence of a simple connection between various elements of the system and, as a result, the emergence of the process of physical and chemical interaction at their boundaries contact [45].

When obtaining reinforced castings with macro-implants, which are placed in the cavity of a casting mold or in a polystyrene pattern, new multi-component systems for the theory of casting processes arise: "metal – model – implant – mold" and "metal – reinforcing phase – mold".

The technological process of manufacturing reinforced castings by casting according to gasified models is carried out according to the following scheme:

- preparation of components (calibration, cleaning and plating of the surface, provision of the reinforcing structure of the required shape and configuration);
- production of expanded polystyrene patterns with reinforcing elements;
- form assembly;
- matrix alloy filling, impregnation;
- holding time for solidification of the liquid phase;
- knocking out of the mold;
- thermal or mechanical treatment of reinforced products.

The AF influence on the formation of the structure and properties of cast reinforced structures was tested on cast reinforced materials from iron-carbon alloys (MA – gray and high-strength cast iron with spherical graphite, RP – metal rods (diameter 2 and 5 mm) made of Steel 20 and steel plate Steel 3 with a thickness of 0.3 and 0.7 mm).

When steel elements are used to reinforce cast iron castings, the intensification of heat and mass exchange processes in the transition zone and the increase in the values of the effective diffusion coefficients of chemical elements occurs due to the significant advantage of the mass of cast iron over steel. At the same time, the higher the degree of doping of the alloys that are joined, the smaller the value of the effective diffusion coefficients due to the lower mobility of the atoms of the alloying elements in the transition zone [45].

During the research, it was established that the steel partition with a thickness of 0.3 mm was deformed under the influence of gas-dynamic flows in the form and in the place where the metal was fed, it melted through in several places. The use of a steel plate made of Steel 3 with a thickness of 0.7 mm ensured complete preservation of the diaphragm (**Fig. 2.16**). The quality of the diffusion connection and the strength properties of the transition layer are determined by temperature conditions and physical and chemical processes at the interphase boundaries. The intense flow of heat and mass exchange processes during the interaction of cast iron with a partition made of St3 steel causes a significant melting of the partition. This is confirmed by the presence of a sufficiently large width of the transition zone – (0.15–0.18) mm (**Fig. 2.16**). In the process of interaction, the steel was intensively saturated with cast iron carbon and a zone with a lamellar pearlite structure (Pt1; PDO.5), characteristic of St5 steel, was formed along the junction boundary. The microstructure of cast iron is a pearlite base with carbide and graphite inclusions.

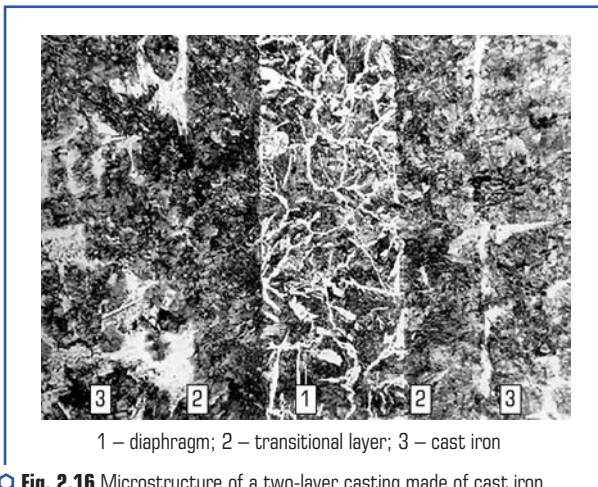


Fig. 2.16 Microstructure of a two-layer casting made of cast iron with a diaphragm made of a steel plate St3 with a thickness of 0.7 mm

Numerous oxidation-reduction reactions take place at the interface between the liquid metal and the solid partition. The process of interaction of liquid cast iron with a steel plate is characterized by high speeds and fairly deep penetration of elements deep into the steel plate due to the large difference in chemical potentials and mass of cast iron compared to the diaphragm.

The active flow of high-temperature oxidation-reduction processes is also facilitated by the long stay of cast iron in a liquid state at the place of metal supply.

Carburization of the surface layer of the steel diaphragm also occurs due to the local accumulation of the liquid carbon phase of the destruction of the model, which depends on hydrodynamic and convective flows in the melt in the process of filling the mold with metal.

A physical model of the mass and heat exchange of reinforcing materials was developed according to the established laws about the conditions of solidification, the movement of matrix alloys (MA) in molds with a macroreinforcing phase (MRP), the interaction of MA, MRP with a polystyrene foam pattern and its thermal destruction products in the form of liquid, gaseous, and solid phases elements and matrix alloy when forming the structure and properties of cast reinforced structures in multicomponent systems new for the theory of foundry processes: "metal – model – MRP – form".

The interaction of the macroreinforcing phase (MRP) with the matrix alloy (MA) in the cavity of the casting mold is shown in (Fig. 2.17). The MA enters the mold under the influence of hydrostatic or elevated pressure P_m , and comes into contact with the reinforcing phase (MRP), which can be located directly in the cavity of the mold or at the boundary of the "liquid metal – mold" system (Fig. 2.17).

When filling the casting mold, microexchange zones are formed around the MRP in the "MA – RP" system with the formation of a transition zone g_m , heat exchange in this system takes place along the contact surface S_f, S_{mp} with a characteristic parameter for RP – R_{RP} . The boundary temperature conditions at the heat exchange boundary of the MA – RP system $T_0 = 450$ °C, and the final temperature at the heat exchange boundary of this system:

$$T_f = \frac{T_L - T_S}{2}, \quad (2.1)$$

where T_L, T_S – the liquidus and solidus temperatures for the matrix alloy, °C.

For the integrated MA – RP system, the heat exchange contact area will be $n \cdot S_f, n \cdot S_{PR}$, respectively, where n is the number of MRP elements located in the cavity of the casting mold, pcs., and their mass will be:

$$m = 0.785 \times n \times g_{MRP} \times R_{MRP}^2 \times L_{MRP}, \text{ kg} \quad (2.2)$$

where g_{MRP} – density, kg/m³; L_{MRP} – the characteristic length of the MRP element, m.

The interaction of the matrix alloy, the macro-aluminous phase, the polystyrene pattern and its thermal destruction products with the liquid and solidifying metal occurs as follows [46]: at the moment when the MA melt (Fig. 2.17, item 2) enters the mold under the action of hydrostatic or increased PM pressure, which leads to rapid heating of the metal rod (MAF) placed

in the polystyrene pattern (**Fig. 2.17, item 1**), which is confirmed by the calculated data of the heating time of the rod along the entire height of the model to its gasification temperature (450 °C), which does not exceed 0.4...0.5 s.

In this and subsequent stages, filling the mold with vertical macreinforcing elements (MRE) installed in it (in our case in the form of rods) complicates the area of liquid metal flow (the mold) and exerts a certain influence on the thermophysical and hydrodynamic processes occurring in it.

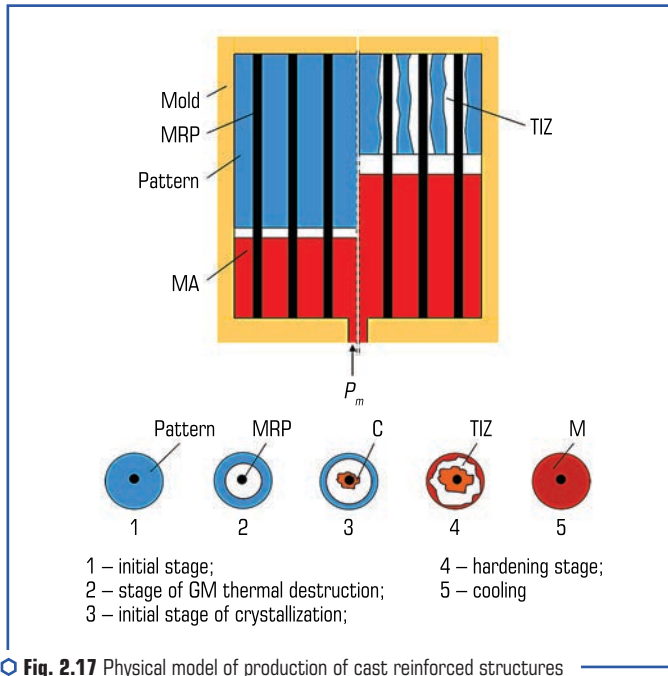


Fig. 2.17 Physical model of production of cast reinforced structures

In the next period of MA movement in the mold with the foam model, the initial stage of gasification of the pattern (**Fig. 2.17, item 2**) occurs in two directions: at the front of the liquid metal flow with the formation of a "metal – model" gap and around the rod with the formation of a "macreinforcing element (MRE) – model" gap. During this period, the products of thermal destruction of the model (vapor-gas phase (VGP), liquid phase (LF)) migrate into the mold through the gaps formed, and the gap "MRE – model" constantly increases and reaches the mold limit.

During the movement of thermal destruction products (VGP, LP and GP), partial condensation occurs on the rod (**Fig. 2.17, item 3**) with the formation of a border around the rod in the pyrocarbon form (PF), which leads to carbonization in the contact zone of the rod, the carbon content of which is clearly lower than in MA (cast iron, medium and high carbon steel). During this period, the

rod melts in the form of a decrease in its melting temperature, which contributes to the formation of a strong transition zone (**Fig. 2.17, item 4**) on the "MRP – MA" contact surface.

2.3.3 RESEARCH OF HEAT AND MASS EXCHANGE PROCESSES IN REINFORCED CASTINGS FROM IRON-CARBON ALLOYS

To evaluate the conditions of heat and mass transfer and solidification in reinforced castings made of iron-carbon alloys, cast samples of carbon steel (Steel 45L) with a size of $\varnothing 50 \times 200$ mm in a hollow sand mold made of loose refractory (LAC process) and a reinforcing phase in the form of rods (Steel 45), occupying 50 % of its cross-sectional area [47].

During computer modeling of the hardening of a casting $\varnothing 50$ mm made of 45L steel in a hollow form, it was established that on the contact surface "metal – form" this alloy reaches the temperature T_l after 8.9 s (**Fig. 2.18**), and the temperature T_s – after 165.0 s. During the same period, at a point located at a distance of 1/4 diameter from the surface of the casting, the alloy reaches the temperature T_l after 14.2 s, and the temperature T_s after 181.5 s. In the center of the casting, during the same period, the alloy reaches the temperature T_l after 8.5 s (**Fig. 2.18**), and the temperature T_s – after 211.5 s, then the liquid phase disappears in all sections of the casting.

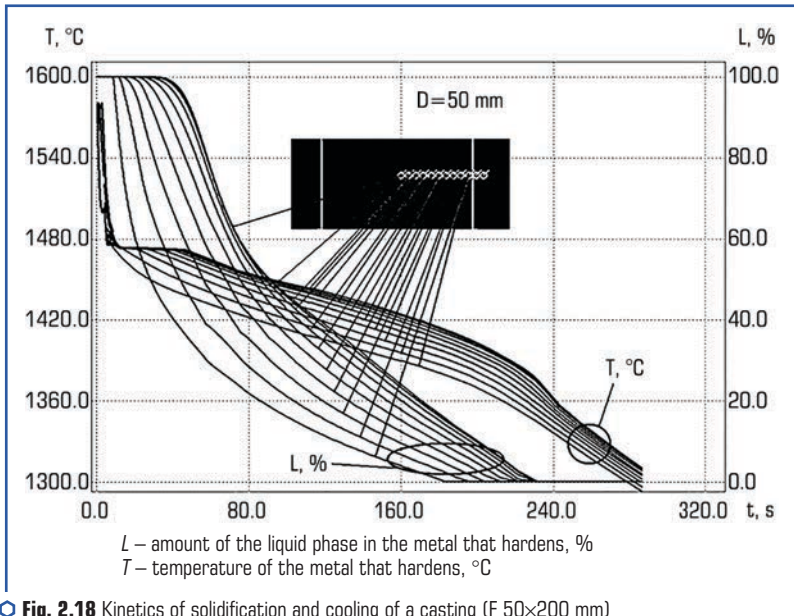


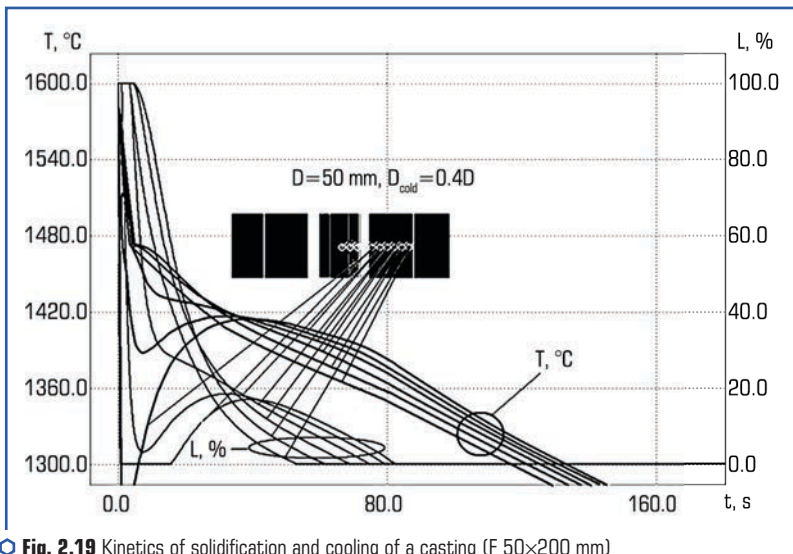
Fig. 2.18 Kinetics of solidification and cooling of a casting (F 50×200 mm) made of 45L steel in a hollow form

During the hardening of a $\varnothing 50$ mm casting made of 45L steel in a mold with MAF, which is $1/2$ of its diameter, it was established that on the contact surface "metal – mold" this alloy reaches the temperature T_l after 5.3 s (**Fig. 2.19**), and temperature T_s – after 42.0 s. During the same period, at a point located at a distance of $1/4$ of the diameter from the surface of the casting, the alloy reaches the temperature T_l after 8.8 s (**Fig. 2.19**), and the temperature T_s – after 124.0 s, and at the "metal – MRP" boundary, the alloy reaches the temperature T_l after 1.8 s (**Fig. 2.19**), and the temperature T_s – after 80.0 s, then the liquid phase disappears in all sections of the casting.

It should be noted that under these conditions, the surface and center of the MRP warms up to a maximum temperature of 1410 °C after 5.0 s, and then cools at a rate of 1.5 – 2.0 °C/s (**Fig. 2.20**).

It is also important to note that the rate of removal of overheating of the melt to the temperature T_l in all experiments differs from each other. Thus, when the sample solidifies in an empty form, this rate is 8.5 – 14.0 °C/s, and the lower value refers to the central part of the casting, and the cooling rate of the latter is already 4.0 – 5.0 °C/s, where the greater value refers to the surface of the rod.

During solidification of the casting in the form where the MRP is located, which is $1/2$ of its diameter, the speed at which the melt reaches the temperature T_l is 15.0 – 70.0 °C/s, and the higher value refers to the part of the casting adjacent to the boundary of the MRP, and the cooling rate of the casting is 2.0 – 3.0 °C/s, where the greater value refers to the "metal – MRP" contact surface.



○ **Fig. 2.19** Kinetics of solidification and cooling of a casting (F 50×200 mm) made of 45L steel in a mold with MRP (0.5D_{cast})

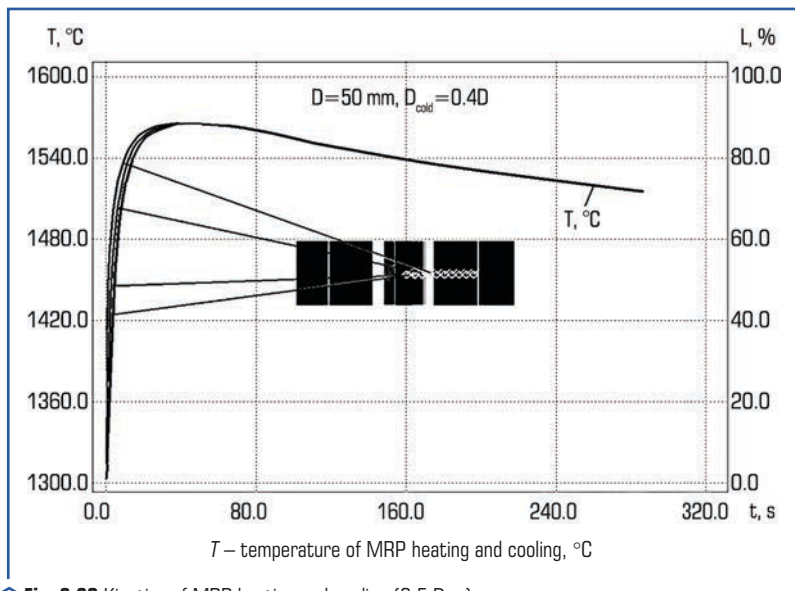


Fig. 2.20 Kinetics of MRP heating and cooling ($0.5 D_{\text{east}}$)

Based on the analysis of the received data, it was established:

- MRP presence creates conditions for increasing the rate of solidification of the alloy in direct proportion to its mass and with its increase in relation to the volume of metal in the mold, while the MRP presence in the mold significantly affects the removal of overheating of the alloy to a temperature T_i , which exceeds the similar one during solidification of the casting in a hollow mold in 1.4...2.0 times;
- MRP presence in the mold affects the cooling of the casting in the same way, but to a lesser extent, the ratio between the cooling rate of the casting in the hollow mold and in the MRP presence is only $1/(1.15...8.0)$;
- it is important to note that on the "MAF – metal" contact surface the hardening process proceeds initially with the rapid formation of a solid phase (freezing), then up to 15...20 % of the solid phase is formed in this layer. The final formation of solid metal around the MRP occurs when the previous layers have already crystallized.

2.3.4 SELECTION OF FUNCTIONAL SCHEMES FOR OBTAINING CAST REINFORCED STRUCTURES AND OPTIMIZATION OF THEIR TECHNOLOGICAL PARAMETERS

The analysis and generalization of methods for optimizing technological parameters, the mutual influence of MS and AF on the characteristics of cast reinforced structures (CRS)

and schemes for their production made it possible to create a system for selecting materials and technologies based on their functional characteristics. This system of choosing the optimal technological process and materials for obtaining high-quality cast products based on iron-carbon and non-ferrous alloys is based on the following functional links and blocks (**Fig. 2.21**):

1. The choice of cast reinforced materials L_0 is made in accordance with the requirements for the cast product, the properties of which are determined by a complex of mechanical, elastic-dynamic, corrosion-resistant and tribotechnical characteristics I_0 . Therefore, the choice of the necessary characteristics, such as mechanical A_{01} , elastic-dynamic A_{03} , corrosion-resistant A_{04} and tribotechnical A_{02} , is determined by the set of data I_0 and they functionally depend on the similar characteristics of the matrix alloy M_{01} – M_{02} and the reinforcing phase A_{01} – A_{02} . So, first, the characteristics of L_{01} – L_{02} are determined using adapted or created databases DB1–DB2, and then on this basis MS and AF are established, the properties of which are determined according to DB1 and DB2. Moreover, it is advisable to initially search for new CRSs from no less than two versions of the "MA₁ – RP₁" and "MA₂ – RP₂" systems, which are implemented as CRM₁ and CRM₂ with similar required characteristics to I_0 . Next, based on the selected characteristics of M_{01} – M_{02} and A_{01} – A_{02} , the chemical composition of M_{03} for M_{10}/M_{20} , as well as the type of A_{03} – A_{04} and the geometrical characteristics of A_0 for A_{10}/A_{20} are established. In order to choose the optimal CRM from n given ones, it is advisable to determine the complex quality indicator of each of them according to the equation of the form:

$$K_c = \sqrt{A^m B^l C^K D^S E^T \dots\dots W^Z Z^d Y^q X^l}, \quad (2.3)$$

where K_c – CRS comprehensive quality indicator; $A, B, C, \dots X$ – factors that determine the CRS properties; $m, l, e, s, \dots t$ are degrees of significance of the CRS qualities.

Moreover, the complex indicator K_c takes into account tribotechnical K_1 , mechanical K_2 , technological K_3 , thermo-mechanical K_4 , foundry K_5 , electrotechnical K_6 and elastic-plastic K_8 properties and economic indicators K_7 (**Fig. 2.21**). The values of the indicated indicators $A\dots X$ and their indices $m\dots l$ are determined by the method of expert evaluation by interviewing at least 25 specialists working in this field. The material for which the value of the K_c coefficient exceeds the analogues by at least 10 % is considered optimal.

2. After the CRS final selection, using the DB3 database, the MA and RP characteristics are set, including thermophysical M_{04} , foundry M_{05} , mechanical M_{01} , elastic-dynamic A_{01} , tribotechnical A_{02} , and finally the same parameters for the CRS (L_{01} – L_{02}). Based on the obtained data, the technological parameters of the process $T_1, t_c, t_p, T_{RP}, T_{MA}, T_f, V, H, P, t_{hard}$ and t_{cool} are determined according to the block diagram "T – t" (**Fig. 2.21**).

3. The choice of material and geometry of the F_0 mold is determined by the geometry of the casting, the thermophysical properties of the mold, the series of castings, and the preparation of a particular casting manufacturer.

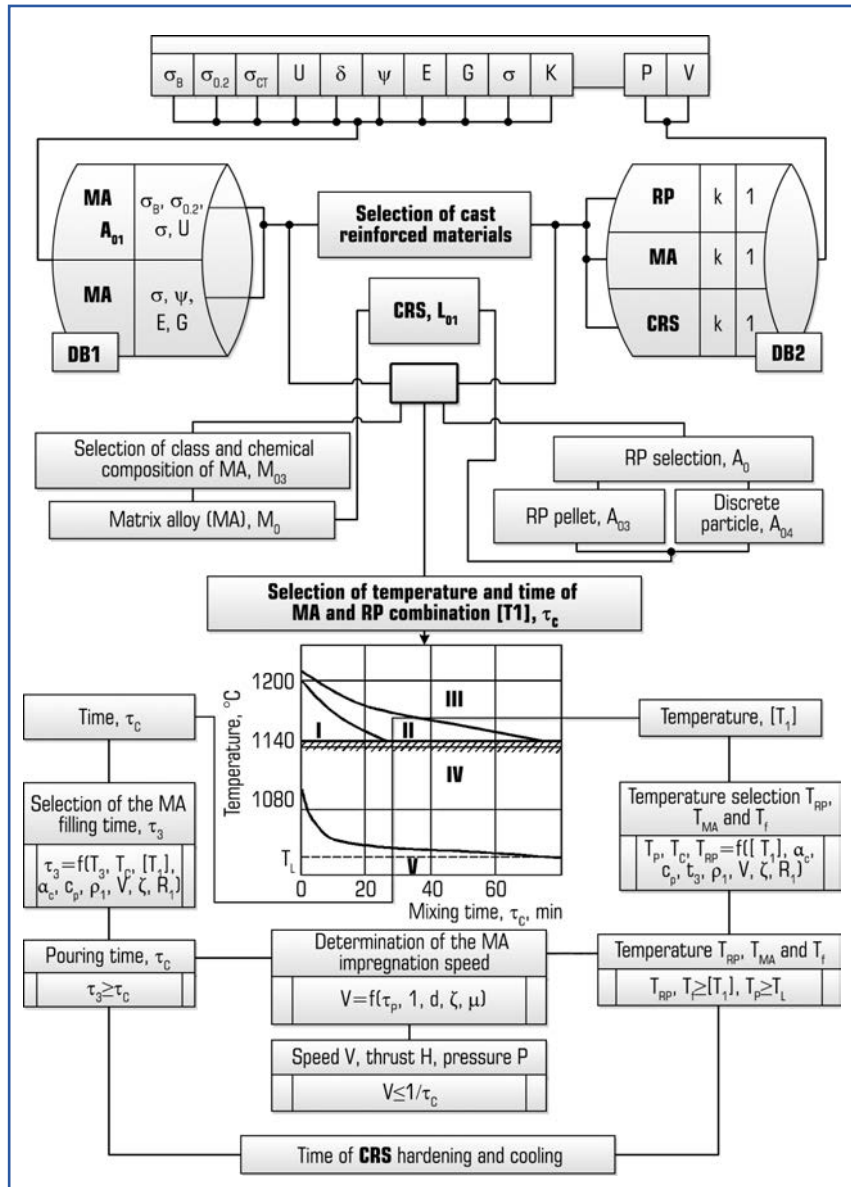


Fig. 2.21 Selection and optimization of materials and basic technological parameters for obtaining reinforced cast structures and castings with differential properties using macroreinforcing phase (MRP)

The method of pouring Z_0 is determined by the RP geometrical parameters, the MA casting properties (M_{05}), the geometry of the form F_0 , the specified speed $[V]$ and its filling time $[t_3]$, as well as the RP temperature $[T_1]$.

4. After choosing all the necessary casting parameters, materials, shape geometry and pouring method, it is advisable to determine the optimal implementation scheme of the technological process of obtaining varnish. The selection is carried out in accordance with the requirements of specific manufacturing processes of casting on gasified models.

CONCLUSIONS

The work presents scientific and practical results regarding the development of modern technological processes for the production of cast products and constructions of responsible purpose from aluminum, iron-carbon and heat-resistant alloys, namely:

- a complex of original equipment developed and used at the Physical and Technological Institute of Metals and Alloys of the National Academy of Sciences of Ukraine for the production of cast structural materials from aluminum alloys under the influence of electromagnetic, plasma kinetic, centrifugal effects on metal systems in a vacuum, which allows intensifying structural and phase transformations in alloys; disperse intermetallics and microgroups in alloys; evenly distribute alloying and strengthening particles in the liquid metal bath; control the rate of crystallization of the alloy; effectively doping alloys with active metals, in particular, using consumable electrodes in plasmatrongs; process alloys with carbon and silicon nanoparticles synthesized by reactions of carbon with silicon-containing media on crystalline metal centers and compounds that are introduced into the melt; increase the efficiency of plasma heating of liquid metal to $\geq 90\%$; to change the structure and properties of cast products by effective plasma effects on alloys;

- the improved design of the casting unit VIM-25-175C with the introduction of additional cooling, which led to the improvement of the cooling process of the crystallizer during directional crystallization and ensured obtaining a regular structure of castings of GTE blades made of heat-resistant alloys;

- a physical model of the heat and mass transfer of reinforcing elements and matrix alloy during the formation of the structure and properties of cast reinforced structures when lost foam casting, and the results of studies of heat and mass transfer processes in reinforced castings from iron-carbon alloys, which made it possible to establish that the MRP presence creates conditions for increasing the speed solidification of the alloy is directly proportional to its mass and with its increase in relation to the volume of metal in the mold, while the MRP presence in the mold significantly affects the removal of overheating of the alloy to the temperature T_i , which is 1.4...2.0 times higher than the similar casting in a hollow mold during solidification, while on the contact surface "MRP – metal" the solidification process proceeds initially with the rapid formation of a solid phase (freezing), then up to 15...20 % of the solid phase is formed in this layer. The final formation of solid metal around the MRP occurs when the previous layers have already crystallized.

The latest technologies have been developed:

- complex ecologically clean processes of processing and pouring of aluminum melts with the help of the created MHD equipment, in which vacuum-plasma systems are installed;
- production of castings of working blades of gas turbine engines with a regular structure by the method of directional crystallization;
- production of cast reinforced structures from iron-carbon alloys by the method of casting according to gasified models, with the possibility of optimizing their technological parameters depending on the initial casting data.

CONFLICT OF INTEREST

The authors declare that they have no conflict of interest in relation to this research, whether financial, personal, authorship or otherwise, that could affect the research and its results presented in this paper.

REFERENCES

1. Polyvoda, S. L., Siryi, O. V., Hordynia, O. M., Puzhailo, L. P. (2017). Pat. No. 119406 UA. Plavylno – lyvarnyi kompleks dlia napivbezperernogo lyttia zlyvkiv z aliuminiievykh splaviv. MPK B22D 11/14. No. u201703178; declared: 03.04.2017; published: 25.09.2017, Bul. No. 18. Available at: <https://uapatents.com/5-119406-plavilno-livarnijj-kompleks-dlya-napivbezperernogo-littya-zlyvkiv-z-alyuminievhikh-splaviv.html>
2. Puzhailo, L. P., Polyvoda, S. L., Siryi, O. V., Hordynia, O. M. (2019). Pat. No. 131179 UA. Sposib pryhotuvannya aliuminiievykh lihatur u mahnitohydrodynamichnykh ustanovkakh. MPK C22B 21/00. declared: 15.06.2018; published: 25.09.2008, Bul. No. 1. Available at: <https://base.uipv.org/searchINV/search.php?action=viewdetails&IdClaim=254473>
3. Polyvoda, S. L., Siryi, O. V., Puzhailo, L. P. (2013). Pat. No. 101343 UA. Method for producing high-strength aluminum wrought alloys containing zinc. MPK C22C 21/06, C22C 21/02, C22B 9/04, C22B 21/00. No. a201007359. declared: 26.12.2011; published: 25.03.2013, Bul. No. 6. Available at: <https://uapatents.com/5-101343-sposib-prigotuvannya-visokomicnikh-alyuminievhikh-deformivnikh-splaviv-z-vmistom-cinku.html>
4. Puzhailo, L. P., Siryi, O. V., Polyvoda, S. L. (2015). Pat. No. 108781 UA. Sposib rafinuvannya aliuminiievoho splavu u vakuumi. MPK C22B 21/00, C22B 9/04. No. a201310432. declared: 27.08.2013; published: 10.06.2015, Bul. No. 11. Available at: <https://uapatents.com/4-108781-sposib-rafinuvannya-alyuminievhogo-splavu-u-vakuumi.html>
5. Polyvoda, S. L., Polyvoda, M. O., Hordynia, O. M., Siryi, O. V., Puzhailo, L. P. (2017). Pat. No. 115590 UA. Sposib vyznachennia vmistu vodniu u ridkomu metali. MPK C22B 21/00,

- G01N 33/20, G01N 27/61, G01N 27/74. No. a201511064. declared: 12.11.2015; published: 27.11.2017, Bul. No. 22. Available at: <https://uapatents.com/6-115590-sposib-viz-nachennya-vmistu-vodnyu-u-ridkikh-alyumniehvikh-splavakh.html>
6. Naidek, V. L., Narivskiy, A. V., Lenda, Yu. P., Hanzha, M. S. (2006). Pat. No. 75166 UA. Vakuump plazmova ustanovka dlia obrobky metalichnykh rozplaviv u vannii. MPK C22B 9/00, H05H 1/26, C21C 7/072, C21C 7/10. No. 2004010693. declared: 30.01.2004; published: 15.03.2006, Bul. No. 3. Available at: <https://uapatents.com/3-75166-vakuump-lazmova-ustanovka-dlya-obrobki-metalichnykh-rozplaviv-u-vanni.html>
 7. Puzhailo, L. P., Polyvoda, S. L., Siryi, O. V., Hordynia, O. M. (2019). Pat. No. 131180 UA. Sposib napivbezperernogo lyttia zlyvkiv z aliuminiievykh splaviv, yaki mistiat lehkookysliuvani komponenty. MPK B22D 11/14, B22D 21/04. No. u201806809. declared: 15.06.2018; published: 10.01.2019, Bul. No. 1. Available at: <https://base.uipv.org/searchINV/search.php?action=viewdetails&IdClaim=254474>
 8. Puzhailo, L. P., Gavriiliuk, V. P., Seryi, A. V., Polivoda, S. L., Gordynia, A. N. (2012). Modelirovanie magnitogidrodinamicheskikh protsessov elektromagnitnogo peremeshivaniia aliuminievo-go splava v kristallizatore i teplovi nasadke pri poluneprieryvnom lite slitkov. Protssesy litia, 5, 54–60.
 9. Mitin, B. S., Petuhov, S. A., Puzhajlo, L. P., Serov, M. M., Frolov, V. D., Popel, P. S. (1995). Svoystva splavov Al-Cr-Zr, poluchennh jekstrakciej rasplava v jelektromagnitnom pole. Fizika i himija obrabotki materialov, 1, 110–116.
 10. Polyvoda, S. L., Siryi, O. V., Hordynia, O. M. (2020). Pat. No. 140659 UA. Ustanovka dlia otrymannia volokon z aliuminiievykh splaviv ekstrahuvanniam rozplavu. MPK B01D 11/00, B22D 11/06, B22D 11/16. No. u201907978. declared: 12.07.2019; published: 10.03.2020, Bul. No. 5. Available at: <https://base.uipv.org/searchINV/search.php?action=viewdetails&IdClaim=266530>
 11. Narivskiy, A. V., Moiseiev, Yu. V., Polyvoda, S. L., Siryi, O. V., Hordynia, O. M. (2020). Pat. No. 144020 UA. Sposib obroblennia splaviv u mahnitodynamichnii ustanovtsi. MPK C22B 9/05, C21C 1/00, B22D 1/00. No. u202001893. declared: 17.03.2020; published: 25.08.2020, Bul. No. 16. Available at: <https://base.uipv.org/searchINV/search.php?action=viewdetails&IdClaim=270921>
 12. Narivskiy, A. V., Shyriaieva, I. V., Hlike, A. P., Fedorov, V. V., Naidek, V. L. (2012). Pat. No. 98903 UA. Sposib rafinuвання splaviv vid domishok. MPK C21C 7/10, C22B 9/04, C21C 7/072. No. a201108029. declared: 25.06.2011; published: 25.06.2012, Bul. No. 12. Available at: <https://uapatents.com/6-98903-sposib-rafinuvannya-splaviv-vid-domishok.html>
 13. Dubodielov, V. I., Naidek, V. L., Narivskiy, A. V., Fedorov, V. V., Fiksen, V. M., Slazhniev, M. A. et al. (2014). Pat. No. 107390 UA. Sposib plazmovoho rafinuвання splaviv u mahnitodynamichnii ustanovtsi. MPK C22B 9/04, C22B 9/05, C21C 7/072, C21C 1/00. No. a201302218. declared: 22.02.2013; published: 25.12.2014, Bul. No. 24. Available at: <https://uapatents.com/6-107390-sposib-plazmovogo-rafinuvannya-splaviv-v-magnitodynamichnij-ustanovci.html>

14. Fikssen, V. M., Dubodielov, V. I., Naidek, V. L., Sychevskiy, A. A., Tunyk, V. O., Narivskiy, A. V., Hanzha, M. S. (2017). Pat. No. 113663. Sposib plazmovoï obrobky splaviv v mahnitodynamichnii ustanovtsi. MPK C22B 9/05, C21C 1/00, C21C 7/072, C22B 9/04, B22D 1/00. No. a201502163. declared: 12.03.2015; published: 27.02.2017, Bul. No. 4. Available at: <https://uapatents.com/6-113663-sposib-plazmovo-obrobki-splaviv-v-magnitodynamichnii-ustanovci.html>
15. Narivskiy, A. V., Dubodielov, V. I., Moiseiev, Yu. V., Hanzha, M. S., Narivskiy, O. A., Davydenko, V. M. et al. (2019). Pat. No. 136171 UA. Sposib plazmovoï obrobky splaviv u mahnitodynamichnii ustanovtsi. MPK C22B 9/05, C21C 7/072, B22D 1/00. No. u201901368. declared: 11.02.2019; published: 12.08.2019, Bul. No. 15. Available at: <https://base.uipv.org/searchINV/search.php?action=viewdetails&IdClaim=260764>
16. Dubodielov, V. I., Narivskiy, A. V., Naidek, V. L., Naumovets, A. H., Seredenko, V. O., Fikssen, V. M. et al. (2020). Pat. No. 121619 UA. Sposib oderzhannia lytykh kompozytsiinykh materialiv na metalevii osnovi. MPK B22D 19/14, B22D 27/20, B22D 27/02, C22F 3/00, C22C 1/03, C22B 9/05, C22C 1/00. No. a201810552. declared: 25.10.2018; published: 25.06.2020, Bul. No. 12. Available at: <https://base.uipv.org/searchINV/search.php?action=viewdetails&IdClaim=269065>
17. Naidek, V. L., Narivskiy, A. V., Hanzha, M. S., Bilenkiy, D. M., Sychevskiy, A. A. (2004). Pat. No. 69091 A UA. Sposib obrobky ridkoho metalu. MPK: C22B 9/04, C22B 9/05. No. 20031210928. declared: 02.12.2003; published: 16.08.2004, Bul. No. 8. Available at: <https://base.uipv.org/searchINV/search.php?action=viewdetails&IdClaim=77511>
18. Naidek, V. L., Narivskiy, A. V., Kurpas, V. I., Bilenkiy, D. M., Hanzha, M. S. (2006). Pat. No. 75829 UA. Sposib vakuum-plazmovoï obrobky kolorovykh splaviv. MPK C22B 9/00, H05H 1/26. No. 20041109751. declared: 26.11.2004; published: 15.05.2006, Bul. No. 5. Available at: <https://uapatents.com/3-75829-sposib-vakuum-plazmovo-obrobki-kolorovykh-splaviv.html>
19. Naidek, V. L., Narivskiy, A. V., Dubodielov, V. I., Smyrnov, O. M., Yakobshe, R. Ya., Kurpas, V. I. et al. (2008). Pat. No. 81701 UA. Sposib obrobky ridkoho metalu v promizhnomu kovshi. MPK C22B 9/04, C22B 9/00, C22B 9/05, C22B 9/22, H05H 1/26. No. a200603972. declared: 10.04.2006; published: 25.01.2008, Bul. No. 2. Available at: <https://base.uipv.org/searchINV/search.php?action=viewdetails&IdClaim=11291>
20. Naidek, V. L., Narivskiy, A. V., Bilenkiy, D. M., Hanzha, M. S., Piontkovska, N. S., Sychevskiy, A. A. et al. (2009). Pat. No. 85988 UA. Sposib vakuumno-plazmovoï obrobky rozplavu metalu. MPK C22B 9/04, C22B 9/05. No. a200806948. declared: 19.05.2008; published: 10.03.2009, Bul. No. 5. Available at: <https://uapatents.com/3-85988-sposib-vakuumno-plazmovo-obrobki-rozplavu-metalu.html>
21. Balitskii, A. I., Kvasnytska, Y. H., Ivaskevich, L. M., Mialnitsa, H. P. (2018). Hydrogen and corrosion resistance of Ni-Co superalloys for gas turbine engines blades. Archives of Materials Science and Engineering, 91 (1), 5–14. doi: <https://doi.org/10.5604/01.3001.0012.1380>

22. Balitskii, A. I., Kvasnytska, Y. H., Ivaskevych, L. M., Kvasnytska, K. H., Balitskii, O. A., Shalevska, I. A. et al. (2023). Hydrogen and Corrosion Resistance of Nickel Superalloys for Gas Turbines, Engines Cooled Blades. *Energies*, 16 (3), 1154. doi: <https://doi.org/10.3390/en16031154>
23. Ivaskevich, L., Balitskii, A., Kvasnytska, I., Kvasnytska, K., Myalnitza, H. (2022). Thermal Stability, Cyclic Durability and Hydrogen Resistance of Cast Nickel-Cobalt Alloys for Gas Turbine Blades. *Advances in Mechanical and Power Engineering*, 147–155. doi: https://doi.org/10.1007/978-3-031-18487-1_15
24. Kvasnytska, Yu. H., Ivaskevych, L. M., Balytskyi, O. I., Maksyuta, I. I., Myalnitza, H. P. (2020). High-Temperature Salt Corrosion of a Heat-Resistant Nickel Alloy. *Materials Science*, 56 (3), 432–440. doi: <https://doi.org/10.1007/s11003-020-00447-5>
25. Kuznetsov, V. P., Lesnikov, V. P., Konakova, I. P., Popov, N. A., Kvasnytska, Yu. G. (2015). Structural and Phase Transformations in Single-Crystal Rhenium- and Ruthenium-Alloyed Nickel Alloy Under Testing For Long-Term Strength. *Metal Science and Heat Treatment*, 57 (7–8), 503–506. doi: <https://doi.org/10.1007/s11041-015-9912-4>
26. Hlotka, A. A., Haiduk, S. V. (2020). Prediction of the Thermodynamic Processes of Phase Separation in Single-Crystal Refractory Alloys Based on Nickel. *Materials Science*, 55 (6), 878–883. doi: <https://doi.org/10.1007/s11003-020-00382-5>
27. Paton, B. E. (Ed.) (1987). *Zharoprochnost liteinykh nikelevykh splavov i zashchita ikh ot okisleniia*. Kyiv: Nauk. Dumka, 256.
28. Fu, H., Geng, X. (2001). High rate directional solidification and its application in single crystal superalloys. *Science and Technology of Advanced Materials*, 2, 197–204. doi: [https://doi.org/10.1016/S1468-6996\(01\)00049-3](https://doi.org/10.1016/S1468-6996(01)00049-3)
29. Wu, X., Makineni, S. K., Liebscher, C. H., Dehm, G., Rezaei Mianroodi, J., Shanthraj, P. et al. (2020). Unveiling the Re effect in Ni-based single crystal superalloys. *Nature Communications*, 11 (1). doi: <https://doi.org/10.1038/s41467-019-14062-9>
30. Konter, M., Kats, E., Hofmann, N. (2000). A Novel Casting Process for Single Crystal Gas Turbine Components. *Superalloys*, 189–200. Available at: https://www.tms.org/Superalloys/10.7449/2000/Superalloys_2000_189_200.pdf
31. Hu, S., Yang, W., Li, Z., Xu, H., Huang, T., Zhang, J. et al. (2021). Formation mechanisms and control method for stray grains at melt-back region of Ni-based single crystal seed. *Progress in Natural Science: Materials International*, 31 (4), 624–632. doi: <https://doi.org/10.1016/j.pnsc.2021.07.004>
32. Specification Z88YF1-S2 for Supplying Remelting Stocks of Alloy CM-88Y, Technical specifications of "Zorya"- "Mashproekt" GTRPC. (2016). Mykolaiv: National Technical University "KhPI".
33. Lapin, J., Gebura, M., Pelachova, T., Nazmy, M. (2008). Coarsening kinetics of cuboidal gamma prime precipitates in single crystal nickel base superalloy CMSX-4. *Kovove Mater*, 46 (6), 313–322. Available at: <http://www.kovmat.sav.sk/issue.php?nr=46&cc=6>

34. Kvasnytska, Y. H., Ivaskevich, L. M., Balitskii, A. I., Kvasnytska, K. H., Mialnitsa, H. P. (2022). Structural and Mechanical Properties of the Nickel Alloy of Gas-Turbine Engine Blades. *Materials Science*, 57 (5), 688–694. doi: <https://doi.org/10.1007/s11003-022-00596-9>
35. Shalevska, I. (2020). Kompleks tekhnolohichnykh protsesiv ekolohichno bezpechnoho vyrobnytstva vylykviv z prohnovozanymy funktsionalnymy vlastyvoistyamy za modeliyamy, shcho hazyfikuiutsia. Kyiv: Fyzyko-tekhnolohichnyi instytut metaliv ta splaviv Natsionalnoi akademii nauk Ukrainy, 416.
36. Chung, D. D. L. (2010). *Composite Materials. Science and Applications*. Springer, 358. doi: <https://doi.org/10.1007/978-3-030-28983-6>
37. Lysenko, T. V., Yasiukov, V. V., Prokopovych, Y. V. (2019). Kontseptsyy upravleniya formoobrazovanyem otlivok. Odessa: Ekolohyia, 272.
38. Shinsky, O., Shalevska, I., Kaliuzhnyi, P., Shinsky, V., Lysenko, T., Shevchuk, T. et al. (2018). Principles of construction and identification of a multilevel system for monitoring parameters of technological cycle of casting. *Eastern-European Journal of Enterprise Technologies*, 5 (1 (95)), 25–32. doi: <https://doi.org/10.15587/1729-4061.2018.141303>
39. Dulska, A., Studnicki, A., Szajnar, J. (2017). Reinforcing cast iron with composite insert. *Archives of Metallurgy and Materials*. 62 (1), 355–357. doi: <https://doi.org/10.1515/amm-2017-0054>
40. Anikeev, A. N., Chumanov, I. V. (2018). Microstructure and Hardness of a Dispersion-Reinforced Casting. *Russian Metallurgy (Metally)*, 12, 1161–1164. doi: <https://doi.org/10.1134/S0036029518120030>
41. Nebozhak, I. A., Sumenkova, V. V., Tkachuk, I. V., Shynskiy, O. Y. (2001). Osoblyvosti strukturoutvorennia SCh20, modyfikovanoho FS75 u porozhnyini lyvarnoi formy za HAMOLYV – protsesom. *Metaloznavstvo ta obrobka metaliv*, 4, 43–49.
42. Włodarczyk-Fligier, A., Dobrzański, L. A., Kremzer, M., Adamiak, M. (2008). Manufacturing of aluminium matrix composite materials reinforced by Al2O3 particles. *Journal of Achievements in Materials and Manufacturing Engineering*, 1 (27), 99–102. Available at: http://jamme.acmsse.h2.pl/papers_vol27_1/27123.pdf
43. Shalevska, I., Kaliuzhnyi, P. (2019). Physical modeling of the hydrodynamic processes of casting molds pouring filled with a locally oriented reinforcing phase. *Technology Transfer: Fundamental Principles and Innovative Technical Solutions*, 55–57. doi: <https://doi.org/10.21303/2585-6847.2019.001042>
44. Shalevska, I. A., Musbah, J. I. (2020). Obtaining Cast Reinforced Structures by Liquid Phase Combination of System Components. *Casting processes*, 1 (139), 69–75. doi: <https://doi.org/10.15407/plit2020.01.069>
45. Shalevska, I. A. (2019). Research of heat-exchange processes in a casting form with reinforcing phase. *Foundry Production and Metallurgy*, 3, 54–59. doi: <https://doi.org/10.21122/1683-6065-2019-3-54-59>
46. Shinsky, I., Shalevska, I., Musbah, J. (2015). Efficiency of influence of a metal macroreinforcing phase on process of solidification of large-sized castings. *TEKA. Edition of Lublin University of technology*, 15 (2), 51–59.

CHAPTER 3

**REGULARITIES OF THE FORMATION OF STRUCTURE,
PHASE COMPOSITION AND TRIBOLOGICAL PROPERTIES
OF HEAT-RESISTANT CHROMIUM-NICKEL ALLOYS "NIKORIN"****ABSTRACT**

In this work, new solutions have been obtained for a scientific and practical problem, which consists in increasing the complex of tribological properties and heat resistance of chromium-nickel alloys for modern mechanical engineering. The composition of heat-resistant chromium-nickel alloys is investigated. The distribution of alloying elements between phases and structural components is studied, the dependence of the change in mechanical properties on the parameters of the structure and phase composition is established.

Calorimetric analysis of the alloys under study during heating/cooling is carried out. The crystallization/melting temperatures of the nickel-chromium alloy "Nikorin" were determined. The structure, phase composition, microhardness of the structural components of the heat-resistant chromium-nickel alloy "Nikorin" after quenching from various temperatures have been studied. The tribological properties of chromium-nickel alloys in the cast state are investigated.

KEYWORDS

Chromium-nickel alloys, structure, austenite, hardness, wear rate, wear resistance index.

Nowadays, chromium and nickel-based alloys – the most complex, have amazing properties of all alloys – are widely used to make parts that are exposed to the most heat. They are used at high homologous temperatures compared to any conventional alloy system.

The main group of such alloys is made up of heat-resistant alloys with high long-term strength and creep limits at a temperature of 700 °C and above. In terms of chemical and phase composition, heat-resistant high-chromium alloys are very diverse, since chromium and nickel have a large number of extremely soluble alloying elements that have a positive effect on their heat resistance. This can explain the significant possibilities and reserves for increasing the heat resistance of high-chromium alloys. As the content of chromium, titanium and aluminum in these alloys increases, their characteristics of long-term strength increase, since these elements

form reinforcing excess phases $\eta(\text{Ni}_3\text{Ti})$, $\gamma'(\text{Ni}_3\text{Al})$, $\text{Ni}_3(\text{Al}, \text{Ti})$, as well as chromium and titanium carbides, which strengthen the alloys. Complications of the chemical composition of high-chromium and chromium-nickel alloys with promising refractory alloying elements in the presence of a sufficient number of hardening phases further increase the heat resistance of high-chromium and chromium-nickel alloys.

From the point of view of the dependence of the technological properties of nickel on the chromium content in the solid solution, attention was drawn to the fact that as the chromium concentration increases, the plasticity of the alloys decreases. Alloys with chromium content above 30 % are quite tough, therefore their processing in a cold state becomes complicated, although the limiting solubility of chromium in nickel is 34–35 %. The combination of physicochemical, electrical and technological properties of chromium-nickel alloys has determined the areas of practical application of alloys of this system.

At present, heat-resistant chromium-nickel alloys have come to one of the first places in terms of their importance and are widely used in various fields of technology.

The experience of domestic and foreign industry and special studies indicate that the most promising structural materials for operation under friction at elevated temperatures and various loads are nickel-chromium alloys "Nikorin". These alloys are used for the manufacture of rolling tools (gauges, mandrels for hot tube rolling mills). The most outstanding properties of high-chromium irons are high wear resistivity (with a low temperature coefficient) and high-temperature strength. This determined a specific and fairly wide area of application of these alloys. They are used for the manufacture of rolls, armor plates, blades of shot blasting machines, grinding balls, rolling tools (gauges and roll mandrels) [1]. The stability of the "Nikorin" alloy mandrels significantly exceeds the stability of the high-chromium iron mandrels in the as-cast condition.

In this regard, the purpose of this work is to study the structure, phase composition and wear resistance of the nickel-chromium alloy "Nikorin".

3.1 A CONTEMPORARY VIEW ABOUT THE PATTERNS OF STRUCTURE FORMATION, PHASE COMPOSITION, MECHANICAL AND TRIBOLOGICAL PROPERTIES OF HIGH-CHROMIUM AND CHROMIUM-NICKEL ALLOYS

3.1.1 PATTERNS OF STRUCTURE FORMATION IN HEAT-RESISTANT HIGH-CHROMIUM AND CHROMIUM-NICKEL ALLOYS

3.1.1.1 FEATURES OF STRUCTURE FORMATION IN HIGH-CHROMIUM ALLOYS

Increasing the service life of machine parts that wear out quickly is the most important problem in modern mechanical engineering. The short service life of parts reduces the economic efficiency of many machines and industrial equipment and leads to irrecoverable loss of metal.

Modern high-chromium alloys are complex-alloyed multicomponent alloys, differing in structure and properties. They represent a separate group of industrial alloys, the hardening of which forms a carbide phase. It is this, in combination with a certain type of matrix, which determines the specific properties of high-chromium alloys and at the same time creates significant difficulties in the production and operation of these alloys.

High chromium alloys have a complex metal matrix structure. Depending on the chemical composition, mass, cooling rate of the ingots or the type of heat treatment, it consists of austenite, martensite and their decomposition products, the ratio of which can vary within wide limits. Until now, no clear position has been formed that determines the optimal phase composition and structure of the metal matrix, both in terms of wear-resisting properties and mechanical properties (impact hardness and strength). Some authors take the martensite matrix as the optimal one, which provides maximum wear-resisting properties [1–3]. Other authors [4, 5] give preference to metastable austenite. There is evidence that the ultimate wear-resisting properties can be obtained with a mixed microstructure – martensite and metastable austenite [6, 7].

A similar picture is observed in the analysis of literature sources, in which the effect of the matrix on the strength characteristics of high-chromium alloys was studied. According to various studies, it is believed that the best is the austenite-martensite base [6], purely austenitic [4], martensitic [8]. There is an opinion [9] that the structure of the metal matrix does not affect the strength of high-chromium alloys at all. Naturally, the complexity of the structure, inhomogeneity of the composition of the solid solution, various methods of obtaining and testing castings lead to ambiguous and contradictory conclusions about the dependence of properties on the type of structure of the metal base.

High chromium alloys are widely used in industry. Parts made of high-chromium alloys operating under abrasive and shock-abrasive wear conditions, both at room temperature and at elevated temperatures. Industrial high-chromium alloys are complex multicomponent systems that contain permanent impurities (phosphorus, sulfur, oxygen, hydrogen, nitrogen), as well as various alloying elements.

By changing the chemical composition, the type of modifying and alloying impurities, the conditions of hardening and cooling in the solid state, it is possible to regulate the physicomechanical and operational properties of wear-resistant high-chromium alloys over a wide range.

The wear resistance of high-chromium alloys is determined by the amount, size, morphology, microhardness of eutectic and secondary carbides and a metal base – the main structural components of these alloys [10].

In wear-resistant high-chromium alloys based on the Fe-C-Cr system, depending on the ratio of carbon and chromium, carbides of the $(\text{Fe}, \text{Cr})_3\text{C}$ type are formed; $(\text{Cr}, \text{Fe})_7\text{C}_3$; $(\text{Cr}, \text{Fe})_{23}\text{C}_6$. The carbide $(\text{Cr}, \text{Fe})_7\text{C}_3$, has the highest hardness, especially along the axis of its crystal lattice [11].

The high wear resistance of the solid phase (in particular, carbides in high-chromium alloys) can manifest itself only when this phase is firmly fixed in the matrix and the degree of plastic deformation of the matrix is low [11]. With weak fixation of even very hard carbides in a soft plastic (for example, ferrite or pearlite) matrix, the high potential stability of carbides during abrasive wear is not realized.

When choosing the alloy composition, first of all, one should take into account the value of the ratio of carbide-forming elements and carbon. This ratio should be such as to ensure that the required amount of carbides is obtained in the alloy. To obtain the most alloyed carbides, the ratio of the carbide-forming element content to the carbon content must reach certain (critical) values. This ratio for chromium is (at. %) $\text{Cr/C} \geq 4.5$ [12]. It is quite obvious that not every increase in the content of carbon or carbide-forming elements will unambiguously increase wear resistance. In complex-alloyed high-chromium alloys, the type of carbides depends on the affinity of the carbide-forming elements to carbon and their quantitative content. With a close atomic content, the leading element in the formation of carbides is the element that is most similar to carbon.

The experience of domestic and foreign industry and special studies indicate that high-chromium and chromium-nickel alloys are the most promising structural materials for operation under shock loads, as well as under friction conditions at room and elevated temperatures.

3.1.1.2 FORMATION OF THE STRUCTURE OF CHROMIUM-NICKEL ALLOYS

At present, nickel-based alloys are used as heat-resistant materials intended for operation at temperatures from 700 to 1100 °C. Heat-resistant nickel alloys, in terms of their importance, have come out on top and are widely used in various branches of technology. This is explained by the fact that heat-resistant nickel alloys successfully combine high heat resistance, scale resistance and manufacturability.

Alloying nickel with chromium (up to 50 %) increases its stability in oxidizing environments, for example, in boiling solutions of nitric and chromic acids.

The main advantage of nickel-chromium alloys (>20 % Cr) is their high corrosion resistance in nitric acid solutions in the presence of a fluorine ion and higher heat resistance at high temperatures.

Many works have been devoted to the study of the Ni-Cr phase diagram. By this time, the most acceptable diagram seems to be given by Taylor and Floyd, which is characterized by a long-focus transformation with the limiting solubility of the components. **Fig. 3.1** shows a refined phase diagram of the Ni-Cr eutectic type system [13], according to which the eutectic crystallizes at 1345 °C and 49 % Cr. On the nickel side, there is a wide region of a γ -solid solution with an fcc lattice (structure of the A1 type, $a=0.358\text{--}0.359$ nm). The solubility of chromium in nickel at 1345, 1100, 600, and 20 °C is 47, 43, 35 and 30 %, respectively. The chromium-based alpha solid solution (structure of type A2, $a=0.288$ nm) has a bcc lattice and exists in a much smaller concentration range than the γ -solid solution.

For a long time, there remained controversial questions about the existence in the Ni-Cr system of a eutectoid transformation due to high-temperature allotropic transformation in chromium, as well as about the possibility of the formation of the σ -phase. For the first time, Blum and Grant, on the basis of X-ray and microscopic studies, concluded that eutectoid transformation occurs in the Ni-Cr system at a temperature of about 1180 °C and 35 % Ni. The assumption about

the possibility of the formation of the σ -phase in the Ni-Cr system was first expressed by A. Sully on the basis of theoretical considerations

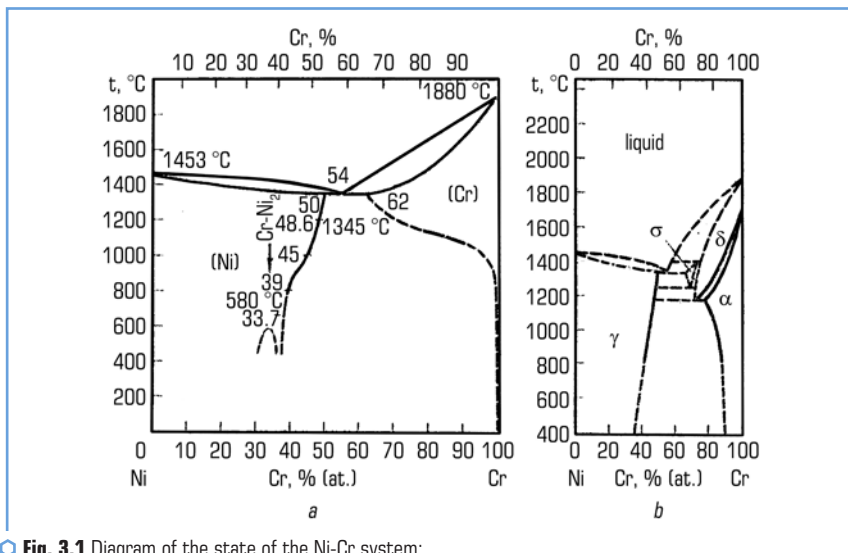


Fig. 3.1 Diagram of the state of the Ni-Cr system: *a* – according to the data [13]; *b* – according to the data [14]

Yukawa, Haida and others [14] investigated by X-ray analysis particles of Ni-Cr alloys with a size of 10–100 nm, obtained by evaporation of alloys in argon under pressure and proposed a state diagram of Ni-Cr, in which, in addition to α - and γ -solid solutions due to the mutual solubility of nickel and chromium, the established limits for the existence of the σ -phase as intermetallic compounds, and the δ -phase (high-temperature allotropic modification of chromium), as shown in **Fig. 3.1, b**. In this case, the σ -phase has a β – U type structure (space group D_{6h}^8 , $a=0.881$ – 0.882 nm). The structure of the δ -phase is assigned to type A15, $a=0.458$ nm.

Another feature of the Ni-Cr system is that in a wide range of chromium concentrations (from 19.0 to 36 % (at)), the γ -solid solution is ordered with the formation of a Ni_2Cr superstructure [15, 16]. Transition temperature order – disorder alloys from 25.0; 29.2; 33.3 (stoichiometric composition) and 36.6 % (at.) Cr, respectively 540, 580, 590, 585 °C [15–17].

Ye. S. Vintaykin and H. H. Urushadze [18–20] proposed a peritectoid type of state diagram at low temperatures. At about 580 °C, an ordered phase (Ni_2Cr), a disordered γ -solid solution, and an α -phase can be in equilibrium.

The study of the structure of the ordered phase, carried out by the methods of X-ray diffraction, neutron diffraction [16, 17], and electron microscopy [21], showed that it belongs to the Pt_2Mo type. This structure is characterized by a layered arrangement of atoms:

parallel to the $\{110\}$ initial fcc lattice, two layers of nickel atoms and a layer of chromium atoms alternate. The unit cell of an ordered Ni_2Cr alloy is orthorhombic (space group $D_{2h}^{25} = \text{Immm}$), contains 4 nickel atoms and 2 chromium atoms. The unit cell parameters of the ordered phase are determined by the relations:

$$a = 3a_{\text{fcc}}/\sqrt{2}; \quad b = a_{\text{fcc}}/\sqrt{2}; \quad c = a_{\text{fcc}}. \quad (3.1)$$

The Curie point of nickel-chromium alloys decreases with increasing chromium content and reaches room temperature at about 8 at. % Cr. Therefore, under normal conditions, none of the industrial alloys has magnetic properties.

3.1.2 STRUCTURAL TRANSFORMATIONS IN CHROMIUM-NICKEL ALLOYS

In nickel alloys with 30–50 % Cr, which are of interest as a basis for heat-resistant materials characterized by high stability at elevated temperatures, the following structural transformations are possible:

- 1) the formation of intermetallic γ' -phases from a fcc lattice of the $\text{Ni}_3(\text{Al}, \text{Ti})$ type;
- 2) the order of the γ -solid solution with the formation of the Ni_2Cr superstructure in alloys with 30–33 % Cr, or 33–36 % (at) at temperatures below 580 °C;
- 3) precipitation of the α -phase from the γ -solid solution in alloys with >39 % Cr at 600–900 °C;
- 4) carbide formation is due to the temperature dependence of the solubility of carbon in the γ -solid solution. The main carbide is Me_{23}C_6 which precipitates mainly along the grain boundaries in the temperature range 600–1000 °C with short holding times.

3.1.2.1 FORMATION OF γ' -PHASE

The amount and nature of the distribution of the γ' -phase in heat-resistant chromium-nickel alloys depend on alloying, cooling rates during solidification of the casting and heat treatment [17].

The γ' -phase is a unique intermetallic phase. When interacting with dislocations, it contributes to the strengthening of the antiphase limits of the γ - γ' -alloy. By the way, the strength of the γ' -phase increases with increasing temperature. In addition, the hereditary plasticity of the γ' -phase prevents strong embrittlement, in contrast to strengthening by phases that have a higher hardness, for example, carbides. Also, its action is directly opposite to strong embrittlement during the formation of brittle σ - or Laves phases. The γ' -phase was first observed in the form of spheroidal particles, then cubic; later it was found that their shape is associated with the magnitude of the mismatch between the lattice parameters of the matrix and precipitates.

According to the observations of Hagel and Beatti, γ' -particles have a spherical shape with a lattice mismatch of 0–0.2 %, cubic – with a lattice mismatch of 0.5–1.0 % and a lamellar shape with values of more than 1.25 % [22].

3.1.2.2 ORDERING BY Ni_2Cr TYPE

Alloys containing up to 39 % Cr are single-phase. However, in the range of chromium concentrations of 30–33 %, there is an ordered Ni_2Cr phase. The ordering temperature in an alloy of stoichiometric composition Ni + 30.5 % Cr is 590 °C. In the quenched state, the structure of an alloy of stoichiometric composition is characterized by short-range order in the arrangement of atoms.

For the development of ordering, substantial hypothermia (~90 °C) is required. However, even at 500 °C, which corresponds to the maximum speed of improvement, the process is sluggish: to achieve an equilibrium degree of the order of Ni_2Cr at 500 °C, it takes ~500 h ordering in the Ni_2Cr system is a first-order phase transition and proceeds according to a homogeneous mechanism [23–25].

The development of the ordering process according to the Ni_2Cr type leads to a significant increase in the strength properties [24] and to the electrosupport [25].

3.1.2.3 FORMATION OF α -PHASE

In accordance with the equilibrium phase diagram of Ni-Cr [26], alloys with 30–40 % Cr (0.03 % C and 0.1 % Si) in the state of quenching from 1100 °C in water have the structure of a γ -solid solution with a grain size No. 5–6 and hardness ~210 HB. In the structure of alloys containing more than 43 % Cr, along with the γ -solid solution after quenching from 1100 °C, the α -phase is present. The amount of the latter increases with increasing chromium content. In an alloy with 50 % Cr, the α -phase appears in the form of relatively large particles with a size of 20–70 and 1–5 microns, elongated along the rolling direction, and also in the form of separate globular precipitates less than 1 micron. The grain size in these alloys during quenching decreases approximately to No. 7 and the hardness increases to 290 HB [24].

Alloys containing more than 39 % Cr are subject to precipitation hardening. Tempering at 600–900 °C causes the decomposition of the γ -solid solution with the release of the α -phase, as well as carbides of the Me_{23}C_6 type.

The morphology, size, distribution and quantity of the α -phase are determined primarily by the content of the main element of chromium in the alloy and the temperature-time regime of tempering; as well as the presence of additional alloying elements in the alloy (Mn, Fe, Ti, Al, C, etc.).

The type of precipitation of the α -phase in Ni – 40–50 % Cr alloys is classified as cellular or discontinuous.

In alloys with 40 % Cr, boundary cellular precipitates of the α -phase (colonies of "pearlite-like" structure) are observed in the structure after 1:00 tempering at 700–800 °C, which practically does not affect the change in the hardness of the quenched alloy (**Fig. 3.1, b**). Tempering at 600–900 °C of alloys with 45, 50 and 55 % Cr causes intense decomposition of the nickel-chromium solid solution, which is accompanied by abundant precipitation of the α -phase throughout the volume [24, 15, 16]. At the same time, in an alloy with 45 % Cr, after 700–800 °C tempering, there is mainly a lamellar α -phase, the size of the plates and the distance between them increase with an increase in the tempering temperature. In an alloy with 50 % Cr, a predominantly globular α -phase is precipitated, which grows larger with increasing temperature. The separation of the α -phase from the supersaturated solid solution leads to an increase in the hardness of the alloy (**Fig. 3.2**).

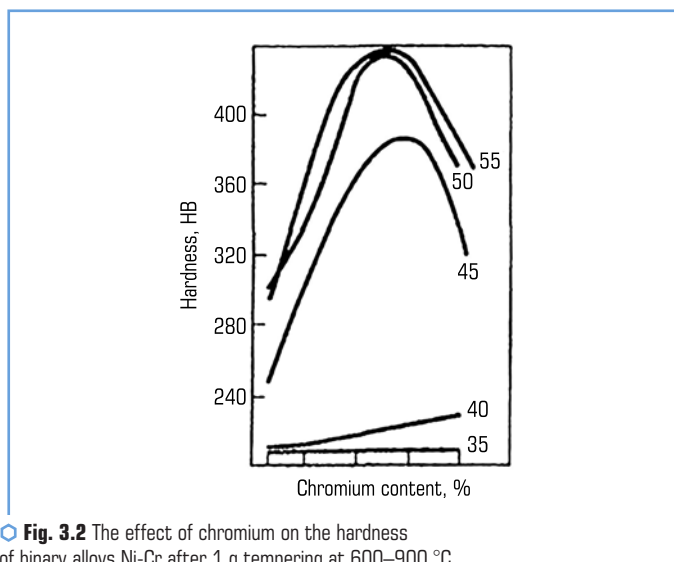


Fig. 3.2 The effect of chromium on the hardness of binary alloys Ni-Cr after 1 g tempering at 600–900 °C. Quenching from 1100 °C in water (figures in Cr % curves) Source [16]

3.1.2.4 CARBIDE FORMING

Depending on alloying and heat treatment, carbide phases of various types are formed in heat-resistant alloys. Most of the carbon is bound in the primary low-soluble titanium carbide of the TiC type, and in the presence of nitrogen – in titanium carbonitrides Ti(CN). Titanium carbides form a eutectic with nickel, which has a lower melting point, which is the reason for their distribution in the middendritic volumes.

The distribution of titanium carbides and nitrides in the cast structure of heat-resistant chromium-nickel alloys depends on the crystallization conditions (pouring temperature and cooling rate). When pouring from high temperatures and slow cooling, carbides and carbonitrides are coarser and, standing out along the grain boundaries, form a network (frame) when rapidly cooling, they are precipitated as smaller formations. On thin sections of titanium carbide or carbonitrides, they look like cubic or polyhedral pink inclusions.

In addition to titanium carbides and carbonitrides, carbon in cast nickel alloys forms double carbides. These carbides are precipitated into carbides of the Cr_{23}C_6 type predominantly along the crystal boundaries in the form of a mesh or rim, which negatively affects the ductility of the alloys. The shape of the distribution of double carbides depends on the heat treatment mode: the higher the hardening temperature, the coarser the precipitation [26, 27].

3.1.3 CARBIDES IN HEAT-RESISTANT CHROMIUM-NICKEL ALLOYS

The role of carbides in heat-resistant alloys is complex and dynamic. Nowadays, most researchers come to the conclusion that carbides actually have an important and beneficial effect on the long-term strength at high temperatures. In addition, it is clear that the morphology of carbides has an effect on ductility. Also, carbides can affect the chemical stability of the matrix through the bonding of electrons interacting with carbon.

In alloyed heat-resistant nickel alloys, such carbides are formed as: MeC , Me_{23}C_6 , Cr_7C_3 and Me_6C . Their type and stability are determined by alloying – the content of carbon and strong carbide-forming elements (tantalum, hafnium, niobium, titanium, etc.), as well as the concentration and ratio in the alloy of other, less strong carbide-forming agents – chromium, tungsten, molybdenum. The morphology of carbides, as well as their size, mainly depend on the conditions of crystallization and alloying.

MeC carbides are formed in heat-resistant alloys at temperatures slightly below their solidification temperature. They exist in the form of individual particles, unevenly distributed in the alloy along the boundaries and within the grains [28, 29]. These carbides have fcc lattice and are the most durable and fairly stable phases. In carbide reactions in alloys, they serve as the main source of carbon, since they are rich in this element in comparison with other carbides. They are stable up to about 1300 °C [28]. They are formed from a simple combination of carbon and reactive or refractory metals and are characterized by a classic formula like TiC or TaC . In order of decreasing their stability, they are arranged in the series of TAC , NbC , TiC and VC . The composition of MeC carbides in real alloys includes tungsten and molybdenum, as well as nickel and chromium in smaller amounts, while the binding forces in MeC carbides weaken and decomposition reactions can occur, leading to the formation of other types of carbides.

Carbides Me_6C are formed in nickel heat-resistant alloys at temperatures of 815–980 °C. They are similar to carbide Me_{23}C_6 , but are usually formed with a high content of refractory metal.

These carbides are formed in alloys with a high content of tungsten and molybdenum and are precipitated both along the grain boundaries and within them. Carbides of the Me_6C type have a complex cubic structure. Me_6C carbides are formed when chromium is replaced by molybdenum or tungsten in other carbides. In contrast to the more stable carbide $Me_{23}C_6$, their compositions can vary within wide limits. Since Me_6C carbides are stable at temperatures higher than those of $Me_{23}C_6$ carbide, their precipitation along the grain boundaries is more preferable and can be used to control the grain size.

The chromium content of more than 8–12 % already leads to the formation in the structure of chromium-nickel alloys of the primary trigonal carbide, which has the formula Cr_7C_3 . Carbides of this type are located in chromium-nickel alloys in the form of irregularly shaped particles. Usually, in alloys with a complex composition, Cr_7C_3 carbides are unstable and can transform into $Me_{23}C_6$ during aging. With a less complex chemical composition, Cr_7C_3 carbides strengthen the structure of heat-resistant alloys.

In the Ni-Cr system, which contains more than 30 % Cr, the main equilibrium carbide phase is $Cr_{23}C_6$, which has a complex fcc lattice (of the D_{34} type) with a cube edge $a=1.060$ nm. The $Me_{23}C_6$ unit cell contains 92 metal atoms and 24 carbon atoms and consists of 8 octants, in each of which the vertices are alternately surrounded by cuboctahedra (48h-position) and simple cubes (32f-position). In addition, metal atoms can also occupy the centers of the cuboctahedron (4a-position of the cell vertex, considered) and one of the most spacious center of each octant (8c-positions). Carbide $Cr_{23}C_6$ is characterized by a very narrow homogeneity region, due to which, in terms of the ratio of metal and carbon atoms, it almost always represents a phase of stoichiometric composition [28]. Compound $Me_{23}C_6$ can be a carbide of one element, for example, chromium ($Cr_{23}C_6$); however, according to the principle of chemical indifference [29], chromium atoms can be replaced by atoms of other elements (Fe, Ni, Mn). In pure $Cr_{23}C_6$, iron can replace up to 30 at. % Cr, while occupying predominantly cubic f-positions [30].

In $Me_{23}C_6$ carbide, each carbon atom is surrounded by eight metal atoms located along the vertices of a quadrangular prism.

With insignificant decarburization, $Me_{23}C_6$ carbides can transform into bcc structures (for example, α -Cr) or into the σ -phase. The actual nature of the $Me_{23}C_6 \rightarrow \alpha$ -phase transition is determined by the structural relationship and diffusion rates.

The solubility of carbon in nickel alloys with 30–45 % Cr is small and decreases with increasing chromium content and decreasing heating temperature.

At 800 °C, the solubility of carbon in alloys with 35–45 % Cr decreases by more than an order of magnitude.

Carbides $Me_{23}C_6$ are formed during heat treatment or operation at 600–1000 °C. They stand out mainly along the grain boundaries, sometimes they can be observed along the twin line and on stacking faults.

The location and size of carbides are determined by the content of chromium, additional and impurity elements in the alloy, and by the heat treatment mode. Carbide $Me_{23}C_6$ dissolves at 1100 °C [27, 24].

In alloys with a chromium content of 30–39 % Cr after tempering at 600–900 °C for 10 min. Up to 100 hours, only particles of $Me_{23}C_6$ carbide are present at the grain boundaries, the size of which increases with increasing temperature and heating duration. In alloys containing more than 39 % Cr, along with precipitates of carbides, cellular precipitates of the α -phase based on Cr are formed. With an increase in the chromium content in the alloy (up to 50 %), the temperature-time interval of its appearance shifts towards lower temperatures and short-term exposures. So, if in an alloy with 40 % Cr after 10 hours of tempering at 600 °C, only $Me_{23}C_6$ carbide is present within the limits, then in an alloy with 50 % Cr after a similar tempering, the α -phase is also present along with carbide.

3.1.4 INFLUENCE OF ALLOYING ELEMENTS ON THE STRUCTURE AND PROPERTIES OF HIGH-CHROMIUM NICKEL ALLOYS

In terms of chemical and phase composition, heat-resistant nickel alloys are very diverse, since nickel has a greater number of extremely soluble alloying elements, which have a positive effect on its heat resistance. This can explain the significant possibilities and reserves for increasing the heat resistance of nickel alloys.

The choice of alloying elements and their optimal composition in heat-resistant nickel alloys must be approached with caution, given their effect on the various properties of the alloys. In particular, chromium, widely used for alloying nickel, which strengthens the nickel solid solution by reducing the rate of diffusion processes, must be added to heat-resistant nickel alloys in different amounts, since the alloys are intended for different operating temperatures.

Chromium is added to heat-resistant chromium-nickel alloys to increase oxidation resistance at high temperatures, and the more, the higher its content in the alloys.

An increase in the chromium content in chromium-nickel alloys strengthens the alloys of this system: the creep resistance at high temperatures approximately doubles.

In alloys with an austenitic matrix, chromium increases the binding energy of the atoms of the crystal lattice of the γ -solid solution, somewhat increases the heat-resistant properties and the recrystallization temperature of doped austenite.

In nickel heat-resistant alloys, chromium reduces the amount of the γ' -phase that is formed during decomposition, worsens the thermal stability of the γ' -phase and thereby negatively affects the durability and ductility. In addition, more than other elements, chromium extends the crystallization range of alloys, worsens their manufacturability. At the same time, a decrease in the chromium content leads to an inevitable deterioration in heat resistance.

Chromium forms with carbon a number of carbides ($Cr_{23}C_6$, Cr_7C_3), which, as a result of quenching and aging, precipitating in a γ -solid solution in a highly dispersive state, strengthen austenite alloys.

Chromium carbides have a relatively low thermal stability, and therefore the increase in the heat resistance of austenitic alloys due to only such carbides is insufficiently effective.

Manganese promotes the expansion of the γ -area of the nickel-chromium system, forming alloys with an austenitic structure. Manganese as iron, cobalt and copper forms a continuous solid solution with nickel at 1000 °C.

As an austenite-forming element, manganese is less effective than nickel, especially with high chromium content. Therefore, it is advisable to introduce small amounts of carbon or nitrogen together with manganese, which promotes the strong development of precipitation hardening processes [25].

Manganese reduces the critical cooling rate and increases quench susceptibility and cross-sectional improvement.

Manganese somewhat increases the solubility of chromium carbides (Cr_7C_3) in austenite, which also depends on the chromium content [26].

Aluminum. As the content of titanium and aluminum in Ni-Cr alloys increases, their characteristics of long-term high-temperature strength increase, since these elements form, reinforcing, excess phases. In this case, aluminum has a strong effect on the amount of γ' -phase in nickel-chromium-titanium alloys. With an increase in the amount of aluminum, the content of alloying elements in the γ' -phase increases sharply. For example, when the aluminum content is 0.6 %, the amount of γ' -phase is 5.1 %; at 1.7 % Al – 25.5 %; at 4.1 % Al – 42.5 %. According to the Ni-Al-Ti phase diagrams, aluminum has a significant effect on the solubility of titanium in nickel. So, at 1150 °C, the titanium solubility in nickel decreases from 13 to 8 % with an aluminum content of up to 5 %. At 750 °C, this phenomenon is even more pronounced. Titanium has a similar effect on the solubility of aluminum in nickel.

Aluminum, introduced into complex alloyed nickel-chromium heat-resistant alloys, causes a very strong effect on the increase of heat-resistant properties of these alloys, and the more, the higher its content. However, if the amount of aluminum is more than 3–4 %, then difficulties arise during forging, which limits the possibility of a stronger alloying with this element of hard-to-form heat-resistant alloys.

Titanium. The region of solid solutions rich in nickel at 1150 °C extends in the nickel-titanium binary system up to 13 % titanium, and in the nickel-chromium-titanium ternary system at 20 % Cr up to about 10 % Ti.

With decreasing temperature, the solubility of titanium in the binary and ternary systems drops sharply. So, at 750 °C in the Ni-Ti binary system the solubility of titanium is already 10 %, and in ternary alloys with 20 % Cr – about 4 %. Apparently, with a further decrease in temperature, the titanium solubility in the Ni – Cr solid solution drops even more sharply, and alloys with a titanium content of less than 4 % at room temperature may already be two-phase. The introduction of up to 3 % titanium into chromium-nickel alloys promotes the formation of highly dispersed intermetallic phases at moderate temperatures, thereby increasing the resistance of the alloy to plastic deformation and increasing the long-term strength at 800 °C to 15 kg/mm².

It was found that the characteristic temperature, long-term strength limits, and internal friction increase with the penetration of titanium into a chromium-nickel alloy. However, the composition of heat-resistant alloys, in addition to titanium, as a rule, includes aluminum [27].

Carbon. Despite the small amount of carbon in heat-resistant nickel alloys, it has a great influence on their structure and properties, as it forms not only hardly soluble titanium carbide, but also chromium carbides Cr_{23}C_6 , Cr_7C_3 , Me_6C .

In chromium-nickel alloys, part of the carbon is bound in primary titanium carbides TiC or carbonitrides (TiCN), and the other part in chromium carbonitrides of the CrCN type.

The introduction of carbon into chromium-nickel alloys promotes the stabilization of austenite in the $\gamma \rightarrow \alpha$ transformation ratio and thereby expands the possibilities of alloying the solid solution with ferrite-flammable elements while maintaining the austenite structure of Cr_{23}C_6 , Cr_7C_3 .

Carbon has a large and variable with temperature solubility in γ -solid solution compared to solubility in α -solid solution, providing austenitic alloys with the ability to precipitation hardening as a result of heat treatment and increasing their mechanical properties at room and elevated temperatures.

Strengthening of austenitic alloys with carbon occurs due to the formation of chromium carbides of the Me_{23}C_6 type. However, the great tendency of chromium carbides to coagulate does not allow obtaining a large strengthening effect at high temperatures, although the mechanical properties at room temperature are greatly enhanced.

The greatest strengthening effect at high temperatures is achieved as a result of complex alloying, when several alloying elements are simultaneously introduced into the solid solution.

Iron. The study of the effect of iron in nickel-based alloys made it possible to establish that in heat-resistant alloys of a simpler composition, it is possible to admit the content of 5–8 % iron in the EI437BU alloy, the introduction of 5 % iron practically does not change the heat resistance and technological properties.

The expansion of the boundaries of the iron content up to 5 % in alloys of the EI437 type allows using ferrochrome instead of metallic chromium in their smelting. Foreign nickel-based nimonic alloys 80A, 90.95 contain up to 5 % Fe, and nimonic alloys 100 and 105 – up to 10 % [31].

In complex-alloyed heat-resistant alloys, the introduction of iron somewhat worsens the heat-resistant properties and its content should not exceed 1–2 %.

Silicon, which is present in heat-resistant nickel alloys with intermetallic reinforcement, has a negative effect on long-term strength. The higher the aluminum and titanium content, the lower the silicon content should be.

According to some data, for a number of alloys there are limitations in technical conditions: the silicon content is allowed no more than 0.3–0.5 %.

The example of the EI787 alloy clearly shows the negative effect of silicon.

Vanadium. Vanadium is sometimes added to austenitic alloys in small amounts (up to 0.3 %) to improve technological characteristics.

The introduction of a large amount of vanadium into these alloys does not have a positive effect on the heat-resistant properties, which is associated with the weakening of the binding energy of atoms in the crystal lattice of the γ -solid solution. In austenitic alloys, vanadium is added

together with carbon, which greatly increases the tendency of the alloy to precipitation hardening. As a result of aging, the strength characteristics of the alloy increase both at room temperature and at elevated temperatures, the plastic properties decrease with an increase in the content of vanadium and carbon.

With the introduction of vanadium and carbon, the strengthening proceeds due to the intensive formation of highly dispersed vanadium carbides VC and chromium carbides Cr_{23}C_6 with some mutual solubility of vanadium in chromium carbide and chromium in vanadium carbide.

Excessive alloying of alloys with vanadium and carbon promotes the intensive formation of carbide particles during aging, which leads to sharp embrittlement of the material during operation at high temperatures. Vanadium increases the heat resistance of alloys as long as it retains a sufficient reserve of plasticity and phase precipitation occurs uniformly [32].

The addition of vanadium together with carbon in chromium-nickel or even better chromium-manganese alloys is very expedient and has a positive effect on the heat-resistant properties of the alloys. However, the addition of only vanadium with carbon does not ensure the fulfillment of the requirements currently imposed on high-temperature alloys.

The best results are obtained when vanadium and carbon are added simultaneously with refractory metals (Mo, W, Nb) in certain combinations. This is explained by the fact that vanadium and carbon impart to the γ -solid solution the ability to develop precipitation hardening processes, and refractory elements inhibit diffuse exchange at higher temperatures, making it difficult for the coagulation of dispersed phases and not strengthening of the alloy.

Molybdenum. The introduction of molybdenum into nickel alloys increases the recrystallization temperature of γ -solid solutions and inhibits their softening.

The activation energy of self-diffusion of iron or chromium increases with an increase in the amount of molybdenum added to the alloy.

In most alloys, alloying with molybdenum, along with an increase in heat resistance, gives an increase in plasticity during short-term and long-term tests.

Molybdenum has a much greater effect on the heat resistance of precipitation-hardening alloys with carbide or intermetallic strengthening.

The effectiveness of the effect of molybdenum on the heat-resistant properties of alloyed alloys increases when they are introduced into the alloy simultaneously with other elements, including elements that cause precipitation hardening processes. In this case, molybdenum inhibits the softening of the alloy at higher temperatures due to the fact that it complicates the diffuse exchange, recrystallization and coagulation of dispersed particles.

In carbide-reinforced nickel-base creep alloys, molybdenum also has a positive effect by increasing creep resistance. In a number of alloys, molybdenum forms phases of the Laves type (Fe_2Mo), which contributes to an even greater increase in heat resistance due to precipitation hardening processes.

3.1.5 HEAT RESISTANCE OF CHROMIUM-NICKEL ALLOYS

The phenomenon of creep of metals under load at high temperatures was known for many years, and the first studies of this phenomenon are about a century ago. At first, however, progress towards improving the properties of metals was rather slow. Serious attempts to develop new materials with higher creep resistance began only from the time when the operating temperatures of steam engines rose so much that ordinary low-alloy steels were unsuitable for the manufacture of parts of these machines [33].

At present, nickel-based alloys are used as heat-resistant materials designed to operate at temperatures from 700 to 1100 °C. They are used in gas turbines for engines of aircraft, ships, power generation systems, in the manufacture of rocket and space technology, in petrochemical equipment. Thus, in an aircraft gas turbine engine, more than 70 % of the mass is made up of heat-resistant alloys based on nickel, chromium-nickel and iron-nickel bases – these are discs, nozzle and rotor blades of turbines, combustion chambers, etc. The use of these alloys in the manufacture of stationary gas turbines has also sharply increased, since an increase in operating temperatures can significantly improve their technical and economic indicators.

The most difficult conditions are for turbine blades operating at temperatures of 850–1050 °C. They are subjected to significant tensile stresses as a result of centrifugal loads; these stresses cause creep of parts. The high-speed gas flow of high aggressiveness and the operating mode cause the occurrence of variable mechanical and thermal loads, which cause high-temperature and thermal fatigue, the active development of gas corrosion and erosion processes. The nozzle blades operate at temperatures up to 1150 °C and low stresses, and the disks – at temperatures of 600–800 °C and higher working loads (up to 500–600 MPa), therefore the heat-resistant alloys used for these groups of parts differ significantly in composition and properties.

Modern nickel heat-resistant alloys are essentially working to their limit, as operating temperatures often reach 0.8–0.85 solidus temperatures.

Therefore, the development of new technological processes, such as directional crystallization, growing parts in a monocrystallite state, the use of alloys reinforced with dispersed oxide particles, and the use of alloys reinforced with refractory wires, is of paramount importance in increasing the temperature level of modern heat-resistant alloys, their reliability and durability.

Modern high-temperature nickel-based alloys are very complex: they are included in 7–9 basic alloying elements and a large amount of impurities, their content should be controlled in the alloy.

Depending on the chemical and phase composition, structure, and basic properties, modern chromium-nickel alloys designed for operation at high temperatures can be divided into three large groups: heat-resistant, corrosion-resistant, and heat-resistant alloys [34].

Heat resistance is the ability of steels and alloys to withstand mechanical loads at high temperatures for a certain time.

Heat resistance is a structural and sensory property and, as such, is essentially determined by the structural features of the structure of the material and, first of all, its defectiveness –

by dislocations, their origin, movement, interaction with obstacles and boundaries and their disappearance. Point and spatial defects are also significant.

The main group of nickel alloys is made up of heat-resistant alloys with high long-term strength and creep limits at a temperature of 800 °C and above.

Nickel forms solid solutions with many elements, provides significant opportunities for achieving high heat resistance of alloys based on it. At 1000 °C, cobalt, iron, manganese and copper form unlimited solid solutions, and such refractory metals as chromium, tungsten, molybdenum, tantalum, niobium, vanadium – limited solid solutions with different regions of homogeneity. The solubility of elements such as titanium and aluminum at 1000 °C is 10 % and 7 %, respectively.

Pure nickel at 800 °C has $\sigma(100) = 40 \text{ Mn/m}^2$ (4 kgf/mm²). With the introduction of 20 % Cr into nickel, the long-term strength $\sigma(100)$ increases only to 50–55 Mn/m² (5–5.5 kgf/mm²), while the addition of titanium up to 2 % and 0.7 % aluminum abruptly increases $\sigma(100)$ to 150 Mn/m² (15 kgf/mm²).

It is important to note that the solubility of alloying elements in multicomponent nickel-based alloys can differ significantly in the direction of decreasing the values obtained in the study of binary nickel alloys – alloying element.

Most alloying elements, soluble in nickel or nichrome, are effective hardeners and increase the creep resistance of nickel-based alloys.

Despite the complexity of reports of heat-resistant nickel alloys, the following basic principles can be formulated that are used in their creation:

1) heat-resistant alloys are the main (matrix) solid solution on a chromium-nickel base, alloyed with cobalt and refractory elements-hardener, and the most effective effect is the heat resistance is the complex introduction of alloying elements. The content of these elements in the alloy depends on its purpose and economic feasibility;

2) titanium and aluminum, sometimes niobium, are necessarily present in the alloys, which mainly provide the formation of the main hardening phase of these alloys (γ' -phase);

3) are present in alloys chromium and aluminum provide resistance to gas corrosion due to the formation of protective films rich in oxides Cr₂O₃ and Al₂O₃;

4) carbon is contained in alloys in small amounts, forming carbides and carbonitrides. The kinetics of precipitation and morphology of carbide phases during crystallization, heat treatment, and during operation also largely determines the heat resistance of nickel-based alloys.

Thus, the high-temperature strength of nickel-based alloys is associated with the optimization of their composition according to the ratio of alloying elements included in the matrix γ -solid solution and strengthening intermetallic and carbonitride phases.

Operating temperature and operating stresses are decisive factors in the development of high-temperature nickel-chromium alloys. If the magnitude of stresses depends on the design of the part, then the level of operating temperatures determines the efficiency and main technical characteristics of the product.

With an increase in temperature, the strength of interatomic bonds decreases, the processes of diffusion and disintegration intensify. The mechanism and rate of gas corrosion, the mechanism of plastic deformation and destruction change depending on the temperature.

The operating mode of the chromium-nickel alloy – the nature of temperature and load changes over time – has a great influence on the heat resistance. In the presence of thermal changes, materials are exposed to thermal fatigue, which can sharply (several times) increase the creep rate or lead to the destruction of the part even in the absence of mechanical loads due to only thermal stresses (thermal fatigue). The action of alternating stresses, causing the development of high-temperature fatigue, can also strongly affect the heat resistance and heat resistance.

The composition of the gas environment can also significantly affect the heat resistance and heat resistance of alloys. The presence of aggressive components in the environment (for example, compounds containing sulfur, vanadium, halogens, alkali metals) causes the formation of low-melting or volatile compounds, destroys protective oxide films, and promotes the development of local types of gas corrosion. In addition, in many cases, the gas environment affects the alloy not in stationary conditions, but dynamically, that is, high-speed gas flows act on the surface of the parts, the speed of which can be hundreds and thousands of meters per second. Such operating conditions are typical, for example, for gas turbine blades, skin parts for high-speed aircraft and rockets. Under the influence of high-speed gas flows, creep processes are enhanced, as a result of which the operational resistance of the parts decreases.

Therefore, when determining the suitability of an alloy for operation in a loaded state at high temperatures, it is necessary to take into account not only the results of standard tests for creep and long-term strength, but also the possible change in these characteristics under operating conditions. This requires complex tests to be carried out as closely as possible to the work of the part in real conditions.

3.1.6 MODERN TRENDS IN THE DEVELOPMENT AND USE OF HIGH-TEMPERATURE NICKEL-CHROMIUM ALLOYS "NIKORIN" FOR THE MANUFACTURE OF MANDRELS FOR TUBE ROLLING MILLS

The mandrel longitudinal rolling states used in tube rolling mills have significantly less variety than the helical rolling states. This is primarily due to the fact that they all perform one function: in these states, the walls are rolled out and a rough pipe is obtained from the sleeve. In addition, only double-roll stands have a mandrel state for longitudinal rolling, which also reduces the type of states.

All states can be divided into two groups. The first group includes states of a linear type, with one or two working stands. Rolling in these states is carried out on a short cone-shaped mandrel fixed at the end of a long rod. Longitudinal rolling is based on the deformation of the metal by rolls located parallel in one plane and rotating in different directions; the metal rolling axis is perpendicular to the major roll axes.

The second group of states – multi-stand continuous states, in which rolling is carried out on a long mandrel (floating or held). Floating mandrel rolling is much more widespread. In our time, they began to use a held mandrel, which moves during the deformation of the pipe at a given speed. Floating mandrels of great length (18–20 m) with a diameter of more than 180–200 mm are quite heavy, difficult to transport, require the use of bulky equipment; great difficulties are caused by the manufacture of such mandrels. This is why, for large continuous states, retained mandrels are used, which are about half the length. Rolling on a retained mandrel increases the accuracy of pipes and is therefore also used for rolling smaller pipes [35].

The continuous mill carries out the rolling process in the most progressive and promising way. These units are characterized by the continuity and flow of production, a high degree of mechanization and automation, the best quality of pipes compared to other production methods. Tube-rolling units with an unrepeatable state allow to increase the rolling speed with a short duration of auxiliary operations and large metal deformations, using thick-walled sleeves for this purpose, increases the productivity of the entire TPA complex. The advantage of continuous rolling is also the possibility of obtaining thin-walled pipes of greater length and higher quality (without risks, scratches, with less transverse and longitudinal ripening). Due to the large length of the pipes, tension-reduction states are more efficiently used.

The states of the first group can be single-cast (automatic-state) or double-cast (tandem mill) with the distance between the stands more than the length of the pipe is rolled. Sometimes the two-state is called semicontinuous. Single-stand automatic states carry out rolling in two (and sometimes three) passes in the same caliber and for the task for each subsequent pass the pipe is turned on the front (input) table with the help of reverse feed friction rollers.

Automatic states can have multi-groove rolls (with a number of caliber up to 11–12) or single-groove rolls. In the first case, as one gauge wears out, they switch to rolling in another. Otherwise wear of the groove means the need to replace the rolls. Single-gauge stands are lighter and transshipment is usually carried out by replacing the stands: instead of a stand with worn rolls, a stand with new rolls is installed, assembled aside on a special stand. A very important advantage of single-gauge stands is their increased rigidity, which ensures higher accuracy of pipes with wall thickness. In recent years, more preference has been given to automatic states with single-gauge rolls [36].

Mandrels for rolling states (mandrels) are used for hot rolling of seamless pipes, when rolling a liner into a rough pipe by thinning its wall and increasing its length in pilgrim, rolling and automatic states. The mandrel in this case controls its own diameter and the inner diameter of the pipe. Due to the abrasive and abrasive action of the material of the rolling sleeves, the mandrels lose their material, which leads to a decrease in their diameter and a decrease in the inner diameter of the resulting pipes and a decrease in the thickness of their walls (**Fig. 3.3**).

The resistance of the mandrel to abrasion is measured by the number of rolling cycles, the mandrel withstands without changing the diameter and is determined by the material from which

the mandrel is made. In this case, the mandrel must meet two requirements at once: high wear resistance, in order to avoid its rapid failure, and low brittleness, to prevent the fracture of the shank due to the stress arising in the mandrel during rolling. Economically, the manufacture of mandrels is limited by the cost of materials for their manufacture. Technologically – the availability and manufacturability of the materials used [37].

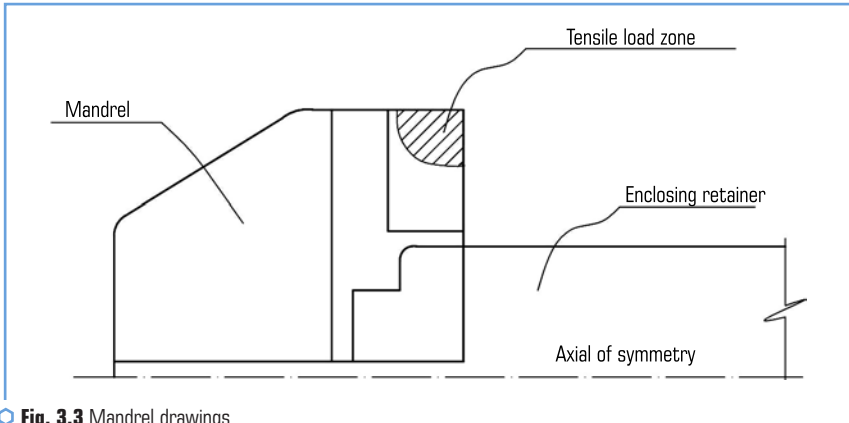


Fig. 3.3 Mandrel drawings
Source [37]

In this work, the choice of material for the manufacture of mandrels is substantiated, which meets all these requirements.

To do this, it is necessary to solve a number of tasks: to analyze the working conditions and determine the requirements for the mandrel material; to characterize the materials suitable for the manufacture of mandrels, to determine the chemical composition of the mandrel materials; determine the formation of the structure and properties of mandrels; justify the choice of material and select the modes of heat treatment of the mandrels.

Today, pipes are used to transport solid (in the form of slurry), liquid and gaseous materials in the event that transportation of these materials by other means is unprofitable. Tubes are made today using the helical rolling method discovered by the Mannesmann brothers in 1885. In this method, the ingot, heated to 900 °C, is carried away by rolls rotating in one direction, it starts to rotate around its axis and between the rolls is pierced with mandrels (**Fig. 3.4**).

The shell obtained in this case is the initial product for further rolling into a rough tube in rolling states. In this case, the shell decreases its thickness and increases its length, turning into a rough tube. This operation is done on automaton states, continuous rolling states and pilgrim states (**Fig. 3.5–3.7**).

When rolling the shell, the inner diameter of the pipe is controlled by the diameter of the mandrel, which is in the pipe during the entire rolling process until it is removed.

During rolling, due to prolonged contact of the mandrel with the workpiece, the mandrel surface heats up to 700 °C, so the mandrel material must withstand heating up to 700 °C without losing its properties. Also, the mandrel material must resist thermal cycling and abrasion, as well as have high surface hardness, resistance to impacts occurring at the beginning of rolling and during the removal of the mandrel.

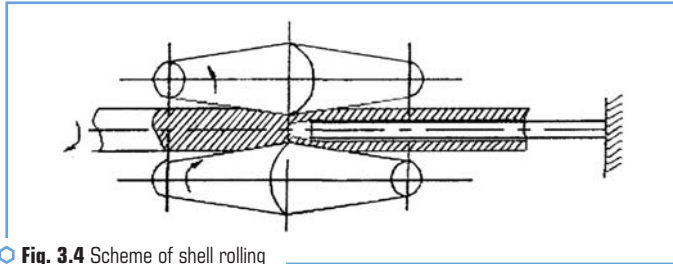


Fig. 3.4 Scheme of shell rolling
Source [37]

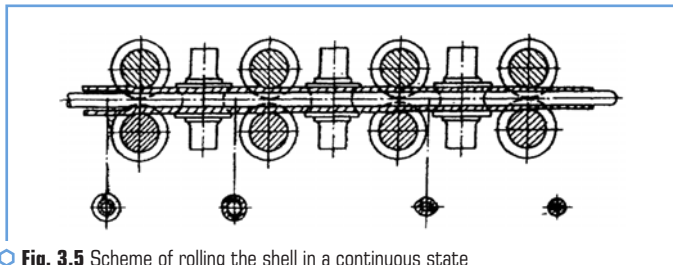


Fig. 3.5 Scheme of rolling the shell in a continuous state
Source [36]

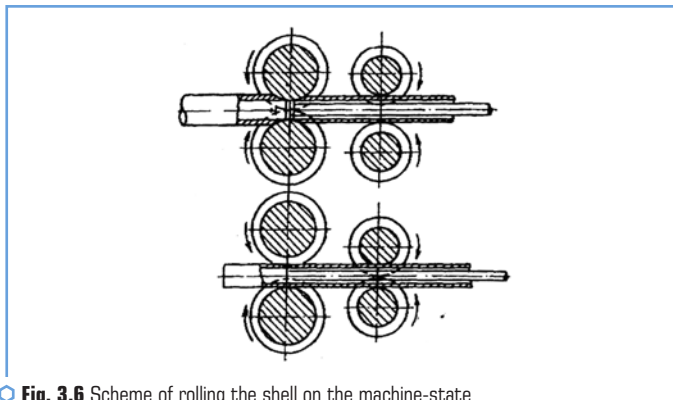


Fig. 3.6 Scheme of rolling the shell on the machine-state
Source [36]

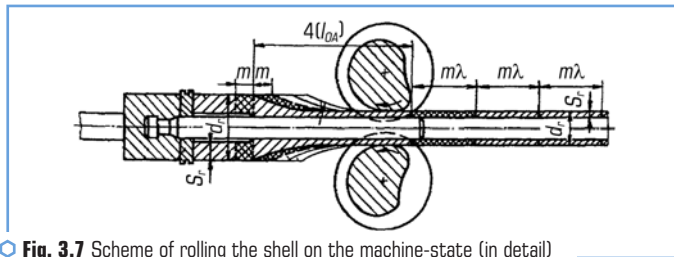


Fig. 3.7 Scheme of rolling the shell on the machine-state (in detail)
Source [36]

Thus, the limiting requirements for a steel mandrel are:

- surface hardness less than 24 HRC;
- heat resistance not less than 700 °C;
- impact strength KCU not less than 90 J/cm²;
- resistance to wear.

There is no normative documentation (technological instructions and technical conditions) that regulates the properties of mandrels made of cast iron and nickel-chromium alloy "Nikorin", which leads to the urgent need to develop requirements for the properties of alloys for mandrels.

3.1.7 STATEMENT OF THE RESEARCH PROBLEM

The object of this paper is to research:

- patterns of formation of the structure of the nickel-chromium alloy "Nikorin" in the initial cast state;
- influence of the structure, phase composition on the properties of the nickel-chromium alloy "Nikorin" in the cast state;
- temperature ranges of phase transformations of the nickel-chromium alloy "Nikorin";
- structure, phase composition, microhardness of phases and structural components of prototypes of the nickel-chromium alloy "Nikorin" after quenching from different temperatures;
- wear resistance of chromium-nickel alloys under friction conditions at elevated temperatures and various loads.

3.2 MATERIAL AND METHODOLOGY OF RESEARCH

Research alloys melted in laboratory conditions were used to carry out studies of phase and structural transformations in nickel-chromium alloys "Nikorin". The chemical composition of the research alloys is shown in **Table 3.1**.

● **Table 3.1** The chemical composition of the prototypes of the nickel-chromium alloy "Nikorin"

Alloy name	Content of alloying elements, %							
	C	Cr	Ni	Mn	Ti	Si	Al	Fe
Chromium-nickel alloy "Nikorin" No. 1	1.8	34.0	57.0	0.2	0.6	0.7	2.5	2.3
Chromium-nickel alloy "Nikorin" No. 2	1.5	36.0	57.2	0.3	0.7	0.6	1.9	1.7
Chromium-nickel alloy "Nikorin" No. 3	2.6	36.0	57.2	0.3	0.7	0.8	2.0	2.2

During melting, the melt was in a quartz tube in an experimental induction furnace. To obtain the required cooling rates during crystallization, a quartz tube with a melt was placed in a Tamman furnace and cooled at a given rate. As a result, samples were obtained that had the content of the main alloying elements within the grade composition for the "Nikorin" chromium-nickel alloy.

The microstructure of the samples of the nickel-chromium alloy "Nikorin" was developed in the Grosbeck reagent followed by thermal digestion. The study of the microstructure was carried out using an optical microscope "Neophot-21".

The determination of the number of phases and structural components in the structure of the research alloys was carried out by the method of A. A. Hlaholev at x400 magnification [38].

The phase identification in the nickel-chromium alloy "Nikorin" was carried out by X-ray structural analysis on a DRON-3M diffractometer in FeK α – radiation. To determine the lattice parameter, the profile of the diffraction maxima (111) g, (002) g, (113) g was recorded along three mutually perpendicular sides of the sample, each side being recorded five times at a rate of (1/8) °/min. The lattice parameter was calculated from the position of the center of mass of the above diffractometric maxima. The results obtained were subjected to statistical processing according to the standard method.

The amount of austenite was determined from the ratio of the integral intensities of the lines (001) and (111) [39–41].

The distribution of alloying elements between the phases and structural components of the nickel-chromium alloy "Nikorin" in the initial state was studied using a JSM-840 electron microscope with a "Link-860/500" microanalysis system ("Link Analytical", England). The studies were carried out in the mode of secondary electrons (SEI) and backscattered electrons (BEI). The beam current was $I = 10^{-7} \dots 10^{-9}$ A. Voltage $U = 20$ kV. The analysis was $t = 100$ s. The beam diameter was 1...1.5 μm . The analysis was performed using the ZAF4/FLS software. Pure samples for each investigated element were chosen as standards (purity was 99.99 %). Standard samples from Link Analytical were used.

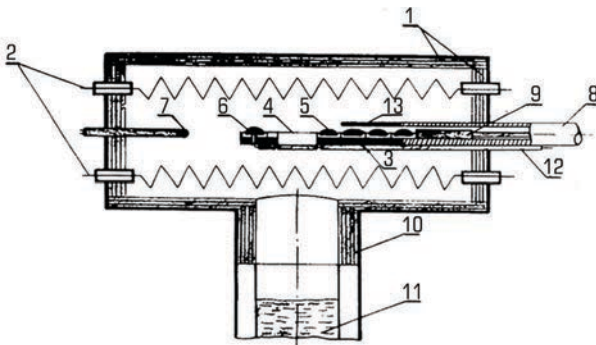
Basic information on the nature and mechanism of phase transformations during hardening was obtained on the basis of differential thermal and quenching microstructural analysis. The regularities of the formation of the structure of the Nikorin alloy were studied by quenching-microstructural analysis on a specially designed installation [13]. Quenching temperatures were selected based on the Ni-Cr diagram [14, 42], as well as in accordance with the heating/cooling

thermogram of the research alloys. This setup allows to systematically record the high-temperature state of the sample with high accuracy by quenching. It was based on a vacuum furnace with a quenching tank (**Fig. 3.8**) of the following design.

The main supporting element of the installation is the furnace body. It has a cylindrical shape and is welded from a sheet of steel X18H10T with a thickness of 3 mm. Flanges made of the same steel are welded to the ends, allowing for quick disassembly and assembly of the furnace. One of the flanges is simultaneously a supporting one for screens, a heater and current drives, assembled into a single block. A sample holder assembly is attached to the second flange (**Fig. 3.9**), it is a crucible made of refractory material (3), rigidly fastened to a molybdenum tube (8).



○ **Fig. 3.8** General view of the installation for hardening-microstructural analysis
Source [42]



○ **Fig. 3.9** Diagram of the working space of the furnace for hardening-microstructural analysis
Source [42]

The design of the holder allows 4 samples to be installed into the furnace at once on flat alundum substrates (5) and sequentially dumped into the quenching bath (11) through a special hole (4). In the working space of the furnace, limited by a coaxial shield (1), it includes the following elements: a pusher (9), with the help of which the sample (5) is dropped through the hole (4) into the shaft (10) into the quenching bath (11) molybdenum standard (6) with a hot junction of the thermocouple BP 5/20 (7), which controls the operation of the temperature setpoint of the heater power supply system; screen (13), which prevents intensive heating of the samples not participating in the experiment.

The samples were hardened in a 10 % solution in sodium chloride, which is constantly cooled by running water. The cooling rate of the sample during quenching was 20 deg/s at a speed of its movement in the bath of about 3 m/s. The heat loss of a sample with a diameter of 5 mm on the way from the working space of the furnace to the meniscus of the quenching liquid does not exceed 2 °C.

Determination of the temperature ranges of transformations was carried out by thermal analysis on a VD-4 calorimeter with heating at a rate of 5 deg/min.

The microhardness of the structural components of chromium-nickel alloys was determined using a PMT-3 device in accordance with GOST 9450-76 at a load of 50 g and an increase of $\times 485$, as an average of 50 measurements. The measurement accuracy of the diagonals of the indentation is 0.3 % of the smallest division of the micrometer scale. The hardness of the samples was determined by the Rockwell method according to the standard method.

The temperature dependence of the hardness of the chromium-nickel alloy Nikorin was studied using a Vickers device. A diamond pyramid was used as an indenter; the exposure of the indenter under a load of 50 g was 10 s. The hardness measurements were carried out at a heating rate of 5 °C/min with a slit of 100 °C. The hardness, which was measured from the indentation of the indenter, characterizes the value of the material resistance [43].

Tribotechnical tests for wear resistance under friction conditions at elevated temperatures and various loads were carried out on a modernized friction device 2070 CMT 1, according to the "shaft-plane" scheme. The counterbody was Art. 45. **Fig. 3.10** shows the appearance of the tribological contact at a load of 1000 N and a sliding speed of 2 m/s [44].

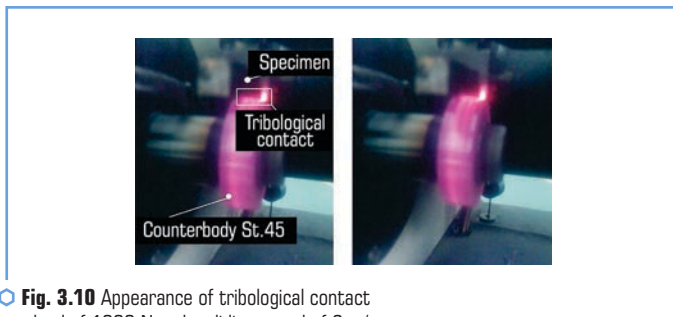


Fig. 3.10 Appearance of tribological contact at a load of 1000 N and a sliding speed of 2 m/s
Source [44]

3.3 INVESTIGATION OF THE REGULARITIES OF THE STRUCTURE FORMATION, PHASE COMPOSITION, PROPERTIES AND DISTRIBUTION OF ALLOYING ELEMENTS BETWEEN THE PHASES AND STRUCTURAL COMPONENTS OF NICKEL-CHROMIUM ALLOYS "NIKORIN" IN THE AS-CAST STATE

The work investigated the structure, phase composition, hardness, microhardness of the structural components of the samples of the nickel-chromium alloy "Nikorin" intended for the manufacture of mandrels for rolling pipes [45, 46].

Analysis of the microstructure of samples (No. 1, 2, 3) of the heat-resistant chromium-nickel alloy "Nikorin" in the initial cast state (**Fig. 3.11–3.13**) indicates that an almost homogeneous structure is formed in these alloys over the section of the casting. Analysis of the microstructure of samples (No. 1, 2, 3) of the heat-resistant chromium-nickel alloy "Nikorin" in the initial cast state (**Fig. 3.11–3.13**) indicates that an almost homogeneous structure is formed in these alloys over the section of the casting. In the structure of three samples of the high-temperature nickel-chromium alloy "Nikorin", chromium carbide Cr_7C_3 is observed both in the longitudinal and in the cross section. In these alloys, due to the high carbon content, crumbling of the Cr_7C_3 carbide is observed.

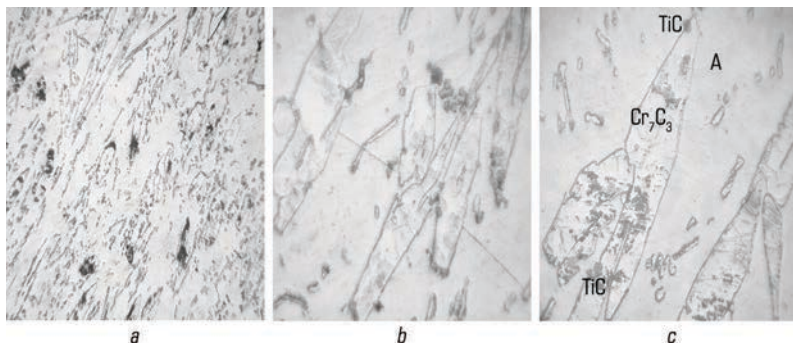
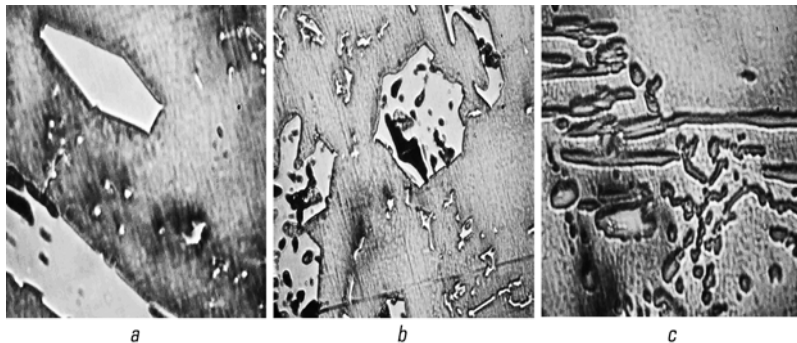


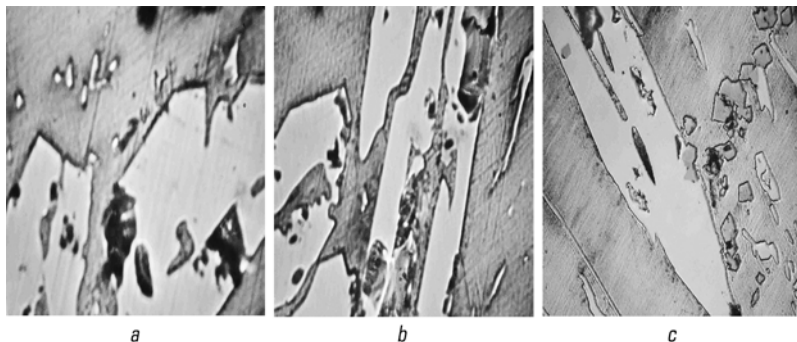
Fig. 3.11 Microstructure of heat-resistant chromium-nickel alloy "Nikorin" (alloy No. 1): *a* – casting surface $\times 150$; *b* – surface of casting $\times 600$; *c* – central part of casting $\times 600$
Source [44–46]

Since alloy 3 contains more carbon (2.62 % C), this phenomenon is much more pronounced in it than in alloys 1 and 2. Due to the fact that there is a sufficiently high carbon content in the alloys, the Cr_7C_3 chromium carbide becomes brittle and during operation (or the manufacture of a microsection), such a carbide crumbles unevenly throughout the carbide volume. Therefore, the higher the carbon content in the alloy, the less stable the carbide becomes. And since the carbide component strengthens chromium-nickel alloys, it can be concluded that parts from such an alloy will be less stable during operation. Another type of TiC carbides (**Fig. 3.11, c, 3.13, c**) is located

unevenly both in the volume of Cr_7C_3 carbides and in the austenitic matrix of the casting. Titanium carbides have a regular cubic shape.

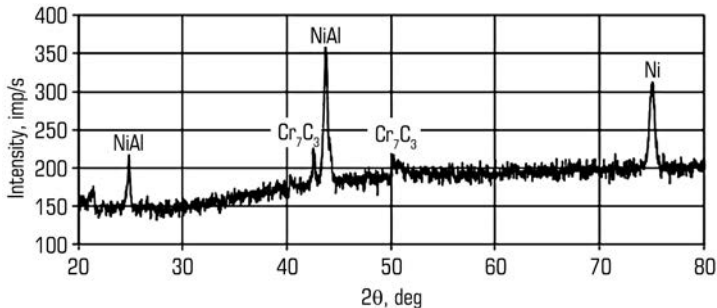


○ **Fig. 3.12** Microstructure of heat-resistant chromium-nickel alloy "Nikorin" (alloy No. 2):
a – longitudinal section of Cr_7C_3 carbides; *b* – cross section of Cr_7C_3 ; *c* – coarsely differentiated
austenite-carbide eutectic based on Cr_7C_3 chromium carbide
Source [44–46]



○ **Fig. 3.13** Microstructure of nickel-chromium alloy "Nikorin" (alloy No. 3):
a – cross-section of Cr_7C_3 ; *b* – longitudinal section of Cr_7C_3 carbides; *c* – carbide *t* and,
which grows together with chromium carbide Cr_7C_3
Source [44–46]

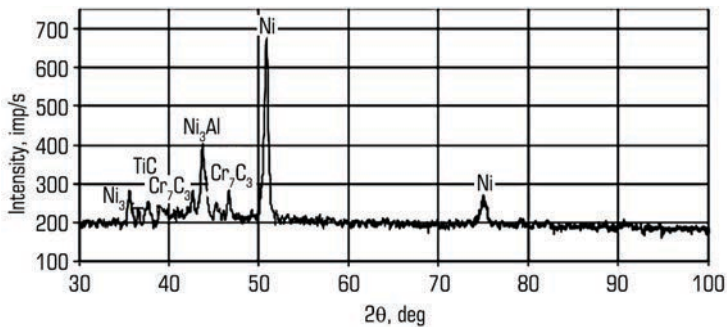
The phase composition of research alloys was studied using X-ray diffraction analysis (**Fig. 3.14–3.16**). **Fig. 3.14** shows the diffraction patterns of the nickel-chromium alloy "Nikorin" (alloy No. 1). In the chromium-nickel alloy, X-ray diffraction analysis has revealed excess and eutectic carbide Cr_7C_3 , as well as high-nickel austenite, as evidenced by the high intensity of its line (111).



○ **Fig. 3.14** Scheme of the diffractogram of the prototype (alloy No. 1) of the nickel-chromium alloy "Nikorin"
Source [44–46]

Fig. 3.15, 3.16 show diffraction patterns of samples of alloys 2 and 3 of the nickel-chromium alloy "Nikorin". In this alloy, X-ray diffraction analysis revealed excess and eutectic carbide Cr_7C_3 , as well as high-nickel austenite, as evidenced by the high intensity of its line (111). In addition, titanium carbide TiC is present in test alloys 2 and 3.

Additionally, carbide analysis was carried out on samples of research alloys No. 2, 3 (**Fig. 3.17, 3.18**), which, in addition to the above-mentioned carbides, made it possible to reveal the σ -phase (FeCr) in the structure of the heat-resistant chromium-nickel alloy. The presence of this phase is undesirable, since it reduces the stability of the alloys during operation. This is due to the fact that the σ -phase has a high hardness, however, it is very fragile.



○ **Fig. 3.15** Scheme of the diffractogram of the prototype (alloy No. 2) of the nickel-chromium alloy "Nikorin"
Source [44–46]

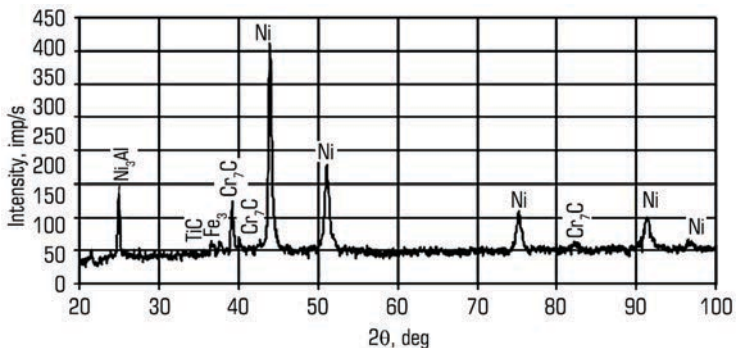


Fig. 3.16 Scheme of the diffraction pattern of the prototype (alloy No. 3) of the nickel-chromium alloy "Nikorin"
Source [44–46]

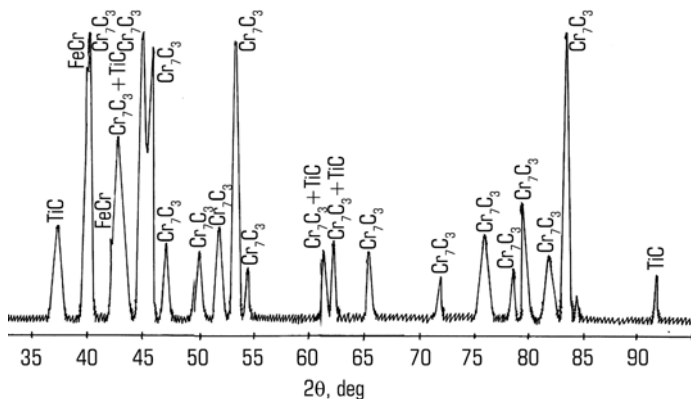
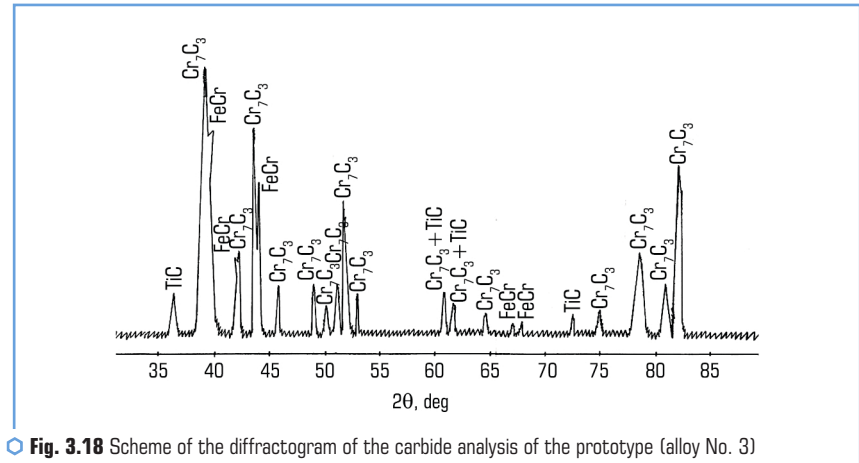


Fig. 3.17 Scheme of the diffraction pattern of the carbide analysis of the prototype (alloy No. 2) of the nickel-chromium alloy "Nikorin"
Source [44–46]

Table 3.2 shows the quantitative data of X-ray structural analysis of prototypes of the nickel-chromium alloy "Nikorin" in the cast state.

Analysis of the data in **Table 3.2** [44–46] indicates that the matrix of the chromium-nickel alloy consists of high-nickel austenite. The hardness of a nickel-chromium alloy "Nikorin" is 47 HRC units.

Table 3.3 shows the measurement data for the microhardness of the matrix and Cr_7C_3 carbide in all research chromium-nickel alloys.



● **Fig. 3.18** Scheme of the diffractogram of the carbide analysis of the prototype (alloy No. 3) of the nickel-chromium alloy "Nikorin"
 Source [44–46]

● **Table 3.2** Quantitative data of X-ray structural analysis of prototypes of the nickel-chromium alloy "Nikorin"

Test chromium-nickel alloys	a_γ by (022) γ %	γ , in the matrix	HRC
Alloy No. 1	3.59	100	47
Alloy No. 2	3.59	100	47
Alloy No. 3	3.59	100	47

Source [44–46]

● **Table 3.3** The value of the microhardness of the matrix and eutectic carbide in research chromium-nickel alloys

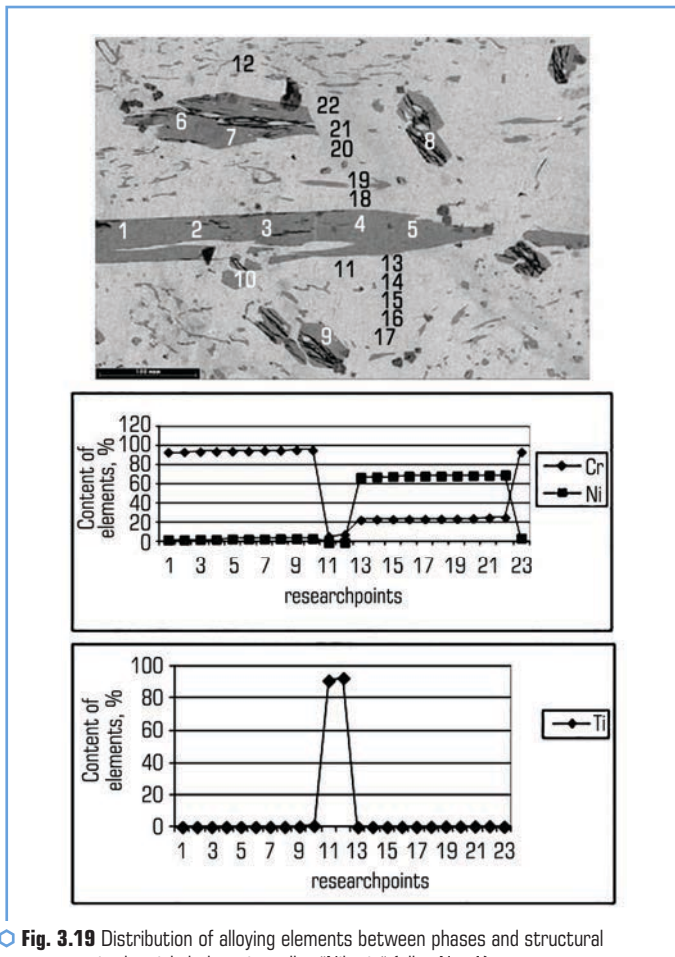
Test chromium-nickel alloys	Microhardness of structural components, MPa	
	Matrix	Carbide
Alloy No. 1	2769	18921
Alloy No. 2	2852	18921
Alloy No. 3	2680	18921

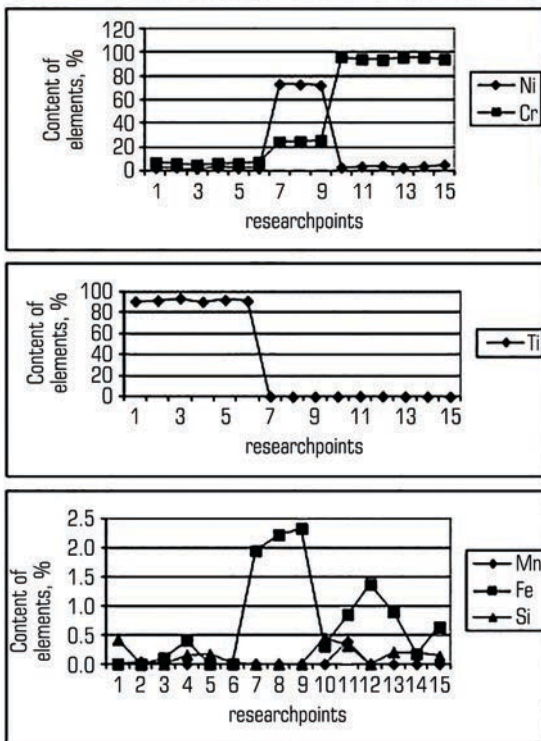
Source [44–46]

The alloys differ from each other in the content of carbon and iron, therefore the microhardness of the matrix of chromium-nickel alloys No. 1, No. 2 and No. 3 is not the same. Due to the high carbon content, crumbling of Cr_7C_3 carbide is observed in these samples, since alloys 1 and 3 contain more carbon, this phenomenon is more pronounced in them than in alloy 2, which explains

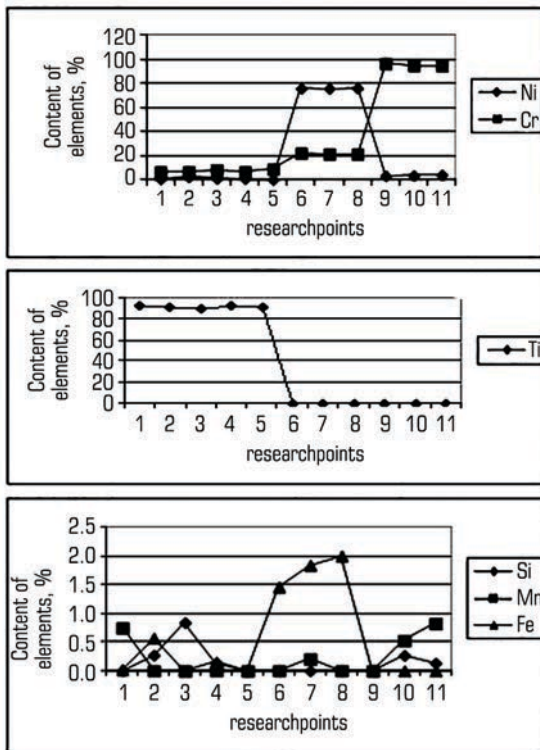
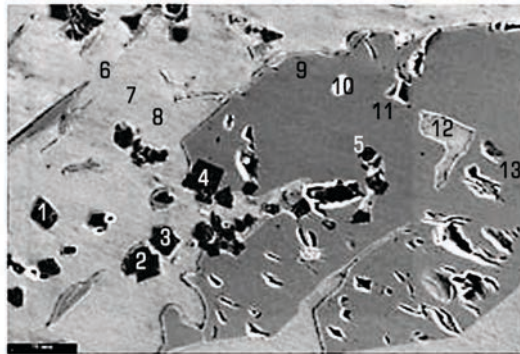
the decrease in the microhardness of the matrix. The microhardness of Cr₇C₃ carbide in all alloys remains unchanged.

The distribution of alloying elements between phases and structural components in research chromium-nickel alloys in the cast state was studied using local X-ray spectral analysis. The research results are shown in **Fig. 3.19–3.21** and in **Tables 3.4–3.6**. Quantitative local X-ray spectral analysis was carried out point by point. The content of alloying elements in the matrix and carbide was analyzed [46–48].





○ **Fig. 3.20** Distribution of alloying elements between phases and structural components in the nickel-chromium alloy "Nikorin" (alloy No. 2)
Source [46–48]



○ **Fig. 3.21** Distribution of alloying elements between phases and structural components in the nickel-chromium alloy "Nikorin" (alloy No. 3)
Source [46–48]

● **Table 3.4** Distribution of alloying elements between phases and structural components in the chrome-nickel alloy "Nikorin" (alloy No. 1)

Structural components	Content of alloying elements in structural components, in %						
	Cr	Ni	Fe	Ti	Si	Mn	Σ alloying elements, %
Matrix	24.66	68.72	2.10	0.21	0.60	0.30	27.87
Carbide Cr ₇ C ₃	94.47	3.77	0.70	0.16	0.15	0.65	5.43
TiC carbide	7.51	0.24	0.13	91.81	0.16	–	8.04

Source [46–48]

● **Table 3.5** Distribution of alloying elements between phases and structural components in the chrome-nickel alloy "Nikorin" (alloy No. 2)

Structural components	Content of alloying elements in structural components, in %						
	Cr	Ni	Fe	Ti	Si	Mn	Σ alloying elements, %
Matrix	24.80	7.90	2.18	0.09	–	–	24.89
Carbide Cr ₇ C ₃	95.32	3.55	0.71	0.18	0.22	0.07	4.73
TiC carbide	6.08	2.34	0.09	91.36	0.13	0.07	8.71

Source [46–48]

● **Table 3.6** Distribution of alloying elements between phases and structural components in the chrome-nickel alloy "Nikorin" (alloy No. 3)

Structural components	Content of alloying elements in structural components, in %						
	Cr	Ni	Fe	Ti	Si	Mn	Σ alloying elements, %
Matrix	21.90	79.13	1.77	0.31	–	0.07	24.04

Source [46–48]

Fig. 3.19 and **Table 3.4** show data on the distribution of alloying elements between phases and structural components in the Nikora chromium-nickel alloy (alloy No. 1). The content of chromium and other alloying elements in the Cr₇C₃ carbide, which is formed in the nickel-chromium alloy "Nikorin", has been determined. The Cr₇C₃ carbide in the chromium-nickel alloy contains 94.5 % Cr, other alloying elements are present in small amounts. The chromium-nickel alloy matrix contains 68.7 % Ni and 24.6 % Cr and is a nickel-based solid solution with a face-centered cubic lattice.

In **Fig. 3.20, 3.21** and **Tables 3.5, 3.6** show data on the distribution of alloying elements between the phases and structural components in the samples of the high-temperature nickel-chromium alloy "Nikorin" (alloys No. 2 and No. 3).

Analysis of the obtained data on the distribution of alloying elements between the phases and structural components (**Fig. 3.20, 3.21, Tables 3.5, 3.6**) shows that the structure of the alloy

is homogeneous. The content of chromium and other alloying elements in the Cr_7C_3 carbide, which is formed in the nickel-chromium alloy "Nikorin", the matrix and titanium carbide TiC , has been determined. The Cr_7C_3 carbide in the prototype alloy No. 2 contains 95.32 % Cr, and in the alloy No. 3 – 95.35 % Cr, all other alloying elements are present in the carbide in small amounts. The matrix of the nickel-chromium alloy "Nikorin" sample No. 2 contains 72.9 % Ni and 24.8 % Cr, and sample No. 3 – 79.13 % Ni and 21.9 % Cr and is a solid solution based on nickel with an fcc lattice. Titanium carbide TiC in sample No. 2 contains 91.36 % Ti, and in sample No. 3 – 90.55 % Ti.

The data obtained indicate that the matrix of the research alloy No. 2 contains 3 % more chromium in comparison with the matrix of the alloy No. 3. The carbides Cr_7C_3 and TiC of alloy No. 2 of iron, silicon and manganese also contain more than alloy No. 3. In the matrix of chromium-nickel alloy No. 3, the content of nickel, iron, titanium is 7 % higher compared to alloy No. 2, the content of iron and titanium in sample No. 3 is slightly higher than in sample No. 2. It should be noted that the prototypes differ only in the content of alloying elements in the matrix, the degree of alloying of Cr_7C_3 and TiC carbides is the same.

Thus, the data obtained indicate that, over the section of the casting, heat-resistant chromium-nickel alloys have a homogeneous structure with a uniform distribution of alloying elements.

3.4 CALORIMETRIC ANALYSIS OF RESEARCH CHROMIUM-NICKEL ALLOYS

Phase transformations in metallic systems are accompanied by the release or absorption of heat, and some of them occur both in the forward and reverse directions (reverse), while others proceed in only one direction (irreversible). The first include the following phase transformations: melting-crystallization, polymorphic transformations, formation and decomposition of chemical compounds. Irreversible processes should include the reactions of transition from unstable, metastable compounds to stable (stable) ones, for example, the decomposition of solid solutions, the transition from an amorphous state to a crystalline state. The thermal effects of irreversible processes appear only on the heating curves and, as a rule, such reactions are exothermic [49, 50].

If no transformations occur during heating in the sample, then the differential record on the thermogram is fixed as a straight line parallel to the temperature axis. Thermal effects of phase transformations are reflected in the thermogram by sharp deviations of the differential curve. However, the onset of the effect is characterized by a sharp kink in the differential curve only for substances with high thermal conductivity. For substances with low thermal conductivity, the beginning of the deviation of the differential curve is always more or less smoothly rounded [50].

Changes in the course of the curve correspond to the start and end temperatures of the conversion. As a rule, the nature of the effect can be determined by the nature of the peaks in the thermogram. However, it should be noted that a large number of thermograms of various substances with a large number of effects, the nature of which has not been deciphered, has been

published so far [50]. One of the factors that make it difficult to decipher thermograms is the superposition of effects on each other. If both merging effects are accompanied, for example, by heat absorption, then one unusually large effect takes place on the thermogram. If, however, two heat effects, opposite in sign, merge, then they superimpose one on the other, mutually reduce the size of the corresponding deviations on the differential curve. The overlapping of peaks of various effects can be deciphered after additional research using other methods.

Considering the above, let's consider the thermograms of the nickel-chromium alloy "Nikorin".

Fig. 3.22 shows the heating and cooling thermograms of the nickel-chromium alloy "Nikorin". It can be seen from the presented curve (**Fig. 3.22, a**) that a horizontal section is observed on the thermogram of heating to a temperature of 490 °C, which indicates the absence of phase transformations, apparently due to the high stability of the initial structure. Heating to a temperature of 490 °C indicates the presence of a stable austenitic structure in this alloy.

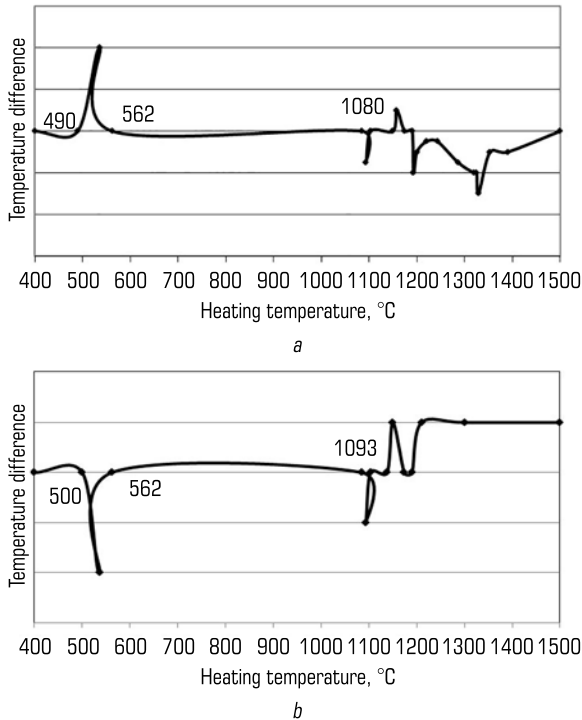


Fig. 3.22 Thermogram of the nickel-chromium alloy "Nikorin":
a – heating; *b* – cooling

In the temperature range 490–562 °C, the ordered phase CrNi₂ is likely to dissolve in the nickel austenite. Upon further heating to a temperature of 1085 °C, the structure of the alloy under study retains its stability, because, according to the thermogram, there are no thermal effects in this gap. On the cooling thermogram, the thermal effects are much less and they are not as intense as during heating.

Table 3.7 shows the temperatures of the onset of crystallization and melting of the high-temperature alloy "Nikorin", determined by thermal analysis during heating and cooling. The melting range of the Nikorin alloy is 104 °C, and the crystallization range is 93 °C. When heated from room temperature to 1286 °C, only one thermal effect is observed in the temperature range 490–562 °C, probably dissolution of the ordered CrNi₂ phase in the nickel matrices.

● **Table 3.7** Temperatures of the onset of crystallization/melting of samples of chromium-nickel alloy "Nikorin" during heating/cooling

Research alloy	Crystallization temperature, °C		Melting point, °C	
	Heat	Cooling	Heat	Cooling
"Nikorin"	1390	1373	1286	1280

3.5 STRUCTURE, PHASE COMPOSITION, MICROHARDNESS OF PHASES AND STRUCTURAL COMPONENTS OF PROTOTYPES OF NICKEL-CHROMIUM ALLOY "NIKORIN" AFTER QUENCHING FROM DIFFERENT TEMPERATURES

The quenching microstructural research method, developed by the staff of the "Bunin School" and widely used to study the mechanism and kinetics of phase transformations in alloys of the Fe-C system, has been successfully applied to alloys of other systems, and makes it possible to obtain comprehensive information about the features of phase transformations and patterns of structure formation in these systems, in particular, in the Ni-Cr system, which is the basis of high-temperature and heat-resistant alloys "Nikorin".

"Nikorin" alloys are intended for the manufacture of rolling tools (calibers and mandrels for rolling pipes) and must have increased strength properties at high temperatures and be resistant to oxidation. Alloying nickel with chromium results in a strong increase in oxidation resistance at high temperatures.

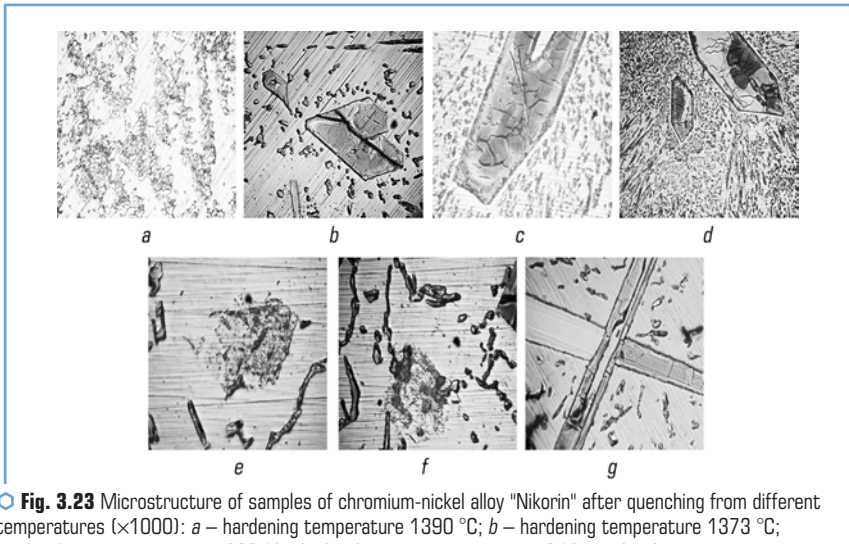
The critical minimum amount of chromium required for a significant increase in the heat resistance of nickel and complex nickel alloys is 20–25 %. The maximum heat resistance in alloys of the Ni-Cr system is observed at 40 % chromium [51].

Alloys of the Ni-Cr system are alloyed with effective reinforcements – aluminum and titanium. These elements in nickel alloys contribute to the formation of a stable dispersed intermetallic compound Ni₃Al(Ti), which causes coherent strengthening of the matrix, hinders the sliding of the

metal under load at high temperatures, and thus increases the strength of the alloy. It has been established that it is the formation of this phase that increases the strength of a number of industrial Ni-Cr alloys at high temperatures [26, 52].

An analysis of the microstructures of the chromium-nickel alloy samples indicates that, depending on the quenching temperature, a different structure and phase composition are formed in the research alloy. As a result of quenching the nickel-chromium alloy "Nikorin" from a liquid state from a temperature of 1390 °C, a quenched liquid with a clearly pronounced cellular structure and well-developed dendrites of the primary γ -Ni solid solution are recorded (**Fig. 3.23, a**).

Quenching from a temperature of 1373 °C indicates the development of the crystallization process, which does not end at this temperature. Austenite dendrites grow together and form a matrix in which chromium carbides Cr_7C_3 are present, as well as near the carbides – quasi-eutectic regions of a quenched liquid (**Fig. 3.23, b, c, d**). When quenched from a temperature of 1280 °C, crystallization also does not have time to complete. A rim of eutectic austenite is formed around coarse crystals of Cr_7C_3 carbides, which indicates the initial stage of eutectic crystallization: $P \rightarrow \text{Cr}_7\text{C}_3 + \gamma$ (**Fig. 3.23, c**). Sections of the quenched liquid solidify in the form of a quasi-eutectic.



○ **Fig. 3.23** Microstructure of samples of chromium-nickel alloy "Nikorin" after quenching from different temperatures ($\times 1000$): *a* – hardening temperature 1390 °C; *b* – hardening temperature 1373 °C; *c* – hardening temperature 1280 °C; *d* – hardening temperature 1170 °C; *e* – hardening temperature 1150 °C; *f* – hardening temperature 1100 °C; *g* – hardening temperature 1100 °C ($\times 500$)
Source [53, 54]

In the samples quenched from a temperature of 1150–1100 °C, together with the carbides Cr_7C_3 , TiC and austenite, the structure contains an intermetallic phase (probably σ is the FeCr phase). The presence of this phase is undesirable, since it reduces the stability of the alloys during

operation under conditions of tensile stresses. This is due to the fact that the σ -phase has a high hardness, however, at the same time, it is very brittle. The presence of the σ – phase is recorded in the structure of the metallurgical tooling parts, obtained by casting from the "Nikorin" alloy [55].

It is known [56–58] that in high-chromium and chromium-nickel alloys during crystallization, peritectic-eutectic transformations are realized:

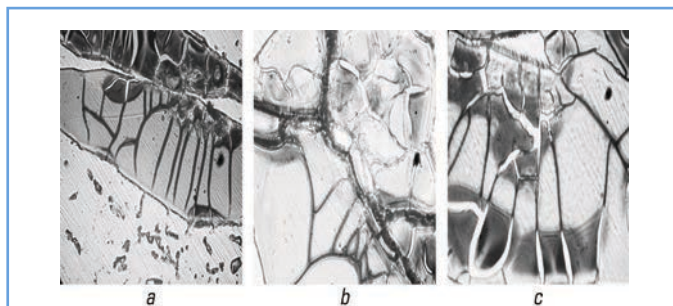


The study of quenched samples confirms the implementation of the peritectic transformation ($P + \gamma \rightarrow Cr_7C_3 + \gamma_{zal} + P_{zal}$) in the nickel-chromium alloy "Nikorin" (Fig. 3.24).

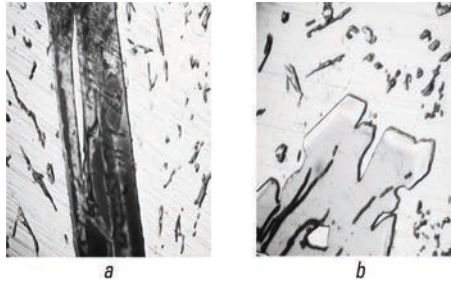
The peritectic transformation leads to a change in the shape and morphology of the primary carbide crystals of Cr_7C_3 as a result of the diffuse interaction of the liquid and γ -Ni austenite crystals; dark channels are formed in the middle of the carbide crystals, through which the liquid enters during the peritectic transformation to the γ/Cr_7C_3 recrystallization front. Regions of retained austenite (white) are observed in the center and periphery of the carbide crystals. Crystallization is completed upon cooling below 1190 °C. In the sample quenched from a temperature of 1085 °C, crystallization is completely completed, as evidenced by the microstructure represented by a matrix and a large amount of Cr_7C_3 carbides. The structure contains dispersed needle-shaped carbides along with large ones (Fig. 3.25, a).

In a specimen quenched from a temperature of 526 °C (Fig. 3.25, b), the structure is represented by an austenite matrix and carbides of various shapes and sizes.

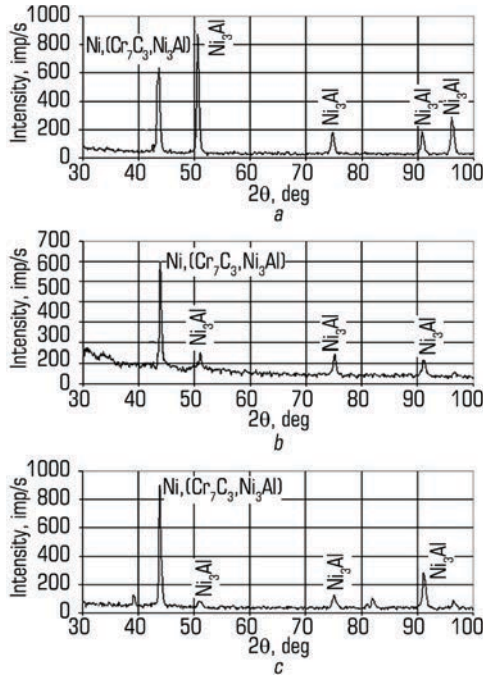
Fig. 3.26–3.28 shows the sections of the diffraction patterns of the samples of the nickel-chromium alloy "Nikorin" after quenching from different temperatures. X-ray diffraction analysis of samples quenched at different temperatures revealed excess and eutectic Cr_7C_3 carbide, high-nickel austenite, as well as the Ni_3Al phase.



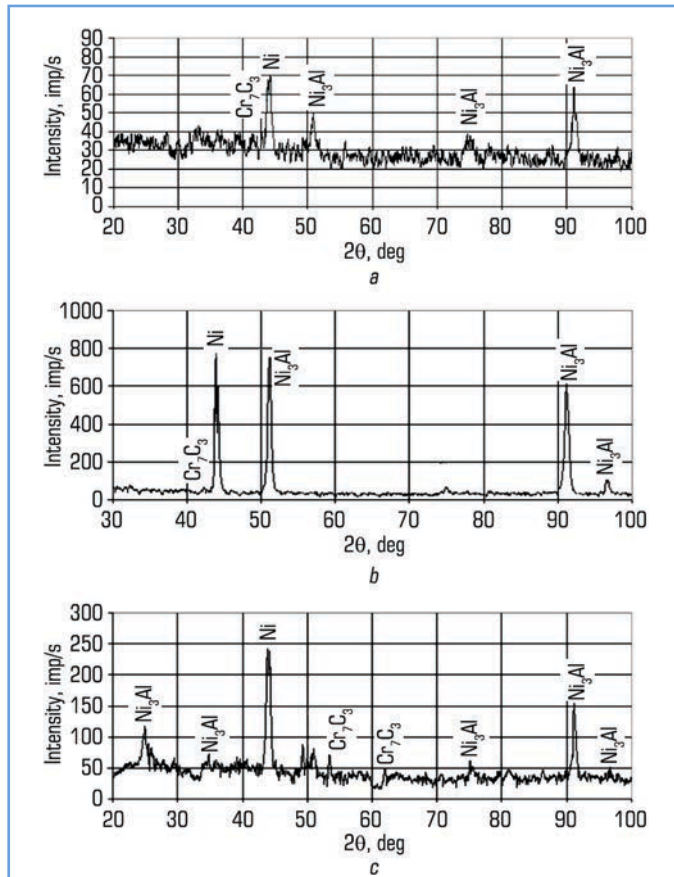
○ Fig. 3.24 Microstructure of a sample quenched from a temperature of 1280 °C: a – $\times 500$; b, c – $\times 1000$
Source [53, 54]



○ **Fig. 3.25** Microstructure of samples, chromium-nickel alloy "Nikorin" after quenching at different temperatures: *a* – hardening temperature 1085 °C; *b* – hardening temperature 526 °C
Source [53, 54]



○ **Fig. 3.26** Schemes of diffraction patterns of the nickel-chromium alloy "Nikorin" after quenching at different temperatures: *a* – hardening temperature 1390 °C; *b* – hardening temperature 1373 °C; *c* – hardening temperature 1286 °C
Source [53, 54]

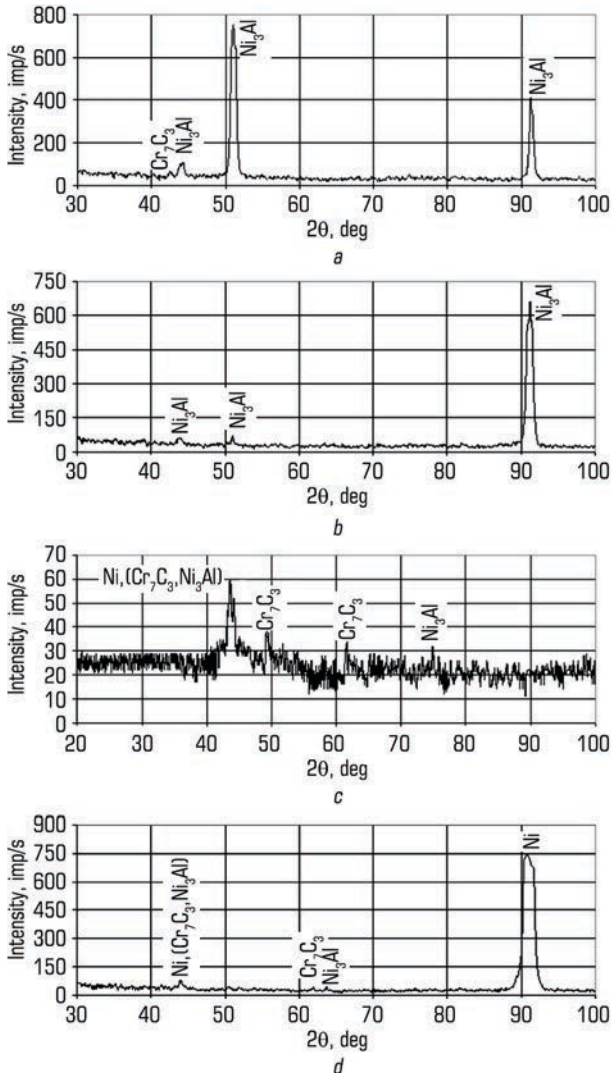


○ **Fig. 3.27** Schemes of diffraction patterns of the nickel-chromium alloy "Nikorin" after quenching from different temperatures: *a* – hardening temperature 1280 °C; *b* – hardening temperature 1190 °C; *c* – hardening temperature 1170 °C
Source [53, 54]

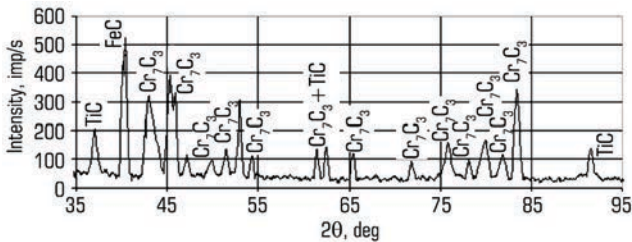
In order to clarify the phase composition of the alloy, carry out carbide analysis. Additionally, carbide analysis was carried out on samples quenched from 1150–1100 °C (**Fig. 3.29, 3.30**), which, in addition to Cr₇C₃ carbide, made it possible to reveal titanium carbide TiC and the σ-phase (FeCr) in the structure of the heat-resistant chromium-nickel alloy.

Table 3.8 shows the measurement data for the microhardness of the matrix and Cr₇C₃ carbide.

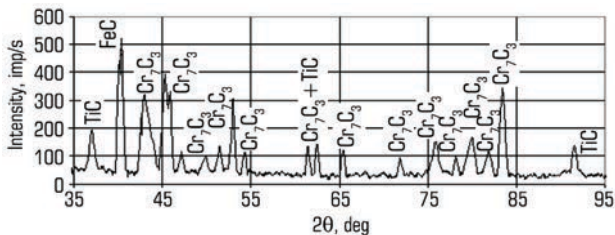
In accordance with the structural changes and the phase composition of the nickel-chromium alloy "Nikorin", the microhardness also changes (**Table 3.8**).



○ **Fig. 3.28** Schemes of the diffraction patterns of the nickel-chromium alloy "Nikorin" after quenching at different temperatures: *a* – hardening temperature 1150 °C; *b* – hardening temperature 1110 °C; *c* – hardening temperature 1085 °C; *d* – hardening temperature 526 °C
Source [53, 54]



● **Fig. 3.29** Schematic of the diffraction pattern of a sample of nickel-chromium alloy "Nikorin" quenched from a temperature of 1150 °C
Source [53, 54]



● **Fig. 3.30** Schematic diffraction pattern of a sample of nickel-chromium alloy "Nikorin" quenched from a temperature of 1100 °C
Source [53, 54]

● **Table 3.8** Microhardness of the matrix and carbides in the samples of the nickel-chromium alloy "Nikorin" after quenching from various temperatures

Sample No.	Quenching temperature of "Nikorin" alloys, °C	Microhardness of research alloys, MPa	
		Matrix	Carbide
1	1390	4120.89	–
2	1373	3405.69	21285.58
3	1286	2294.99	16483.55
4	1280	2043.68	23361.05
5	1190	2595.67	25755.55
6	1170	2227.98	25755.55
7	1150	1933.23	16483.55
8	1110	2365.06	16483.55
9	1085	2438.39	15239.97
10	526	3532.99	16483.55

Source [53, 54]

Data analysis **Table 3.8** shows that in the temperature range 1286–1280 °C, where peritectic-eutectic transformations are realized, the microhardness of the carbide changes extremely, which is probably associated with a change in the quantitative ratio of carbides. In the temperature range 1150 °C–1110 °C, the microhardness of the carbide is stable and amounts to 16483.55 MPa. However, at a temperature of 1150 °C, a significant decrease in the microhardness of the matrix (up to 1933 MPa) is observed, which is probably associated with the precipitation of the σ -phase. Quenching from a temperature of 526 °C leads to an increase in the microhardness of the matrix to 3533 MPa.

Based on the data in the table, it is possible to conclude that, as a result of grating from different temperatures, a redistribution of alloying elements occurs, which leads to jumps in the values of microhardness.

3.6 INFLUENCE OF THE STRUCTURAL-PHASE STATE ON THE MECHANICAL AND TRIBOLOGICAL PROPERTIES OF CHROMIUM-NICKEL ALLOYS IN THE CAST STATE

The work carried out the measurement of hardness at elevated temperatures of samples of chromium-nickel alloy "Nikorin" in the initial state.

This type of study allows one to make an express assessment of the heat resistance characteristics of a given material without expensive tensile tests. The hardness, which is measured by the indentation of the indenter, characterizes the value of the resistance of the material [43].

Table 3.9 shows the data of hardness measurements at high temperatures on samples of the nickel-chromium alloy "Nikorin" in the cast state.

● **Table 3.9** Measurement data of the high-temperature hardness of the nickel-chromium alloy "Nikorin"

Test temperature, °C	300	400	500	600	700	800	950
Hardness HV1, GPa	2.41	3.15	2.3	3.09	2.56	1.92	0.98

Source [59, 60]

The analysis of the table shows that at a test temperature of 300 °C the hardness of the chromium-nickel alloy is small and amounts to 2.41 GPa, with an increase in temperature to 400 °C the hardness of the alloy slightly increases (3.15 GPa). A temperature of 500 °C leads to the fact that the hardness index drops sharply and amounts to 2.3 GPa. Thereafter, the hardness of the research chromium-nickel alloy increases.

On the curve of the temperature dependence of the hardness of the heat-resistant chromium-nickel alloy "Nikorin" (**Fig. 3.31**) in the temperature range of 500–600 °C, there is a sharp change in hardness. Probably, in this temperature range, dissolution of secondary excess carbides in nickel austenite occurs, which explains the sharp drop in hardness at 500 °C.

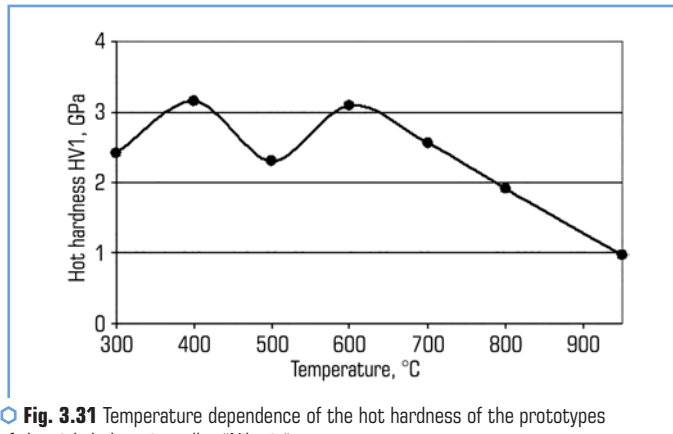


Fig. 3.31 Temperature dependence of the hot hardness of the prototypes of the nickel-chromium alloy "Nikorin"
Source [59, 60]

Also, tests were carried out for wear resistance under friction conditions at elevated temperatures and various loads of samples of the nickel-chromium alloy "Nikorin" in the cast state. The research results are shown in **Tables 3.10, 3.11**.

Table 3.10 shows the results of tribotechnical tests of samples of chromium-nickel alloy "Nikorin" in the cast state at room temperature.

- **Table 3.10** Results of studies on the wear resistance of the nickel-chromium alloy "Nikorin" under friction conditions at various loads

State of research samples	Specific load, kg/mm ²	Speed m/s	Sliding distance, km	Wear rate <i>i</i>	Wear resistance index <i>n</i>
Chromium-nickel alloy "Nikorin"	0.02	1	7.2	2.6×10^{-8}	7.58
	0.03	1	7.2	4.92×10^{-8}	7.3
	0.04	1	7.2	7.3×10^{-8}	7.13

Source [61–63]

- **Table 3.11** The results of studies on the wear resistance of the nickel-chromium alloy "Nikorin" under friction conditions at elevated temperatures and a load of 500 N

State of research samples	Load, [N]	Speed m/s	Sliding distance, km	Wear rate <i>i</i>	Friction coefficient μ	Wear resistance coefficient, <i>n</i>
Chromium-nickel alloy "Nikorin"	500	2	0.6	9.3×10^{-7}	0.4	6.03

Source [61–63]

Analysis of the results of tribological studies carried out at specific loads of 0.02–0.04 kg/mm² (**Table 3.10**) indicates that with an increase in the specific load, an increase in the intensity of wear (i) of the nickel-chromium alloy "Nikorin" in the cast state is observed with 2.6×10^{-8} to 7.3×10^{-8} , and the wear resistance coefficient (n) decreases (from 7.58 to 7.13).

Fig. 3.32 shows the dependence of the wear rate on the specific load of the nickel-chromium alloy "Nikorin". Analysis of the graphical dependencies indicates that the wear rate of the nickel-chromium alloy "Nikorin" increases significantly with increasing specific load. At a specific load of 0.04, this indicator is the highest.

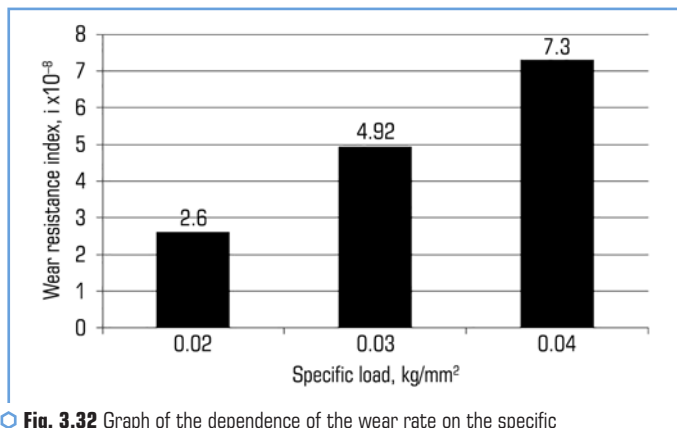


Fig. 3.32 Graph of the dependence of the wear rate on the specific load of the nickel-chromium alloy "Nikorin"

Fig. 3.33 shows the dependences of the wear resistance index of the nickel-chromium alloy "Nikorin" on the specific load at room temperature of tests. The analysis of the graphical dependencies indicates that the wear resistance indicator decreases with an increase in the specific load.

The work also carried out tribotechnical studies of samples of the nickel-chromium alloy "Nikorin" in the cast state at a load of 500 N. The test temperature in contact was 950 °C (**Table 3.11**).

Analysis of the test data for wear resistance under frictional conditions (**Table 3.11**) indicates that at a load of 500 N the nickel-chromium alloy "Nikorin" has a high wear rate (9.3×10^{-7}) and, accordingly, a low wear resistance coefficient (6.03), and the coefficient friction (μ) is 0.4. With an increase in loads to 600–750 N, the nickel-chromium alloy "Nikorin" began to collapse during testing.

Thus, the nickel-chromium alloy "Nikorin" in the cast state demonstrates the best wear resistance at loads of 0.02–0.04 kg/mm² (minimum wear rates and maximum wear resistance rates).

Frictional wear leads to a change in the structure, phase composition and properties of the nickel-chromium alloy "Nikorin".

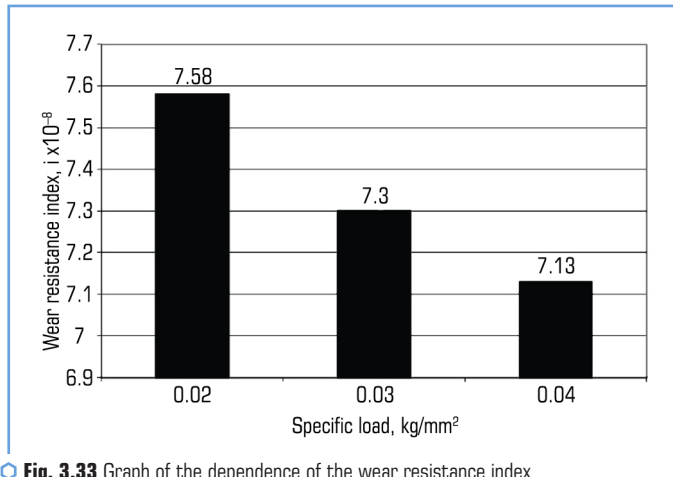


Fig. 3.33 Graph of the dependence of the wear resistance index of the nickel-chromium alloy "Nikorin" on the specific load

In Fig. 3.34 shows the structure of the nickel-chromium alloy "Nikorin" in the cast state after tribological tests at room temperature. The structure contains TiC carbides, which are located in the bulk of Cr_7C_3 carbides, which indicates their initial role in crystallization. Cr_7C_3 carbides are also destroyed during drift. However, since the chromium carbide in this alloy is not alloyed, its destruction occurs to a lesser extent and mainly at the TiC/ Cr_7C_3 interface. Significant fracture zones were also found at the TiC/matrix interface.

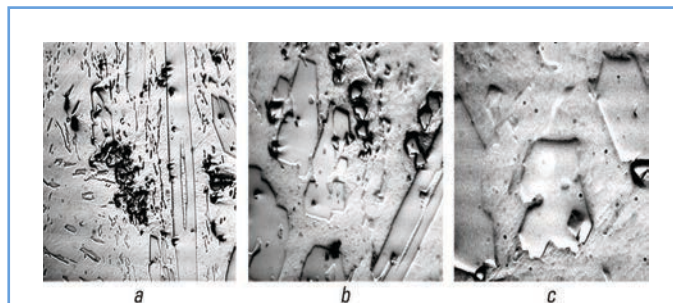


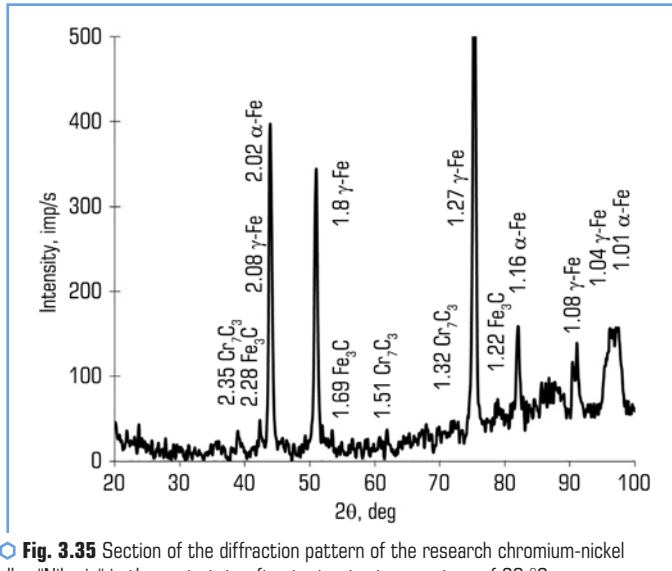
Fig. 3.34 Microstructure of the nickel-chromium alloy "Nikorin" in the cast state after testing at a temperature of 20 °C and a specific load of 0.04 kg/mm²: a – $\times 200$; b – $\times 500$; c – $\times 1000$

Friction wear of the nickel-chromium alloy "Nikorin" at a test temperature of 20 °C leads to a change in its phase composition.

In **Fig. 3.35** shows the diffraction patterns of the nickel-chromium alloy "Nikorin" in the cast state after tests at room temperature and a specific load of 0.04 kg/mm^2 . Phase X-ray diffraction analysis made it possible to reveal in the "Nikorin" alloy Cr_7C_3 carbide, Fe_3C carbide and a matrix consisting of 14 % austenite and 86 % ferrite.

Table 3.12 shows the quantitative data of X-ray structural analysis of the research chromium-nickel alloy "Nikorin" before and after friction wear: the value $\beta_{0.5}$ of the (011) line_a, characterizing the degree of imperfection of the-phase; amount of retained austenite (% γ); the residual austenite parameter (a_γ) and the α -phase parameter (a_α).

Data analysis **Table 3.12** indicates that the structure of the chromium-nickel alloy after frictional drift contains the α -phase, the degree of imperfection ($\beta_{0.5}$) of the lattice of which is 0.43, and the lattice parameter (a_α) is 2.91.



○ **Fig. 3.35** Section of the diffraction pattern of the research chromium-nickel alloy "Nikorin" in the cast state after tests at a temperature of $20 \text{ }^\circ\text{C}$ and a specific load of 0.04 kg/mm^2

● **Table 3.12** Quantitative data of X-ray structural analysis of the research chromium-nickel alloy "Nikorin" before and after friction wear at room temperature

Test temperature	a_α to (011) α		a_γ to (022) γ		Imperfection degree α - phase ($\beta_{0.5}$)		% γ , in the matrix	
	before wear	after wear	before wear	after wear	before wear	after wear	before wear	after wear
+20 $^\circ\text{C}$	–	2.91	3.59	3.57	–	0.43	100	14

In the process of testing, measurements were made of the microhardness of the decomposition products of austenite, the eutectic component and the hardness of prototypes of the nickel-chromium alloy "Nikorin". **Table 3.13** shows the data of measurements of the microhardness of the matrix, eutectic carbide and the hardness of samples of the chromium-nickel alloy "Nikorin" before and after wear by friction at room temperature and a specific load of 0.04 kg/mm².

● **Table 3.13** Microhardness of matrix, eutectic carbide and hardness of samples of chromium-nickel alloy "Nikorin" before and after friction wear

Test temperature	Microhardness of structural components, MPa				Hardness, HRC	
	Decomposition products of austenite		Eutectic carbides		before wear	after wear
	before wear	after wear	before wear	after wear		
+20 °C	2769	2468	18921	17886	47	33

The frictional wear of the nickel-chromium alloy "Nikorin" leads to a decrease in the microhardness of the matrix (from 2769 MPa to 2468 MPa), carbide (from 18921 MPa to 17886 MPa) and the general rigidity of the test specimens. The hardness of the Nikorin chromium-nickel alloy after tribological tests is 33 HRC.

This nature of the change in the microhardness of the matrix, carbide and the total rigidity of the prototypes of the nickel-chromium alloy "Nikorin" is due to structural changes, as well as the redistribution of alloying elements between phases and structural components in the process of friction wear.

CONCLUSIONS

The structure, phase composition and properties of the nickel-chromium alloy "Nikorin" in the cast state were investigated:

- it has been found that the structure of the heat-resistant chromium-nickel alloy in the initial cast state consists of high-nickel austenite, high-chromium carbide Cr₇C₃, titanium carbide TiC and intermetallic compound Ni₃Al;
- by the method of X-ray structural analysis, the phase composition has been studied and the carbide analysis of research alloys has been carried out. It has been shown, that:
 - the presence of high-chromium carbides ensures high hardness of research alloys;
 - the σ-phase has been found in the nickel-chromium alloy "Nikorin", which negatively affects the operational properties of the alloy;
 - Ni₃Al intermetallic compounds have been found in the structure of the "Nikorin" alloy;

- the distribution of alloying elements between the phases and structural components in the nickel-chromium alloy "Nikorin" in the cast state has been studied;
- it has been established that heat-resistant chromium-nickel alloys have a homogeneous structure with a uniform distribution of alloying elements over the section of the casting;
- calorimetric analysis of research alloys during heating/cooling has been carried out. The crystallization/melting temperatures of the nickel-chromium alloy "Nikorin" were determined;
- specific structure, phase composition, microhardness of the structural components of the heat-resistant chromium-nickel alloy "Nikorin" after quenching from different temperatures;
- a carbide analysis has been, which confirmed the presence in the structure of a heat-resistant chromium-nickel alloy quenched from a temperature of 1150, 1100 °C of the σ -phase (FeCr);
- a comprehensive study of structure formation and phase transformations during crystallization and in the solid state of the nickel-chromium alloy "Nikorin" confirms the realization of peritectic-eutectic transformation in these alloys;
- a high-temperature hardness of the nickel-chromium alloy "Nikorin" in the cast state has been investigated;
- tests for wear resistance have been conducted under friction conditions at room and elevated temperatures and various loads of samples of nickel-chromium alloy "Nikorin" in the cast state;
- it has been found that the best indicators of wear resistance (minimum indicators of wear intensity and maximum indicators of wear resistance coefficient) are demonstrated by samples of nickel-chromium alloy "Nikorin" in the cast state at loads of 0.02–0.04 kg/mm². Frictional wear leads to a change in the structure, phase composition and properties of the nickel-chromium alloy "Nikorin";
- a decrease in the microhardness of the decomposition products of austenite, eutectic carbide and the total hardness of the tested samples has been observed. The hardness of the "Nikorin" chromium-nickel alloy after tribological tests is 33 HRC.

CONFLICT OF INTEREST

The authors declare that they have no conflict of interest in relation to this research, whether financial, personal, authorship or otherwise, that could affect the research and its results presented in this paper.

REFERENCES

1. Rozhkova, E. V., Vatkovskaia, I. E. (1985). Prokalivaemost iznosostoikikh chugunov. Liteinoe proizvodstvo, 1, 33–35.
2. Stepina, A. I., Stupitckii, A. M., Kleis, I. R. (1977). Vlianie struktury na iznosostoikost chugunov. Liteinoe proizvodstvo, 9, 26–36.

3. Romanov, O. M., Rozhkova, E. V., Kozlov, L. Ia., Shveikhsman, A. O. (1981). Iznosostoikie lopatki drobemetnykh apparatov. Liteinoe proizvodstvo, 6, 26–30.
4. Leshchenko, A. D., Kutuzov, A. D., Lunev, V. V. (1988). Sostav khromistogo chuguna s zadannyimi svoystvami. Liteinoe proizvodstvo, 6, 8–12.
5. Komarov, O. S., Susina, O. A., Urbanovich, N. I. et al. (1997). Vliianie struktury metallicheskoj osnovy vysokokhromistykh splavov na ego tribotekhnicheskie kharakteristiki. Lite i metallurgii. Inf. Biulleten, 7–9, 22–24.
6. Shebatinov, M. P., Romanov, L. I., Prokhorov, M. I. et al. (1984). Issledovanie uslovii iznosostoikosti chuguna. Trudy Gorkovskogo instituta vodnogo transporta, 206, 99–109.
7. Slabodinskii, I. N., Kirievskii, B. A., Smoliakov, L. G. (1972). Issledovanie poverkhnostnykh sloev vysokokhromistykh chugunov pri gidroabrazivnom iznose. Lite iznosostoikie materialy. Sbornik IPL AN USSR. Kiev, 21–26.
8. Frost, R. H., Maewski, T., Krouss, G. (1984). Impact fracture behavior of high-chromium-molibdenium white cast iron. Transactions of the American Foundrymen's Society, 94 (11–15), 293–322.
9. Iurasov, S. A., Kozlov, L. Ia., Rozhkova, E. V. et al. (1984). Vliianie struktury metallicheskoj osnovy na prochnost khromistykh splavov. MITOM, 7, 18–20.
10. Bunin, K. P., Taran, Ia. N. (1972). Stroenie chuguna. Moscow: Metallurgii, 160.
11. Grigorovich, V. K. (1970). Elektronnoe stroenie i termodinamika splavov zheleza. Moscow: Nauka, 213.
12. Samsonov, G. V., Vinnitskii, I. M. (1976). Tugoplavkie soedineniia. Moscow: Metallurgii, 560.
13. Shank, F. A. (1973). Struktury dvoynykh splavov. Moscow: Metallurgii, 760.
14. Yukawa, N., Hida, M., Imura, T., Mizuno, Y., Kawamura, M. (1972). Structure of chromium-rich Cr-Ni, Cr-Fe, Cr-Co, and Cr-Ni-Fe alloy particles made by evaporation in argon. Metallurgical Transactions, 3 (4), 887–895. doi: <https://doi.org/10.1007/bf02647663>
15. Girshovich, N. G., Ioffe, A. Ia. (1958). Zharostoikie chuguny. Leningrad: Mashprom, 20.
16. Ulianin, E. A., Svistunova, T. V., Levin, F. L. (1986). Korrozionnoostoikie stali i splavy na osnove zheleza i nikelia. Moscow: Metallurgii, 262.
17. Issledovaniia po zharoprochnym splavam. Vol. 2 (1957). Izd. AN SSSR, 13–19.
18. Vintaikin, E. Z., Urushadze, G. G. (1969). Obrazovanie dalnego poryadka v splavakh nikel-hrom. DAN SSSR, 184 (3), 589–592.
19. Vintaikin, E. Z., Urushadze, G. G. (1970). Neytronno-difraktsionnoe issledovanie uporiadocheniya atomov v splavakh nikelya i hroma. Ukrainskiy biokhicheskii zhurnal, 15, 133–135.
20. Vintaikin, E. Z., Urushadze, G. G. (1969). Uporiadochenie splavov nikel-khrom. Fizika Metallov i Metallovedenie, 27, 895–903.
21. Zakharov, M. V., Zakharov, A. M. (1972). Zharoprochnye splavy. Moscow: Metallurgii, 384.
22. Sabol, G. P., Stickler, R. (1969). Microstructure of Nickel-Based Superalloys. Physica Status Solidi, 35 (1), 11–52. doi: <https://doi.org/10.1002/pssb.19690350102>
23. Khimushin, F. F. (1969). Zharoprochnye stali i splavy. Moscow: Metallurgii, 749.

24. Svistunova, T. V., Runova, Z. K., Kireeva, T. S., Tarasenko, V. A., Kostenko, A. G. (1976). Korroziionnaya stoykost nikelhromistyykh splavov v plavikovo-azotokislotnykh travilnykh rastvorah. *Stal*, 9, 851–853.
25. Svistunova, T. V., Kireeva, T. S., Runova, Z. K. (1983). Struktura i korroziionnoe povedenie khromonikelevyykh splavov tipa KhN60 v azotofloridnom rastvore. *Zashchita metallov*, 19 (2), 212–219.
26. Bannykh, O. A. (1994). Zharoprochnyye i zharostoikiye stali i splavy na nikelevoi osnove. Moscow: Nauka, 245.
27. Melnikova, N. A., Pakchanin, L. M., Petrenko, P. V. (1974). Issledovanie vozvrata ehlektroprotivleniya v splavakh nikel-khrom. *Fizika Metallov i Metallovedenie*, 37 (6), 1159–1163.
28. Struktura i svoystva zharoprochnyykh metallicheskiykh materialov (1967). Izd. Nauka, 349.
29. Pridantsev, M. V. (1973). Zharoprochnyye stareiushchie splavy. Moscow: Metallurgiya, 183.
30. Betteridzh, Tc. (1961). Zharoprochnyye splavy tipa nimonik. Moscow: Metallurgiya, 381.
31. Lanskaia, K. A. (1969). Zharoprochnyye stali. Moscow: Metallurgiya, 245.
32. Khimushin, F. F. (1962). Legirovanie, termicheskaya obrabotka i svoystva zharoprochnyykh staley i splavov. Moscow: Oborongiz, 320.
33. Salli, A. (1953). Polzuchest metallov i zharoprochnyykh svoystv. Moscow: Oborongiz, 290.
34. Khimushin, F. F. (1958). Zharoprochnyye gazoturbinnyye stali i splavy. Sovremennyye splavy i ikh termicheskaya obrabotka. MDNTP im. F. E. Dzerzhinskogo. Mashgiz, 348.
35. Rakhmanov, S. R. (2007). Dinamika strezhnevoi sistemy mekhanizma uderzhanii opravki proshivnogo stana truboprolatnogo agregata. Sovremennyye napravleniia proizvodstva svarynykh i besshovnykh trub iz chernyykh i tsvetnykh metallov. Dnepropetrovsk, 45–51.
36. Danchenko, V. N., Kolikov, A. P., Romantsev, B. A., Samusev, S. V. (2002). Tekhnologiya trubnogo proizvodstva. Moscow: Intermet – Inzhenering, 640.
37. Grudnev, A. P., Mashkin, L. F., Khanin, M. I. (1994). Tekhnologiya prokatnogo proizvodstva. Moscow: Metallurgiya, 650.
38. Saltykov, S. A. (1970). Stereometricheskaya metallografiya. Moscow: Metallurgiya, 375.
39. Wilson, F. R., Harding, R. A. (1984). The X-Ray Study of ADI. *BCIRA Journal*, 318–331.
40. Mirkin, L. I. (1979). Rentgenostrukturnyi kontrol mashinostroitelnykh materialov. Moscow: Mashinostroenie, 250.
41. Gorelik, S. S., Rastorguev, A. N., Skakov, Iu. A. (1963). Rentgenograficheskii i elektronno-graficheskii analiz metallov. Moscow: Metallurgiya, 218.
42. Kalinushkin, E. P. (2007). Peritekticheskaya kristallizatsiya legirovannykh splavov na osnove zheleza. Dnepropetrovsk: Porogi, 172.
43. Westbrook, J. H., Conrad, H. (Eds.) (1973). The Science of Hardness Testing and its Research Application. American Society for metals. Ohio: Metal Park, 520.
44. Kutcova, V. Z., Kovzel, M. A., Nesterenko, A. M., Zhivotovich, A. V. (2008). Struktura i fazovyi sostav zharoprochnogo khromonikelevogo splava "Nikorin". *Stroitelstvo, materialovedenie, mashinostroenie*, 45 (3), 44–51.

45. Kutcova, V. Z., Kovzel, M. A., Zhivotovich, A. V. (2008). Issledovanie struktury, fazovogo sostava i svoystv zharoprochnykh khromonikelevykh splavov v litom sostoianii. Oborudovanie i tekhnologii termicheskoi obrabotki metallov i splavov (OTTOM – 9), 1, 23–28.
46. Kutcova, V. Z., Zhivotovich, A. V., Kovzel, M. A., Kravchenko, A. V. (2008). Struktura, fazovyi sostav i fazovyi rentgenospektralnyi analiz zharoprochnogo khromonikelevogo splava "Nikorin". Metallofizika i noveishie tekhnologii, 30, 235–243.
47. Kutsova, V. Z., Kovzel, M. A., Grebeneva, A. V., Myrgorodskaya, A. S. (2012). Structure, phases and alloying elements distribution of Nikorim (high-temperature strength Ni-Cr alloy) in its cast form. Metallurgical and Mining Industry, 4 (1), 40–44.
48. Kutsova, V. Z., Kovzel, M. A., Velichko, O. O., Stradomski, Z. (2013). Structure, phases and alloying elements distribution of Nikorim (high-temperature strength Ni-Cr alloy) in its cast form. Metallurgy 2013. New technologies and achievements in metallurgy, material engineering and production engineering. Czestochowa, 31 (2), 99–105.
49. Berg, L. G. (1961). Vedenie v termografiiu. Moscow: Izd. AN SSSR, 368.
50. Piloian, G. O. (1984). Vvedenie v teoriyu termicheskogo analiza. Moscow: Izd. AN SSSR, 257.
51. Miroshnichenko, I. S. (1982). Zakalka iz zhidkogo sostoianii. Moscow: Metallurgiya, 168.
52. Lanskaia, K. A., Kobozaeva, Z. T. (1970). Spetsialnye stali i splavy. Moscow: Metallurgiya.
53. Petrushin, N. V., Logunov, A. V., Dolzhanskii, Iu. M. (1981). Prognozirovaniye zakonomernosti izmeneniya svoystv v zavisimosti ot legirovaniya Cr, Co, Nb, W. Metallovedenie i termicheskaya obrabotka metallov, 5, 10–15.
54. Kutsova, V. Z., Kovzel, M. A., Hrebeneva, A. V. (2011). Zakonomernosti formyrovaniya strukturi khromonykelevogo splava "Nikorim". Novi materialy i tekhnologii v metalurhii ta mashynobuduvanni. Zaporizhzhia, 1, 59–66.
55. Kutsova, V. Z., Kovzel, M. A., Hrebeneva, A. V. (2012). Struktura, fazovyi sklad khromonikelevogo splavu "Nikorim" u termoobroblenomu stani. Metaloznavstvo ta termichna obrabotka metaliv, 1, 31–34.
56. Bunin, K. P., Malinochka, Ia. N., Taran, Iu. N. (1969). Osnovy metallografii chuguna. Moscow: Metallurgiya, 416.
57. Bobro, Iu. G., Tikhonovich, V. I., Bobro, A. Iu. (1990). Upravlenie strukturoi metallicheskoj matritcy iznosostoikikh chugunov. Protsesty litia, 1, 31–35.
58. Diagrammy sostoianii metallicheskih sistem tematiceskii spravochnik (1978). Moscow, 308.
59. Kutcova, V. Z., Kovzel, M. A., Grebeneva, A. V., Gorna, I. D., Velichko, O. O. (2012). Vpliv izotermichnogo gartuvannia na mekhanichni vlastivosti visoko khromistikh splaviv. Metallurgicheskaya i gornorudnaia promyshlennost, 7, 255–261.
60. Kutcova, V. Z., Kovzel, M. A., Velichko, O. A., Stradomski, Z. (2013). Iznosostoikost vysokokhromistikh splavov v shirokom intervale temperatur. Metallurgy 2013. New technologies and achievements in metallurgy, material engineering and production engineering. Czestochowa, 31 (2), 81–87.

61. Kindrachuk, M. V., Kutcova, V. Z., Kovzel, M. A., Velichko, O. O. (2013). Vpliv izotermichnogo gartuvannia na znosostiikist visokokhromistikh splaviv v umovakh tertia pri pidvishchenikh temperaturakh. *Mashinoznavstvo*, 7–8 (193–194), 59–63.
62. Kutcova, V. Z., Kovzel, M. A., Grebeneva, A. V., Velichko, O. O. (2014). Tribotekhnicheskie svoistva vysokokhromistykh splavov v litom i termoobrabotannom sostoianii pri komnatnoi i povyshenoi temperature ispytanii. *Metallurgicheskaia i gornorudnaia promyshlennost*, 3, 69–74.
63. Kindrachuk, M. V., Kutcova, V. Z., Kovzel, M. A., Grebeneva, A. V., Danilov, A. P., Khlevina, Iu. L. (2012). Tribotekhnicheskie svoistva vysokokhromistykh splavov v litom i termoobrabotannom sostoianii. *Problemi tribologii (Problems of Tribology)*, 2, 58–63.

CHAPTER 4

THE INFLUENCE OF EXTERNAL ACTIONS AND METHODS OF
ALLOYING ALLOYS ON THE OPERATIONAL CHARACTERISTICS
OF CAST PRODUCTS

ABSTRACT

The chapter presents the results of scientific research on the influence of electromagnetic stirring and alloying on the properties of deformable aluminum alloys, the influence of alloying elements on the phase state and structural stability of heat-resistant corrosion-resistant alloys, which are used for the manufacture of turbine blades of gas turbine engines (GTE), is analyzed. The results of studies on the effect of alloying a heat-resistant nickel-based alloy with tantalum and rhenium on its operational characteristics are presented.

The influence of excess pressure on the properties and quality of castings from iron-carbon alloys during lost foam casting is determined.

It is determined that under the controlled influence of technological factors and excess pressure (2...6 MPa) on liquid metal and during its crystallization, it is possible to increase the mechanical strength and reduce the porosity of cast iron and steel castings by 15...30 %, compared to gravity casting according to models, which are gasified.

The latest technological processes for the production of ordinary and reinforced castings with specified properties by casting according to gasified models, using excess pressure on the metal, have been developed.

The work carried out by the authors at the Physical and Technological Institute of Metals and Alloys of the National Academy of Sciences of Ukraine is of high scientific and practical importance for the production of high-quality foundry products and will be useful for foundry product manufacturers, scientific and scientific-pedagogical workers of the specialty "Metallurgy" (Foundry production).

KEYWORDS

Deformable aluminum alloys, vacuum magnetohydrodynamic complex, heat-resistant alloy, gas turbine engine, turbine blade, continuously cast aluminum ingots, modification, iron-carbon alloys, lost foam casting, thermal destruction of polystyrene, physical and mechanical properties of cast structures, influence of pressure on metal.

The high quality of structural materials can be ensured by using the latest methods of preparing alloys, based on the intensification of the processes of interaction of gas, liquid and solid phases with the melt. The use of plasma, centrifugal and electromagnetic actions on metal systems in a vacuum provides wide opportunities for the creation of effective technologies for mass and special purpose metal production, based on the processes of treating alloys with dispersed and active reagents in a highly reactive state. The creation of such breakthrough technologies for obtaining high-quality structural materials with economical consumption of energy resources and materials is relevant and meets the requirements of science and practice at the current stage.

To achieve greater efficiency of gas turbines in the fields of aviation power and ship gas turbine construction, an important task is to increase the operating temperatures at the turbine inlet. However, different types of turbines are designed to work on different types of fuel and in different operating conditions. Therefore, there is a need to use heat-resistant nickel alloys with different chemical compositions and physical properties to meet the specifications and requirements of different turbines in these industries. The relevance and economic significance of research is due to the intensive development of unique technology and the growing need for materials with increased or new functional characteristics.

In order to achieve the guaranteed quality and strength of cast structures due to the increase in the mechanical properties of iron-carbon alloys, the effect of regulated pressure on the metal in the mold during lost foam casting was investigated.

4.1 MODERN PROCESSES OF PRODUCTION OF CAST STRUCTURAL MATERIALS FROM ALUMINUM ALLOYS FOR PRODUCTS OF RESPONSIBLE PURPOSE

4.1.1 THE INFLUENCE OF EXTERNAL ACTIONS AND MELT ALLOYING METHODS ON THE STRUCTURES AND PROPERTIES OF PRODUCTS MADE OF DEFORMABLE ALUMINUM ALLOYS

Deformable aluminum alloys with a unique complex of mechanical and operational properties have low density, sufficiently high strength and machinability, are an irreplaceable structural material for the aerospace, automotive and shipbuilding industries, as well as for the production of special military equipment.

Many years of experience have established a direct dependence of the mechanical and technological properties of ingots on their primary structure, which is formed in the process of crystallization during continuous casting. Ingots with a uniform fine-crystalline (non-dendritic) structure have the highest properties, which ensures:

- 1.5–2.0 times increase in plasticity in the cast state with high resistance to cracking of ingots;
- reduction by 2–3 times of the duration of homogenizing annealing of ingots before plastic deformation;

- a 4–6-fold reduction in the pressing force of semi-finished products and an increase in crack resistance during hot deformation;
- 20–30 % increase in strength and 1.3–1.8 times the plasticity of products made from these ingots compared to semi-finished products with a dendritic structure.

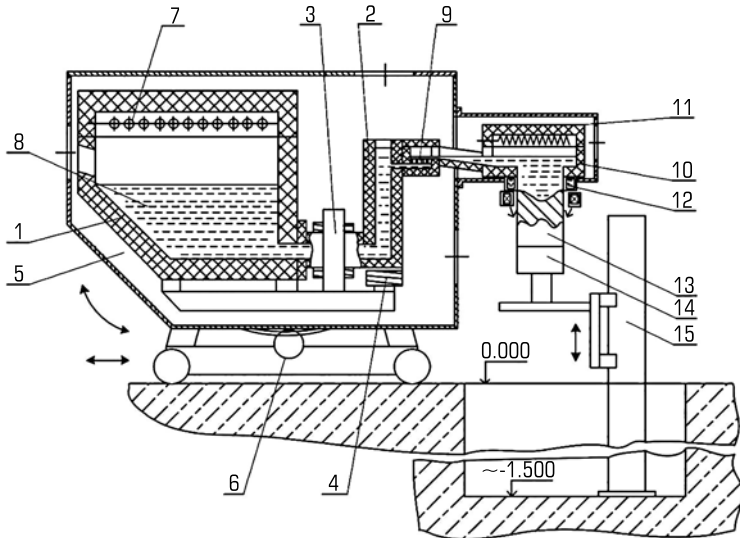
The structure in ingots is dispersed by modifying alloys with manganese, chromium, zirconium, scandium and other elements. The primary structure in ingots is crushed also when ultrasonic, electromagnetic, vibrational vibrations and other external influences are applied to the liquid metal.

The Physics and Technology Institute of Metals and Alloys of the National Academy of Sciences of Ukraine has developed and successfully operates a melting and pouring complex, which includes a vacuum magnetodynamic mixer (MHD-mixer) and a continuous ingot casting machine (CICM) [1] (**Fig. 4.1**). The use of such a complex for the preparation of aluminum alloys and the continuous casting of ingots from them allows [2]:

- constantly stir the liquid metal with electromagnetic forces during the preparation of alloys. Due to this, increase the degree of assimilation of alloying elements by the melt and evenly distribute them in cast products;
- refine the alloy in a vacuum (dilution ~1 mm Hg) with constant electromagnetic stirring of the alloy and reduce the hydrogen content in the ingots to 0.05–0.12 cm³/100 g of metal;
- pass the melt through a ceramic filter and effectively remove oxide inclusions until their final concentration in the alloy is ≤0.05 vol. %;
- create a protective atmosphere of inert gases above the melt in the MHD unit and during feeding into the crystallizer, which excludes additional gas saturation and oxidation of the alloy;
- regulate the intensity of electromagnetic mixing of the alloy in the crystallizer and control the process of structure formation in ingots.

Most deformable aluminum alloys, especially high-strength ones, contain refractory elements Mn, Cr, Ti, Zr, etc. As a rule, ligatures are used for their introduction into the alloy. One of the main advantages of preparing aluminum alloys in a vacuum MHD mixer is the intensification of the dissolution processes of elements, including pure refractory metals. Their dissolution occurs in the active zone – the section of the mixer channel, where the magnetic fields of the inductor and the electromagnet interact, thus creating the maximum magnetohydrodynamic factors of influence on the melt [3]. So, for example, it was shown [4] that with the optimal combination of the magnitude and direction of action of volumetric electromagnetic forces in the active zone of the MHD mixer, pure chromium in the amount of 3.0 wt. % can be dissolved in aluminum in ~20 minutes without significantly overheating the metal.

The properties of deformable aluminum alloys are largely determined by their hydrogen content, the presence of which leads to the development of macro- and microporosity, prevents the welding of discontinuities formed during pressure treatment. The influence of vacuum refining of the melt in the MHD mixer on the quality of continuous cast ingots from the secondary aluminum alloy AD31 [5] is shown on the example of experimental melts, the technological regimes of which are given in **Table 4.1**. The quality of ingots from the AD31 alloy must meet the requirements of the standards of regulatory documentation.



- 1 – crucible;
 2 – metal conduit;
 3 – inductor;
 4 – electromagnet;
 5 – vacuum chamber;
 6 – vacuum chamber rotation drive;
 7 – heating elements;
 8 – liquid metal;
 9 – camera with foam ceramic filter;
 10 – thermal nozzle;
 11 – filling device;
 12 – crystallizer;
 13 – ingot;
 14 – seed;
 15 – mechanism of vertical movement of the crystallizer

○ **Fig. 4.1** Vacuum MHD complex for the preparation of aluminum alloys and continuous casting of ingots from them

● **Table 4.1** Technological parameters of the preparation of secondary alloy AD31 and continuous casting of ingots from it

Melting No.	Melting of the charge on the "dry floor"	Overflow to the MHD-mixer through the KS11LA filter mesh	Modification with Al-Ti-B ligature	Modes of vacuum refining		Filtration through a porous ceramic filter	Ingot casting modes	
				Vacuum, mm Hg	Refining duration		Temperature, °C	Casting speed, mm/min
1	+	+	–	–	–	+	690–705	110
2	+	+	+	–	–	+	690–705	110
3	+	+	+	1	30	+	690–705	110

It can be seen that in ingots made of alloys without melt processing in a vacuum (melts No. 1, 2), the hydrogen content is 0.4–0.5 cm³/100 g of metal, which exceeds the requirements of regulatory

documentation ($\leq 0.3 \text{ cm}^3/100 \text{ g}$). The concentration of hydrogen in vacuum metal ingots (melt No. 3) is $0.05\text{--}0.07 \text{ cm}^3/100 \text{ g}$.

The macrostructure of the ingots (melts No. 1 and No. 2) is coarse-grained fan-shaped with a clear arrangement of dendrites in the radial direction (**Fig. 4.2, a**).

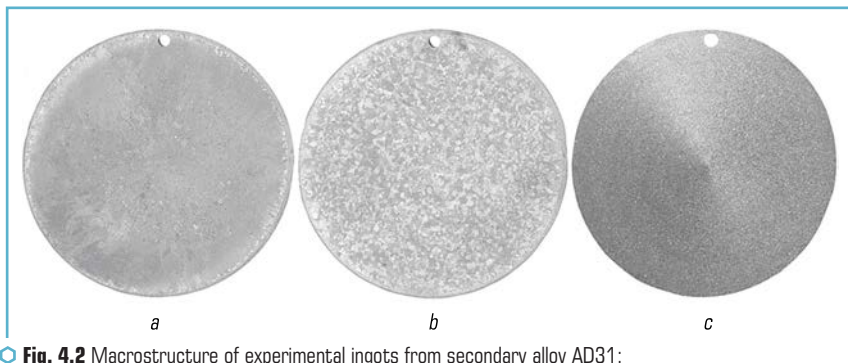


Fig. 4.2 Macrostructure of experimental ingots from secondary alloy AD31: *a* – melt No. 1; *b* – melt No. 2; *c* – melt No. 3

Alternating zones of fan-shaped and coarse-grained equiaxed structures, as well as light veins and non-metallic inclusions are also observed (**Fig. 4.2, b**). The macrostructure of the ingots (melt No. 3) obtained from the vacuum-refined alloy is fine-grained, homogeneous, without light spots and non-metallic inclusions (**Fig. 4.2, c**) and fully meets the requirements of the standards. In this way, vacuum refining makes it possible to obtain ingots from the secondary AD31 alloy, which in terms of their properties are at the level of cast metal made from primary materials.

During the vacuum refining of high-strength aluminum alloys, one of the main alloying elements – zinc – evaporates, the content of which can reach $\sim 10\%$. To eliminate the evaporation of zinc, the rarefaction above the alloy in the vacuum chamber must be higher than the value of its vapor elasticity. Thus, in industrial technologies for the preparation of such alloys with vacuum treatment in a ladle or mixer, the rarefaction above the melt during refining is maintained at a level of $\geq 10 \text{ mm Hg}$. With such a vacuum, a lot of hydrogen remains in the ingots after crystallization ($0.27\text{--}0.29 \text{ cm}^3/100 \text{ g}$ of metal). For the preparation of high-strength aluminum alloys with a high zinc content in a vacuum MHD unit, a technology has been developed that allows eliminating losses of this alloying element by evaporation and reducing the hydrogen content in ingots to $0.05 \text{ cm}^3/100 \text{ g}$ of metal [6].

For the preparation of high-quality aluminum alloys, a refining method was developed [7] using successive vacuum pulses, which ensures a residual concentration of hydrogen in ingots at the level of $0.01\text{--}0.03 \text{ cm}^3/100 \text{ g}$ of metal. Methods of operational control of the hydrogen content in liquid metal [8] were also created, which made it possible to automate the process of preparing alloys in the MHD-unit.

The quality and properties of ingots made of deformable aluminum alloys significantly depend on the concentration of oxide inclusions, in particular, Al_2O_3 in them. To eliminate (reduce) oxidation of the liquid metal, all components of the vacuum MHD complex (mixer crucible, dispensing chamber and crystallizer) are hermetically connected. Such a connection allows creating a protective environment of inert gases over the metal at all stages of ingot production from melting to casting. The creation of a protective environment is especially relevant when preparing alloys that contain easily oxidizable elements, for example, magnesium (alloys 1560, 1575, 1545, etc.).

The oxide film formed on the surface of aluminum alloys of the Al-Mg system during their melting has low strength and is destroyed when the liquid metal is stirred. Therefore, during the preparation of alloys with magnesium, the surface film does not protect the melt from oxidation. To protect such alloys from oxidation, small beryllium additives are introduced into the melt, which form a dense film of beryllium-magnesium oxides on the surface of the liquid metal bath. Such a film significantly reduces the oxidation of alloys and the content of non-metallic inclusions in ingots. However, beryllium and its compounds are poisonous, and its use in the production of alloys is dangerous. Therefore, the task of excluding beryllium from the technologies of preparing alloys of the Al-Mg system is urgent. The effectiveness of using a protective argon environment against metal oxidation in the production of ingots from the experimental alloy 1545 containing 4.5 % by mass. magnesium, shown in **Table 4.2**. It can be seen that the ingots (melt No. 1), obtained without protection of the melt from oxidation, have a tensile strength of 30 %, and the relative elongation is 2.4 times less than that of ingots from an alloy that protected against oxidation (melts No. 2 and No. 3).

● **Table 4.2** Conditions for experimental melting of alloy 1545 and results of mechanical tests of samples in the cast state

Melt- ing No.	Melting peculiarities	Mechanical properties		
		$\sigma_{0.2}$, MPa	σ_B , MPa	δ , %
1	Without the use of measures to protect the melt from oxidation	132	215	5
2	With the use of a ligature Al-5 wt. % Be (based on 0.0003 wt. % Be in the alloy)	204	294	12
3	With the use of protective argon environment	207	292	13

An important factor affecting the crystallizing metal is electromagnetic stirring. To regulate the intensity of mixing of the alloy during the crystallization of the ingot, a low crystallizer with a thermal nozzle and an electromagnetic stirrer is installed on the continuous casting machine (**Fig. 4.3**). The design of the crystallizer is designed so that the magnetic field of the stirrer affects the alloy in the liquid and liquid-solid state.

With the help of electromagnetic stirring, it is possible to influence the nature and speed of movement of liquid metal in the crystallizer [9]. In order to exclude bubbling in the crystallizer and tightening of oxide films from the alloy surface into the middle of the ingot, the melt movement should

be laminar (value $Re < 6900$). If this indicator is exceeded, the quality of the ingot deteriorates and liquid metal may break through the surface layer of the ingot, which has begun to crystallize.

The use of electromagnetic stirring during continuous casting also allows for the alignment of the crystallization front of the alloy, which helps to reduce the anisotropy of properties and internal stresses in the ingot. At the same time, the structural components in the alloy are crushed. Mixing is advisable when introducing modifiers into the melt, which intensifies the process of nucleation in the alloy and contributes to the uniform distribution of crystallization centers near the solidification front of the ingot. The movement of liquid metal in the crystallizer during electromagnetic stirring is shown in **Fig. 4.3**.

The effectiveness of the influence of electromagnetic stirring of the B96C alloy during its crystallization on the structure of a continuously cast ingot with a diameter of 90 mm is shown in **Fig. 4.4**. The part of the ingot produced without electromagnetic stirring of the alloy during the casting process (**Fig. 4.4**, upper part) has an uneven coarse crystal structure with a micrograin size ~ 350 microns. The ingot part that was cast using electromagnetic stirring has a uniform fine crystal structure with a micrograin size of $\sim 100 \mu\text{m}$ (**Fig. 4.4**, lower part).

The positive effect of electromagnetic mixing of the alloy in the ingot during its crystallization can be shown on the example of the production of a ligature bar Al-2.5 % by mass. Zr with an improved structure for modifying alloys directly in the crystallizer of a continuous casting machine [10].

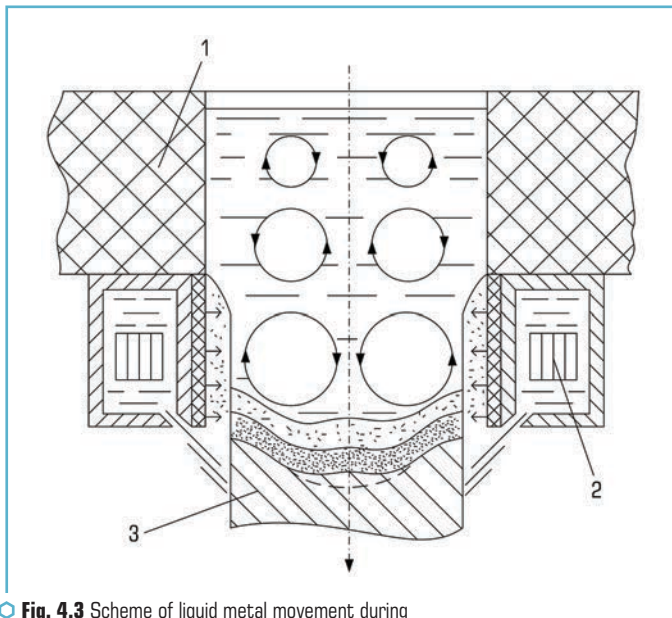


Fig. 4.3 Scheme of liquid metal movement during electromagnetic stirring in the crystallizer



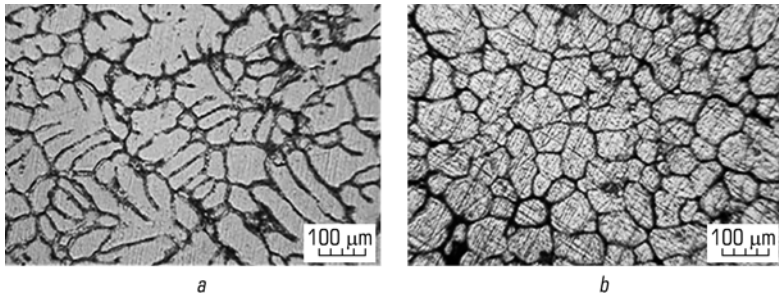
Fig. 4.4 Macrostructure of the longitudinal section of a continuously cast ingot $\varnothing 90$ mm from the B96Ts alloy: the upper part – without electromagnetic stirring; the lower one – with electromagnetic stirring of the alloy in the ingot

Technology of preparation of ligature alloy Al–2.5 % by mass. Zr from primary materials (aluminum grade A85 and zirconium grade KTC) consists in dissolving crushed zirconium in aluminum in the active zone of the MHD mixer at a temperature of 820 °C, followed by its increase to 1000 °C and exposure for 20 minutes. To avoid oxidation of the alloy, melting was carried out in a protective argon atmosphere. A continuously cast ingot with a diameter of 50 mm was produced. One part of the ingot was obtained without electromagnetic stirring of the alloy, the second – with stirring at an electromagnetic stirrer current of 160 A.

Part of the ingot of the ligature alloy, made without electromagnetic stirring, contains large (up to 100 μm) acicular Al_3Zr intermetallics, which reduce the mechanical properties of the alloy. Part of the ingot made with electromagnetic mixing of the alloy contains a modifying phase of 3–10 μm . Thus, the use of electromagnetic mixing of the alloy during ingot crystallization allows the structure to be dispersed in aluminum ligatures containing various refractory elements.

The modifying ability of the ligature bar Al–2.5 wt. % Zr and the influence of its modification of the alloy in the crystallizer on the mechanical properties of ingots were determined on the B96C1 alloy. The alloy was prepared in a vacuum MHD mixer from primary materials. The zirconium content in the alloy was 0.10 wt. %. Two ingots of $\varnothing 150$ mm were cast from the prepared alloy. The first of them was obtained by continuous modification of the alloy in the crystallizer with a ligature rod Al–2.5 wt. % Zr. This rod was produced by continuous casting with electromagnetic stirring of the ligature during the crystallization process. With the help of a rod, an additional 0.03 wt. % of zirconium was introduced into the alloy. After dissolving the rod, the total concentration of zirconium in the alloy was ~ 0.13 % by mass.

After casting the first ingot into the alloy remaining in the MHD mixer, crushed zirconium was added to its content in the alloy ~ 0.13 wt. % and produced a second ingot using the usual technology without bar modification. The structures of the experimental ingots are shown in **Fig. 4.5**. The average grain size in the ingot obtained by conventional technology is ~ 280 μm , and in the ingot from an alloy modified with a ligature rod ~ 80 μm . After the homogenization annealing of the ingots, pressing and heat treatment according to the standard regimes for the B96C1 alloy, samples for mechanical tests were made, the results of which are presented in **Table 4.3**.



● **Fig. 4.5** Microstructure of continuously cast ingots with a diameter of 150 mm from the B96Ts1 alloy: *a* – produced according to traditional technology; *b* – modified with a ligature bar Al–2.5 % by wt. Zr

● **Table 4.3** Mechanical properties of hot-pressed billets from the B96C1 alloy

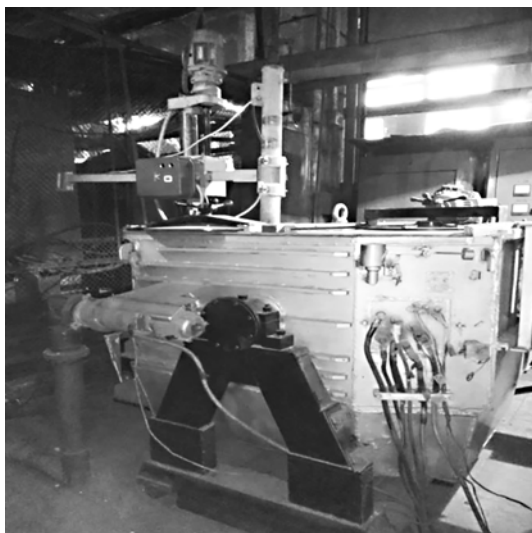
Manufacturing technology	σ_B , MPa	$\sigma_{0.2}$, MPa	δ , %
Modification with a ligature bar Al–2.5 % by mass. Gold	669	642	7.2
Traditional	632	611	4.5

It can be seen that after continuous modification with a rod made of ligature Al–2.5 % wt. Zr obtained using electromagnetic mixing of the alloy in the crystallizer, the grain size in the ingots decreases by 3.5 times, the tensile strength and yield strength (σ_B , $\sigma_{0.2}$) of the pressed products increases by 5–6 %, the relative elongation – by 35–40 % compared to experimental blanks made from an alloy that was modified according to traditional technology.

The created melting and pouring MHD equipment can be combined with plasmatrons and develop effective processes for preparing alloys and obtaining cast products from them [11, 12]. An example of such technologies can be the method of plasma nitriding of aluminum alloys in the MHD mixer (**Fig. 4.6**).

The high-strength aluminum alloy B93pch was melted in a mixer. The first ingot with a diameter of 250 mm was obtained from the prepared alloy by continuous casting. In the melt that remained

in the mixer after the production of the first ingot, a ligature of Al–5 % by mass was introduced. Ti based on the calculation of the titanium content in the alloy ~ 0.05 % by mass. Then, the titanium-doped alloy was treated with a plasma nitrogen jet immersed in the liquid metal. Nitriding of the alloy was carried out for 1.5–2 min at a voltage on the plasmatron of 60..65 V, a constant current of 380÷400 A, and a nitrogen consumption of ~ 7.5 l/min. After plasma nitriding of the melt, the B93pch+Ti+PN alloy was obtained, which was further refined in a vacuum and a second ingot with a diameter of 250 mm was cast from it.



○ Fig. 4.6 Vacuum MHD mixer with plasmatron

It was determined that the first Ingot from the B93pch alloy has a dendritic heterogeneous structure. The average grain size in it is 25÷30 % larger than in a cast made of a plasma-nitrided alloy (Fig. 4.7, a). In an alloy ingot doped with titanium and nitride by plasma, the structure is dispersed with a uniform distribution of grains of the same size (Fig. 4.7, b).

After the homogenization annealing of the ingots, isothermal pressing and heat treatment of the pressed products were carried out according to the T1 mode. The mechanical properties of the samples of the obtained products are shown in Table 4.4. It can be seen that after alloying with titanium and MHD-plasma nitriding of the alloy, the mechanical properties of pressed parts from continuously cast ingots increase: the tensile strength and yield strength (σ_B , $\sigma_{0.2}$) increase by 7÷10 %, relative elongation – by 20÷25 % compared to the requirements of OST 1 90073-85 for stampings made of alloy B93pch.

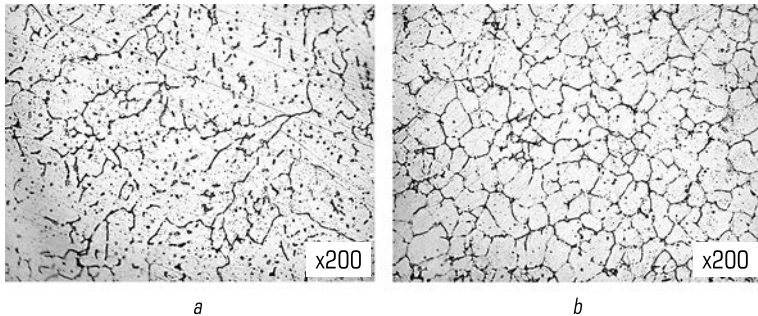


Fig. 4.7 Microstructure of continuously cast ingots with a diameter of 250 mm from experimental alloys: *a* – B93pch; *b* – B93pch+Ti+PN

Table 4.4 Mechanical properties of products from experimental alloys

Alloy	Mechanical properties		
	σ_B , MPa	$\sigma_{0.2}$, MPa	δ , %
B93pch	486	447	6.9
B93pc+Ti+PN	517	472	7.3
Requirements of OST 1 90073-85 for stampings from alloy V93pch	480	440	6.0

It is advisable to use the results of the performed research at enterprises that produce metal products of responsible and special purpose from aluminum alloys, as well as at foundry and metallurgical mini-plants.

4.2 INFLUENCE OF ALLOYING ELEMENTS ON SPECIAL PROPERTIES OF HEAT-RESISTANT ALLOYS

The problem of the resistance of marine gas turbine materials to high-temperature salt corrosion (HSC) is critical, especially compared to aircraft turbines that operate on refined kerosene, a light fuel, where HSC is not a problem. To ensure resistance to HSC, it is often necessary to increase the chromium content in materials, but this can lead to a decrease in the strength of alloys at high temperatures. In the case of aircraft alloys, the chromium content is usually limited to 6–8 wt. %, which is not feasible for alloys used in marine gas turbines. This creates an actual problem, since the temperature of the working environment in aircraft turbines is higher than in marine ones, and increasing this temperature becomes such an important task [13–15]. Unlike air turbines, marine turbines operate on heavy fuel with a high content of sulfur and other harmful impurities, as well as in the presence of water vapor and sea salts, which contribute to HSC.

The problem of creating multi-component heat-resistant nickel-based alloys for the blades of stationary gas turbine units (GTU) requires improving the structural and phase stability of materials. This improvement contributes to the reliability of the materials during long-term operation, which can be from 50 to 100 thousand hours at a temperature from 750 to 950 °C. It is especially important to achieve this stability under conditions of exposure to fuel with aggressive sulfur and vanadium impurities, which can affect the material.

The results of the assessment of the strength and durability of the main components and parts of the stationary gas turbine engine indicate the need to improve the operational characteristics of the working blades of the 1st and 2nd stages of the gas turbine. **Table 4.5** shows the chemical composition of modern global heat-resistant alloys for high-pressure gas turbine blades.

Heat-resistant corrosion-resistant alloys such as IN792 and CMSX-4 are known for their structural stability due to the balanced content of elements such as tantalum (Ta), molybdenum (Mo) and tungsten (W) (**Table 4.5**) [16, 17]. However, despite this stability, these alloys show insufficient long-term strength and corrosion resistance at the average surface temperature of the blades, which is up to 850 °C.

According to literature data [18–20], rhenium and tantalum are elements that exhibit the properties of effective hardeners of austenitic solid solution (rhenium) and active carbide and γ' -phase formers (tantalum). This helps to increase the heat resistance of the alloy. The structural stability of alloys containing rhenium and tantalum with the appropriate chromium content and the presence of topologically densely packed phases (TDPP-phases) will be determined both by the total content of refractory elements and their mutual ratio.

● **Table 4.5** Chemical composition of modern global heat-resistant alloys for high-pressure turbine blades of gas turbines

Alloy brand	Cr	Ni	Co	Mo	Re	W	Al	Ti	Ta	Nb	Hf
IN 738LC	16.0	base	8.5	1.7	–	2.6	3.4	3.4	3.4	0.9	–
CMSX-11C	14.9	base	3.0	0.4	–	4.5	3.4	4.2	5.0	0.1	0.04
SC PWA 1483	12.8	base	9.0	1.9	–	3.8	3.6	4.1	5.0	–	–
Rene 80H	14.1	base	9.2	4.0	–	4.0	3.1	4.7	–	–	0.74
DC GTD 111	14.0	base	9.5	1.5	–	3.8	3.0	4.9	2.8	–	0.15
CMSX-4	6.5	base	9.6	0.6	3.0	6.4	5.6	1.0	6.5	–	0.10
CM88Y	15.9	base	11.0	1.9	–	5.3	3.05	4.6	–	0.2	0.30

Elements such as chromium, molybdenum, tungsten, niobium, rhenium, and tantalum have the properties of both solid solution strengtheners and active carbide formers (chromium, tantalum, tungsten), and they are preferentially distributed in the γ -solid solution. The introduction of these elements into the alloy of the considered type may be justified to ensure phase-thermal stability

during engine operation, but this is possible only with a certain balance of tungsten, molybdenum and chromium content. When complex alloying with refractory metals, it is important to take into account their liquidation coefficients, especially when forming alloys with an oriented structure. The introduction into the composition of the alloy of elements that increase the difference in density between the main melt and the liquid (such as Al, Ti, Nb, and others), as well as refractory elements (W, Re, Mo, and others), can contribute to the formation of surface defects of liquidation origin during process of directional crystallization, especially at low crystallization rates.

The heat-resistant corrosion-resistant nickel-based alloy CM88Y [9] (**Table 4.5**) with a long-term strength of 280 MPa (900 °C, 100 h) was taken as the object of research. The purity of the alloy in terms of the content of harmful impurities must meet the requirements of the AMC 2280 standard. This alloy is used to make the working blades of the 1st and 2nd stage GTE turbines.

The alloying complex of SM88Y type alloys was optimized by adding to it the refractory elements of rhenium and tantalum as promising for additional alloying. These elements contribute to the strengthening of the austenitic solution, increase the structural stability of the alloy as a whole by reducing the diffusion mobility of the elements in the alloy, especially at high temperatures, significantly strengthening the solid solution and stabilizing the strengthening γ' -phase. Taking into account the results of our own experiments and literature data, it was established that alloying heat-resistant alloys with elements that have large atomic radii, such as rhenium and tantalum, is justified. These elements, with atomic radii exceeding the radius of nickel (the ratio for rhenium is 1.063), have a positive effect on the correspondence of crystal lattice periods in the γ -solid solution and the strengthening γ' -phase, which leads to an increase in the long-term strength of alloys at high temperatures. Rhenium also inhibits the processes of coagulation of the γ' -phase in the structure of the alloy and helps increase its thermal stability.

During the selection of the optimal metal alloying method and the study of the effect of individual elements on the structure and properties of the castings, the optimal chemical composition of the alloy was analyzed using linear regression analysis and taking into account the predicted structural stability of the alloy, which was determined by the PHACOMP program [21]. This method is based on the calculation of the possibility of the formation of the σ -phase in the γ -solid solution of complex heat-resistant alloys. The intensity of σ -phase formation depends on the number of electron vacancies N_v in the alloy matrix, excluding those that form carbides and borides in the alloy.

To determine the concentration of electron vacancies, it is necessary to establish the sequence of formation of phases in alloys and the sequence of their formation in the γ -matrix. This sequence includes the following stages: first, the formation of borides ($\text{Mo}_{0.5}\text{Ti}_{0.15}\text{Cr}_{0.25}\text{Ni}_{0.1}\text{B}_2$) occurs, then the formation of carbides occurs, in particular mono carbides ZrC, HfC, TaC, NbC, TiC and complex carbides Me_6C , Me_{23}C_6 and the formation of strengthening γ' -phase ($\text{Ni}_{0.88}\text{Co}_{0.08}\text{Cr}_{0.04}$)₃ (Al, Ti, Ta, Nb, Hf, V). After studying these reactions, the composition of the residual matrix can be established, which allows to calculate the number of electron vacancies $N_{v, av}$. According to the calculations, the N_v of the experimental alloy with the addition of rhenium and tantalum is 2.3, and that of the SM88Y alloy is 2.35. According to literature data, this indicator should not exceed 2.4 [22].

The obtained values of the coefficients in the regression equations (**Table 4.6**) showed that chromium has the greatest influence on the mass loss (Lg Metal loss), with an increase in chromium, the corrosion properties of the alloy increase. Rhenium also has a positive effect on the corrosion properties of the experimental alloy. Rhenium and titanium have a positive effect on the amount of the strengthening γ' -phase, when their content in the alloy increases, the volume of the γ' -phase increases (**Table 4.7**). Alloying heat-resistant alloys with rhenium and tantalum allows to increase the heat resistance of the cast metal (**Table 4.7**). This is achieved by increasing the amount of dispersed γ' -phase and strengthening the γ -phase due to cobalt, chromium, molybdenum, tungsten and rhenium. Even with a chromium content of 12.75 % by mass, the corrosion resistance of the experimental alloy remains at the level of the SM88Y alloy.

● **Table 4.6** Results of calculations of the composition of the experimental alloy with the addition of rhenium and tantalum using linear regression analysis

Alloy index	Regression equation
Corrosion resistance: Lg Metal loss (mass loss index)	$1.47437 - 0.602207 \times C - 0.146826 \times Cr + 0.0201633 \times Ti - 0.293672 \times Re$ $R^2 = 99.985 \%$
Lg corros Rate (corrosion rate indicator)	$1.52 - 0.0376815 \times Cr - 0.219755 \times Ti - 0.185562 \times Re$ $R^2 = 97.9276 \%$
The number of γ' , at. %	$16.7844 - 39.5125 \times C + 9.47215 \times Ti + 3.33362 \times Re$ $R^2 = 99.1566 \%$

● **Table 4.7** Characteristics of experimental alloys

Alloy brand	The volume of the γ' -phase in the alloy structure, %	Dissolution temperature of the γ' -phase, °C	Liquidus temperature, T_L , °C	Solidus temperature, T_S , °C	Long-term strength of the alloy at 900 °C for 100 hours, MPa	Corrosion resistance according to the mass loss index LgMetalloss	Corrosion rate in depth, LgcorrosRate
Experimental alloy	44.8	1170	1385	1320	330	-1.611	-0.161
CM88Y	43.2	1180	1320	1270	275	-1.372	0.115

According to the calculations, the optimal content of the experimental alloy with the limit alloying with refractory metals was determined by mass %: Ni base; (0.04–0.07) C; (12.3–13.2) Cr; (3.0–3.5) Al; (1.8–2.3) Thos; (6.8–7.5) So; (0.03–0.05) Zr; (0.45–0.50) Fe; (0.9–1.4) Mo; (6.0–6.6) W; (0.1–0.5) Nb; (2.5–4.3) Yes; (3.7–4.3) Re [23]. Samples of the above composition were melted by vacuum-induction melting, and for comparative studies of the SM88Y alloy, the temperature of pouring the melt into molds was 1560–1580 °C, the temperature of the mold was 800 °C.

Studies of the microstructure of the samples in the as-cast state confirm that the phase-structural state corresponds to the characteristics of the alloy of the considered type, and includes a γ -solid solution with the presence of the γ' -phase and carbides. **Fig. 4.8** clearly illustrates the microstructures of samples of heat-resistant alloy SM88Y and the experimental alloy.

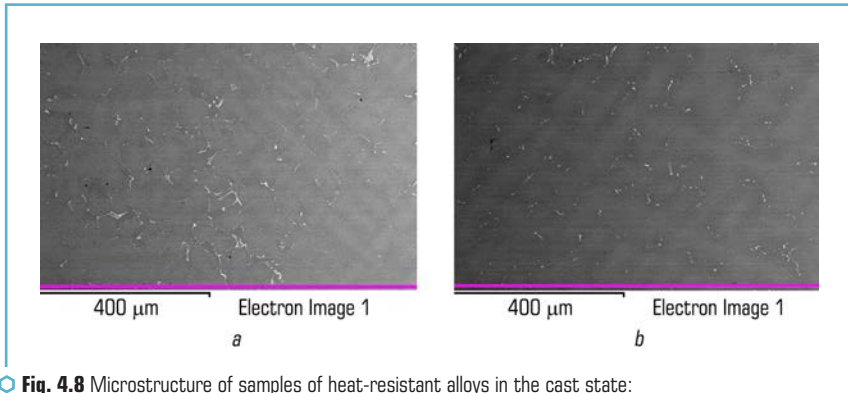


Fig. 4.8 Microstructure of samples of heat-resistant alloys in the cast state: *a* – CM88Y; *b* – experimental alloy

With the help of a high-precision synchronous thermal analyzer STA 449F1 of the company "NETZSCH" (Germany), the temperatures of phase transitions in the experimental alloys were determined using a specially developed method. The addition of rhenium and tantalum to the alloy resulted in an upward shift of the solidus (T_s) and liquidus (T_l) temperatures to approximately 1320 °C and 1385 °C, respectively, compared to values of 1270 °C and 1320 °C without these additions elements, which makes it possible to raise the operating temperature of turbine blades by more than 50 °C compared to the SM88Y alloy. In addition, the dissolution temperature of the strengthening intermetallic γ -phase of the experimental alloy remains at the level of the SM88Y alloy (**Table 4.7**).

Based on the obtained temperatures of phase transitions, the heat treatment mode was set: 1220 °C, 4 h+1050 °C, 4 h+870 °C, 20 h, cooling after each stage of heat treatment in air [24]. The results of tests on short-term strength showed that the level of mechanical properties of all samples of the experimental alloy meets the requirements of the technical documentation for this product (**Table 4.8**).

The study of resistance to high-temperature salt corrosion of experimental alloys was carried out on cylindrical samples with a diameter of 8 mm in a salt solution of 25 % NaCl+75 % Na₂SO₄ (density 2.5 g/cm³) for 30 hours. Corrosion indicators were determined by measuring mass loss and conducting metallographic studies, including analysis of the depth of corrosion in the metal (**Table 4.9**) [25–27].

● **Table 4.8** Mechanical properties of samples of experimental alloys

Test temperature, °C	Alloy	σ_B , MPa	$\sigma_{0.2}$, MPa	δ , %	ψ , %
20	CM88Y	1173	880	16.0	12.0
	Exp. alloy	1212	912	12.0	10.5
600	CM88Y	942	745	8.8	12.7
	Exp. alloy	1005	706	16.0	17.8
900	CM88Y	879	683	24.0	42.2
	Exp. alloy	880	673	19.2	42.2

● **Table 4.9** Corrosion indicators of experimental alloys

Alloy	Sample No.	Specific mass loss, mg/cm ²	Corrosion rate, mg/cm ² /h	Depth of external corrosion, mm	Depth of internal corrosion, mm
CM88Y	1	35.26	1.175	0.05	0.12–0.15
	2	28.85	0.962	0.24	0.10–0.12
Experimental	3	28.70	5.896	0.28	0.05–0.10
	4	27.82	9.627	0.05	0.05–0.10

The conducted set of studies showed that the increase in the volume fraction of the strengthening γ' -phase is achieved due to the optimal combination of such elements as aluminum (Al), titanium (Ti) and tantalum (Ta). After the introduction of rhenium and tantalum into the alloy, an increase in the dissolution temperature of the γ' -phase is noted, which has a positive effect on its heat resistance. Phase stability and strengthening of the γ -solid solution is ensured by alloying with refractory elements, such as tungsten (W), molybdenum (Mo) and rhenium (Re). In addition, the optimal combination of alloying elements has been established in order to minimize the probability of formation of topologically densely packed phases in castings of heat-resistant corrosion-resistant alloys for gas turbine blades. Reducing the chromium (Cr) content in the experimental alloy ensures its corrosion resistance. Optimization of the content of carbon (C), boron (B), zirconium (Zr), hafnium (Hf) and yttrium (Y) was performed in order to improve the quality and durability of the alloys.

4.3 THE INFLUENCE OF EXCESS PRESSURE ON THE PROPERTIES AND QUALITY OF CASTINGS FROM IRON-CARBON ALLOYS WHEN LOST FOAM CASTING

4.3.1 FEATURES OF THERMAL DESTRUCTION OF POLYSTYRENE UNDER THE ACTION OF EXCESS PRESSURE

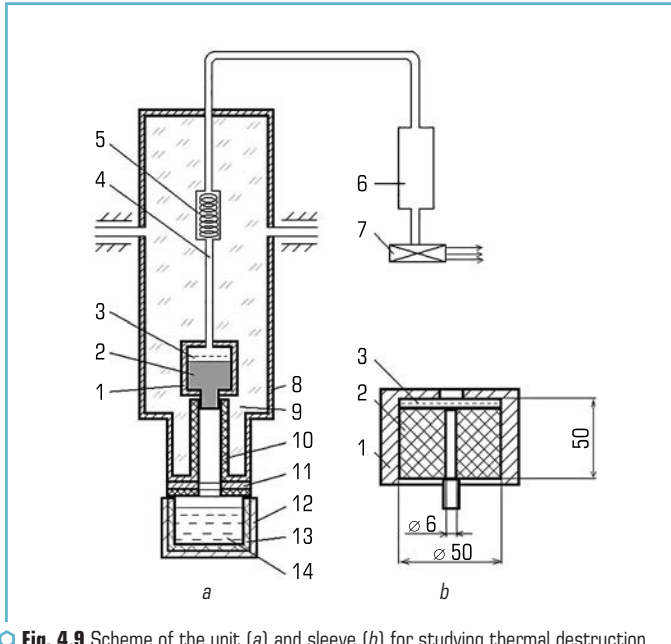
The phase composition and ratio of thermal destruction products of the model plays a major role in shaping the quality of castings obtained by casting on gasified models. It was established

that when filling the form with metal, the model material undergoes all the main stages of transformation when heated – melting, evaporation, partial oxidation and gasification with the formation of liquid, solid and gaseous phases [28]. At the same time, the effect of high pressure created in the "metal – model" system on the conditions of thermal destruction of polystyrene foam has not been studied.

To study the processes of destruction of the polystyrene pattern under the conditions of metal pouring under excessive pressure, a special technique and equipment were developed, which are schematically presented in **Fig. 4.9**.

The unit includes a steel sleeve 1, in which the investigated polystyrene sample 2 is placed and a metal mesh 3, which is designed to prevent metal from entering the pipeline 4, which removes destruction products from the sleeve, trap 5 for trapping the vapor-liquid phase, cylinder 6 for trapping the gaseous phase with a known volume, gas pressure sensor 7, which is connected to the automatic control system (ACS). The installation kit also includes a foundry container 8 with refractory filler 9, a ceramic riser 10, a punch 11 and a pressing chamber 12 with a case 13, into which liquid metal 14 is poured.

Fig. 4.9, b shows the assembled sleeve. For research, a sample with dimensions $\text{Ø}50 \times 50$ mm, weight 2.5 ± 0.2 g, which corresponds to the density of the model $\rho_s = 25\text{--}26 \text{ kg/m}^3$, was selected.



○ **Fig. 4.9** Scheme of the unit (a) and sleeve (b) for studying thermal destruction of polystyrene when high pressure is applied to the metal

A central hole $\varnothing 6$ mm is provided in the center of the sample for the release of destruction products during pyrolysis. The sample is installed in the sleeve at a height of 10 mm from the bottom edge so that decomposition products do not enter the mold cavity at the moment of contact of the sample with the metal. A layer of non-stick, non-gas-forming coating is applied to the inner surface of the sleeve, which is dried at a temperature of 230–250 °C for 1.5–2.0 hours.

After installing the sample, the nozzles for the release of decomposition products from the sleeve are hermetically connected by a pipeline 4 to the trap 5, which is filled with glass wool, where part of the vaporous decomposition products condenses at room temperature.

Another part of the solid destruction products settles on the inner surface of the sleeve above the sample. After the trap, the gaseous decomposition products enter cylinder 6 through a sealed pipeline. The temperature of the gas in the cylinder is measured by a thermoelectric sensor. At the moment of contact of the sample with liquid metal, its decomposition begins. The release of gaseous products leads to an increase in the pressure in the system, which is perceived by the pressure sensor 7 and controlled by the ASC.

The volume of gas released during sample decomposition was calculated according to formula (4.1):

$$V = V_0' - V_0, \quad (4.1)$$

where V_0' – the total volume of air in the system brought to normal conditions and released during gas decomposition, m^3 ; V_0 – the volume of the system brought to normal conditions, m^3 .

The amount of vapor phase (VP) condensed in the trap was determined as the difference between the mass of the trap before and after the experiment: G_1 and G_2 , respectively, and the mass of soot products as the difference between the mass of the trap G_3 after removing the condensed liquid fractions by keeping the trap at 200 °C and by the mass of the trap to experiment G_1 .

The mass of the resulting gas mixture (GM) was determined by the known density ($\rho = 0.67 \text{ kg/m}^3$) and the experimentally determined volume.

The thermal destruction conditions of the polystyrene pattern of the real shape were determined in the temperature range of 1050–1520 °C by filling the mold with GM carbon steel ($T = 1520$ °C) and cast iron ($T = 1300$ – 1450 °C). During the implementation of this series of experiments, the metal lifting speed varied in the range of 25–150 mm/s, and the constant parameters were the pressure on the liquid metal ($P_m = 0.5 \text{ MPa}$) and the density of the model ($\rho_s = 25.5 \pm 0.5 \text{ kg/m}^3$).

The analysis of the data on the thermal destruction of the model shows that an increase in the metal lifting speed from 25 to 150 mm/s leads to a decrease in the specific gasification rate of polystyrene a_5 by 2.4–3.2 times. At the same time, a change in the temperature of the melt within one value of the speed W_1 has no significant effect on the change in the value of a_5 . In this case, the deviation of the value of a_5 from the average does not exceed 5–10 %. This allows to determine the kinetics of the change in the value of Q_5 as an average \bar{Q}_5 for each value of the rate of rise of the metal in the form of W_1 . In this case, the kinetics of the change in the gasification

coefficient Q_5 can be imagined as a dependence $y = A \cdot X^B$ that determines the functional relationship between the time of filling the mold with the sample (X) and its gasification coefficient (Y).

To find the values of the coefficients A and B , mathematical data processing was used, which is based on the method of minimum errors, which made it possible to obtain the equation of the kinetics of thermal destruction of the polystyrene foam pattern in real form when pouring alloys in the temperature range of 1050–1520 °C, which has the form:

$$Q_5 = 58.5\sqrt{t_3}, \text{ cm}^3/\text{h}. \quad (4.2)$$

Graphical interpretation of the gasification kinetics of the model on the basis of the data obtained according to equation (4.2) in the setting of full-scale experiments is presented in **Fig. 4.10**.

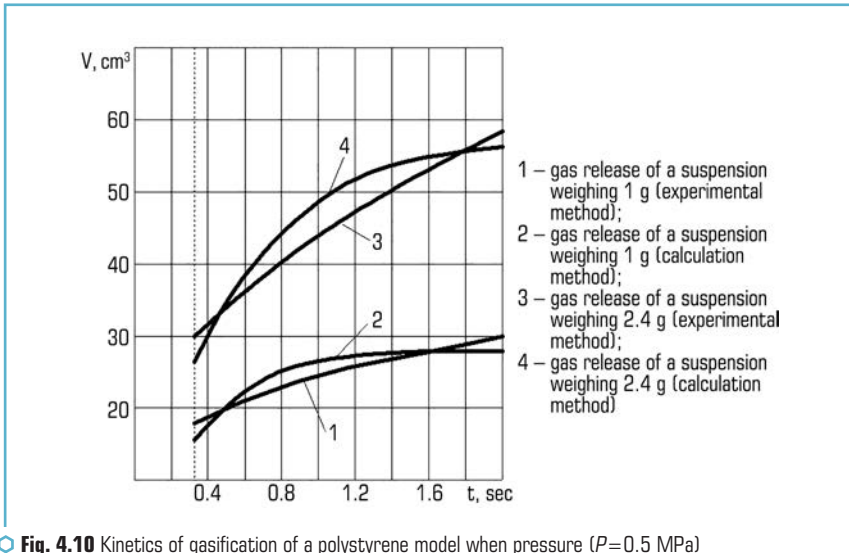


Fig. 4.10 Kinetics of gasification of a polystyrene model when pressure ($P=0.5$ MPa) is applied to the crystallizing liquid metal

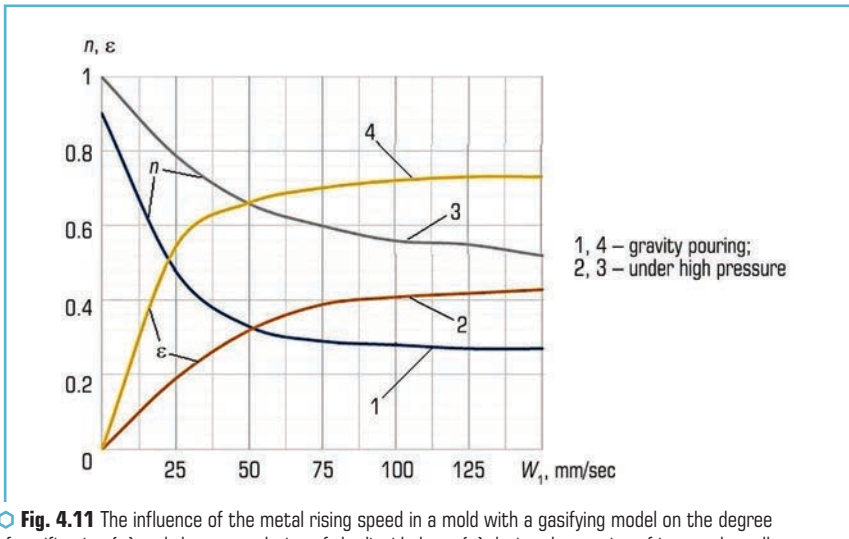
When comparing the calculated (**Fig. 4.10**, curves 2, 4) and experimental (**Fig. 4.10**, curves 1, 3) curves describing the gasification kinetics of the model, a fairly high commonality between the calculated and experimental data was established. It was determined that the relative error between the data is within 2–12.5 %. This allows to assert that experimental data and mathematical calculations can be used in the analysis of the conditions of thermal destruction of polystyrene foam in a form with the imposition of high pressure P_1 , as well as in technological calculations for predicting the quality of cast blanks when lost foam casting, with the imposition of pressure on liquid and crystallising metal.

Generalized data on the number of gaseous, vapor-gas, and solid phases depending on the speed of metal ascent in the form of W are presented in **Table 4.10**.

When analyzing these data (**Table 4.10**), it was found that when the speed of W_1 increased from 25 to 150 mm/s, the amount of gaseous phase (GP) and solid phase (SP) decreased by 2.5 and 1.5 times, respectively, and the amount of vapor-gas phase (VGP) increases by 3.2 times (**Fig. 4.11**).

● **Table 4.10** Number of gaseous, vapor-liquid and solid phases during thermal destruction of a polystyrene foam sample weighing 2.4 g

Amount of phase, g, (%)	Phase name	Metal lifting speed in the form of mm/s					
		25	50	75	100	125	150
	Gaseous	0.160 (7)	0.114 (5)	0.094 (4)	0.08 (3.3)	0.072 (3.0)	0.066 (2.7)
	Vapor gas	0.32 (13)	0.701 (30)	0.818 (34)	0.906 (36.7)	0.976 (40)	1.004 (42.3)
	Solid	1.92 (80)	1.585 (65)	1.488 (62)	1.414 (60)	1.352 (57)	1.330 (55)



○ **Fig. 4.11** The influence of the metal rising speed in a mold with a gasifying model on the degree of gasification (n) and the accumulation of the liquid phase (ϵ) during the casting of iron-carbon alloys under high pressure ($P > 0.5$ MPa)

This character of the change in the volume (mass) of GP, VGP differs from similar ones during the thermal destruction of GM during gravity casting (**Fig. 4.11**, curves 3, 4), which indicates a change in the mechanism of thermal destruction of polystyrene foam when pressure is applied to liquid metal and metal that crystallizes.

It is important, on the basis of the available data, to determine the gasification coefficient ε , liquid phase accumulation ξ as parameters used for mathematical prediction of the quality of castings obtained by the LGM process [29]. In this case, the coefficients n and ε depending on the rate of rise W , and the kinetics of their change are presented in **Fig. 4.11**.

The analysis of these data shows that with an increase in the speed of W_1 , the degree of gasification increases from 0.2 to 0.45 (**Fig. 4.11**, curve 2), and the value of the coefficient ε naturally decreases from 0.8 to 0.55 (**Fig. 4.11**, curve 1). This character of the change in n and ε during gravity filling, as well as their kinetics of change, is reversed (**Fig. 4.11**, sections 3, 4).

Further, on the basis of the obtained data, it is advisable to determine the gasification coefficients of the a_5 model, as a parameter used in the calculation of the volume, mass and degree of GM gasification.

To determine the relative coefficient a_5 , let's use equation (4.2), but since the interaction between the metal and the Styrofoam model occurs in a plane perpendicular to the vector of the melt movement speed, it can be represented in the following form:

$$V_d = a_5 F_5 \sqrt{\tau}, \text{ cm}^3. \quad (4.3)$$

At the same time, the physical content of the introduced equation (4.3), the physical content of the coefficient a_5 , which determines the amount of gas released from a unit of the interaction surface in the "metal – part" system per unit of time τ , should be clarified. In this case, if:

$$a_5 F_a = 169.37, \text{ and since } F = 19.34 \text{ cm}^2,$$

$$a_5 = \frac{169.34}{19.34} \text{ and finally, } a_5 = 8.76.$$

At the same time, the rate of gas evolution at the destruction temperature of the polystyrene pattern can be represented in the form of an equation:

$$\frac{dV}{d\tau} = \frac{a_5 F_5}{2\sqrt{F}}, \quad (4.4)$$

destruction of the V_M model in the form of an equation:

$$V_M = b_5 F_5 \sqrt{\tau}, \quad (4.5)$$

and since $\frac{V_M}{V_d} = \frac{b_5 F_5 \sqrt{\tau}}{a_5 F_5 \sqrt{\tau}}$, then the coefficients of destruction of the model:

$$b_5 = a \frac{V_M}{V_d} = \frac{8.76 \times 96t}{545} = 1.55,$$

where b_5 – the destruction coefficient of the model; 545 – the amount of gas formed during complete gasification of the model weighing 2.4 g.

In this case, the kinetics of gasification V_G of the V_M model during high-pressure GM casting for iron-carbon alloys in the range of 1050–1570 °C is described by an equation of the following form:

$$V_f = 8.76F_5\sqrt{\tau}, \text{ cm}^3; \quad (4.6)$$

$$V_M = 1.55F_5\sqrt{\tau}, \text{ cm}^3. \quad (4.7)$$

Therefore, the mass P_5 of the destroyed model at this moment in time is determined by the expression:

$$G_5 = 1.55\rho_5F_5\sqrt{\tau}. \quad (4.8)$$

The amount of liquid phase at any moment of time is determined according to the equation:

$$G_b = G_5 - 8.76\rho_D F_5\sqrt{\tau}, \text{ g}. \quad (4.9)$$

Equations (4.8) and (4.9) will make it possible to predict the conditions for the LP appearance on the surface of the front of the metal flow and the casting, which solidifies when excess pressure is applied.

It should be especially noted that during the setting of a series of experiments and the analysis of the obtained data on the thermal destruction of the expanded polystyrene pattern during pressure casting of iron-carbon alloys, the nature of the kinetics of thermal destruction was established, which is significantly different from the similar one during gravity casting. These differences can be explained by another mechanism of thermal influence in the "metal – model" system, which is based on the following: firstly, when the pressure is increased, the inequality is fulfilled: $P_1 \gg P_p + \sigma_5$, and it cannot be realized during gravity casting, so as well as $P_M < P_p + \sigma_5$, when $W_5 > 50$ mm/s, ($P_M^{\text{max}} < 0.08$ MPa), σ_5 – the thermomechanical resistance of GM, ($\sigma_5 \geq 0.15$ MPa); secondly, the filling of the form at $W_1 > 40$ mm/s leads to the formation of a new system of thermodynamic influence – "metal – vapour-gas gap – spheroids of the liquid phase – model". These initial conditions, which differ from gravity casting along GM, change the mechanism of thermodynamic interaction. When pouring the mold, the gap – "metal – model" is filled with a liquid phase, which under pressure P_1 is pressed into the mold and the heat flow from the melt to the model q_5 is transmitted through the LP with a thickness Δ , which is a thermal resistance and depends on the value of Δ . As the speed of W_1 increases, the thickness of the gap decreases and the thermal resistance decreases, which leads to an increase in the power of the heat flow q_5 and, therefore, the gasification rate of the polystyrene foam pattern increases. On the contrary, during gravity casting ($W_1 \leq 40$ mm/s), a "metal-model" gap is first formed, and the surface of the flow front

is partially covered by LP. In this case, the heat transfer from the melt to the model is mainly transmitted by radiant energy, where $q_r = f(T_4)$, which explains that during gravity casting, the degree of gasification of polystyrene foam is higher than during pressure casting and significantly depends on the temperature of the metal being poured T_1 , which is not observed during pressure casting.

Thus, on the basis of the conducted research, the mechanism of heat-force interaction of the metal with the polystyrene foam pattern, the conditions, the kinetics of its gasification depending on the casting parameters were established, and a mathematical apparatus was created that allows predicting the formation of defects in the casting caused by the interaction of the metal with the GM and determining the optimal parameters of GM casting under high pressure.

4.3.2 THE INFLUENCE OF TECHNOLOGICAL PARAMETERS OF LOST FOAM CASTING UNDER REGULATED PRESSURE ON THE PHYSICAL AND MECHANICAL CHARACTERISTICS OF CAST STRUCTURES MADE OF IRON-CARBON ALLOYS

It is known that applying pressure to the metal at the time of its hardening contributes to the formation of a denser structure in castings and reduces porosity [29, 30].

Research on the influence of casting parameters, in particular high pressure, on the physical and mechanical properties of castings was carried out on objects in the form of iron-carbon alloys – carbon and stainless steel, cast iron with spherical and vermicular graphite.

In order to study the thermodynamic influence on the development of the crystallization processes of the formation of castings during GM casting, a methodology was developed and special equipment was created, the scheme of which is presented in **Fig. 4.12**, and the levels of variation by variable factors are in the **Table 4.11**.

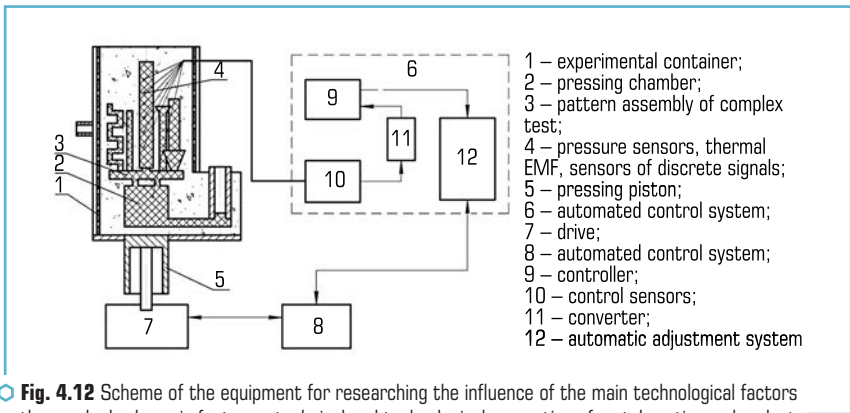


Fig. 4.12 Scheme of the equipment for researching the influence of the main technological factors on the gas-hydrodynamic features, technical and technological properties of metal castings when lost foam casting, under excess adjustable pressure

● **Table 4.11** Experiment planning matrix

Factors	Experiment No.															
	1	2	3	4	5	6	7	8	9	10	11	12	13	14	15	16
Pressure P_1 , MPa	3	6	3	6	3	6	3	6	3	6	3	6	3	6	3	6
Overheating, θ_1	1.25	1.25	1.05	1.05	1.25	1.25	1.05	1.05	1.25	1.25	1.05	1.05	1.25	1.25	1.05	1.05
Speed W_1 , mm/s	80	80	80	80	20	20	20	20	80	80	80	80	20	20	20	20
Model density ρ_5 , kg/m ³	50	50	50	50	50	50	50	50	20	20	20	20	20	20	20	20

As a result of mathematical processing of research data, performed in accordance with the experiment planning matrix (**Table 4.11**) with the application of the application program package, coefficients and regression equations were determined for each of the responses in the following form:

1. For carbon steel (Steel 45L):

a) strength limit σ_B , MPa:

$$Y = 35.1 + 5.68X_{16} + 24.3X_{17} - 0.103X_{18} - 0.226X_{19} - 4.536X'_6 + 0.0248X'_7 + 0.0446X'_8, \quad (4.10)$$

where $X'_6 = X_{16}X_{17}$, $X'_7 = X_{16}X_{18}$, $X'_8 = X_{16}X_{19}$;

b) porosity, P , %:

$$Y = -7.10 + 1.336X_{16} + 7.18X_{17} + 0.1193X_{18} - 0.01067X_{19} - 1.316X'_6 - 0.0216X'_7 + 0.00348X'_8 - 0.1059X'_9 + 0.00553X'_{10} - 0.0000574X'_{11} + 0.1937X'_{12} - 0.001619X'_{13}, \quad (4.11)$$

where $X'_9 = X_{17}X_{18}$, $X'_{10} = X_{17}X_{19}$, $X'_{11} = X_{18}X_{19}$, $X'_{12} = X'_{11}X_{17}X_{18}$, $X'_{13} = X_{16}X_{17}X_{19}$;

c) shrinkage ε , %:

$$Y = 4.18 + 1.493X_{19} + 5.555X_{17} + 0.09X_{18} - 0.0006X_{19} + 0.348X'_6 - 0.0213X'_7 + 0.000252X'_9 + 0.00638X'_{10} + 0.000049X'_{11} + 0.0182X'_{12}. \quad (4.12)$$

2. For high-alloy steel (type X18H10TЛ):

a) strength limit σ_B , MPa:

$$Y = 78.5 + 1.182X_{16} - 18.32X_{17} - 0.346X_{18} - 0.0499X_{19} - 0.879X'_6 + 0.0138X'_7 + 0.001239X'_8 + 0.287X'_9; \quad (4.13)$$

b) porosity, P , %:

$$Y = 2.80 + 0.655X_{16} + 3.238X_{17} + 0.0563X_{18} - 0.0253X_{19} - 0.695X'_6 - 0.00499X'_7 - 0.0015X'_8 - 0.05122X'_9 + 0.0175X'_{10} - 0.000499X'_{11} + 0.00928X'_{12}; \quad (4.14)$$

c) shrinkage ε , %:

$$Y = -2.44 + 0.971X_{16} + 4.15X_{17} + 0.0662X_{18} - 0.0088X_{19} - 0.907X'_6 - 0.013X'_7 + 0.000X'_8 - 0.057X'_9 + 0.0126X'_{10} - 0.0115X'_{12}. \quad (4.15)$$

3. For cast iron with spherical graphite:

a) strength limit σ_B , MPa:

$$Y = 154 - 3.483X_{16} - 96.65X_{17} - 0.184X_{18} - 1.84X_{19} + 3.608X'_6 + 0.0048X'_7 + 0.01954X'_8 + 0.186X'_9 + 1.45X'_{10} + 0.0004737X'_{11}; \quad (4.16)$$

b) shrinkage ε , %:

$$Y = 1.66 - 0.1349X_{16} - 0.2867X_{17} - 0.00455X_{18} + 0.0003753X_{19} + 0.029X'_6 + 0.00055X'_7 + 0.000374X'_8; \quad (4.17)$$

c) porosity, P , %:

$$Y = -0.984 + 0.2352X_{16} + 1.365X_{17} + 0.017X_{18} - 0.00428X_{19} - 0.2647X'_6 - 0.00347X'_7 + 0.0008337X'_8 - 0.01689X'_9 + 0.333X'_{10}. \quad (4.18)$$

4. For cast iron with lamellar graphite:

a) strength limit σ_B , MPa:

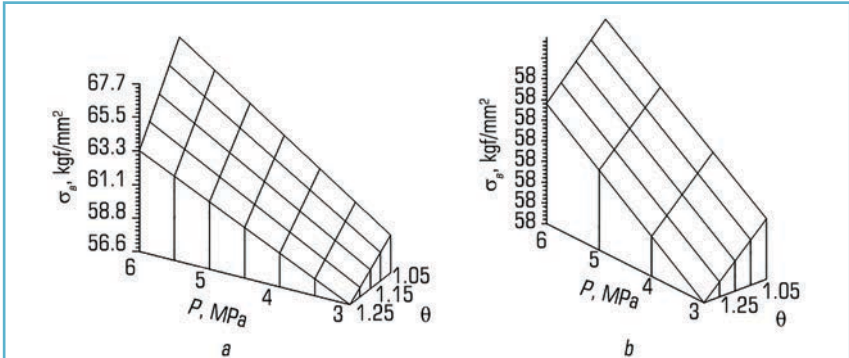
$$Y = 61.4 - 1.479X_{16} - 22.59X_{17} - 0.0894X_{18} - 0.6204X_{19} + 1.118X'_6 + 0.0145X'_7 - 0.002098X'_8 + 0.002239X'_9 + 0.4301X'_{10} + 0.001424X'_{11}; \quad (4.19)$$

b) shrinkage ε , %:

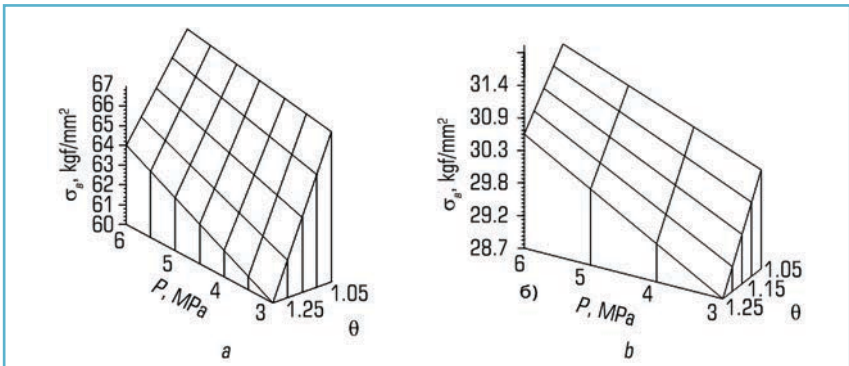
$$Y = 1.72 - 0.1645X_{16} - 0.2492X_{17} - 0.004X_{18} - 0.00125X_{19} + 0.0207X'_6 + 0.0005833X'_7 + 0.001042X'_8. \quad (4.20)$$

The assessment of the adequacy of the obtained mathematical dependencies to the experimental data was carried out using the Fisher statistical test, and the significance of the regression coefficients was checked using the Student's t-test.

To assess the effect of pressure P_1 and the overheating degree θ , on the formation of the physical and mechanical properties of the metal of castings obtained by lost foam casting, it is advisable to use the graphical interpretation of the regression equation for σ_B , P_1 , ε , which are presented in **Fig. 4.13–4.18**.



○ **Fig. 4.13** Influence of pressure P_1 and the degree of metal overheating on the strength σ_B in:
 a – carbon steel; b – alloy steel



○ **Fig. 4.14** Influence of pressure P_1 and the degree of metal overheating θ , on the strength σ_B of:
 a – high-strength cast iron; b – gray cast iron

Based on the analysis of these graphical data, it was established that an increase in pressure P_1 leads to an increase in the strength characteristics for all studied alloys. Moreover, the maximum increase in strength is achieved with minimal overheating of the melt θ_1 . Thus, the increase

in the value of σ_B for castings made of carbon and alloy steels, gray and high-strength cast iron amounted to 23 %, 17 %, 17 %, and 19 % (Fig. 4.13, 4.14), respectively.

At the same time, an increase in the degree of overheating from 1.05 to 1.25 reduces the value of pressure P_1 by σ_B and reduces these values compared to B_{max} by 10 %, 6 %, 9.6 %, and 4 %, respectively.

The nature of the effect of pressure P_1 and overheating σ_B^{max} on the kinetics of changes in porosity P during casting of various alloys on GM is inversely related to their strength characteristics. Thus, increasing the pressure P_1 to a value of 6 MPa reduces the porosity in carbon, stainless steel castings by 3.75 and 2.35 times (Fig. 4.15, 4.16), respectively.

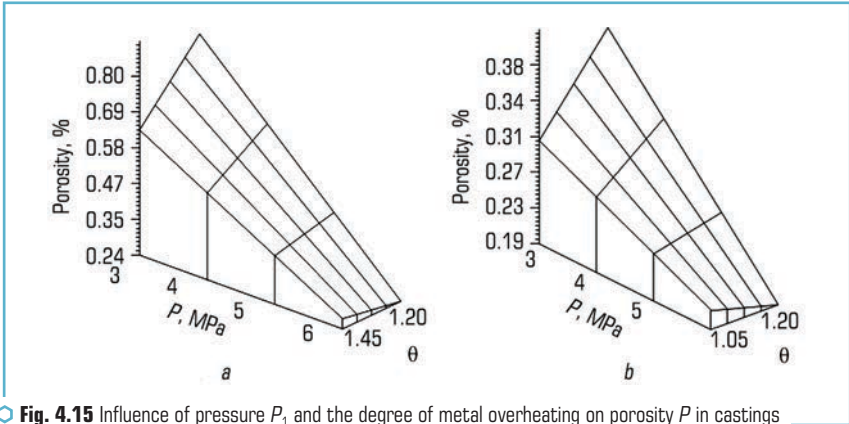


Fig. 4.15 Influence of pressure P_1 and the degree of metal overheating on porosity P in castings made of: a – stainless (X18H10) steel; b – carbon steel

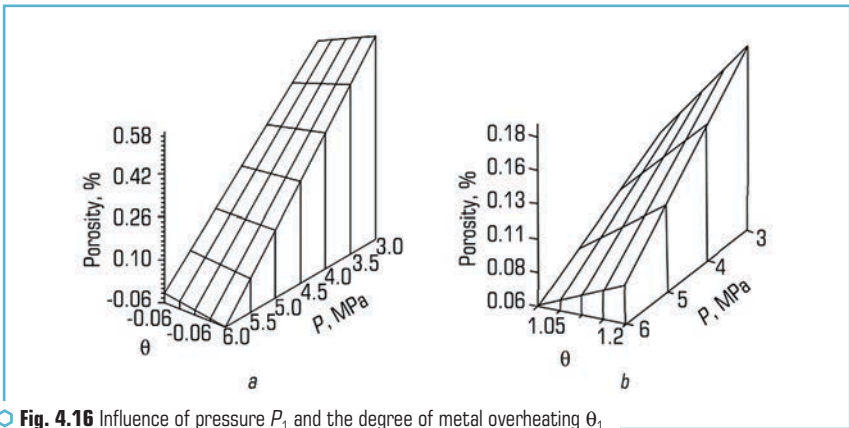


Fig. 4.16 Influence of pressure P_1 and the degree of metal overheating θ , on the porosity of: a – high-strength cast iron; b – gray cast iron

Moreover, the maximum porosity P^{\max} in castings made of carbon steel was 2 times higher than in castings made of stainless steel (Fig. 4.15, a, b).

The influence of the degree of overheating in the melt at P^{\max} and P^{\max} on porosity is ambiguous. At a high level of pressure P^{\max} , overheating practically does not affect the porosity, which changed only by 0.02 % and 0.03 %, respectively. At a low pressure P^{\max} , the influence of the degree of overheating is significant. Thus, decreasing the value of θ_1 from 1.25 to 1.05 causes an increase in porosity in stainless steel and carbon steel castings by 0.3 and 0.12 %, respectively (Fig. 4.15).

A similar effect on the kinetics of porosity change with increasing pressure P_1 is observed in high-strength and gray cast iron castings (Fig. 4.16). Thus, increasing P_1 to a value of 6 MPa leads to a decrease in porosity in high-strength and gray cast iron castings from 0.73 to 0.06 % and from 0.24 to 0.06 %, respectively.

It should be noted that porosity in high-strength cast iron castings at low and high pressure does not depend on the degree of overheating θ_1 . On the contrary, the porosity in gray cast iron castings increases with increasing superheat θ_1 , although its absolute values are lower than those of high-strength cast iron by a factor of 3.

The nature of the kinetics of changes in the linear shrinkage of carbon and stainless steels when pressure P_1 is applied is identical.

As the pressure P_1 increases to 6 MPa, the shrinkage of carbon and stainless steels decreases from 2.35 to 2.27 % and from 2.37 to 2.20 %, respectively (Fig. 4.17). Moreover, the absolute values of ϵ^{\min} and ϵ^{\max} for both types of steel are practically equal (Fig. 4.17).

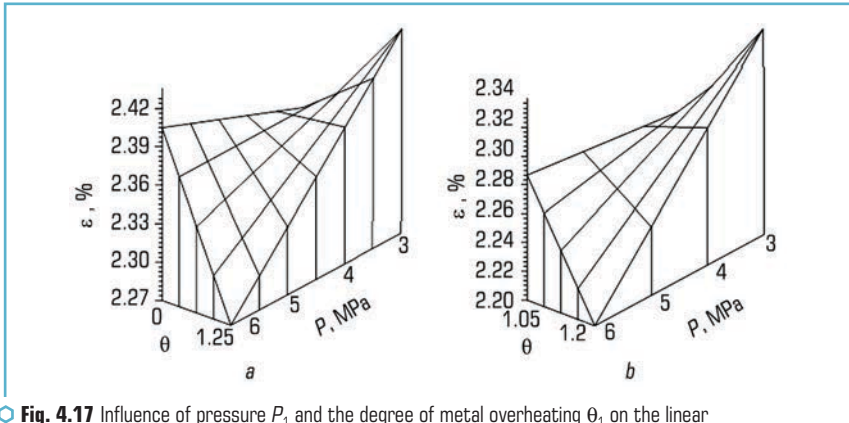


Fig. 4.17 Influence of pressure P_1 and the degree of metal overheating θ , on the linear shrinkage of: a – carbon (Steel 45L) steel; b – alloy (X18H10) steel

Overheating of alloys above T_s in the studied temperature range also insignificantly changes the value of ϵ , although this value is more typical for carbon steels.

The influence of P_1 on the kinetics of change in casting shrinkage of cast iron with spherical and lamellar graphite is more noticeable. Here, increasing the pressure P_1 from 3 to 6 MPa reduces the casting shrinkage for cast iron with compact graphite and plate-vermicular graphite by 1.6 and 2.3 times, respectively (**Fig. 4.18**).

Imposition of pressure P_1 on liquid metal and crystallizing metal, the value of which ($P_1 > 0.5$ MPa) significantly exceeds the metallostatic pressure H_1 during gravity casting by GM, where $H_1 < 0.08$ MPa. In connection with this, the conditions of thermal interaction in the "metal – form" system change. Firstly, during pressure casting, there is no "gap" δ for a long period after pouring, which significantly increases the heat transfer coefficient α – in the "metal – form" system compared to heat exchange in the "metal – thermal gap – form" system during gravity casting.

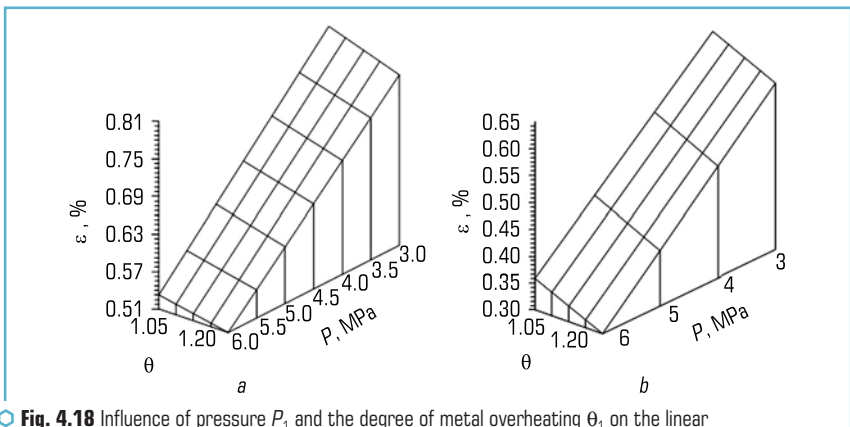


Fig. 4.18 Influence of pressure P_1 and the degree of metal overheating θ , on the linear shrinkage of: *a* – gray cast iron; *b* – high-strength cast iron

For example, with regard to the conditions of solidification of a casting made of carbon steel (Steel 45L), it was established that the influence of pressure P_1 on the liquid metal in the range of 3.0–6 MPa increases the rate of removal of overheating and crystallization of the metal in comparison with gravity casting, which is in the first 40 s 4.25–2.75 °C/s versus 1 °C/s (**Fig. 4.19**), respectively. At the same time, it should be noted that a decrease in pressure of less than 4.5 MPa leads to an equalization of the cooling rates of the casting. Thus, already 360 s after pouring, the integral coefficient of the cooling rate became equal and amounted to 1.81 °C/s, respectively.

When studying the influence of the P_1 value on the crystallization of gray iron castings, it was established that increasing the P_1 pressure increases the cooling rate of the casting, which was 1.0 °C/s for pressure casting and 0.7 °C/s for gravity casting (**Fig. 4.20**).

The influence of pressure on the amount of linear shrinkage ϵ of iron-carbon alloys, the nature of the kinetics of change, which is the same for all studied alloys, is determined by the creation with the help of its "ideally rigid form" and the development of deformation processes in the initial

stage of metal solidification, since in this period $P_1 > \sigma_b^I$, where σ_b^I is the strength limit casting at high temperatures. In addition, an undeformed "hard" shape creates conditions for compensation of shrinkage due to pre-shrinkage expansion of cast iron.

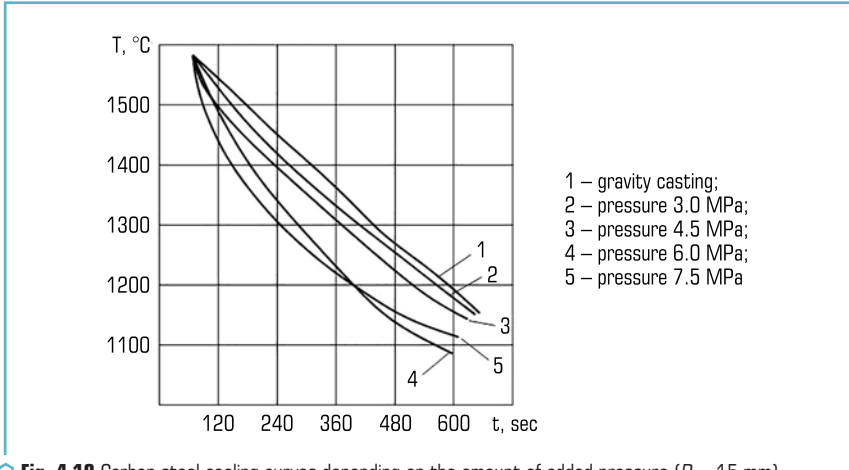


Fig. 4.19 Carbon steel cooling curves depending on the amount of added pressure ($R_1=15$ mm)

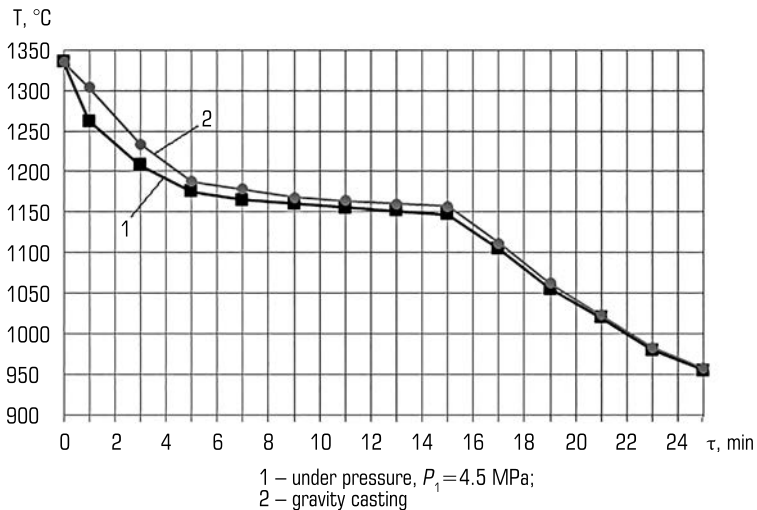


Fig. 4.20 Solidification kinetics of a cast iron casting ($R_1=15$ mm) during gravity casting and lost foam casting

Melt overheating θ in the investigated temperature ranges of the alloys being poured has a specific effect on the physical and mechanical properties of castings due to the intensification of heat removal during the pouring period. Thus, it was previously established [31] that additional removal of overheating due to losses due to thermal destruction of GM (30–50 °C for cast iron, 50–70 °C for steel) and an earlier transition to the liquid-solid and even solid-liquid state occurs, the latter possible only when applying high pressure. Thus, due to the removal of significant overheating and the presence of a solid phase of the metal in the initial stage of pouring, the characteristic effect of the value θ_1 on the physical and mechanical properties of castings from iron-carbon alloys is determined.

In conclusion, it should be especially noted that applying pressure to liquid metal and crystallizing metal allows to increase the strength characteristics of castings from iron-carbon alloys in comparison with gravity casting in hollow molds according to GM, including carbon and stainless steels, high-strength and gray cast iron by 10 and 15 %, 12 and 15 %, respectively.

4.3.3 TECHNOLOGICAL SCHEME OF OBTAINING REINFORCED CASTINGS BY LOST FOAM CASTING UNDER REGULATED PRESSURE

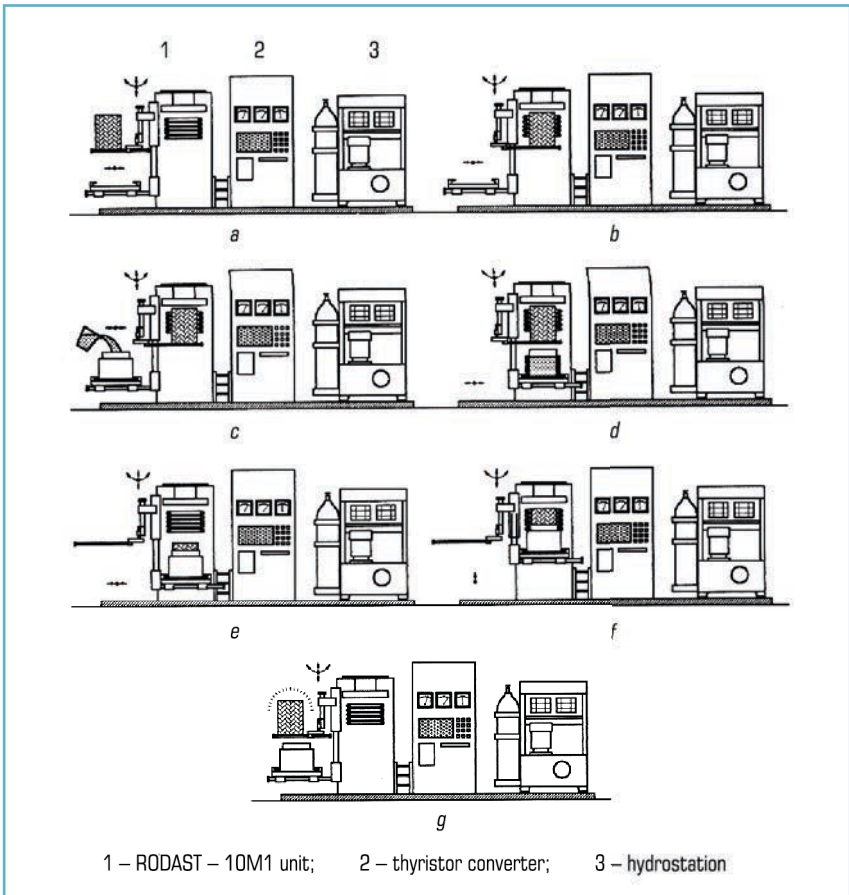
The implementation of this method of obtaining reinforced cast structures of various weights and dimensions using the method of casting into vacuum molds with a macro reinforcing phase of polystyrene foam pattern developed at the PTIMA of the National Academy of Sciences of Ukraine using regulated pressure. At the same time, it is also possible to use expanded polystyrene patterns with oriented porosity of various types – both in the form of bodies of rotation, conical and shaped parts of various and complex configurations.

There are two options for implementing the introduction of heterogeneous elements into the body of the polystyrene pattern: mixing these materials into foamed polystyrene before sintering the pattern, and also by introducing reinforcing elements into a previously prepared cavity in the body of the polystyrene pattern [32].

The technological scheme of obtaining reinforced castings by filling a vacuum mold with a macro-reinforcing phase, which is placed in a gasifying model under excess external pressure, is presented in **Fig. 4.21**.

After the production of the model block, the operation of forming it into a foundry container with sand filler is carried out. Next, the container is installed on the filling of the "RODAST" unit with the help of a movable traverse. Lifting of the mold and edging of the casting container is carried out. The container is vacuumed to a vacuum of 0.07...0.08 MPa. Next, liquid metal is poured into the mold, after which the press piston is raised at a speed set by the controller, which depends on the type, configuration, and thermophysical characteristics of the reinforced system. Pressing is carried out under a pressure of 0.5...20 MPa. After the pressing is finished, the press piston is disconnected from the container and the press residue is separated. After that, the auxiliary

hopper is connected, the forming mixture is removed. Castings are sent for punching, cutting and cleaning, and molding sand for thermal regeneration.



◉ **Fig. 4.21** Technological scheme of obtaining LAM castings using external pressure: *a* – mold installation on the movable traverse; *b* – heating of the mold; *c* – pouring of the matrix alloy (MCA into the receiving bowl); *d* – transfer of the bowl from the MA to the pouring position; *e* – setting of the mold to the pouring position; *f* – filling of the form and LAM solidification under pressure; *g* – cooling the mold and removing the bowl

Thus, the main technological schemes for obtaining cast reinforced structures from iron-carbon alloys, which can be used for non-ferrous alloys, have been created. The main technological schemes created make it possible to obtain reinforced structures that work in extreme and normal conditions.

CONCLUSIONS

After vacuuming in the MHD mixer of liquid metal, which is stirred by electromagnetic forces, in continuously cast ingots from high-strength aluminum alloys, the hydrogen content decreases to 0.03...0.07 cm³/100 g of metal, the concentration of oxide inclusions – to 0.04 vol. % and the solubility of alloying and modifying elements introduced into the melt increases.

In the production of continuously cast ingots from aluminum alloys, which contain easily oxidizable elements (Mg, Zn, etc.), it is necessary to create a protective environment of inert gases at all technological operations from melting to metal pouring. It is shown that in ingots made of alloy 1545 with a magnesium content of 4.5 % by mass, which were protected from oxidation, the breaking strength is 30 %, and the relative elongation is 2.4 times greater than in products obtained without the formation of a protective medium over metal.

Electromagnetic stirring of the alloy in the crystallizer significantly affects the structure and properties of continuously cast ingots. The use of electromagnetic stirring in ingot production processes allows controlling the speed of metal movement in the crystallizer and aligning the crystallization front of the alloy. As a result, the anisotropy of the properties and internal stresses in the ingots decreases, the nucleation process in the liquid metal intensifies, and the alloy structure is crushed. Thus, the ingots obtained without electromagnetic stirring of the B96C alloy in the crystallizer have a coarse crystal structure with a grain size of ~350 μm. In the ingots made from the alloy that was stirred, the structure is dispersed with a grain size of ~100 μm.

It is shown that after alloying the B93pch alloy with titanium in the amount of ~0.5 % by mass and subsequent plasma nitriding, a fine crystalline structure with the same grain size is formed in the ingots, which is 25–30 % smaller than in products made of non-nitrided metal. Complex MHD-plasma processing of the melt allows to increase the mechanical properties of pressed products from continuously cast ingots: the breaking strength and yield strength (σ_B , $\sigma_{0.2}$) increase by 7–10 %, relative elongation by 20–25 % compared to the requirements for stamped parts from alloy B93pch.

The above research results showed the optimal combination of such alloying elements as aluminum (Al), titanium (Ti), tantalum (Ta), tungsten (W), molybdenum (Mo), chromium (Cr) and rhenium (Re), which made it possible obtain high heat resistance, ensure phase stability of the alloy and its corrosion resistance.

The simultaneous influence of technological factors and excess pressure on liquid metal and crystallizing metal allows to increase the mechanical strength and reduce the porosity of the material of castings from carbon, stainless steel, high-strength and gray cast iron by 15–30 %, compared to gravity casting of GM.

Mathematical dependencies have been obtained for determining the mechanical and technological properties of castings made of carbon, stainless steel, high-strength and gray iron in the presence of excess pressure on the liquid metal, which crystallizes, which allows optimizing the technological parameters to obtain castings with the necessary operational properties.

The latest technological processes for the production of reinforced castings by the method of lost foam casting, using excess pressure on the metal, have been developed.

CONFLICT OF INTEREST

The authors declare that they have no conflict of interest in relation to this research, whether financial, personal, authorship or otherwise, that could affect the research and its results presented in this paper.

REFERENCES

1. Polyvoda, S. L., Siryi, O. V., Hordynia, O. M., Puzhailo, L. P. (2017). Pat. No. 119406 UA. Plavylno – lyvarnyi kompleks dlia napivbezperernoho lyttia zlyvkiv z aliuminiievykh splaviv. MPK B22D 11/14. No. u201703178; declared: 03.04.2017; published: 25.09.2017, Bul. No. 18. Available at: <https://uapatents.com/5-119406-plavilno-livarnij-kompleks-dlya-napivbezperernogo-littya-zlyvkiv-z-alyuminiievikh-splaviv.html>
2. Puzhailo, L. P., Serii, A. V., Polivoda, S. L. (2010). Tekhnologii i oborudovanie dlia poluchenia slitkov iz vysokoprochnykh aliuminiievykh deformiruemyykh splavov metodom poluneprieryvnoho littia. Visnyk Donbaskoi derzhavnoi mashinobudivnoi akademii, 3 (20), 227–229. Available at: http://www.dgma.donetsk.ua/science_public/ddma/2010-3-20/article/10PLDMSL.pdf
3. Polyvoda, S. L., Siryi, O. V., Puzhailo, L. P. (2012). Pat. No. 100231 UA. Apparatus for manufacturing and electromagnet casting alloys into casting molds. MPK B22D 39/00, B22D 35/00, H05B 6/02. No. a200907285. declared: 10.07.2009; published: 10.12.2012, Bul. No. 23. Available at: <https://uapatents.com/4-100231-ustanovka-dlya-prigotuvannya-ta-elektromagnitnogo-rozlivannya-splaviv-u-livarni-formi.html>
4. Puzhailo, L. P., Polyvoda, S. L., Siryi, O. V., Hordynia, O. M. (2019). Pat. No. 131179 UA. Sposib pryhotuvannya aliuminiievykh lihatur u mahnitohidrodynamichnykh ustanovkakh. MPK C22B 21/00. declared: 15.06.2018; published: 25.09.2008, Bul. No. 1. Available at: <https://base.uipv.org/searchINV/search.php?action=viewdetails&IdClaim=254473>
5. Puzhailo, L. P., Gavriiliuk, V. P., Polivoda, S. L., Seryi, A. V., Gordynia, A. N. (2012). Issledovanie protsessa poluneprieryvnoho litia slitkov iz vtorychnogo aliuminievoho splava AD31. Metall i lite Ukrainy, 7, 20–22.
6. Polyvoda, S. L., Siryi, O. V., Puzhailo, L. P. (2013). Pat. No. 101343 UA. Method for producing high-strength aluminum wrought alloys containing zinc. MPK C22C 21/06, C22C 21/02, C22B 9/04, C22B 21/00. No. a201007359. declared: 26.12.2011; published: 25.03.2013, Bul. No. 6. Available at: <https://uapatents.com/5-101343-sposib-prigotuvannya-visokomicnikh-alyuminiievikh-deformivnikh-splaviv-z-vmistom-cinku.html>

7. Puzhailo, L. P., Siryi, O. V., Polyvoda, S. L. (2015). Pat. No. 108781 UA. Sposib rafinuvannia aluminievoho splavu u vakuumi. MPK C22B 21/00, C22B 9/04. No. a201310432. declared: 27.08.2013; published: 10.06.2015, Bul. No. 11. Available at: <https://uapatents.com/4-108781-sposib-rafinuvannya-alyumniehvogo-splavu-u-vakuumi.html>
8. Polyvoda, S. L., Polyvoda, M. O., Hordynia, O. M., Siryi, O. V., Puzhailo, L. P. (2017). Pat. No. 115590 UA. Sposib vyznachennia vmistu vodniu u ridkomu metali. MPK C22B 21/00, G01N 33/20, G01N 27/61, G01N 27/74. No. a201511064. declared: 12.11.2015; published: 27.11.2017, Bul. No. 22. Available at: <https://uapatents.com/6-115590-sposib-viznachennya-vmistu-vodnyu-u-ridkikh-alyumniehvikh-splavakh.html>
9. Puzhailo, L. P., Gavriiliuk, V. P., Seryi, A. V., Polyvoda, S. L., Gordynia, A. N. (2012). Modelirovanie magnitogidrodinamicheskikh protsessov elektromagnitnogo peremeshivaniia aluminievogo splava v kristallizatore i teplovi nasadke pri polunepreryvnom lite slitkov. Protsesty litia, 5, 54–60.
10. Narivskiy, A., Polyvoda, S., Voron, M., Siryi, O. (2022). MHD-processes and equipment for continuous casting of aluminum alloy ingots. Casting Processes, 4 (150), 22–27. doi: <https://doi.org/10.15407/plit2022.04.022>
11. Narivskiy, A. V., Shyriaieva, I. V., Hlike, A. P., Fedorov, V. V., Naidek, V. L. (2012). Pat. No. 98903 UA. Sposib rafinuvannia splaviv vid domishok. MPK C21C 7/10, C22B 9/04, C21C 7/072. No. a201108029. declared: 25.06.2011; published: 25.06.2012, Bul. No. 12. Available at: <https://uapatents.com/6-98903-sposib-rafinuvannya-splaviv-vid-domishok.html>
12. Fiksen, V. M., Dubodielov, V. I., Naidek, V. L., Sychevskiy, A. A., Tunyk, V. O., Narivskiy, A. V., Hanzha, M. S. (2017). Pat. No. 113663. Sposib plazmovo obrobky splaviv v mahnitodynamichnii ustanovtsi. MPK C22B 9/05, C21C 1/00, C21C 7/072, C22B 9/04, B22D 1/00. No. a201502163. declared: 12.03.2015; published: 27.02.2017, Bul. No. 4. Available at: <https://uapatents.com/6-113663-sposib-plazmovo-obrobki-splaviv-v-magnitodynamichnij-ustanovci.html>
13. Holländer, D., Kulawinski, D., Weidner, A., Thiele, M., Biermann, H., Gampe, U. (2016). Small-scale specimen testing for fatigue life assessment of service-exposed industrial gas turbine blades. International Journal of Fatigue, 92 (5), 262–271. doi: <https://doi.org/10.1016/j.ijfatigue.2016.07.014>
14. Balitskii, A. I., Kvasnitska, Y. H., Ivaskevich, L. M., Mialnitsa, H. P. (2018). Hydrogen and corrosion resistance of Ni-Co superalloys for gas turbine engines blades. Archives of Materials Science and Engineering, 1 (91), 5–14. doi: <https://doi.org/10.5604/01.3001.0012.1380>
15. Glotka, O. A., Olshanetskii, V. Yu. (2023). Mathematical Prediction of the Properties of Heat-Resistant Nickel Alloys After Directional Crystallization. Materials Science, 58 (5), 679–685. doi: <https://doi.org/10.1007/s11003-023-00716-z>
16. Wahl, J. B., Harris, K. (2016). CMSX-4 plus single alloy development, characterization and application development. Superalloys 2016: Proc. Of the 13th International Symposium on Superalloys. TMS, 25–33. doi: <https://doi.org/10.1002/9781119075646.ch3>

17. Cueto-Rodriguez, M. M., Avila-Davila, E. O., Lopez-Hirata, V. M., Saucedo-Muñoz, M. L., Palacios-Pineda, L. M., Trapaga-Martinez, L. G., Alvarado-Orozco, J. M. (2018). Numerical and Experimental Analyses of the Effect of Heat Treatments on the Phase Stability of Inconel 792. *Advances in Materials Science and Engineering*, 2018, 1–16. doi: <https://doi.org/10.1155/2018/4535732>
18. Kuznetsov, V. P., Lesnikov, V. P., Konakova, I. P., Popov, N. A., Kvasnitskaya, Yu. G. (2015). Structural and Phase Transformations in Single-Crystal Rhenium- and Ruthenium-Alloyed Nickel Alloy Under Testing For Long-Term Strength. *Metal Science and Heat Treatment*, 57 (7–8), 503–506. doi: <https://doi.org/10.1007/s11041-015-9912-4>
19. Wu, X., Makineni, S. K., Liebscher, C. H., Dehm, G., Rezaei Mianroodi, J., Shanthraj, P. et al. (2020). Unveiling the Re effect in Ni-based single crystal superalloys. *Nature Communications*, 11 (1). doi: <https://doi.org/10.1038/s41467-019-14062-9>
20. Klochykhin, V. V., Pedash, O. O., Danilov, S. M., Tyomkin, D. O., Naumyk, O. O., Naumyk, V. V. (2022). Hot Isostatic Pressing in the Manufacture of ZhS3DK-VI Alloy Turbine Blades with 50 % Returns in the Charge. *Strength of Materials*, 54 (6), 1043–1049. doi: <https://doi.org/10.1007/s11223-023-00479-7>
21. Zhang, J. S., Matsugi, K., Murata, Y., Morinaga, M., Yukawa, N. (1992). Evaluation of the phase stability of modified IN738LC alloys with New Phacomp. *Journal of Materials Science Letters*, 11 (8), 446–448. doi: <https://doi.org/10.1007/bf00731099>
22. Balyts'kyi, A. I., Kvasnyts'ka, Yu. H., Ivas'kevich, L. M., Myal'nitsa, H. P. (2018). Corrosion and Hydrogen-Resistance of Heat-Resistant Blade Nickel-Cobalt Alloys. *Materials Science*, 54 (2), 230–239. doi: <https://doi.org/10.1007/s11003-018-0178-z>
23. Kvasnytska, Yu. H., Kliass, O. V., Kreshchenko, V. A., Mialnytsia, H. P., Maksyuta, I. I., Shynskiy, O. Y. (2016). Pat. No. 110529 UA. Zharomitsnyi koroziiinostiikiy splay na nikellevii osnovi dlia lopatok hazoturbinnykh dvyhuniv. MKP C22C 19/05, C22C 19/00, C22C 19/03. No. a201401359. declared: 12.02.2012; published: 12.01.2016, Bul. No. 1. Available at: <https://base.uipv.org/searchINV/search.php?action=viewdetails&IdClaim=219233>
24. Kvasnytska, Y. H., Ivaskevich, L. M., Balitskii, A. I., Kvasnytska, K. H., Mialnitsa, H. P. (2022). Structural and Mechanical Properties of the Nickel Alloy of Gas-Turbine Engine Blades. *Materials Science*, 57 (5), 688–694. doi: <https://doi.org/10.1007/s11003-022-00596-9>
25. Ivaskevich, L., Balitskii, A., Kvasnytska, I., Kvasnytska, K., Myal'nitsa, H. (2022). Thermal Stability, Cyclic Durability and Hydrogen Resistance of Cast Nickel-Cobalt Alloys for Gas Turbine Blades. *Advances in Mechanical and Power Engineering*, 147–155. doi: https://doi.org/10.1007/978-3-031-18487-1_15
26. Kvasnytska, Yu. H., Ivaskevych, L. M., Balytskyi, O. I., Maksyuta, I. I., Myal'nitsa, H. P. (2020). High-Temperature Salt Corrosion of a Heat-Resistant Nickel Alloy. *Materials Science*, 56 (3), 432–440. doi: <https://doi.org/10.1007/s11003-020-00447-5>
27. Balitskii, A. I., Kvasnytska, Y. H., Ivaskevych, L. M., Kvasnytska, K. H., Balitskii, O. A., Shalevska, I. A. et al. (2023). Hydrogen and Corrosion Resistance of Nickel Superalloys for

- Gas Turbines, Engines Cooled Blades. *Energies*, 16 (3), 1154. doi: <https://doi.org/10.3390/en16031154>
28. Shinsky, O., Shalevska, I., Kaliuzhnyi, P., Shinsky, V., Lysenko, T., Shevchuk, T. et al. (2018). Principles of construction and identification of a multilevel system for monitoring parameters of technological cycle of casting. *Eastern-European Journal of Enterprise Technologies*, 5 (1 (95)), 25–32. doi: <https://doi.org/10.15587/1729-4061.2018.141303>
29. Niakan, A. A., Idris, M. H., Ourdjini, A., Karimian, M. (2012). Effect of Applying Air Pressure on Gas Porosity in Lost Foam Casting of Al-Si Alloy. *Advanced Materials Research*, 628, 150–155. doi: <https://doi.org/10.4028/www.scientific.net/amr.628.150>
30. Kaliuzhnyi, P. (2020). Influence of Sand Fluidization on Structure and Properties of Aluminum Lost Foam Casting. *Archives of Foundry Engineering*, 20 (1), 122–126. doi: <https://doi.org/10.24425/afe.2020.131293>
31. Shinsky, I., Shalevska, I., Musbah, J. (2015). Efficiency of influence of a metal macroreinforcing phase on process of solidification of large-sized castings. *TEKA. Edition of Lublin University of technology*, 15 (2), 51–59.
32. Kaliuzhnyi, P., Shalevska, I., Sliusarev, V. (2023). Microstructure of reinforced cast iron produced by lost foam casting. *Archives of Metallurgy and Materials*, 68 (4), 1369–1375. doi: <https://doi.org/10.24425/amm.2023.146202>

STRUCTURAL MATERIALS: MANUFACTURE, PROPERTIES, CONDITIONS OF USE

Orest Ostash, Svitlana Polyvoda, Andrii Titov, Kostyantyn Balushok, Roman Chepil,
Natalia Zlochevska, Anatoliy Narivskiy, Oleg Shinsky, Inna Shalevska, Yuliia Kvasnitska,
Pavlo Kaliuzhnyi, Maksym Kovzel, Valentyna Kutzova

Collective monograph

Technical editor I. Prudius
Desktop publishing T. Serhiienko
Cover photo Copyright © 2023 Canva

TECHNOLOGY CENTER PC
Published in December 2023
Enlisting the subject of publishing No. 4452 – 10.12.2012
Address: Shatylova dacha str., 4, Kharkiv, Ukraine, 61165
